UNIVERSITY OF CALIFORNIA

San Diego

Circumstellar Grains and the Intrinsic Polarization of Starlight

A dissertation submitted in partial satisfaction of the requirements for the degree Doctor of Philosophy in Physics

by

William John Forrest

Committee in charge:

Professor Wayne A. Stein, Chairman
Professor Robert J. Gould
Professor Ralph H. Lovberg
Professor Huey-Lin Luo
Doctor D. Asoka Mendis, Lecturer

1974

The dissertation of William John Forrest is approved, and it is acceptable in quality and form for

University of California, San Diego

1974

DEDICATION

I dedicate this overlong thesis to my parents, my sister Ann, and all my friends who have put up with me these six years in graduate school. I also dedicate it to Earl Scruggs who turned me on to bluegrass banjo picking.

TABLE OF CONTENTS

LIST OF FIGURES

LIST OF TABLES

ACKNOWLEDGMENTS

I would like to thank sincerely Mrs. Dawn Pedersen and Mrs. Del Crowne for doing much of the hard work that makes a thesis. Del drew the beautiful figures, each of which is worth a thousand words (more or less), and Dawn typed the thousands of words. Dawn was especially stalwart in the final days when my mind was fuzzy from late night work and the thesis had to be beaten into final form.

Primary credit for my introduction to and initiation into the field of infrared astronomy goes to my science advisors at UCSD, Drs. Wayne A. Stein and Frederick C. Gillett. Fred designed and built the dewars and detectors on which this study is based and initiated me in the art of infrared observation atop Kitt Peak and Mt. Lemmon in Arizona. He taught me to scan the horizons for those evil entities "clouds" and beware of other gremlins which can turn the best intentioned of observations into garbage. He also commanded a deep knowledge of what the observations meant and which observations were important. Wayne suggested this thesis project and was always available for discussion and critical comment on whatever particular tangent I was on; he was quick to grasp and suggest which tangents might be fruitful. He has been the source of such dicta as "nothing radiates better than a blackbody..." and other practical knowledge in the field of astronomy.

I also wish to thank Drs. K. Serkowski and H. M. Dyck for contributing unpublished polarization measurements and Dr. S. J. Shawl for contributing his thesis and helpful discussions on the matter of the intrinsic polarization of stars.

My work would not have been nearly as fun and productive without the discussions with and observations contributed by many colleagues. In particular, K. M. Merrill, D. W. Strecker, H. S. Hudson, B. T. Soifer, T. W. Jones, N. J. Woolf, E. P. Ney, N. Z. Scoville, R. R. Treffers and D. P. Gilra have been helpful.

Mr. Paul Brissenden should be given credit for help in assembling and maintaining the observing equipment in La Jolla and on Mt. Lemmon.

Finally, the American Taxpayer should be thanked for financing this scientific investigation.

VITA

May 18, 1945 - Born - San Francisco, California

1968 - B.S., Antioch College, Yellow Springs, Ohio
1968-1969 - Teaching Assistant, University of Pennsylvania Philadelphia, Pennsylvania
1969 - National Science Foundation Traineeship
1969 - Research Assistant, University of Pennsylvania, Philadelphia, Pennsylvania (summer)
1970-present - Research Assistant, University of California, San Diego, La Jolla, California

PUBLICATIONS

"Visual Intrinsic Polarization and IR Excess of Cool Stars" (with H. M. Dyck, F. C. Gillett, R. D. Gehrz, W. A. Stein, N. J. Woolf and S. J. Shawl), 1971, Ap. J. 165, 57.

"Variability of Radiation from Circumstellar Grains Surrounding R CrB" (with F. C. Gillett and W. A. Stein), 1971, Ap. J. (Letters) 170, L29.

"IR Measurements of R CrB Through Its March-June Minimum" (with F. C. Gillett and W. A. Stein), 1972, Ap. J. (Letters) 178, L129.

"Spectrum of BNKL, 2.8 μ - 13.5 μ" (with F. C. Gillett), 1973, Ap. J. 179, 483.

"8-13 μ Spectrum of NGC 7027, BD +30° 3639 and NGC 6572" (with F. C. Gillett and K. M. Merrill), 1973, Ap. J. 183, 87.

"Discovery of Large 10 μ Linear Polarization of the Becklin-Neugebauer Source in the Orion Nebula" (with H. M. Dyck, R. W. Capps and F. C. Gillett), 1973, Ap. J. (Letters) 183, L99.

"8-13 μ Observations of Titan" (with F. C. Gillett and K. M. Merrill), 1973, Ap. J. (Letters) 184, L93.

"The 7.5-13.5 μ Spectrum of Saturn" (with F. C. Gillett), 1974, Ap. J. (Letters) 187, L37.

"Circumstellar Grains and the Intrinsic Polarization of Starlight" (with F. C. Gillett and W. A. Stein), submitted to Ap. J., 1974.

FIELD OF STUDY

Major Field: Physics

Studies in Astrophysics.
Professors Wayne A. Stein, William G. Matthews, and Frederick C. Gillett

Studies in Classical Electrodynamics.
Professors Michael Cohen and Robert J. Gould

ABSTRACT OF THE DISSERTATION

Circumstellar Grains and the Intrinsic
Polarization of Starlight

by

William John Forrest

Doctor of Philosophy in Physics
University of California, San Diego, 1974
Professor Wayne A. Stein, Chairman

Twenty-four late-type variable stars exhibiting intrinsic variable polarization have been monitored over the range 3.5 μ to 11 μ for several cycles. No conclusive evidence for gross changes in the amount of circumstellar grains have been found. Thus, circumstellar infrared emission is attributed to the total abundance of grains surrounding the star which does not change by a large amount with time while intrinsic polarization is attributed to more localized scattering and absorption effects or possibly to aligned grains. Spectrophotometry with $\Delta\lambda/\lambda \approx 0.015$ over the 7.5-13.5 μ wavelength range of several stars with different chemical composition indicate excess emission characteristic of 3

types of grains: (1) "blackbody" grains, (2) silicate grains and (3) silicon carbide grains.

It is found that the Mira carbon stars and V Hya have an energy distribution that is qualitatively different than the semi-regular carbon stars and the oxygen-rich stars. In addition to the spectral feature due to silicon carbide grains, which also appears in the semi-regular carbon variables, a major fraction, from 0.3 to 0.8, of the observed energy from the Mira carbon stars appears as a cool component characterized by an approximately 950 °K blackbody. Thus, the ratio silicon carbide to "blackbody" excess appears to vary greatly among the carbon stars. A plausible mechanism to explain the excess over all wavelengths seen in the carbon Miras is absorption of starlight and thermal re-radiation by graphite grains in the circumstellar envelope.

Similar infrared observations of the variable star R CrB over the period 1970-1974 have been made and discussed in terms of a single or double star model for this object. On the single star model it is found that dust made on or about JD 2,441,033 was subsequently ejected from the star with an apparent recessional velocity of 27 km/s. There was no visual event directly associated with this infrared activity but if the apparent recession is extrapolated linearly back in time, the material would have left the stellar surface on JD ~ 2,440,400, and about this time there was a visual event. Spectrophotometry with $\Delta\lambda/\lambda \approx 0.02$ over the 3-4 μ and $\Delta\lambda/\lambda \simeq 0.015$ over the 8-12.5 μ wavelength ranges show

an excess emission which is completely smooth and featureless to the accuracy obtained, in distinct contrast to the spectra of all the M and C stars observed in this study which do show features.

Models to explain the intrinsic polarization of starlight in terms of scattering and absorption by circumstellar dust grains are discussed. It is found that the rapid variability of polarization and the optical depth of the shell inferred from infrared measurements put severe constraints on the asymmetric envelope models and suggest small clouds, perhaps close to the star, must be responsible for the polarization. Alternatively, it is found that asymmetric grains in the extended circumstellar envelope may be aligned by the Davis-Greenstein paramagnetic relaxation mechanism. The time scales for alignment would be 1-3 days and if the field is dipolar (1) a stellar surface field of approximately 16-100 gauss is required, and (2) the expected infrared polarization may not necessarily be large.

The mass loss from late-type stars has been re-investigated and it is found that the observed persistence of dust grains in the circumstellar envelope requires continuous condensation and ejection of grains leading to a minimum gas loss rate $\gtrsim 10^{-6}$ $M_\odot$/yr necessary to restrain the grain outflow. The grains must be momentum coupled to the gas as suggested by Gilman for otherwise they would exit too rapidly. In addition, it is found that the momentum coupling of gas to dust and the minimum gas loss rate consistent with the observed dust loss rate limits the supersonic

terminal velocity of dust grains relative to the gas to approximately 5-10 km/s. For the oxygen-rich Mira variables the calculated mass loss rates (using a simplified model for the circumstellar envelope) are $\sim 3\text{-}7 \times 10^{-6}$ $M_\odot$/yr and the dust loss rate is $\sim 1/300$ of this in silicate grains. For the carbon Miras the gas and graphite dust loss rates are approximately twice this and, in addition, the calculated rates agree with the lower limit to mass loss given by the minimum radiation pressure exerted on the grains (consistent with the observed infrared excess and conservation of energy) and the conservation of momentum. Thus, the idea of Gehrz and Woolf and Gilman that mass loss in late-type stars may be driven by radiation pressure on the circumstellar dust grains is supported.

I. INTRODUCTION

This study was stimulated by the discovery (Dyck et al. 1971) that there was a good correlation (Fig. 1) between the average intrinsic visual polarization and the infrared excess of cool stars as measured by the flux ratio $F_{11\mu}/F_{3.5\mu}$, where F_λ is the apparent flux, $W/cm^2\ \mu$, from the star at wavelength λ. This correlation was understandable on the model that infrared excesses are caused by re-radiation of thermalized starlight from circumstellar dust grains and these same grains, through their scattering and absorptive properties, polarized the initially unpolarized starlight. Since the polarization was known to be time variable (Shakhovskoi 1964; Serkowski 1966 a, b; Zappala 1967), it was desirable to obtain simultaneous infrared and polarization measurements to see if the large and sometimes rapid variations in visual polarization were associated with corresponding variations in the infrared flux.

In addition, the identification of silicate mineral grains as the radiating material around cool M stars (Gillett, Low, and Stein 1968; Woolf and Ney 1969) and the identification of a similar material as a component of the interstellar dust, viz. the emission spectrum of the Trapezium obtained by Stein and Gillett (1969), led Gehrz and Woolf (1971) to consider cool stars, specifically M-type Mira variables, as candidates for the production of this type of dust. They concluded, from their calculated mass loss rates and the distribution of Mira variables in the galaxy, that M-type Mira variables appeared sufficient to supply all of this type of material to the interstellar medium. In addition, Hoyle and Wickramasinghe

Fig. 1: Average polarization as a function of infrared excess as measured by the flux ratio $F_{11\mu}/F_{3.5\mu}$ from Dyck et al. (1971)

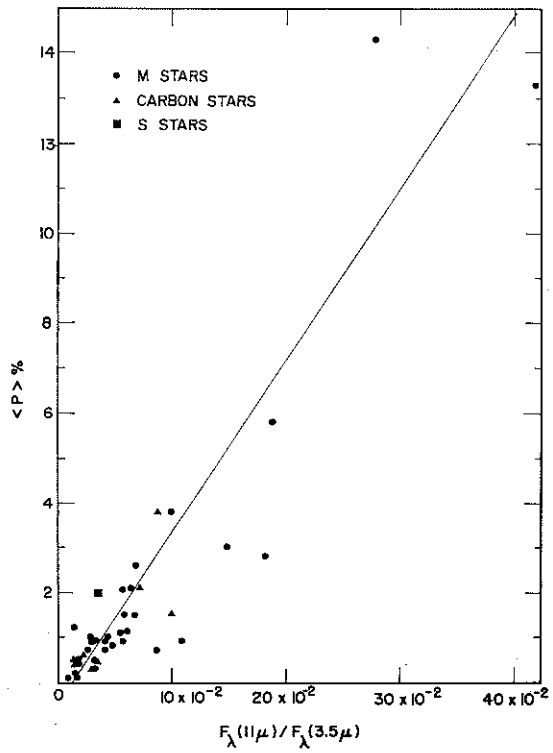

(1962) had, before the discovery of circumstellar dust shells, suggested that carbon Miras might be the seat of production of at least some of the interstellar grains. They speculated on the conditions necessary for the formation and subsequent ejection of graphite grains from these cool-star atmospheres. It was thus potentially very interesting to try and study the detailed dynamics and other aspects of this dust production, i.e., does dust production occur steadily or sporadically, are the dust grains (as exemplified by their infrared spectra) the same for all M-type stars? How do the carbon stars (C-type) and S-type stars fit into this picture?

To this end, light curves (F_λ vs. time) at broad band infrared wavelengths λ_o = 3.5, 4.9, 8.4, and 11.2 μ have been measured for the approximately 25 late type, variable stars and R CrB in Table 1. R CrB is a peculiar hydrogen-deficient, carbon-rich variable whose visual light curve (Loreta 1934; O'Keefe 1939) and infrared excess (Stein et al. 1969) suggest the existence of circumstellar dust grains. In addition, medium resolution spectra ($\Delta\lambda/\lambda \sim 0.015$) have been obtained for some of the stars and related objects, mostly in the wavelength range λλ 7.5-13.5 μ but also, in a few cases, λλ 3-5 μ. These spectra, along with flux measurements at longer and shorter wavelengths may be used to interpret the broad band energy distributions and light curves in terms of the model: star + dust.

II. TECHNIQUE

The photon flux received at earth from a celestial source can be characterized by its four Stokes parameters [intensity (flux = F_λ, W/cm^2 μ), linear polarization (P_λ, %) and position angle (θ_λ, °), and circular polarization (Q, ± %] vs. wavelength (λ,μ) and time. If the source is extended, which all will be to some extent, there is also information as to the angular distribution on the sky. In the present study, intensity (flux) received at infrared wavelengths vs. time for a list (Table 1) of variable stars was made. The techniques used to do this will be briefly described below.

The infrared receiver employed for this study was designed and built at UCSD by F. C. Gillett. The dewar consists of a L He inner flask surrounded by a L N_2 outer flask and encased in a room temperature enclosure -- the inside is evacuated but the L N_2 and L He run at ambient pressure. The detector employed for the most part was a Hg-doped Ge photoconductor (sensitive to photons with $h\nu \gtrsim$ band gap, $\lambda \lesssim 15$ μ) run at L He temperatures in order to (1) reduce the number of thermally excited charge carriers and (2) reduce the thermal background flux on the detector. The ~ f/11 field of view of the detector, appropriate for the Mt. Lemmon telescope, is defined by a L He field lens at the focal plane and a L N_2 baffle. The wavelength resolution is provided by interference filters in the field of view of the detector. Fixed band pass, $\Delta\lambda/\lambda \sim$ 10-20%, filters are used for the broad band measurements and variable band-pass, $\Delta\lambda/\lambda \sim$ 1-2%, for the medium resolution spectra. The filters run at L N_2 temperatures to reduce the thermal background flux on

the detector.

A fundamental difficulty of measurements made at the wavelengths considered here is the existence of a large thermal background (BG) due to the ~ 300 °K terrestrial sources (namely the telescope and the sky) in the field of view of the detector. At $\lambda \sim 10$ μ, even for the brightest sources BG/sig ~ 10^3 and for the faintest sources BG/sig $\gtrsim 5 \times 10^4$, so a reliable method of detecting the small signal from the "star" in the presence of this large background flux must be devised. The problem is analogous to trying to do visual photometry during the day with a fluorescent telescope. The signal from the (discrete) star is extracted from that of the (diffuse) sky by "chopping." An oscillating diagonal mirror near the focal plane shifts the field of view of the detector alternately between a beam which contains only sky and an adjacent beam which contains star + sky. The preamplified detector signal (S_1) is fed into a synchronous demodulator (phase sensitive detector) which detects only the part of the signal which is at the chopping frequency (typically 5-10 Hz). This signal (S_2) would be directly proportional to the flux from the star except for (1) the offset caused by the warm telescope itself and (2) possible differences between the two sky beams (i.e., even with no star in either beam, $S_2 \neq 0$). This effect is cancelled by "wobbling" the telescope, the star being put alternately in one (S_2) and then the other (S_2') sky beam, the reference beam being alternately on one side and then the other side of the star. The net signal, which is proportional to the flux

from the star, is then $S_3 = S_2 - S_2'$. The signals S_2 are recorded directly on a chart recorder and also digitized and sent into an integrator where the differencing to get S_3 is performed. Wobbling is done once every 10-30 sec, in the case of a faint source many S_3 are combined to give an average signal, S, and standard deviation of the mean, σ_m.

For all the measurements described here, a 22" beam diameter and 30" chopping-wobbling distance, as projected on the sky, was employed. The broad band filters used had central wavelengths λ_o and widths $\Delta\lambda$ (FWHM) given approximately by:

λ_o	2.28 μ	3.5 μ	4.9 μ	8.4 μ	11.2 μ	12.5 μ	18 μ
$\Delta\lambda$	0.5 μ	1.0 μ	1.0 μ	0.8 μ	2.0 μ	1.7 μ	4 μ
		Monitor (light curve) wavelengths					

And the narrow band filter wheels covered the ranges

$\lambda\lambda$ 2.8-5.5 μ $\Delta\lambda/\lambda \sim 2.2\%$

$\lambda\lambda$ 7.5-13.6 μ $\Delta\lambda/\lambda \sim 1.5\%$.

The observations were made, almost exclusively, during the night using the 60" metal-mirror telescope of the U. Minnesota-UCSD Infrared Observatory on the peak ($\sim$ 9300 ft. high) of Mt. Lemmon, Arizona. Flux measurements are made by comparing the signal S_λ from a target object at a particular wavelength to that from a "standard" star or stars. In the first approximation, the flux will be

$$F_\lambda(\text{object}) = S_\lambda(\text{object}) \frac{F_\lambda(\text{standard})}{S_\lambda(\text{standard})} \quad . \qquad \text{(II-1)}$$

A. Broad Band

The broad band flux from "standard" stars (Table 2a) is derived by this technique using the fundamental stardard star αLyr (Sp:A 0 V) and the flux for zero magnitude [$F_\lambda(0\text{ mag}) = F_\lambda(\alpha\text{Lyr})$] given by Gillett, Merrill and Stein (1971). In addition, the secondary standard star αC Ma (Sp: A IV) was used for calibrating the standards assuming $F_\lambda(\alpha\text{CMa})/F_\lambda(\alpha\text{Lyr}) = 3.44$, const. At wavelengths other than those given by Gillett et al. (1971) the flux for zero magnitude was extrapolated using a 10,000 °K black body appropriate for αLyr, αCMa, for $\lambda > 1$ μ and using the calibration of Johnson (1965) for $\lambda < 1$ μ. The broad band fluxes at a wavelength λ are conveniently expressed in "magnitudes," [λ], where

$$F_\lambda(\text{star}) = F_\lambda(0\text{ mag}) 10^{-[\lambda]/2.5} \quad . \qquad \text{(II-2)}$$

The (assumed) magnitudes for αLyr, αCMa and derived magnitudes for the other standard stars are given in Table 2a along with the assumed flux for zero magnitude. In general, the repeated measurements of standards were consistent with (1) the magnitudes listed and (2) no time variability, within $\sim \pm 5\%$. The absolute flux calibration is less certain and could differ by as much as ± 20% from that listed.

Standard stars were measured regularly through the night at all wavelengths used to establish the sensitivity of the system [i.e., $S_\lambda(*)/F_\lambda(*)$] and possible variations in sensitivity or deviations from eq. (II-1) due to:

(1) Telescope focus

(2) Sky transparency vs:

(a) time

(b) zenith angle, θ_Z

(c) azimuth angle, ϕ

(3) Detector beam alignment

(4) Guiding errors

(5) Non-linearity of detector system

(6) Other.

These measurements were combined to give the adopted sensitivity through the night which was applied to the target stars (eq. II-1) to give the observed fluxes (magnitudes). In general, target stars were observed near meridian transit so as to minimize the corrections due to differing zenith angles.

The errors to be assigned to the broad band measurements are difficult to assess a posteriori. In most cases the statistical errors were very small ($\ll \pm 5\%$) and the true error is probably of a systematic nature. Variable sky transparency was most troublesom at 3.5 μ and, especially, 4.9 μ where the filter bandpasses overlap the wings of the atmospheric H_2O absorption. The 8.4 μ and, especially, 11 μ filters are placed in much cleaner atmospheric windows. A statistical analysis of the systematic errors was made by comparing measurements of the same bright target star made more than once during a week's observing run. We assume the star's flux did not vary on a few days' timescale and the measurements (Q_i) are distributed normally about the

mean ($\overline{Q}$), i.e., the probability $P(Q_i)$ is given by:

$$P(Q_i) = \text{const. } e^{-(Q_i-\overline{Q})^2/2\sigma^2} .$$

Then if $\Delta = \sqrt{2}\,|Q_1 - Q_2|/(Q_1 + Q_2)$, the average standard deviation is given by $\langle\sigma/\overline{Q}\rangle = (1/2)\langle\Delta^2\rangle^{1/2}$. The average from ~ 60 independent pairs and gave for $\langle\sigma/\overline{Q}\rangle$:

Time	[3.5 μ]	[4.9 μ] -[3.5 μ]	[8.4 μ] -[3.5 μ]	[11.2 μ] -[3.5 μ]	[11.2 μ] -[8.4 μ]
1970.8-1972.0	0.07	0.07	0.07	0.07	0.05
1972.0-1974.0	0.04	~~0.07~~ 0.04	0.04	0.04	0.04

i.e., the 1 σ systematic errors improved from about ± 7% during the first year to ± 4% for the last two years.

B. Narrow Band

The primary standards for the narrow band spectra λλ 8-13 μ were αBoo and αTau, assumed to be 4000 °K and 3500 °K black bodies respectively normalized to their broad band fluxes (Table 2a). The standard and target stars were measured at close to the same zenith distance (within ~ 0.2 sec θ_z) but different times, the flux is then given by eq. (II-1). Broad band measurements (at 8.4 μ, 11.2 μ, and 12.5 μ) were also made as a cross check on the corrected spectra. At these wavelengths the primary atmospheric absorbers are water ($\lambda \lesssim 8$ μ), ozone (λλ 9-10 μ peaking

at $\sim 9.6\ \mu$) and CO_2 ($\lambda > 13\ \mu$). The ozone and CO_2 absorptions seemed to be fairly stable through a night and from night to night but the H_2O could be highly variable, especially on "wet" nights. As a check on the procedures, two spectra $\lambda\lambda$ 8-13 μ of the asteroid Ceres were obtained. The corrected spectra followed a $\sim 220\ ^\circ K$ black body within the statistical ($\sim 5\%$) errors, so it is believed there are no gross systematic errors being introduced by this procedure.

The errors in a given spectra for $\lambda > 8\ \mu$ can be estimated by:

(1) Scatter in adjacent points (we take ~ 2 points per resolution element)

(2) Statistical errors arrived at in averaging two or more spectra together.

Method (2) is to be preferred, especially when one is looking for real features in the spectra.

III. THE STARS

The program stars (Table 1) are all of late spectral type (excluding R CrB, described more fully in Chapter VI), which implies a low effective surface temperature ($T_* \sim 2000$-$3000\ ^\circ K$). The stars are all "giants" or "supergiants," which implies a much larger stellar radius ($r_* \sim 10^2$-$10^3\ r_\odot$) and a much higher luminosity ($\mathcal{L}_* \sim 10^3$-$10^5\ \mathcal{L}_\odot$) than stars of corresponding spectral type on the main sequence. The masses of the stars are not well known; for the M-type Mira variables and R CrB it is believed $M_* \sim 1$-$2\ M_\odot$. The structure of the stars consists of a hot, dense core ($M_{core} \sim 0.5\ M_*$) where the prodigious luminosities are generated by nuclear reactions; this energy is transported by convection to the stellar "surface" and thence radiated to the observer. For the late type stars the "surface" is actually an extended atmosphere; the atmospheric scale height ($h = kT/mg$) is comparable to the stellar radius ($h/r_* \sim 0.05$). The chemical composition of the observed atmospheric layers is indicated by the spectral type. The M-type stars have close to solar abundances for most elements. The carbon stars (C-type) are defined by $N_C > N_O$, and there are other abundance anomalies. The S-type stars are notable for the relative over-abundance of heavy metals of the fifth and sixth periods of the periodic table (Sr, Y, Zr, Nb, Tc, Ba, and La). M and C stars may also exhibit some S star characteristics in their spectra. R CrB is hydrogen deficient and carbon rich. The abundance anomalies

are believed to be the result of nuclear processing of initially solar-type material at some time in the stars' past. In this regard the existence of Tc^{99} in some M, S, and C stars, with a half-life of 2×10^5 years is especially significant. The nuclear reactions must have occurred in the recent past and there must be fairly rapid delivery of processed material to the observed atmospheric layers.

The stars are also variable in luminosity to some extent (Pettit and Nicholson 1933; Strecker 1973). The period of variation is given approximately by the free-fall time $\tau \sim (G\rho_*)^{-1/2}$. The Mira variables (15 of the program stars) have regular periods around one year in which they vary in spectral type, temperature ($T_{max}/T_{min} \sim 2500\ °K/2000\ °K \sim 1.25$), luminosity ($\sim 1$ mag = factor of 2.5) and radius ($r_{max}/r_{min} \sim 1.35$).

In addition to the abundance anomalies there are various spectral peculiarities of which we mention the (1) "veiling" or apparent weakening of the stellar absorption lines, (2) occasional appearance of strong emission lines (hence the "e" in M6e) in the spectrum, and (3) existence of very narrow absorption lines with an approximately constant velocity blueshifted (i.e., to shorter wavelengths) $\sim$ 10-20 km/s from the stellar velocity. In the Mira variables the "veiling" effect is variable from cycle to cycle and could be due to (a) opacity effects (i.e., turbulence, etc.) in the "reversing layer" where the absorption lines are formed, (b) overlying continuous emission which reduces the contrast seen in the underlying stellar spectrum, or (c) scattering

of the starlight off a radially expanding circumstellar envelope. The existence of emission lines in such cool ($T_* \sim 2500\ °K$) stars is quite unusual and indicates some energetic, non thermal-equilibrium processes are taking place. Some of the emission lines (hydrogen, calcium) are believed to originate, at least in part, from below the reversing layer (Merrill 1960) while others ([Mn I], [Fe II]) probably originate above it (Nussbaumer and Swings 1972). The narrow, blueshifted absorption lines probably originate in cool, circumstellar gas in our line of sight to the star which is flowing smoothly away from the star. This implies there is mass loss occurring from these stars (redshifts are never seen). The majority opinion holds that the Mira variables are relatively old stars which have evolved away from the main sequence. Kukarkin (1955) proposed the opposite view that Miras are young, pre-main sequence which should tell us about the conditions of star formation.

The stars are linearly polarized at visual ($\lambda\lambda$ 0.35-1 μ) wavelengths. At least some of this polarization must be intrinsic to the star because (1) the polarization is variable with time, (2) many of the stars with large polarization are at high galactic latitudes, and (3) the wavelength dependence of the polarization is quite different than that of interstellar polarization. The polarization is variable both in degree and in position angle. The variation is, in general, quite chaotic but there is often a tendency in the Mira variables for the maximum polarization

to occur at visual minimum or, in some cases, on the rise to maximum light. The degree of polarization can change (increase or decrease) by factors of 2 or 3 on a timescale of $\lesssim$ 30 days ($\lesssim$ 0.1 period). The angle of polarization can also change by $\sim 90°$ on these short timescales. The degree of polarization generally increases toward the blue and is quite small by $\lambda \sim 1\ \mu$.

IV. BROAD BAND OBSERVATIONS

Table 1 summarizes the stars observed in this study. In addition to the star name, the spectral type, variability class and period are summarized from Kukarkin et al. (1969). The day of zero phase [$D_o(0)$] in column (7) is described in Section C. The range of visual variation from Kukarkin et al. (1969) and the observed range in [3.5 μ] are shown along with limits to the observed variations in infrared colors in columns (8)-(13). In the case of the Mira variables and R CrB the ± numbers refer to the author's estimate of the actual range of variation from the observed light curve, in the case of the SR variables they refer to upper limits to the amount of variation.

A. Energy Distributions, M and S Stars

In order to interpret the observed light curves (flux vs. time) in terms of radiation from the star on the one hand and radiation from its associated circumstellar dust grains on the other, one must make an attempt at separating these two contributions to the observed flux. Appendix A gives the model adopted here to guide this interpretation: The observed flux is the sum of attenuated starlight plus the radiation from the circumstellar shell. The relative bolometric excess α = ratio of total apparent flux from the shell to the total observed flux is one measure of the amount of excess. The monochromatic excess $\beta_\lambda = [F_\lambda(\text{total}) - F_\lambda(\text{continuum})] \times F_\lambda^{-1}(\text{continuum})$ measures the size of an emission feature relative

TABLE 1

Stars Included in the Observing Program

(1) Name	(2) HD	(3) IRC	(4) Spectrum	(5) Variability	(6) Period (days)	(7) D_o(O) J.D. 2,440,000+	(8) Visual Magnitude	(9) [3.5 μ]*	(10) [4.9 μ]-[3.5 μ]*	(11) [8.4 μ]-[3.5 μ]*	(12) [11 μ]-[3.5 μ]*	(13) [11 μ]-[8.4 μ]*
oCet	14386	-00030	M5e-M9e	M	331.7	820	3.7-9.2	-3.48, -2.83	-0.30±0.05	-0.90±0.06	-1.68±0.08	-0.76±0.06
Z Eri	17491	-10040	M4 III	SRb	80 (746)		6.4-7.8	+0.10, +0.26	+0.17±0.07	-0.28±0.10	-1.04±0.11	-0.76±0.10
W Per	237008	+60097	M5	SRb	469		8.7-11.8	-1.57, -1.30	-0.15±0.05	-1.00±0.10	-2.58±0.10	-1.56±0.10
R Lep	31996	-10080	$C7_6e$	M	432.5 (40 yr)	800	6.8-9.6	-1.23, -0.68	-0.30±0.10	-1.20±0.10	-1.90±0.10	-0.66±0.05
Y Tau	38307	+20121	$C7_4e$	SRa	240.9 (1750)		6.8-9.2	-0.40, -0.15	-0.04±0.04	-0.76±0.06	-1.46±0.10	-0.67±0.07
U Ori	39816	+20127	M6e-M8e	M	372.5	782	6.3-12.0	-1.70, -1.00	-0.35±0.05	-0.90±0.10	-1.70±0.15	-0.78±0.10
TV Gem	42475	+20134	M1 Iab	SRc	182		6.6-8.0	+0.50, +0.66	-0.10±0.08	-0.92±0.08	-1.90±0.09	-0.97±0.04
UU Aur	46687	+40158	$C5_4$	SRb	235 (3500)		5.1-6.8	-1.28, -1.08	+0.08±0.04	-0.53±0.04	-0.94±0.06	-0.42±0.04
R Gem	53791	+20171	S3,9e-S6,9e	M	369.6	728	7.1-13.5	+1.12, +2.04	-0.24±0.05	-0.88±0.05	-1.22±0.18	-0.30±0.20
R Cnc	69243	+10185	M6e-M8e	M	361.7	595	6.8-11.2	-1.35, -0.90	-0.40±0.08	-0.82±0.10	-1.30±0.10	-0.48±0.08
R LMi	84346	+30215	M7e-M8e	M	372.3	610	7.1-12.6	-1.35, -0.80	-0.40±0.08	-0.92±0.06	-1.70±0.10	-0.72±0.05
R Leo	84748	+10215	M6.5e-M9e	M	312.6	740	5.8-10.0	-3.23, -2.68	-0.30±0.07	-0.75±0.10	-1.48±0.10	-0.72±0.05
V Hya		-20218	$C6_3e$	SRa	529 (18 yr)		6.0-12.5	-1.90, -1.50	-0.52±0.05	-1.75±0.08	-2.30±0.05	-0.55±0.06
V CVn	115898	+50276	M4e-M6e	SRa	191.9		6.8-8.8	+0.66, +0.80	-0.27±0.07	-1.16±0.10	-2.22±0.08	-1.07±0.09
R Hya	117287	-20254	M6e-M8e(S)	M	388.0	875	4.5-9.5	-3.04, -2.68	-0.05±0.05	-0.55±0.07	-1.15±0.10	-0.60±0.10
S CrB	136753	+30272	M6e-M8e	M	360.4	640	7.3-12.9	-0.75, -0.37	-0.35±0.10	-1.20±0.15	-2.20±0.20	-0.92±0.10
R CrB	141527		cFpep	R CrB			5.8-14.8	+1.27, +2.95	-1.05±0.25	-2.32±0.48	-2.64±0.60	-0.30±0.10
V CrB	141826	+40273	C6,2e	M	357.8	930	7.5-11.0	+0.40, +1.28	-0.65±0.10	-1.25±0.15	-1.94±0.15	-0.65±0.06
X Her	144205	+50248	M6e	SRb	95.0 (746)		6.3-7.4	-1.71, -1.63	-0.04±0.07	-0.55±0.05	-1.36±0.05	-0.80±0.06
U Her	148206	+20298	M6.5e-M8e	M	405.4	920	7.5-12.5	-1.24, -0.65	-0.40±0.05	-0.90±0.10	-1.75±0.06	-0.82±0.08
T Dra		+60255	C8e	M	421.7	995	9.6-12.3	-0.30, +0.64	-0.83±0.08	-1.86±0.14	-2.42±0.16	-0.60±0.05
χ Cyg	187796	+30395	S7,1e-S10,1e	M	406.8	890	5.2-13.4	-3.20, -2.42	-0.12±0.10	-0.70±0.15	-1.40±0.20	-0.70±0.06
RW Cyg		+40424	M3Ia	SRc	586		7.7-9.4	-0.04, +0.10	0.0 ±0.04	-0.92±0.06	-2.63±0.08	-1.71±0.09
V Cyg		+50338	C7,4e	M	421.3	650	9.1-12.8	-1.65, -0.83	-0.83±0.08	-1.80±0.15	-2.41±0.15	-0.60±0.06
R Cas	244490	+50484	M6e-M8e	M	431.0	610	7.0-12.6	-2.84, -2.06	-0.38±0.08	-1.10±0.10	-2.04±0.10	-0.92±0.06

*Quoted values represent those results actually observed. None of the stars were observed through all phases of variability.

to an assumed continuum which may refer to the stellar continuum but in some cases may include a continuum from the shell. In the case the shell is optically thin at infrared wavelengths, α and β_λ may be simply related to the amount of dust surrounding the star. Table 2a gives the broad band magnitudes for the program stars and the Trapezium measured at a particular time; these may be converted to fluxes using the "flux for zero magnitude" at the bottom of the table and eq. (II-2). In addition to the star name, day of observation, and derived phase of observation for the Mira variables, columns (4)-(16) give the λλ 2.3-18 μ data from the present study and observations at other wavelengths from other sources. At the bottom of the table are the adopted magnitudes of the standard stars and at the very bottom the adopted "flux for zero magnitude" as described in Chapter II. Energy distributions for selected stars appear in Fig. 2.

The energy distributions of the M and S stars, both Mira and semi-regular variables, seem to be fit by the two-component model: star + dust grains. The star, characterized by a blackbody plus absorptions with $T_* \sim 1800$-2600 °K, dominates the observed flux for $\lambda < 8$ μ while in the λλ 8-14 μ and λλ 16-24 μ regions there is, in addition, an excess which we attribute, following Woolf and Ney (1969), to radiation from cooler circumstellar grains. Using the model of Appendix I we can recover the excess emission due to dust by

$$F_\lambda^{dust} = F_\lambda^{obs} - F_\lambda^{*} \quad ,$$

TABLE 2a

Energy Distributions of Program Stars, Adopted Magnitudes for Standard Stars, and Adopted Flux for Zero Magnitude

(1)	(2)	(3)	(4)	(5)	(6)	(7)	(8)	(9)	(10)	(11)	(12)	(13)	(14)	(15)	(16)
Star	JD 2,440,000+	$\phi(\mu)$	[0.55 μ] *	[0.84 μ] *	[1.04 μ] *	[1.25 μ] *	[1.65 μ] *	[2.3 μ] *	[3.5 μ]	[4.9 μ]	[8.4 μ]	[11.2 μ]	[12.5 μ]	[18 μ] *	[20 μ] *
σ Cet	1982	0.48(3)	(8.7)		(- 0.6)			- 2.50	- 3.08	- 3.34	- 3.90	- 4.63	- 4.56	(- 5.37)	(- 5.33)
Z Eri	1965	SRb	(~ 7)	(3.57)				+ 0.37	+ 0.12	+ 0.24	- 0.18	- 0.84	- 0.63		
W Per	1950	SRb	(~ 10)	(6.1)				+ 1.91	+ 1.29	+ 1.12	+ 0.30	- 1.36	- 1.23	(- 2.3)	(- 2.3)
R Lep	1980	0.73(3)	(8.2)	(4.3)	(3.3)	(2.66)	(1.19)	+ 0.13	- 0.69	- 1.31	- 2.03	- 2.70	- 2.56		(- 2.60)
Y Tau	1982	SRa	(8.2)	(4.25)	(2.7)			+ 0.28	- 0.35	- 0.44	- 1.09	- 1.71	- 1.61		(- 1.78)
U Ori	2015	0.33(3)	(9.4)	(3.4)	(1.3)			- 0.96	- 1.48	- 1.78	- 2.31	- 3.02	- 3.02	(- 3.52)	
TV Gem	1965	SRc	(~ 7)	(4.26)				+ 0.90	+ 0.45	+ 0.35	- 0.34	- 1.30	- 1.12		
UU Aur	1978	SRb	(6.2)	(3.25)	(1.65)	(1.07)	(- 0.07)	- 0.52	- 1.07	- 1.05	- 1.66	- 2.12	- 2.01		(- 2.08)
R Gem	mean curve	0.45	(11.7)	(6.6)	(4.3)			+ 1.81	+ 1.30	+ 1.08	+ 0.4	+ 0.2			
R Cnc	2015	0.91(3)	(8)	(3.5)	(1.2)			- 0.46	- 1.1	- 1.57	- 1.98	- 2.47	- 2.60		(- 2.92)
R LMi	2015	0.79(3)	(10.5)	(3.32)	(1.6)			- 0.38	- 1.05	- 1.49	- 1.92	- 2.66	- 2.74		(- 3.2)
R Leo	2015	0.84(4)	(6)		(- 0.91)			- 2.88	- 3.30	- 3.55	- 3.92	- 4.60	- 4.72		(- 5.1)
V Hya	1950	SRa	7.5	(4.0)	2.0	(1.66)	(0.23)	(- 0.75)	- 1.90	- 2.40	- 3.57	- 4.03			- 4.23
V CVn	mean	SRc	7.5	(4.2)				(+ 1.1)	+ 0.73	+ 0.46	- 0.43	- 1.49			
R Hya	mean curve	0.30	(7.5)		(- 0.51)				- 2.98	- 3.03	- 3.52	- 4.08			(- 4.66)
S CrB	1950	0.64(3)	(12.8)		(2.76)			+ 0.50	- 0.17	- 0.40	- 1.23	- 2.08	- 1.95		(- 2.58)
R CrB	1033	~ max IR	6.0		5.2			+ 3.13	+ 1.27	+ 0.98	- 0.58	- 0.77		- 0.87	
	1740	~ min IR	6.0					+ 4.33	+ 2.94	+ 1.64	+ 0.16	- 0.29			(- 0.9)
V CrB	mean curve	0.22	(9.9)	(6.2)	(4.9)	(3.92)	(2.46)	(+ 1.56)	+ 0.44	- 0.11	- 0.66	- 1.36			
X Her	1950	SRb	(6.7)					- 1.37	- 1.64	- 1.63	- 2.27	- 2.98	- 2.88		(- 3.58)
U Her	1950	0.54(2)	(12.3)		(2.68)			+ 0.06	- 0.67	- 0.91	- 1.62	- 2.47	- 2.46		(- 2.77)
T Dra	1950	0.26(2)	11.5	(7.35)	(6.58)			+ 1.84	+ 0.22	- 0.60	- 1.66	- 2.26	- 2.14		(- 2.1)
X Cyg	1854	0.35(2)	(11)		(0.95)			- 2.42	- 2.96	- 3.08	- 3.58	- 4.34	- 4.40		(- 4.64)
RW Cyg	mean	SRa	(9)	(4.8)				+ 0.49	- 0.03	- 0.02	- 0.86	- 2.62	- 2.45		(- 3.35)
V Cyg	1845	0.80(2)	(11.4)	(7.1)	(5.7)	(4.1)	(2.2)	+ 0.65	- 0.93	- 1.85	- 2.80	- 3.41	- 3.28		(- 3.41)
R Cas	1946	0.14(3)	(7.5)		(0.1)			- 2.22	- 2.85	- 3.08	- 3.84	- 4.77	- 4.65		(- 5.2)
Trapezium†	1785, 1982		--						+ 4.17	+ 2.94	- 0.68	- 2.66	- 2.64	- 4.95	
Standards -- Adopted Magnitudes and Fluxes for Zero Magnitude															
α Ari								- 0.66	- 0.79	- 0.68	- 0.74	- 0.75	- 0.75		
α Tau								- 2.83	- 3.07	- 2.92	- 3.00	- 3.04	- 3.04		
α CMa	Assumed Constant							- 1.34	- 1.34	- 1.34	- 1.34	- 1.34	- 1.34		
β Gem								- 1.11	- 1.23	- 1.21	- 1.29	- 1.22	- 1.22		
α Boo								- 3.02	- 3.15	- 3.02	- 3.09	- 3.18	- 3.18		
α Lyr								0.0	0.0	0.0	0.0	0.0	0.0		
β Peg								- 2.23	- 2.44	- 2.26	- 2.45	- 2.52	- 2.52		
Flux for Zero Magnitude (10^{-16} W cm^{-2} μ^{-1})			3.9×10^{4}	1.01×10^{4}	5.2×10^{3}	2840	1140	343	71	20	2.45	0.79	0.52	0.122	0.080

* A parenthesis implies the measurement has been adopted (with respect to visual phase) from an earlier time. The $\lambda\lambda$ 2.3-18 μ data are from the present study. Additional data are from the following sources:

0.55 μ: AAVSO (Mayall 1973)
0.84 μ: Neugebauer and Leighton (1969)
1.04 μ: Baumert (1972), Lockwood and Wing (1971), Lockwood (1972)
1.25 μ and 1.65 μ: Frogel and Hyland (1972)
2.3 μ: V CrB and V Hya, Frogel and Hyland (1972); V CVn, Neugebauer and Leighton (1969)
20 μ: Morrison and Simon (1973)

† The Trapezium was measured with a 22" diameter field aperture.

Fig. 2: Energy distributions of selected stars and the Trapezium region of the Orion Nebula. The data is from Table 2a, and is displayed in the format log (λF_λ) + const vs. log λ. Displayed in this manner, blackbody functions of different temperatures have the same shape but are displaced in wavelength and blackbody functions with the same height correspond to equal total flux, $\mathcal{F} = \int_0^\infty F_\lambda \, d\lambda$.

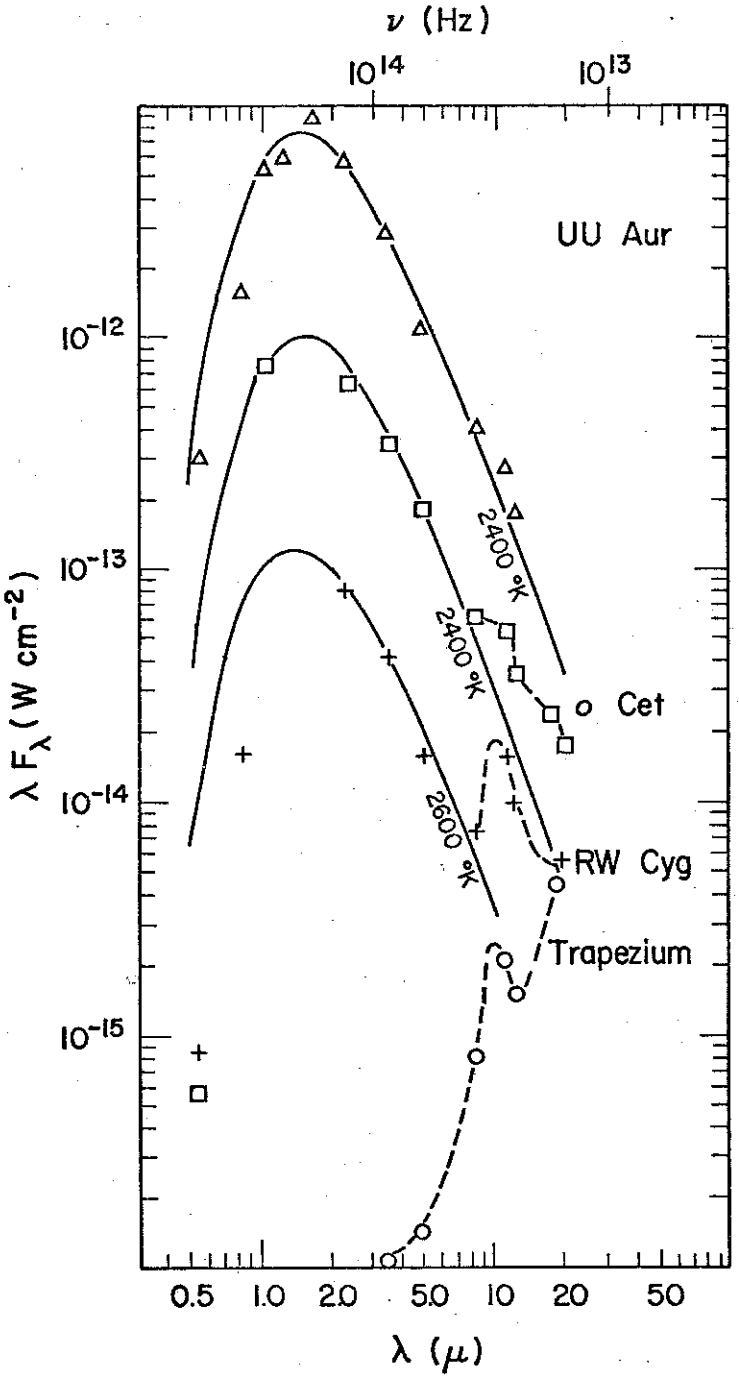

where F_λ^* is assumed to be represented by the blackbody which fits the shorter wavelength data, continued to $\lambda > 8\ \mu$. The parameters α, β_λ, and the color temperature of the excess T_c^{exc} derived on this model and the T_* adopted appear in columns (2)-(6) of Table 2b. The bolometric excess α is found to be quite small, ranging from $\sim$ 0.01-0.03 for the Mira variables to a maximum of $\sim$ 0.05 for the supergiants RW Cyg and W Per. Thus, less than 10% of the total observed energy is radiated by dust grains and the assumption of an optically thin shell would seem to be appropriate. This question is discussed further in Chapters V, VII, and VIII.

B. Star X

The Mira variables are known to exhibit cyclic temperature and luminosity variations (Pettit and Nicholson 1933; Strecker 1973). In order to separate this effect on the observed infrared fluxes from possible variations in the amount of dust around the star, a synthetic star - Star X - has been constructed. The flux from the star is initially taken to be a blackbody with the temperature and luminosity variation through the cycle given by Strecker (1973) for the variable χ Cyg. The phase dependence and range of temperature variation of χ Cyg was fairly typical of the M and S stars studied by Strecker (1973) and Pettit and Nicholson (1933). To this has been added a dust component which radiates a constant fraction 0.02 of the total energy (i.e., $\alpha = 0.02$) with a spectral dependence (β_λ) given by the observed spectrum (Table 2a, Fig. 2, Chapter V) of the Trapezium. In addition, the color temperature

TABLE 2b

Derived Source Parameters from the Data in Table 2a on the Model $F_\lambda^{obs} = F_\lambda^* + F_\lambda^{exc}$

(1)	(2)	(3)	(4)			(5)
Star	α	$\beta(\lambda_o)$ *	$T_c^{exc}(\lambda_1, \lambda_2)$ (11.2 μ, 18 μ)	(11.2 μ, 20 μ)	(3.5 μ, 8.4 μ)	T_* +
oCet	0.013	1.4	410	440		2400
Z Eri	0.003	0.65				3000
W Per	0.046	6.0	360	400		2600
R Lep	0.30	1.1 (3.5 μ)			950	2350
Y Tau	0.0044	0.80				2200
U Ori	0.013	1.3	550			2300
TV Gem	0.011	2.2				3000
UU Aur	0.0020	0.51				2400
R Gem	0.0066	0.60				2400
R Cnc	0.0058	0.60		440		2400
R LMi	0.011	1.2		580		2400
R Leo	0.0069	0.97		500		2600
V Hya	0.40	1.6 (3.5 μ)			900	2400
V CVn	0.023	2.9				2600
R Hya	0.0052	0.65		440		2500
S CrB	0.025	2.6		680		2300
V CrB	0.40	1.4 (3.5 μ)			1000	2200
X Her	0.0075	1.05		420		2600
U Her	0.020	1.6		880		2000
T Dra	0.79	8.0 (3.5 μ)			900	2200
X Cyg	0.0125	1.4		950		2300
RW Cyg	0.041	5.5		480		2600
V Cyg	0.84	9 (3.5 μ)			950	2000
R Cas	0.024	1.9		740		2100
Trapezium	--	--	200			--

* λ_o = 11.2 μ except for those designated as λ_o = 3.5 μ

+ T_* refers to the best "blackbody fit" to F_λ^* which is used to derive F_λ^{exc} and columns (2)-(4) as described in the text. Briefly, F_λ^* is assumed to be represented by the best "blackbody" fit" to the short wavelength data extended to longer wavelengths. Then

$F_\lambda^{exc} = F_\lambda^{obs} - F_\lambda^*$, where F_λ^{obs} is the observed flux

$\beta(\lambda) = F_\lambda^{exc}/F_\lambda^*$

$\alpha = \int_0^\infty F_\lambda^{exc} d\lambda / \int_0^\infty F_\lambda^{obs} d\lambda$, and

$T_c^{exc}(\lambda_1,\lambda_2)$ = color temperature of the excess between λ_1 and λ_2.

of the dust, T_c(11 μ, 18 μ), tracks the star's luminosity according to the law

$$T_c \sim (\mathcal{L}_*)^{1/4}$$

expected (eq. A-10) for dust at a fixed distance from the illuminating source. The observed energy is divided into the 8-14 μ regions and 16-20 μ regions according to the ratio $B_{10\mu}(T_c)/B_{18\mu}(T_c)$, where $B_\lambda(T)$ is the Planck function. The fraction of grain energy occurring in the 16-20 μ window varied from ~ 0.20 (T_* = 2300 °K, T_c(dust) ≃ 460 °K) to ~ 0.26 (T_* = 1750 °K, T_c(dust) ≃ 350 °K), so this latter assumption is not too important. The light curve of this star is given in Fig. 3. Plotted vs. phase (ϕ) are the visual magnitude for χ Cyg (AAVSO mean light curve, Campbell 1955), the average color temperature T_c(1.04 μ, 3.5 μ) of χ Cyg (Strecker 1973), and the calculated 3.5 μ magnitude [3.5 μ] and colors: [4.9 μ] - [3.5 μ], [8.4 μ] - [3.5 μ], [11 μ] - [3.5 μ], and [11 μ] - [8.4 μ] for Star X. The magnitude at a wavelength λ_1, $[\lambda_1]$, is a logarithmic measure of flux as discussed in Chapter II [eq. (II-2)]. The color $[\lambda_1]$ - $[\lambda_2]$ is a logarithmic measure of a flux ratio, i.e. using eq. (II-2)

$$\frac{F\lambda_1}{F\lambda_2} = \frac{F_{\lambda_1}(\text{zero mag})}{F_{\lambda_2}(\text{zero mag})}\ 10^{-([\lambda_1]-[\lambda_2])/2.5} ,$$

which is zero for a hot blackbody such as α Lyr (T_* ~ 10,000 °K) and becomes increasingly negative if there is a relative excess in F_λ at λ_1. Thus, a negative color $[\lambda_1]$ - $[\lambda_2]$ indicates either an excess at λ_1 or a deficiency at λ_2 relative to a hot blackbody.

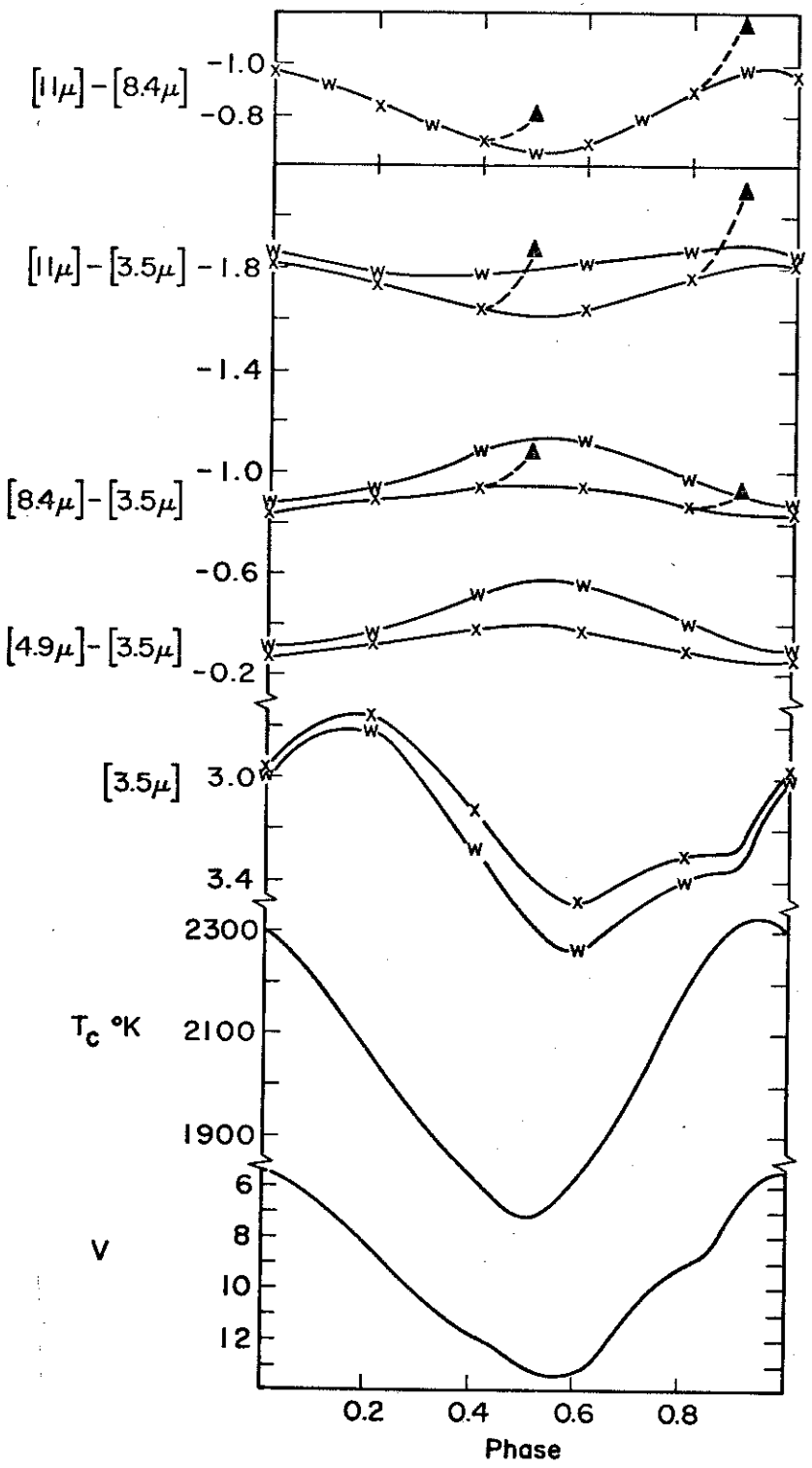

Fig. 3: Characteristics of a hypothetical variable star surrounded by circumstellar dust (Star X) as described in the text. The curves labelled "W" include the possible effect of H_2O absorption at [3.5 μ] and the solid triangles indicate the expected change in the infrared due to a 50% increase in the amount of silicate dust.

The visual magnitude ($V \equiv [0.55\ \mu]$) follows the temperature variation because $\lambda = 0.55\ \mu$ is on the exponential tail of the blackbody; this is accentuated by the increased molecular opacities at 0.55 μ at lower temperatures (Smak 1964; Strecker 1973). The (negative) [4.9 μ] - [3.5 μ] color peaks at minimum temperature because this is just the color temperature of the blackbody assumed for the star. The [11 μ] - [3.5 μ] color on the other hand shows a minimum at temperature minimum. This reduced contrast of dust to star at 11 μ is mostly due to the lower temperature of the star; for a lower star temperature relatively more of the star's total flux appears in the 11 μ band while the change in the relative amount of flux from the dust in this band due to changing temperature is much smaller. Briefly, $\beta_{11\mu}$ decreases from ~ 2.0 at $T_* = 2300$ °K to ~ 0.92 at $T_* = 1750$ °K. The [11 μ] - [8.4 μ] color, which is an indicator of the amount of silicate-type excess (Chapter V), shows the effect of the reduced contrast more strongly with a deeper minimum at temperature minimum.

As a first order treatment of the possible effects of molecular opacities the effect of H_2O absorption on Star X has been considered in a semi-empirical manner. Spectra obtained by Woolf et al. (1964) in the 1-3 μ region of the late-type M stars oCet and R Leo showed strong absorption bands (centered at 1.4 μ, 1.9 μ, and 2.7 μ) which were attributed to the opacity of hot water vapor. Subsequent calculations (Tsuji 1966; Auman 1966, 1967) confirmed H_2O vapor as a major source of opacity for these spectral types. Spectra in the 3-14 μ range (Gillett et al. 1968) of oCet showed

an approximate blackbody continuum ($T \sim 2500$ °K) for $\lambda\lambda$ 3.5-5.5 μ with a "rollover" or apparent absorption $\lambda < 3.5\ \mu$ which was attributed to H_2O absorption in the wings of the 2.7 μ feature. This absorption will reduce the flux of the star as measured by our 3.5 μ ($\lambda\lambda$ 3.0-4.0 μ) filter.

In addition Frogel (1971) has measured H_2O absorption at 2.1 μ in the wings of the 1.9 μ feature in late-type M Miras and finds the absorption varies with phase, reaching a maximum approximately at visual (i.e. temperature) minimum and vice versa. To estimate the possible effect of this variation with phase on the observed 3.5 μ broad band fluxes we have used the following procedure. Using the observed spectral shape $\lambda\lambda$ 3-4 μ (in addition to oCet we have obtained spectra of R Cas, R Leo, and S CrB which show a similar "rollover" $\lambda < 3.5\ \mu$) we calculate the expected reduction of the flux in the 3-4 μ band Δ for a given monochromatic absorption at 3.25 μ and find

$$\Delta \equiv \frac{\int_{3\mu}^{4\mu} F_\lambda(\text{observed})\, d\lambda}{\int_{3\mu}^{4\mu} F_\lambda(\text{cont})\, d\lambda} \simeq 0.5 \left(1 + \frac{F_{3.25\mu}^{(\text{obs})}}{F_{3.25\mu}^{(\text{cont})}}\right) .$$

The few available spectra, in comparison with Frogel's measurements at a similar phase, indicate that absorption at 3.25 $\mu \simeq$ absorption at 2.1 μ. We take this to be an equality, average all of Frogel's 2.1 μ absorption vs. phase data on M-type Miras, calculate the expected depression, Δ, on the 3-4 μ flux for a given 2.1 μ (and therefore 3.25 μ) depression, and apply this to Star X. The observed 3.5 μ magnitude including the effect of water absorption,

$[3.5\ \mu]_W$, will be related to the un-absorbed magnitude $[3.5\ \mu]_X$ by

$$[3.5\ \mu]_W = [3.5\ \mu]_X - 2.5 \log \Delta$$

With corresponding changes in the colors involving the 3.5 μ magnitude. The results are shown in Fig. 3 (W's). It should be emphasized that other possible effects of molecular opacity, for instance H_2O absorption at shorter and longer wavelengths and CO absorption in the 4.9 μ band, have been ignored here.

It is seen that adding water to Star X can change the observed colors considerably. In particular the [11 μ] - [3.5 μ] color no longer shows a minimum at temperature minimum but now looks rather flat. In addition, variations from the average H_2O absorption as seen by Frogel (1971) can change this from cycle to cycle for a real star. The [11 μ] - [8.4 μ] color is, by assumption, not affected by H_2O absorption and therefore may be a better index to watch for possible variations in the amount of dust.

C. Light Curves

1) M-Type Miras

Light curves for selected M-type Mira variables are plotted in Figs. 4-9. The ordinates of these figures is "instantaneous phase" $\phi_I(N)$ where for each cycle N the day for zero phase, $D_o(N)$ and period P(N) has been determined from the visual observations of the AAVSO supplied by Mayall (1973). The instantaneous phase for day D is then

$$\phi_i(N) = \frac{D - D_o(N)}{P(N)}$$

Typically the periods vary less than ~ 10% from the average period P given in Table 1 so the approximate expression for the phase

$$\phi_I(N) \simeq \phi(N) = \frac{D - D_o(0)}{P} - N$$

may be used with the day for zero phase, $D_o(0)$, given in Table 1 to retrieve the approximate Julian dates of the observation. The different cycles, N, are denoted by symbols:

N:	-5	-4	-3	-2	-1	0	1	2	3	4
Symbol:	✱	♦	■	▲	●	X	○	△	□	◇

with time increasing with increasing cycle number.

The observations plotted are, from the bottom up, (1) visual magnitude estimates of the AAVSO (Mayall 1973). The solid line is the AAVSO mean light curve ~ 1920-1950 given by Campbell (1955). (2) [3.5 μ], the 3.5 μ flux expressed in magnitudes. (3) The colors [4.9 μ] - [3.5 μ], [8.4 μ] - [3.5 μ], [11 μ] - [3.5 μ], and [11 μ] - [8.4 μ]. The dashed curves are the author's estimate of the mean behavior and error bars represent typical estimated ± 1 σ errors as discussed in Chapter II. Above these photometric measurements are plotted linear polarization measurements in the visual region (U = [0.36 μ], B = [0.44 μ], V = [0.55 μ]), using the same convention for cycle number and phase described above. The polarization data has been taken from the following sources:

1. Serkowski 1974a
2. Dyck 1972
3. Zappala 1967
4. Vardanian 1968
5. Dombrovskii 1970
6. Dyck 1968
7. Serkowski 1966a, b
8. Dombrovskii et al. 1973
9. Kruszewski et al. 1968
10. Shawl 1972
11. Dyck and Sanford 1971

The phase coverage of any one star is somewhat limited by the time it was available as a nighttime object. The infrared measurements were made almost exclusively at night and only if the star could be measured near meridian transit to minimize atmospheric extinction effects. Thus, there is an ~ 0.25-0.50 gap in the phase coverage and since the periods are all the order of 1 year these gaps usually tend to overlap from cycle to cycle.

Description of Light Curves

Studies of the temperature, radius, and luminosity variations of M and S type Mira variables have been made by Pettit and Nicholson (1933) and Strecker (1973). Lockwood and Wing (1971) and Lockwood (1972) discuss the near infrared behavior in the 1 μ region. Frogel (1971) has studied the 2 μ spectra and the variations of the 2.1 μ H_2O absorption and 2.3-2.5 μ CO $\Delta v = 2$ absorption bands in these stars. Various authors (Dombrovskii 1970; Serkowski 1971; Shawl 1972) have measured and commented on the variable, intrinsic linear polarization of these stars.

The 4 λ infrared light curves presented here are typical of all the M *'s observed in this program. The peak 3.5 μ flux comes at phase ~ 0.1-0.2 near the maximum stellar luminosity as noted by Strecker (1973). In general the observed color variations are fit fairly well by Star X, allowing for possible variations in the H_2O absorptions from the average. Real deviations in the observed [4.9 μ] - [3.5 μ] colors from those of Star X could be due to (1) different stellar temperatures, (2) different amounts of H_2O absorption in the 3.5 μ band, (3) molecular absorptions in the 4.9 μ band as due, for instance, to CO or H_2O, (4) possible contribution of dust emission in the 4.9 μ band, or (5) any combination of the above. The [11 μ] - [3.5 μ] should be a good indicator of the amount of dust (solid triangles, Fig. 3) but there is still uncertainty due to possibly variable H_2O absorption in the 3.5 μ band.

The [11 μ] - [8.4 μ] color, which is also a good indicator of "silicate type" excess and is possibly less affected by stellar absorptions, shows very little variation with phase. This is in contrast to the predicted behavior of Star X (Fig. 3) which has a minimum (negative) color at $\phi = 0.5$ as discussed earlier. To improve the phase coverage and statistical significance the (normalized) [11 μ] - [8.4 μ] colors of all the M stars were averaged

vs. phase. The result confirmed this impression, i.e. the average [11 μ] - [8.4 μ] color was constant ± ~ 0.05 mag = ± 5% from ϕ = 0.0 to 1.0. This seems to imply that there is a tendency for more dust to be present (i.e., larger α) near the visual and temperature minimum of these stars. A 0.2 mag increase in this color at minimum relative to Star X corresponds to an increase in α by a factor ~ 1.5-1.8, which is a significant amount. It is believed the principal assumptions of Star X which would affect this result are (1) a smooth, or at least constant with phase, continuum of the star λλ 8-13 μ. This assumption draws support from the agreement of at least some star excesses with the Trapezium flux (Chapter V) derived using this assumption. (2) Dust grains are equally efficient at absorbing the stellar radiation as the star temperature changes. This requires the absorption efficiency (Appendix A, B) $Q_{abs}(\lambda)$ of the grains to be approximately constant for λ ~ 1.7-1.25 μ. Unfortunately, optical constants for realistic silicate materials aren't available in this region. If $Q_{abs}(\lambda) \downarrow \lambda$, as for graphite, the expected minimum in [11 μ] - [8.4 μ] would be even more pronounced. (3) Effect of H_2O on total stellar luminosity. Woolf et al. (1964) noted that ~ 25% of the stellar flux was absorbed compared to the blackbody assumption adopted here. If this fraction varied with phase, it could affect the apparent "amount of dust." Again, if (bolometric H_2O absorption) $\downarrow T_*$, as found by Frogel (1971) for the 2.1 μ H_2O absorption, the expected minimum would be even more pronounced. In summary it appears that the M Mira light curves imply more dust is present (i.e., larger α) at minimum than

maximum; this question should be investigated further to see if this can be definitely established.

(a) oCet

The photometric and polarization data in the U band for oCet is shown in Fig. 4. Mira (the "Wonderful") is the prototype of its variable class, discovered to be variable in modern times by David Fabricius, August 13, 1596. Infrared observations for all the stars in this study were made during the ~ one week per month observing runs. When possible, more than one measurement was made during the week to check for possible systematic errors (or sudden variations). The points plotted are the averages of these measurements, plotted at the average phase (day) for the week.

The light curve of oCet seems to be adequately described by Star X, plus possible varying amounts of H_2O absorption in the 3.5 μ band. It appears that the [11 μ] - [8.4 μ] light curve is flatter than for Star X, which may imply more dust at minimum as discussed earlier. There are no large increases in this color or the [11 μ] - [3.5 μ] color as due, for instance, to the sudden production of new dust during the observing period. There does seem to be a significant change in the [11 μ] - [8.4 μ] color from the early spectrum by Gillett et al. (1968) taken 17 October 1967 when $\phi(-4)$ = 0.96 which is indicated as a solid diamond on the light curve. It is estimated that this color change would indicate an increase in α by a factor ~ 1.8-2.3 over the present epoch. The

Fig. 4: Polarization and photometric data on oCet. The convention used for denoting different cycles and a description of the plotted data is given in the text.

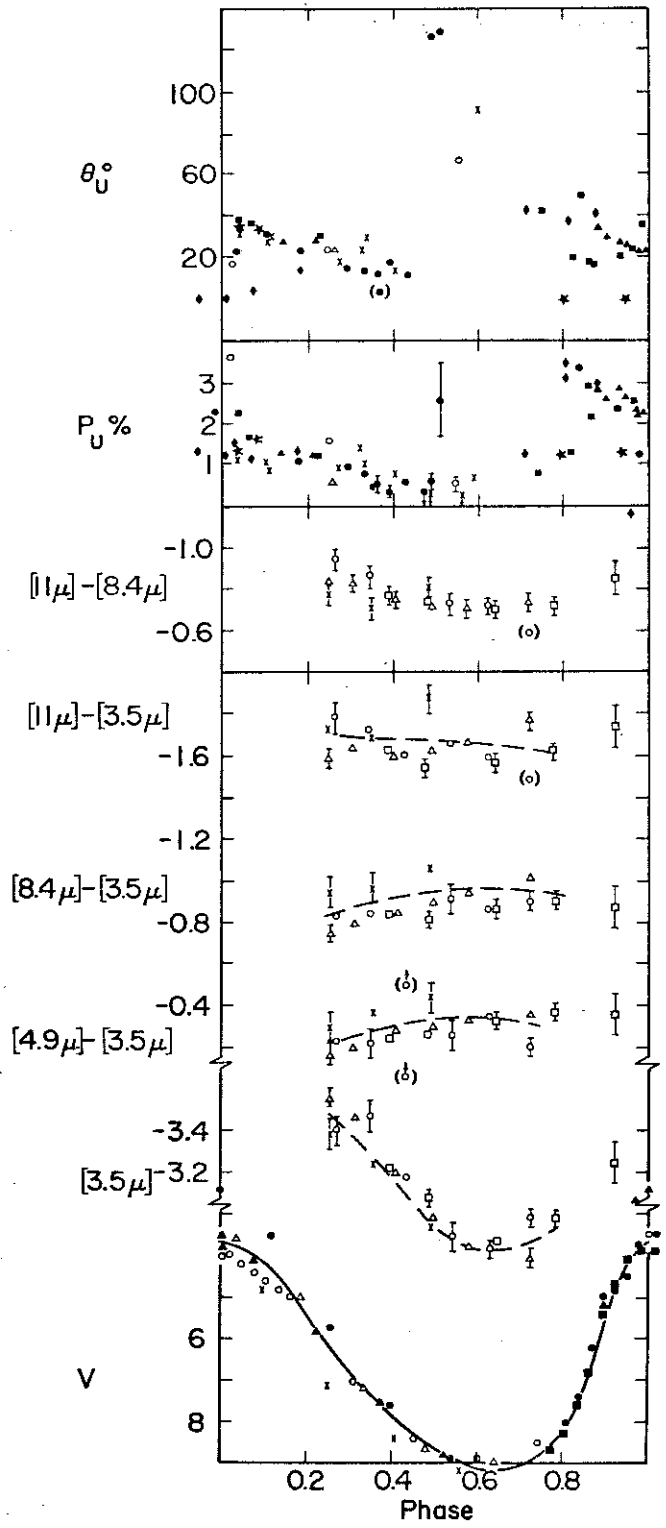

change is also evident in the narrow band spectra discussed in Chapter V. Thus, a secular decrease on a timescale ~ 4 years in the amount of dust by $\sim$ a factor of 2 seems to have occurred for oCet. During the current observation period, $\sim$ late 1971 - early 1974, no further changes in the broad band colors and only small changes in the narrow band spectra (Chapter V) are evident.

The U band polarization data show the large and sometimes rapid variation in both degree and position angle mentioned earlier. Shawl (1971, 1972) has discussed the polarization extensively and points out that there is a sudden increase in polarization near $\phi \sim 0.8$-0.9, i.e. when the visual light is rapidly increasing. The data plotted show this trend (at least for cycles N = -5 to -2) but also that polarization can be high at other phases ($P_U = 3.6\%$, $\phi(1) = 0.03$, P_U goes from $\sim 0.5\%$ to 2.6% for $\phi(-1) \sim 0.49$ to 0.51, i.e. in ~ 10 days). Unfortunately most of the polarization coverage is in the past and there is little coverage of phases 0.5 to 0.8. The available infrared data in the 0.8-0.9 phase region (only cycle 3) indicate no large increase in the [11 μ] - [3.5 μ] or [11 μ] - [8.4 μ] colors as would be expected for the injection of a large amount of new dust. The angle of polarization usually seems to wobble around between $\theta_U \sim 0°$-$40°$, there being no large angle changes associated with the polarization changes at $\phi \sim 0.8$-0.9. During the -1 cycle, however, the angle went from $\theta_U \sim 10°$ to $\sim 130°$ from $\phi(-1) \sim 0.43$ to 0.49, i.e. a change in angle of at least 60° in only 20 days, and decayed back to $\theta_U \sim 50°$ by $\phi(-1) = 0.84$, i.e. another $\Delta\theta$ of at least 80°. The other measurements between phases 0.5 and 0.6 also gave angles ($\sim 70°$ and $\sim 90°$) larger than at other phases.

The simultaneous infrared and polarization data during the 0-2 cycles indicates (1) changes in polarization by factors of 2 or 2 vs. phase during a given cycle and (2) similar changes in polarization at phase ~ 0.25 vs. cycle number, all with no large changes in or noticeable correlation with the [11 μ] - [3.5 μ] or [11 μ] - [8.4 μ] infrared colors. Thus the changes in the amount of dust during the polarization changes must be at most small.

(b) U Ori

The visual, infrared, and polarization data for U Ori is given in Figure 5. U Ori is a 1.35 cm H_2O maser and 18 cm OH "main line" maser source (Schwartz and Barrett 1970a; Wilson and Barrett 1970). The infrared light curve is again described fairly well by Star X. The larger [11 μ] - [3.5 μ], [8.4 μ] - [3.5 μ], and [4.9 μ] - [3.5 μ] colors during the first (0's) cycle could be due to depression in the 3.5 μ band as would be caused by an increase in H_2O absorption. The [11 μ] - [8.4 μ] color again shows a tendency to be constant with phase, averaging around -0.75 to -0.80. The polarization data is meager and no large "events" occurred during the infrared monitor period. There was an ~ 80-$90°$ θ flip in B and U on a short timescale near $\phi(-1) \sim 0.45$ and a subsequent decay through $\sim 80°$ in θ_V during the next cycle [$\phi(0) \sim 0.35$-0.53].

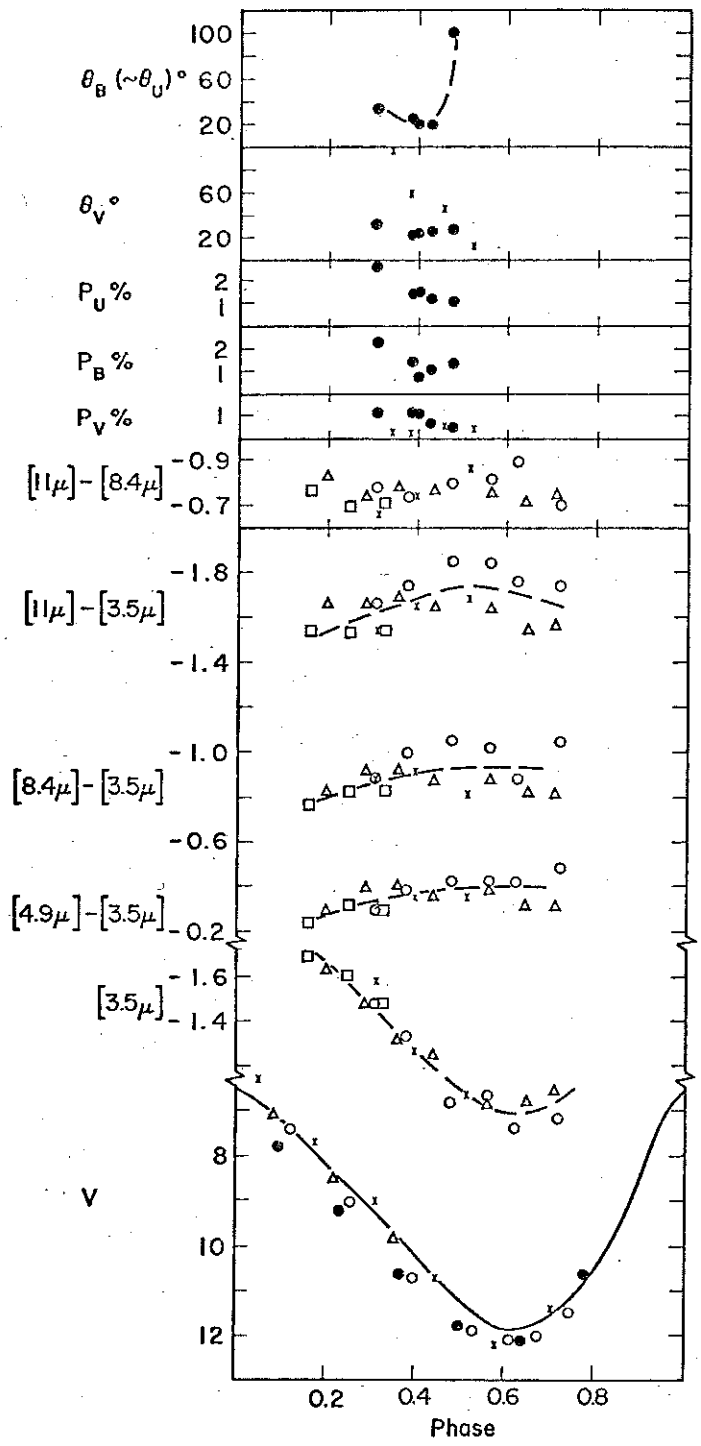

Fig. 5: Polarization and photometric data on U Ori.

(c) R Leo

The photometric and polarimetric data for R Leo are shown in Fig. 6. The spectrum of the excess in R Leo seems different than that of the Trapezium (see Chapter V) but probably still represents circumstellar emission from silicate-type grains.

The 3.5 μ light curve peaks at ~ 0.1-0.2 phase as for the other Mira variables. The [4.9 μ] - [3.5 μ] light curve is adequately described by Star X but the [8.4 μ] - [3.5 μ] color is more nearly like the star alone (~ - 0.6 to - 0.8) than the star plus Trapezium - like excess of Star X. This supports the finding in Chapter V that the spectral excess for R Leo has relatively less flux λλ 8-9 μ than the Trapezium. The [11 μ] - [8.4 μ] color seems approximately constant with phase here (~ -0.75) rather than following Star X. Coverage near $\phi \sim 0.8$ shows no sudden increase at this phase.

There is quite good polarization coverage of this star. In particular there is a polarization "event" which occurred during the infrared monitoring of the zeroth (X's) cycle. The polarization at B and V started at a low value ($P_V \sim 1.1\%$, $P_B \sim 1.8\%$) at $\phi(0) \sim 0.68$ reached a maximum ($P_V \sim 2.4\%$, $P_B \sim 3.7\%$) at $\phi(0) \sim 0.78$ and then decayed back to the original values by $\phi(0) \sim 0.9$. On the next cycle, the polarization reached even lower values ($P_V \sim 0.3\%$, $P_B \sim 0.7\%$) at $\phi(1) = 0.9$. During this time the [11 μ] - [8.4 μ] and [11 μ] - [3.5 μ] colors were approximately constant -- if anything the [11 μ] - [8.4 μ] color was actually higher at $\phi(1) \sim 0.9$. Again, the infrared is not correlated with the polarization changes.

Fig. 6: Polarization and photometric data on R Leo.

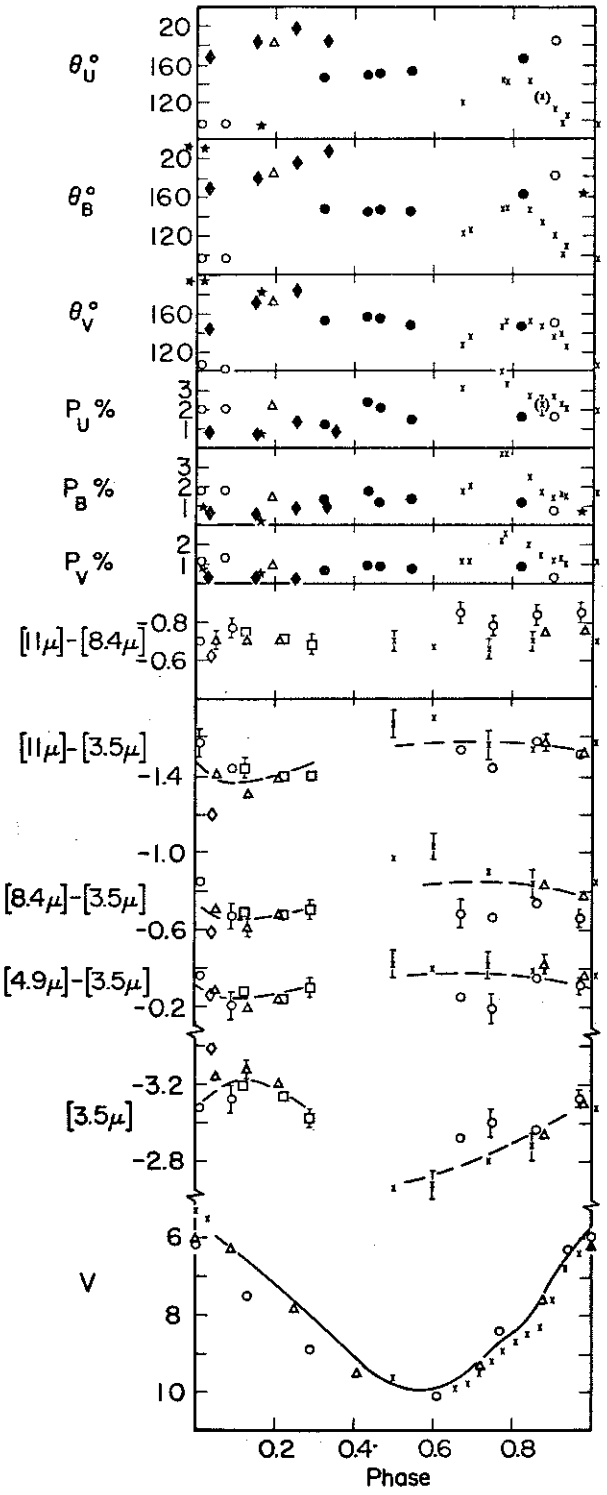

Neither can the polarization event be explained by a sudden blockage of the direct, unpolarized starlight by a fortuitously placed cloud of dust grains which moved, or was formed, on our line of sight to the star (as discussed in Chapter VII). On this model, an increase by a factor of two in polarization requires a reduction of the unpolarized light by the same amount ($\sim$ 1 mag decrease) and this is not seen in the visual light curve. Rather the increase in polarization would seem to require an actual increase (and subsequent decrease) in the polarized intensity on these short, $\lesssim$ 30 days, timescales. Since the infrared measurements indicate no large change in the "amount of dust" as measured by α, it would seem to require either (1) rapid changes in the polarizing efficiency of the existing envelope, either through changes in geometry, or grain alignment (see Chapter VII), (2) injection of a small amount of new dust grains which are very efficient polarizers, (3) injection of new dust grains with low absorptivity, so they don't contribute to the observed infrared or (4) a mechanism other than scattering and absorption by circumstellar grains to explain the polarization.

The position angle of polarization also shows interesting variations. Sometimes the angle is $\theta \sim 80$-$100°$, sometimes $\theta \sim 0$-$20°$, and sometimes $\theta \sim 140°$-$160°$, i.e. halfway between. During the event discussed above $\theta_{U,B}$ started at $\sim 145°$ at polarization maximum ($\phi(0) \sim 0.78$), decayed to $\sim 100°$ by $\phi(0) \sim 0.92$, i.e. $\Delta\theta \sim 45°$ in $\sim$ 45 days. By the end of the next cycle [$\phi(1) \sim 0.9$] $\theta_{B,V} \sim 4°$, i.e. approximate polarization reversal ($\Delta\theta = 90°$). Another $\sim 90°$ θ change occurred in the U band at $\phi \sim 0.15$ between the -5 (★'s) and -4 (♦'s) cycles.

(d) R Hya

The light curve and polarization data on R Hya appears in Fig. 7. The [4.9 μ] - [3.5 μ] color (~ 0.0 to -0.1) is less than for Star X, even leaving out water. This corresponds to a color temperature ~ 5000-10,000 °K which is much too high for the spectral type (M6e-M8e) so it must be due to either excess emission in the 3.5 μ band or absorption in the 4.9 μ band. The latter is more likely and could be due to the $\Delta v = 1$ fundamental vibration-rotation system of CO as suggested by Solomon and Stein (1966). The [8.4 μ] - [3.5 μ] color (~ -0.5 to -0.6) is again lower than for Star X and corresponds to a color temperature of ~ 2200-2500 °K. This may indicate a spectral excess more like R Leo than oCet (Chapter V); Hackwell's (1971, 1972) spectrum in the 8-13 μ region supports this. The [11 μ] - [8.4 μ] color is fit somewhat better by color = constant than by Star X.

The polarization again shows variation in both position angle and amount. The polarization seems to peak at $\phi \sim 0.5$, i.e. minimum light, rather than ~ 0.85 as for oCet. The "preferred" position angle seems to be $\theta \sim 120°$ but there are excursions down to ~ 60° and up to ~ 180°, somewhat like R Leo. The quasi periodic variation in position angle, with a period twice the visual period, has been discussed by Serkowski (1970).

A polarization "event" occurred during the infrared monitoring in the zeroth (X's) cycle. The polarization started at $P_{V,B,U} \sim 0.2\%, 0.3\%, 0.5\%$ at $\phi(0) \sim 0.3$ and shot up to $P_{V,B,U} \sim$

Fig. 7: Polarization and photometric data on R Hya.

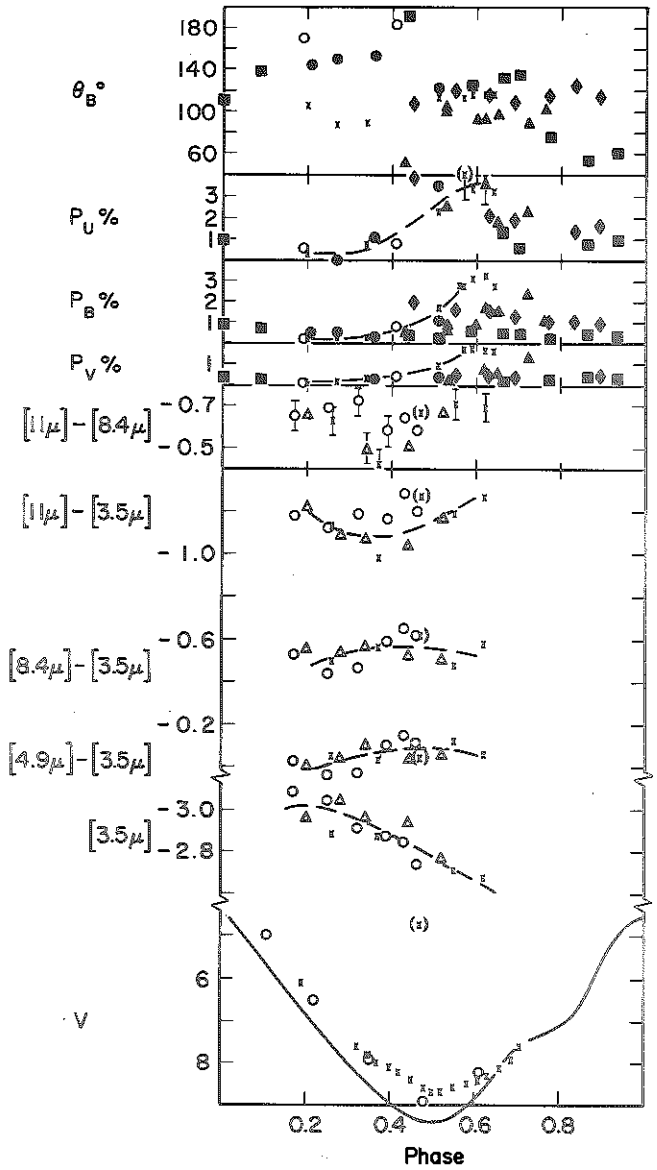

1.7%, 3%, 4% by $\phi(0) = 0.6$. By the next cycle [$\phi(1) \sim 0.2$] the polarization had returned to small values again, though θ_B was $\sim 80°$ different than θ_B at $\phi(0) \sim 0.3$. During this time the [11 μ] - [8.4 μ] color was approximately constant at ~ -0.68 except for one low measurement at $\phi(0) = 0.37$. In particular, there was no sudden increase in this color during the ~ 40 days from $\phi(0) \sim 0.5$ to 0.6 when the polarization was increasing by approximately a factor of 2. As in the case of the polarization event in R Leo described earlier, the absence of significant infrared change or a sudden decrease in visual light here puts severe constraints on models which explain the polarization in terms of scattering and absorption by circumstellar grains.

(e) S CrB

The polarization, infrared, and visual data for S SrB are presented in Fig. 8. S CrB is a 1.35 cm H_2O maser and 18 cm OH "main-line" maser source (Wilson and Barrett 1970; Schwartz and Barrett 1970a). The infrared excess for this star (and R Cas following) is the largest of the M and S Miras in Table 1 and larger than Star X. In addition, the [4.9 μ] - [3.5 μ] and especially the [8.4 μ] - [3.5 μ] colors are larger than expected for the star temperature and the amount of Trapezium-like "silicate" excess indicated by the [11 μ] - [8.4 μ] color. Part of the color may be due to increased H_2O absorption in the 3.5 μ band but the large [8.4 μ] - [3.5 μ] color may also indicate a smooth "black body" component to the excess in addition to the Trapezium-like excess

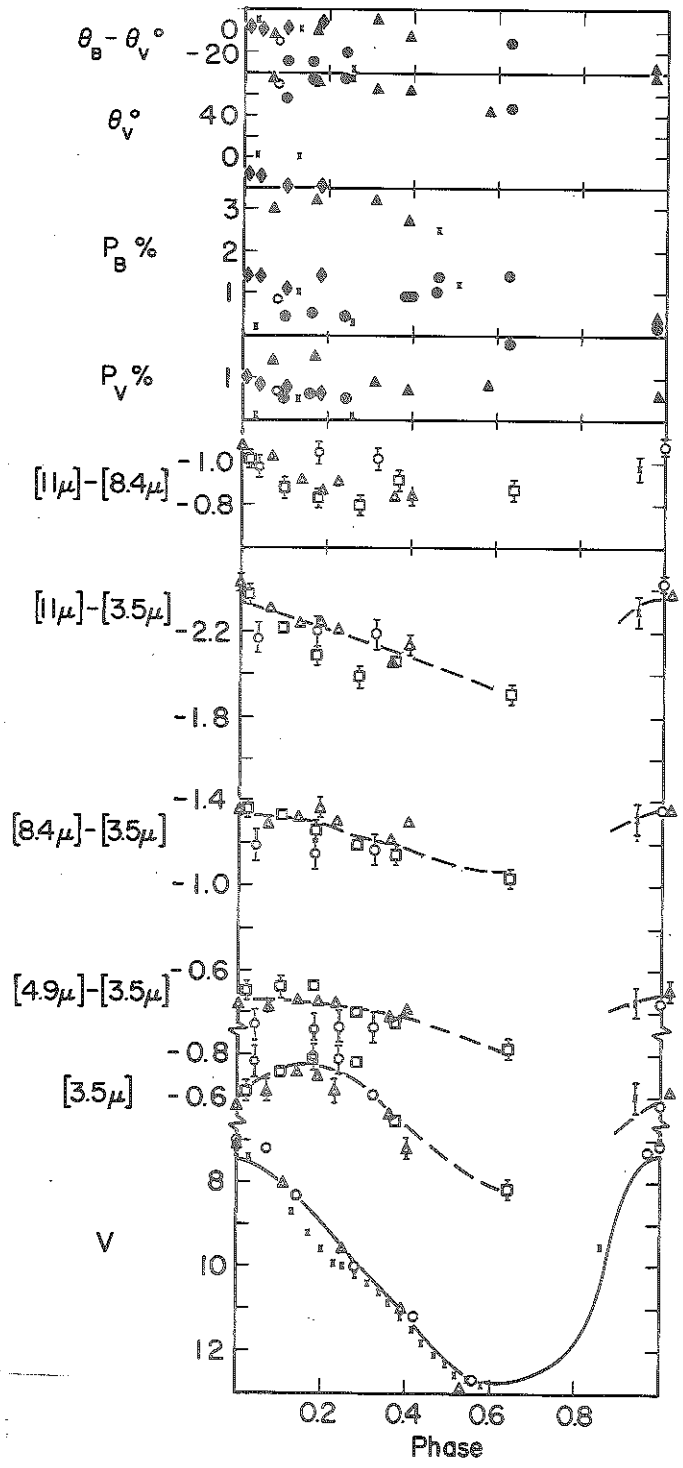

Fig. 8: Polarization and photometric data on S CrB.

indicated by its infrared fluxes (Tables 1, 2a). Another possible indication of an extra component in the 8.4 μ band is the tendency for the [8.4 μ] - [3.5 μ] to reach a minimum at $\phi \sim 0.5$, contrary to Star X with or without H_2O absorption. This is an intriguing possibility but better spectral coverage and resolution (to establish the stellar "continuum" at shorter wavelengths and the shape of the resulting excess) or spatial resolution (to separate the fluxes from the star and circumstellar shell at $\lambda \sim 8$ μ) would be needed to definitely establish it.

The behavior of the [11 μ] - [8.4 μ] color vs. phase seems to follow the "Star X" curve, indicating an approximately constant amount of dust, rather than the approximately constant color of other stars, though the scatter is large. There is an indication of larger amoungs of dust than average on cycle 1 (0's) and smaller than average on cycle 3 (□'s) during $\phi \sim 0.1$-0.3.

The polarization shows the typical Mira star chaos. Polarization can apparently be high anywhere between $\phi \sim 0.0$ and 0.6. There seems to be a "preferred angle" of polarization $\theta \sim 60$-80° but during the -1 and zeroth cycles θ_V went from ~ 70° down to ~ 0° and back up to ~ 70°, the latter transition taking place in $\Delta\phi \sim 0.11 \sim 40$ days. In addition at $\phi(-4) = 0.1$, $\theta_V \sim 150°$ which is ~ 80° the other way from the "preferred angle." Again we see the large and sometimes rapid position angle fluctuations, of the order 90°, which Mira variables can exhibit (though in this case when the polarization is very high the position angle is at the "preferred" angle). The polarization "event" in P_B at $\phi(0) \sim 0.46$ would, as

for R Leo and R Hya, seem to represent an actual increase in the polarized flux since there isn't any corresponding depression in visual light at this time.

(f) R Cas

The photometric data for R Cas is given in Fig. 9; no polarization measurements could be located but this star was included because of the fairly good phase coverage, the large excess, and the extensive series of λλ 8-13 μ spectra (Chapter V) which have been obtained. R Cas is an 18 cm OH "main line" maser source (Nguyen-Quang-Rieu et al. 1971). The [3.5 μ] light curve shows the characteristic peaking at $\phi \sim 0.1$-0.2. The [4.9 μ] - [3.5 μ], [8.4 μ] - [3.5 μ], and [11 μ] - [3.5 μ] color curves are fairly well explained by Star X (with a little more Trapezium excess) affected by varying amounts of absorption in the 3.5 μ band. In particular there is no extra emission in the 8.4 μ band evident. The [11 μ] - [8.4 μ] color curve seems to be fit slightly better by color ~ -0.9, constant than by Star X (α constant); this is also seen in the series of spectra (Chapter V) taken at different phases. There is no evidence for any large changes (> 0.2 mag) in this color over the monitoring period.

(g) Other M-Type Miras

Light curves of the remaining M-Miras (R Cnc, R LMi, and U Her) are not presented but they continue the trends found above.

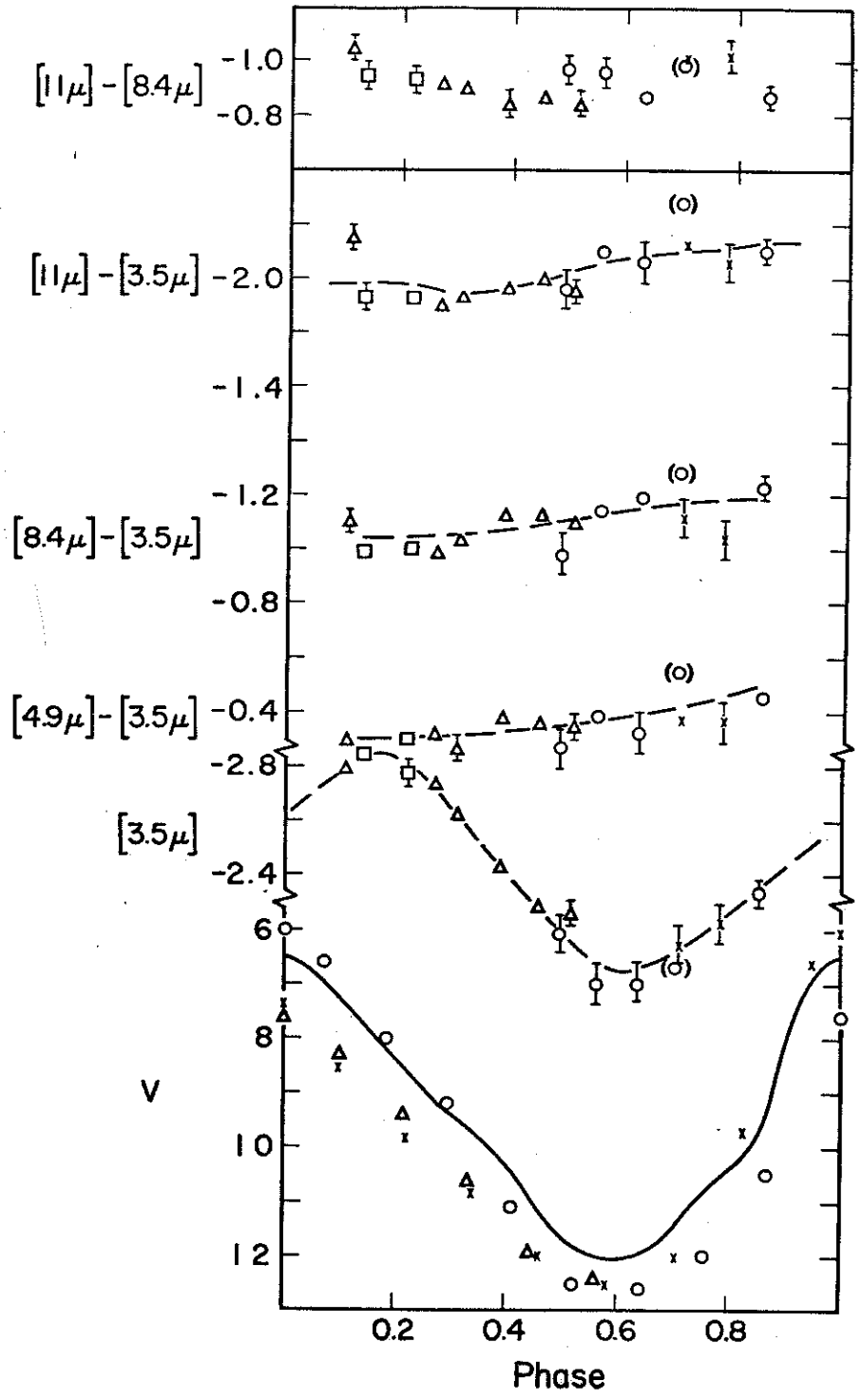

Fig. 9: Photometric data on R Cas.

R Cnc has the smallest infrared excess of all the M stars studied here, with [11 μ] - [8.4 μ] ≃ -0.5 approximately constant $\phi \sim 0.8$ to 1.3. There is no evidence for any large increase in this color after $\phi \sim 0.8$. From the beginning to the end of the zeroth cycle, the position angle θ_V went from ~ 0° to ~ 90° while the amount of polarization didn't change ($P_V \sim 0.5\%$).

R LMi is a (weak) 18 cm OH "main line" maser source (Fillit et al. 1972). The phase coverage is $\phi \sim 0.78$ to 1.32 and the infrared color curves are fairly well represented by Star X. Again, the tendency is for the [11 μ] - [8.4 μ] color to be approximately constant at ~ -0.75 and there are no large excursions from this during the observing period or near phase ~ 0.8 to 0.9. No polarization measurements could be found.

U Her is an 18 cm OH "main line" maser and 1.35 cm H_2O maser source (Schwartz and Barrett 1970a; Wilson and Barrett 1970). The infrared coverage is $\phi \sim 0.17$ to 0.55 and the polarization coverage (in the past) is from $\phi \sim 0.6$ to 1.05, i.e. orthogonal coverage. The infrared color curves are explained fairly well by Star X. The tendency for the [11 μ] - [8.4 μ] color to remain constant (at ~ -0.8) occurs, but there is an indication that the color is even larger (~ -0.9) near minimum, i.e. opposite to Star X and indicative of more dust (larger α) near minimum. The polarization can be high anywhere from $\phi \sim 0.6$ to 1.0. The "preferred angle" is $\theta \sim 70°$ but there are occasional excursions up to $\theta \sim 130°$ and down to $\theta \sim 0°$. During the -2 cycle from $\phi(-2) = 0.81$ to 0.88 (i.e. ~ 30 days) P_B went from 1.5% to 3.0% while θ_B went from +70° to -10°, i.e. an 80° θ-flip.

ii) Semiregular M Stars

Compared with the Mira variables, the semiregular variables are nearly constant, $\Delta V \lesssim 1$ mag, $\Delta[3.5\ \mu] \lesssim 0.3$ mag. The stellar temperatures are, therefore, very nearly constant and we may inspect the colors directly (without resort to Star X) to look for possible changes in luminosity, stellar opacity (absorptions), and/or in the "amount of dust." The spectral excesses of the semi-regular variables (Chapter V) seem very similar to the Trapezium so the [11 μ] - [3.5 μ] and [11 μ] - [8.4 μ] colors should be a direct measure of the "amount of dust," at least in the silicate component.

(a) V CVn

The infrared, visual, and polarization light curves for V CVn are given in Fig. 10. The variation in V (~ 1 mag) apparent in the earlier (JD ~ 2,440,200) data had damped down by the time (JD ~ 2,441,000) the infrared monitoring began. Consequently, there is no well defined "phase" and the data is plotted vs. time (JD). It is seen that the infrared magnitudes and colors can all be fairly well represented by everything constant. The dotted lines in Fig. 10 are the average of all the measurements JD 2,440,980-2,441,845. The standard deviations of the measurements from the mean (Table 1) are only slightly larger than those expected due to systematic errors alone (Chapter II) so the true variation during this time must be at most the order of ± 5%-7% in the infrared magnitudes and colors. A change in the [11 μ] - [8.4 μ] color of ~ 0.1 mag would

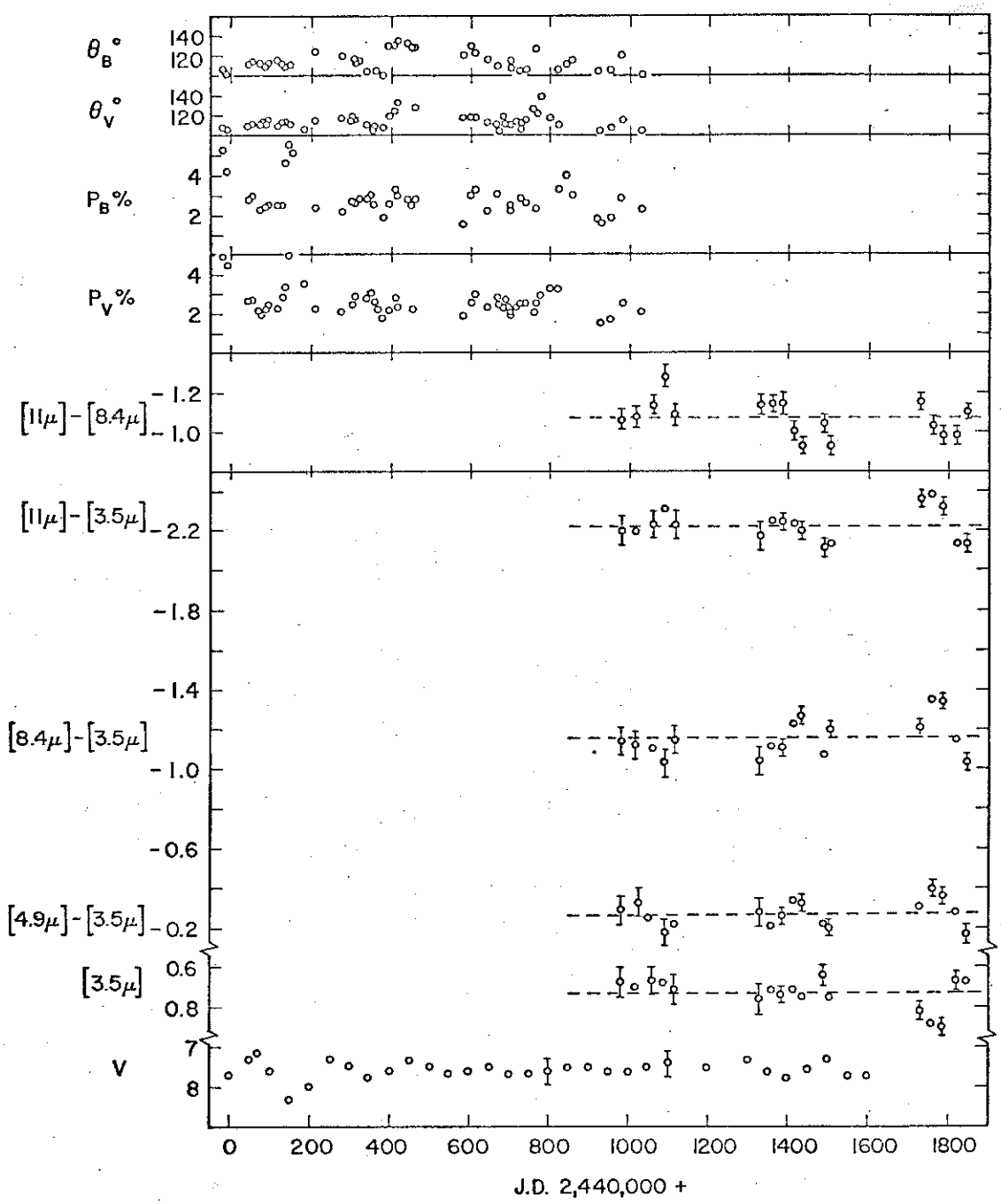

Fig. 10: Polarization and photometric data on V CVn.

correspond to a change by a factor of ~ 1.25 in α and a change in the [11 μ] - [3.5 μ] color of 0.1 mag would correspond to a change in α of a factor of ~ 1.12. Inspection of the light curves shows that the changes in α ($\sim$ "amount of dust" Appendix A) are at most $\sim$ 10%-20% during the monitoring period. In addition, the colors found here agree with the earlier measurements of Gillett et al. (1971).

The energy distribution (Tables 1, 2a) indicate an ~ 0.2 mag excess in the 8.4 μ band in addition to the excess expected for a Trapezium-like excess with the observed [11 μ] - [8.4 μ] ~ -1.07 color. As for S CrB this may indicate a second, "blackbody" like component to the excess emission, but more observations would be needed to establish this. Interestingly, Shawl (1972) in fitting the observed polarization with circumstellar grain scattering models found it impossible to fit V CVn with small silicate grains, because of the relatively flat wavelength dependence of the amount of polarization, but he could get fits using iron or graphite grains. These grains could give a blackbody type excess.

The large variations in polarization for V CVn have been discussed by Kruszewski et al. (1968), Dombrovskii (1970), and Shawl (1971, 1972). Unfortunately, almost no polarization data simultaneous with the present infrared data could be found. Shawl (1972) notes some similarities of the polarization of V CVn with the extreme infrared star VY CMa, i.e. a polarization minimum at 1.65 μ rising to 2.2 μ and an $\sim 90°$ θ change from ~ 1 μ to 2.2 μ.

(b) RW Cyg

The infrared and visual light curves of RW Cyg are presented in Fig. 11. No polarization measurements could be found but this star was included because it has the largest [11 μ] - [8.4 μ] and [11 μ] - [3.5 μ] colors and largest α ($\sim$ 5%) of the M stars studied here. The energy distribution is given in Fig. 2 and the 8-13 μ spectrum is discussed in Chapter V. No large variations are evident in the AAVSO visual (V) estimates and, as for V CVn, the infrared light curves appear to be constant. A 0.1 mag change in the [11 μ] - [3.5 μ] color corresponds approximately to a 10% change in α here so that over the 1080 days of monitoring this star, the "amount of dust," as reflected by α, has changed at most $\sim \pm$ 10-15%. In addition the colors here are in agreement with the earlier measurements of Gillett et al. (1971). Thus, even in the absence of temperature and luminosity variations (V, [3.5 μ] $\sim$ constant) this star has managed to maintain a large and stable dust shell.

(c) Other SR M Stars

The remaining SR variable M stars continue the trends noted above (i.e. nearly constant) and are not plotted. W Per has an excess approximately as large as RW Cyg. There are small variations in V ($\sim$ 1 mag) and [3.5 μ] ($\sim$ 0.2-0.3 mag) during the monitoring period (JD +825 to +1675). The "amount of dust" as indicated by [11 μ] - [3.5 μ] and [11 μ] - [8.4 μ] colors, has changed $\lesssim$ 10-20% during this period. Polarization measurements on JD +910 and 955

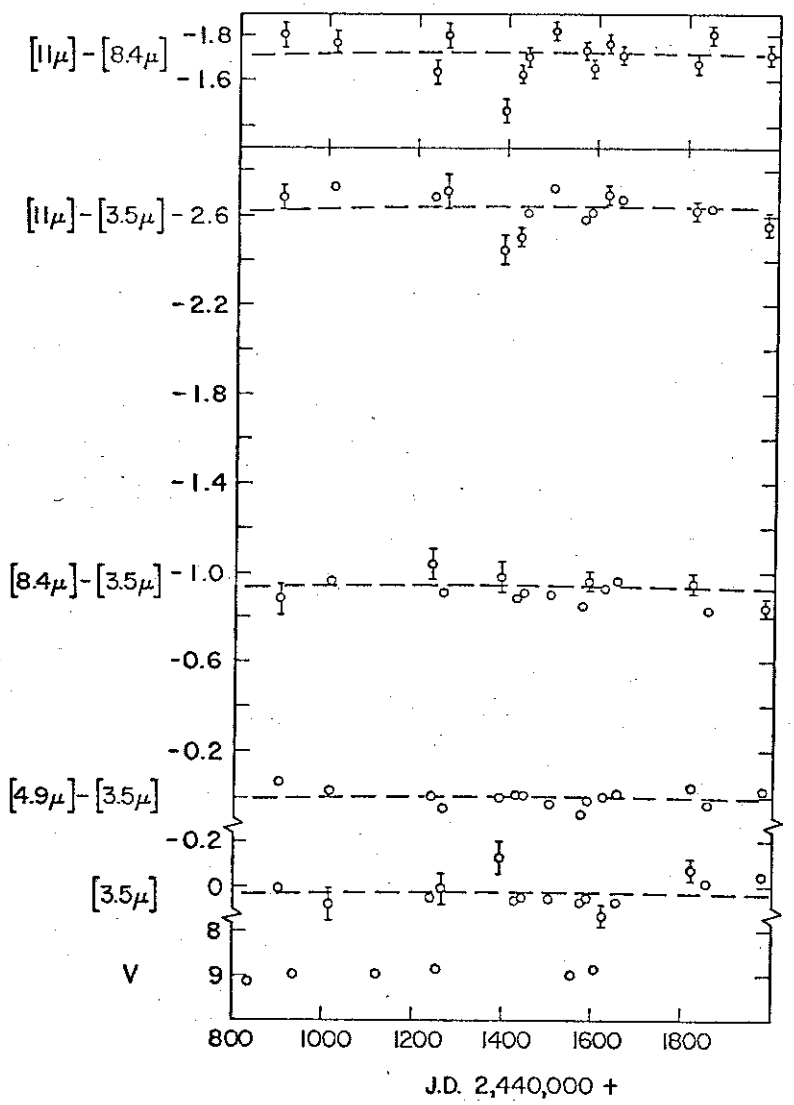

Fig. 11: Photometric data on RW Cyg.

give $P_B \sim P_V \sim 3.7\%$ which is high but its position near the galactic plane ($b_{II} = -2°$) make this inconclusive regarding intrinsic polarization. TV Gem is like W Per but with a smaller excess (small variations in V and [3.5 μ], $\Delta\alpha/\alpha \lesssim 10\text{-}20\%$). Likewise X Her and Z Eri, though there may be a small secular decrease in α of $\sim 20\text{-}40\%$ from JD +900 to +2000 for Z Eri. Z Eri has a smaller [8.4 μ] - [3.5 μ] color and a larger [12.5 μ] - [11.2 μ] color (Table 2a) than would be expected from the amount of excess observed at [11.2 μ], similar to R Leo, but higher resolution spectra would be needed to determine the source of these anomalies.

iii) S-Type Miras

(a) χ Cyg

The infrared, visual, and polarization data for χ Cyg is given in Fig. 12. The energy distribution (Tables 1, 2a, b), spectral excess (Chapter V) and temperature and luminosity variations (Strecker 1973) for at least some S Miras are similar to the M Miras so a comparison with Star X (Fig. 3) regarding possible changes in the amount of dust is valid. Spinrad et al. (1966) and Frogel (1971) find that S and MS type Miras (including χ Cyg) have less H_2O absorption relative to the pure M-types so the appropriate curves would be those without the inclusion of water (X's). The [3.5 μ] flux peaks at $\phi \sim 0.2$, similar to the other Mira variables in this study. The apparent hump or flat area on the rising branch of the [3.5 μ] light curve between $\phi \sim 0.7$ and $\phi \sim 0.85$ was

Fig. 12: Polarization and photometric data on χ Cyg.

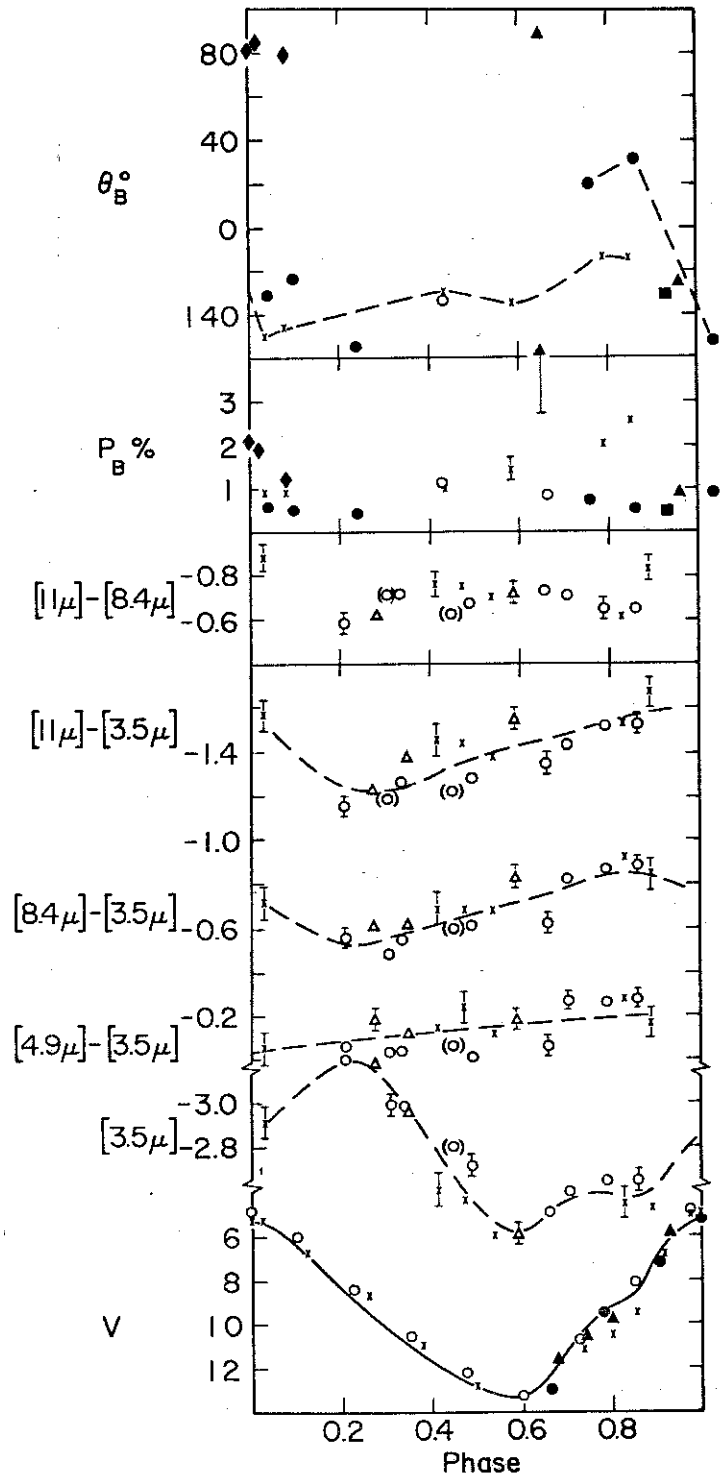

discovered by Strecker (1973) with much better phase coverage and is undoubtedly real. It corresponds to a less pronounced hump in the visual light curve.

The [4.9 μ] - [3.5 μ] color is less negative than expected for Star X and also doesn't show the peak at $\phi \sim 0.5$ as expected -- this could be due to the effects of stellar opacity (absorption) in the broad band 4.9 μ filter -- the 2.3 μ CO $\Delta v = 2$ bands are known to be strong in χ Cyg (Frogel 1971) so the 4.6 μ $\Delta v = 1$ CO fundamental bands could be one source. The 0.2 to 0.4 mag variations in the [8.4 μ] - [3.5 μ] and [11 μ] - [3.5 μ] colors are probably real-minimum colors coming at $\phi \sim$ 0.2 and maximum color at $\phi \sim 0.85$. The [8.4 μ] - [3.5 μ] color is more like the -0.6 to -0.8 color expected for a star without silicate excess and could represent a deficiency in the $\lambda < 9$ μ spectrum of the excess similar to that observed in R Leo and T Cas (Chapter V). The variations in color could be due to a combination of the change in stellar temperature and opacity (absorption) in the 3.5 μ band. The approximate constancy of the [11 μ] - [8.4 μ] color with phase could indicate a relative increase in the "amount of dust" of approximately a factor 1.5-2 near minimum or could be due to changes in stellar opacity in the 8-13 μ region with phase.

The polarization data shows the large and sometimes rapid variations in both amount and position angle of polarization, which are typical of the Mira variables in this study. Of particular interest are the position angle changes during the -1(●) cycle. From $\phi(-1) \sim 0.24$ to $\phi(-1) \sim 0.76$ the position angle went from

$\theta_B \sim +125°$ to $\theta_B \sim 20°$, i.e. $\Delta\theta_B \sim +75°$. Then from $\phi(-1) \sim 0.86$ to $\phi(-1) \sim 1.03$ ($\sim$ 60 days) θ_B went from $\sim +30°$ back to $\sim 130°$, i.e. $\Delta\theta_B \sim -80°$. All the while during this cycle, the degree of polarization changed very little, $P_B \sim 0.5$-0.9%. The slow and steady increase in polarization and rotation of position angle during the zeroth (X) cycle were not accompanied by any large increase in the [11 μ] - [3.5 μ] or [11 μ] - [8.4 μ] colors, indicating the change in amount of dust was at most quite small ($\lesssim 50\%$) during this cycle.

(b) R Gem

The infrared, visual, and polarization data for R Gem are given in Fig. 13. R Gem is the only "pure" S star in this study. It is similar in spectral type (S3,9e) visual range ($\Delta V = 6.4$ mag) and in the [3.5 μ] light curve over the phase covered to the S star R Cyg studied by Strecker (1973). R Cyg had the largest [3.5 μ] ($\sim$ 1.2 mag) and bolometric ($\sim$ 1.4 mag) ranges of the stars studied by Strecker; the large variation in [3.5 μ] observed here for R Gem, $\sim$ 1 mag, is probably correct and would probably be even larger if observations at earlier phases were made. The [4.9 μ] - [3.5 μ] is approximately constant with phase and is probably consistent to the small changes expected due to changes in the stellar temperature.

R Gem is the faintest star in this study at infrared wavelengths so the errors in the 8.4 μ and 11 μ measurements are larger than for the other stars. The [8.4 μ] - [3.5 μ] color is approximately constant with phase at ~ -0.9 but the [11 μ] - [3.5 μ] color

Fig. 13: Polarization and photometric data on R Gem.

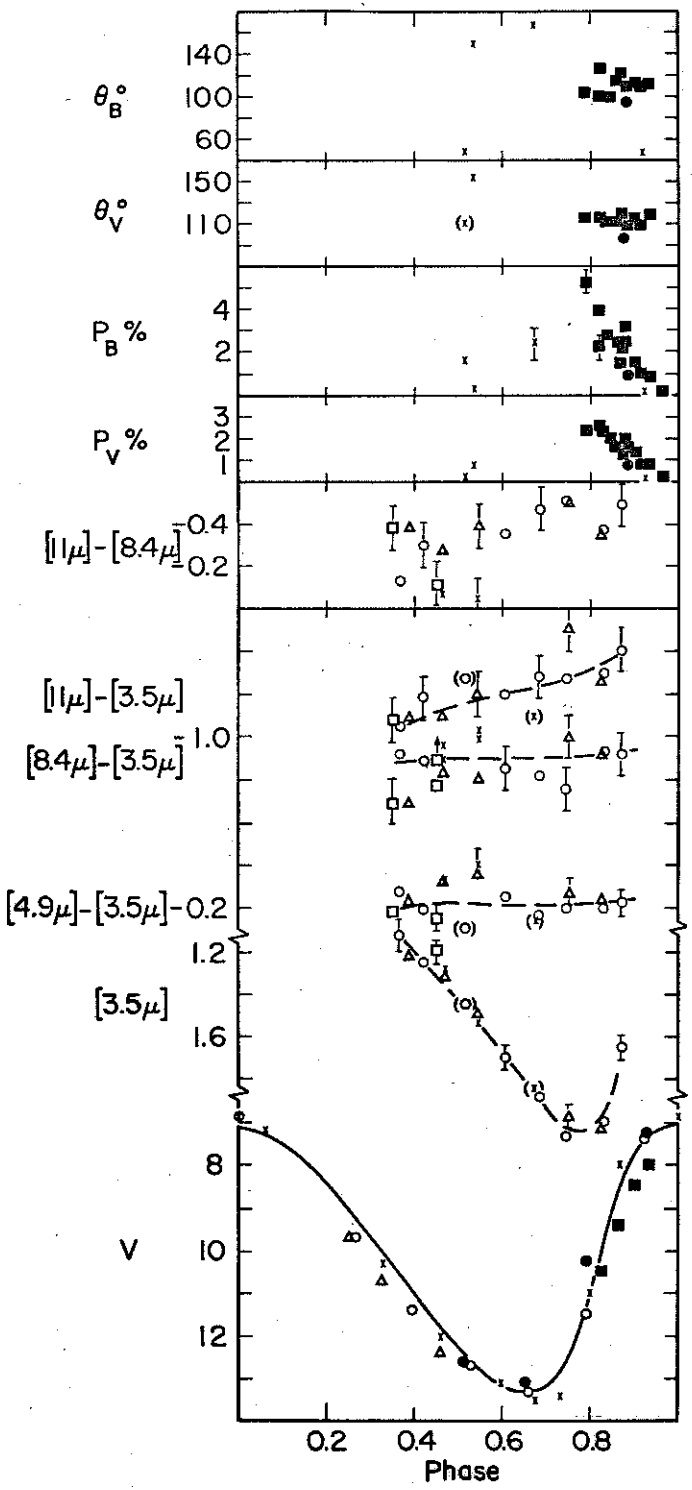

appears to increase from ~ -1.05 at ϕ = 0.35 to -1.4 at ϕ = 0.85. If a blackbody through the $\lambda < 8$ μ points (Table 2a) is adopted for the stellar continuum, then there is an approximately equal excess (~ 0.4 mag) in the [8.4 μ] and [11 μ] filters at $\phi \sim 0.35$ but a considerably larger excess (~ 0.75 mag) at [11 μ] at ϕ = 0.85. The origin of this apparent spectral variation of the excess is unknown at present; there appears to be a small amount of dust present at all phases but the spectrum changes. This could be due to variations in the stellar continuum or could be due to a varying ratio of "blackbody" grains as seen in the S star W Aql to "silicate" grains as seen in the S star R And (Chapter V). The [11 μ] - [8.4 μ] color, which is subject to larger statistical errors, doesn't show the apparent spectral variation with phase as clearly, but does seem at least to indicate an increase in the color from the zeroth cycle (~ -0.1 mag) and the earlier measurements of Gillett et al. (1971) (~ -0.18 mag) to the measurements in later cycles (~ -0.4 mag). This slower timescale variation could be understood in terms of production of more silicate grains with a relatively constant amount of blackbody grains present. More pure S stars should be monitored at these wavelengths to see if these possible phase and/or secular variations in spectral excess are widespread.

The polarization shows large and sometimes rapid changes in amount and position angle with time. During the -3 cycle (■) the polarization decayed from $P_B \sim 4$–5% at $\phi(-3) \sim 0.8$ to $P_B \sim 1\%$ by $\phi(-3) \sim 0.9$, i.e. a factor of 4 decrease over approximately 37

days; while the position angle was constant at $\theta_B \sim 110°$. During this time there was no corresponding increase of visual flux as would occur if the star were coming out from behind an obscuring cloud and contributing relatively more unpolarized direct starlight. These rapid decreases in polarization are quite difficult to understand on the assymetric shell model (Chapter VII) as they seem to require either (1) a rapid change in the initially aligned shell or (2) rapid dissipation through evaporation of dust grains. The polarization during the zeroth cycle (X) also showed interesting and rapid variations in polarization. P_B went from $\sim 0.9\%$, down to $\sim 0.3\%$ and up to $\sim 2.4\%$ in the space of ~ 0.15 cycle ~ 55 days and returned to $\sim 0.1\%$ by cycle's end. θ_B made a rapid transition from $\sim 50°$ to $\sim 150°$ and then returned to $\sim 50°$ by cycle's end. Unfortunately the infrared data during this time is rather meager but at least there doesn't seem to be any large increase in the [11 μ] - [3.5 μ] color which should accompany the injection of new dust.

D. Energy Distributions -- Carbon Stars

The infrared magnitudes taken at a particular time for the carbon stars in this study are given in Table 2a. Broad band energy distributions for selected carbon stars are plotted in Figs. 2, 14, and 15. The energy distributions of the semi-regular variables UU Aur and Y Tau are similar to the M-type stars in that they can be fit by a blackbody of typical stellar temperatures, $T_* \sim 2000\text{-}2500$ °K

Fig. 14: Energy distribution of the carbon stars V Hya, R Lep and Y Tau. The data is from Table 2a and the format is the same as Fig. 2.

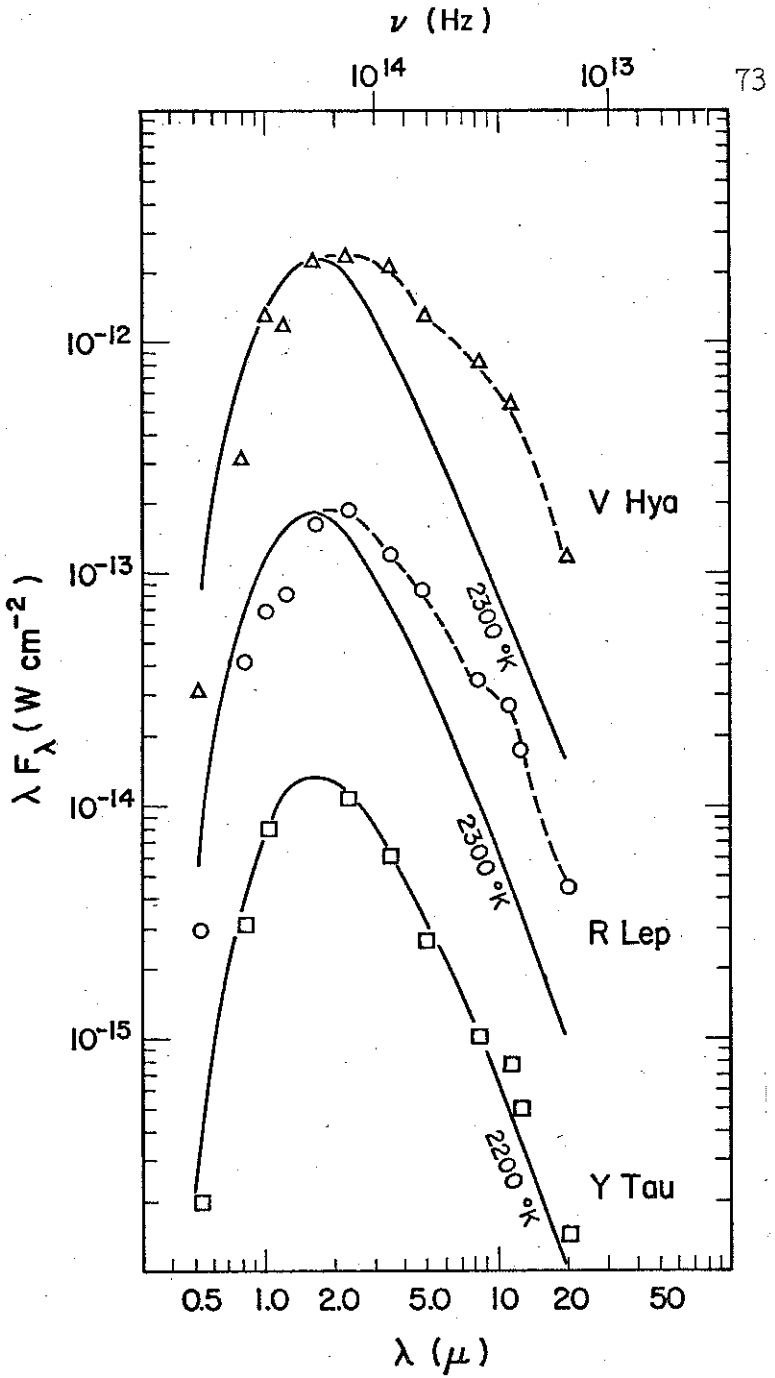

Fig. 15: Energy distribution of the carbon stars T Dra and V Cyg. The data is from Table 2a and the format is the same as Fig. 2.

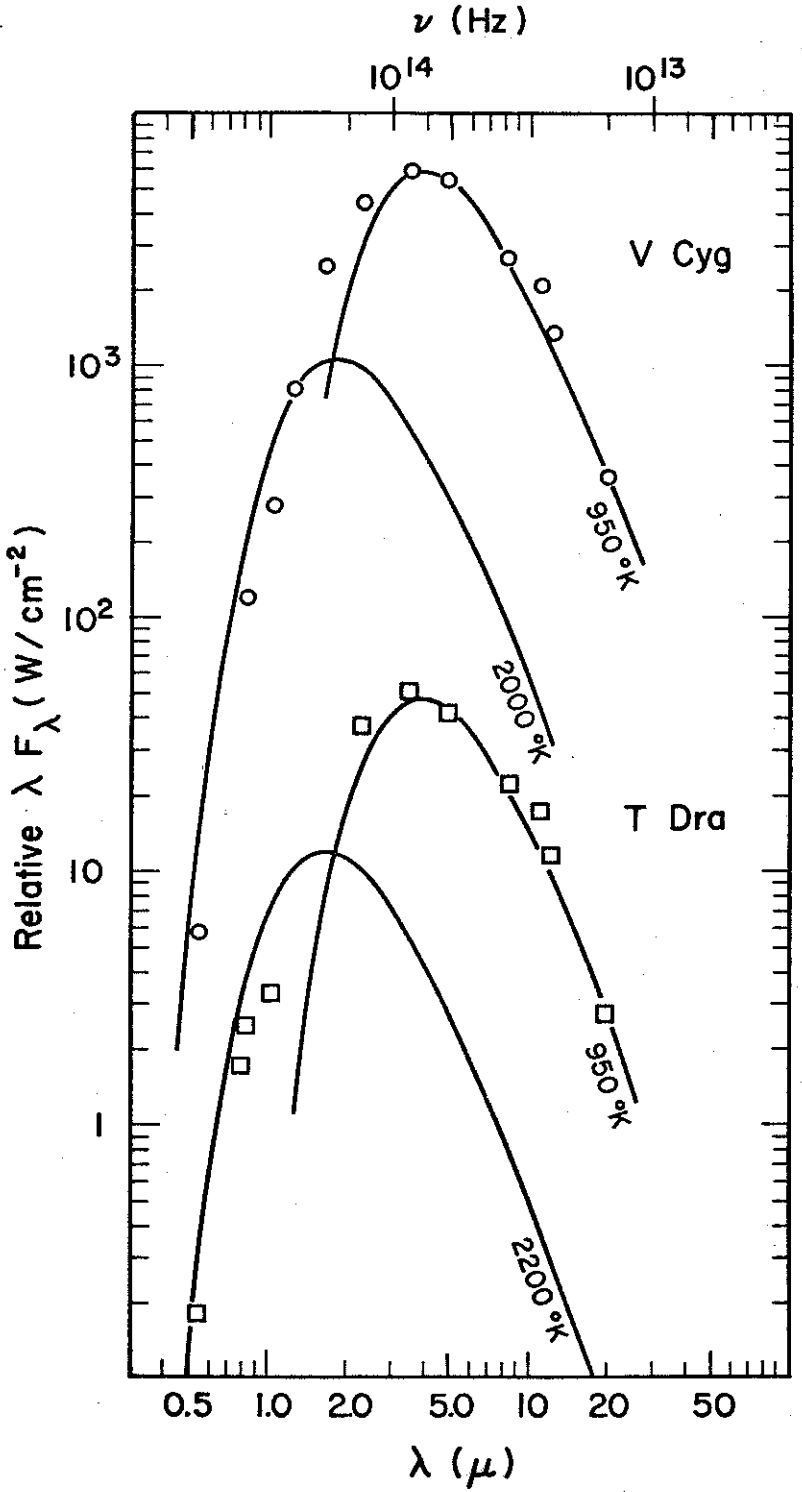

to which is added a small amount of "excess" at $\lambda > 8$ μ. The $\lambda\lambda$ 8-13 μ spectrum of the excess (see Chapter V) is different than the M stars and there is no large excess at 20 μ as for M stars. The apparent "amount of excess" as measured by α is very small ($\alpha \sim 0.2\%$ UU Aur, $\alpha \sim 0.44\%$ Y Tau) using this separation of "star" from "dust" in the observed flux. Deviations from the stellar blackbody are evident at $\lambda < 8$ μ due to the wavelength dependent stellar opacities, but the overall shape and level seems fairly well defined. The temperatures assigned here agree fairly well with temperatures assigned by other means. Fujita (1966) analyzes the relative strengths of atomic lines arising from different levels of the same atom and derives a temperature sequence vs. carbon subtype (Keenan-Morgan system). He finds $C_5 \sim M_3$; $T_* \simeq 2750$ °K to $C_8 \sim M_8$; $T_* \simeq 2350$ °K. Thus the carbon star sequence would be roughly comparable to the M_* sequence in terms of photospheric temperature. Empirical studies of the slope of the continuum (i.e. flux level between strong absorption features) indicate similar temperatures. Fay et al. (1973) made scanner observations between 0.51 μ and 0.69 μ of carbon stars (including 6 of the 7 stars studied here) and found "continuum" color temperatures ranging from ~ 2200 °K for the Mira variables V Cyg, T Dra, R Lep, and V CrB and the semi-regular variable V Hya (C_6 to C_8) to ~ 3000 °K for UU Aur (C_5). Baumert (1972), using narrow band filters in the range $\lambda \sim 0.71$ μ to 1.10 μ, found similar "continuum" color temperatures for these stars T ~ 2100-2900 °K.

For the Mira carbon stars and V Hya, the situation is different. There the observed energy distributions (Figs. 14 and 15) are broader than a single blackbody. This broadness is not a function of spectral type, i.e. compare V Cyg C7,4e with Y Tau C7$_4$e, but rather of variable type. The Mira variables (and V Hya) have the broader energy distribution while the semi-regular variables do not. The extreme examples in this study are V Cyg and T Dra. If a blackbody of temperature corresponding to their spectral type, say T ~ 2000 °K, is run through any wavelength, there will be an apparent excess longward and an apparent deficiency shortward of that wavelength. We therefore propose that the observed energy distribution is actually the sum of the flux of the star, possibly modified by circumstellar attenuation, plus the flux from a circumstellar shell. For the star we propose to adopt a blackbody with temperature given by the spectral type and the near infrared ($\lambda\lambda$ 0.6-1.1 μ) measurements mentioned above, i.e. $T_* \sim 2000$-2500 °K. This will be normalized at near infrared wavelengths ($\lambda \sim 1$-1.5 μ) taking into account the departures from a blackbody shown by real carbon stars of approximately the same spectral type (i.e. UU Aur, Y Tau here). The amount of excess flux at longer wavelengths will then be attributed to radiation from the circumstellar envelope. Only in the case of V Cyg and T Dra (Fig. 15) does this procedure result in a well-defined separation of star from dust. For these stars the star blackbody which fits the short wavelength fluxes falls far short of explaining the energy observed at $\lambda > 2$ μ. The flux left over (excess) can be fit by an ~ 1000 °K blackbody plus

a spectral feature in the $\lambda\lambda$ 10-12.5 μ region which is discussed in Chapter V. In addition, this cool excess represents most of the observed flux, i.e. here $\alpha \sim 0.80$. This means the shell is going optically thick, i.e. $1 - e^{-\langle \tau_{abs} \rangle} \sim \alpha \Rightarrow \langle \tau_{abs} \rangle \sim 1.7$. The problem of interpreting the observed fluxes is now quite difficult because the observed stellar flux will now be modified by (Appendix A)

$$F_\lambda^{obs} = F_\lambda^* \left(e^{-\tau_\lambda}\right) + F_\lambda^{dust} \quad ,$$

and now τ_λ, the effective attenuation of starlight by the dust shell, is not small and will be a complicated function of cloud geometry and grain opacities whose solution is given only by a complete radiation transfer treatment which will not be attempted here. We shall try and derive some simple consequences of the observations.

(1) The broad band energy distribution of the excess is represented fairly well by a T ~ 1000 °K blackbody. If this is an actual temperature of the emitting region, then $R_{shell}/r_* \geq (T_*/T_{shell})^2 \sim 4$. The most plausible emission mechanism to explain this is radiation from circumstellar dust grains. The dual energy distribution might indicate a binary system but the infrared varies with the same period as the visual (see light-curves) so it appears the dust grains derive their energy from the stellar radiation field.

(2) Radiation from the dust begins to be a significant fraction of the observed flux at wavelengths as short as $\lambda = 2$ μ for V Cyg and T Dra. This means that the stellar absorption features should appear weakened ("veiled") relative to a star with no dust

excess. This effect has been observed by Frogel and Hyland (1972) who found the 2.3 μ bands of CO in carbon stars were weaker in the Mira variables relative to the semi-regular variables of the same spectral class. This weakening was correlated to the redness of the infrared colors, i.e., the Mira variables (and V Hya) had redder [3.5 μ] - [1.25 μ] and [11 μ] - [3.5 μ] colors than the semi-regular variables. The authors concluded this might be due to the result of overlying radiation from a circumstellar shell. The extreme example of the stars they studied was V Cyg, for which the CO bands were just barely visible. This agrees with the interpretation of the observed energy distributions proposed here, i.e. for V Cyg (and T Dra) circumstellar radiation represents ~ 2/3 of the observed radiation at [2.3 μ] ($\beta_{2.3\mu} = 2$), so we would expect stellar features to be ~ 1/3 as strong.

An extreme example of this effect is the infrared star IRC +10216. The star has very red colors (~ 600 °K blackbody 2-5 μ, excess at longer and shorter λ's) and the 1.5 μ - 2.5 μ spectra (Becklin et al. 1969) show no discernible stellar absorption features. Spectra in the 1 μ region (Miller 1970; Herbig and Zapalla 1970) show characteristic carbon star absorption features and result in its being classified as a late-type carbon star (~ like V CrB). The supposition that circumstellar emission is responsible for the "veiling" at longer wavelengths was confirmed by lunar occultation measurements of the source (Toombs et al. 1972) which showed the 2-5 μ radiation came from a ~ 0.4" disk with brightness temperature ~ 600 °K ~ color temperature, i.e. an optically thick source much

larger than a 2000 °K star ($\theta_* \sim 0.05$") would be. For IRC +10216 a separation of "star" from "shell" as done for V Cyg results in $\beta_{2.3\mu} \sim 10$ and $\alpha \sim 0.995$.

With this proposed interpretation of the energy distribution of carbon stars the situation regarding separating star from dust and possible time variations in α becomes quite difficult. The [3.5 μ] - [1.04 μ] color no longer measures T_* (as for M stars) and the 3.5 μ flux is no longer directly related to the total apparent flux from the star $\mathfrak{F}* \equiv \int_0^\infty F_\lambda^* \, d\lambda$, as there is a contribution at 3.5 μ due to the circumstellar envelope (dust grains). In addition $\alpha \ll 1$ no longer holds so $\langle \tau_{abs} \rangle \ll 1$ and the assumption of an optically thin envelope (Appendix A) is not valid. This means the observable parameter $\alpha = \mathfrak{F}^{dust}/(\mathfrak{F}^{dust} + \mathfrak{F}*)$ is no longer a linear measure of the amount of dust (eq. 15-19 Appendix A). For instance for V Cyg, $\alpha \sim 0.82 \Rightarrow \langle \tau_{abs} \rangle \sim 1.8$ and a 50% increase in $\langle \tau_{abs} \rangle$ as due, for instance, to the injection of a large amount of new dust would only increase α to ~ 0.93. The colors in the infrared might change even less. In this case, the shorter wavelengths become a better measure of the amount of dust, at least along our line of sight to the star, due to the exponential attenuation $\sim e^{-\tau_\lambda}$ (eq. A-1 Appendix A) of the starlight. If the grain opacity is a decreasing function of wavelength, as for small graphite grains (Appendix B), then an increase by 50% in $\langle \tau_{abs} \rangle \sim \tau_{1.5\mu}$ for V Cyg would result in a decrease by more than a factor of 2.5 (i.e. > 1 mag) in the visual (λ = 0.55 μ) flux from the star, assuming the shell is spherically symmetric.

The additional possibility that the circumstellar shell be non-spherically-symmetric, as well as optically thick, makes the interpretation of observed fluxes in terms of "amounts of dust" more difficult. It is easy to imagine situations in which the observed total flux, $\mathfrak{F}^{obs} = \mathfrak{F}^{dust} + \mathfrak{F}^{*}$ is less than the total apparent flux from a star alone $\mathfrak{F}^{*}(\tau = 0)$ (without dust cloud), e.g. a single small, optically thick occulting cloud $r_{*} < r_{cloud} \ll R_{cloud-*}$. It is even possible to imagine a shell which will give $\mathfrak{F}^{obs} > \mathfrak{F}^{*}$ $(\tau = 0)$ for an observer in a preferred direction (thermal focussing). Energy conservation of course requires $\int \mathfrak{F}^{obs} D^{2} d\Omega = \int \mathfrak{F}^{*}$ $(\tau = 0)$ $D^{2} d\Omega = \mathfrak{L}_{*}$, where $\mathfrak{L}_{*}$ = luminosity of the star and D = distance star-earth, but $\mathfrak{F}^{obs}$, $\mathfrak{F}^{dust}$ need not be spherically symmetric for optically thick shells.

In summary, the semi-regular variable carbon stars UU Aur and Y Tau have energy distributions which are similar to the M stars studied here with the star dominating the energy distribution for $\lambda < 8$ μ and a small excess at longer wavelengths ($\alpha < 0.05$). The Mira carbon stars (and V Hya) on the other hand, appear quite different, with excess "blackbody" like radiation at $\lambda > 2$ μ which represents a considerable fraction ($\alpha \gtrsim 0.3$) of the observed energy. If the excess is attributed to circumstellar grains, then the early near infrared measurements of V Cyg by Pettit and Nicholson (1933) which indicated an extremely low temperature ($T \sim 1350$ °K) should probably be considered the first (unknowing) detection of an infrared excess due to circumstellar grains. Definitive tests of this model might be (1) high spatial resolution measurements, as for IRC +10216,

to determine the size of the emitting/scattering regions at various wavelengths; (2) high spectral resolution measurements from 1 μ to 5 μ. On this model one expects increased weakening ("veiling") of the stellar absorption features as α (or β_{λ}) increases. The "veiling" should increase with wavelength and be much stronger in the Mira variables and V Hya (large α, β_{λ}) than the semi-regular variables.

E. Light Curves -- Carbon Stars

Besides the effect of optical depth discussed earlier, the temperature and luminosity variations of the Mira variables will affect the shape of the light curves. The luminosity variations are clear from the infrared light curves (Figs. 16-20) and temperature variations are indicated by the ~ 2 to 3 magnitude variations in visual light. An estimate of the stellar temperature and luminosity variations was made using the [1.04 μ] "continuum" measurements of Baumert (1972) and the V magnitude given by the AAVSO (Mayall 1973). The 1.04 μ flux is thought to be relatively near the "continuum" at these wavelengths ($\lesssim 0.2$ mag depression) and is a short enough wavelength so that emission from the ~ 1000 °K excess can be ignored. The V = [0.55 μ] magnitude is blanketed but includes the "continuum" region at $\lambda > 0.57$ μ (Fay et al. 1973). A color temperature was calculated for the available data and plotted vs. phase. The color temperature for V Cyg, with the best phase coverage tracked ~ 50-100 °K below the assumed temperature of Star X (Fig. 3). The color temperatures of R Lep and V CrB tracked at

$\sim$ 100-150 °K above that of Star X. Thus it seems that the carbon Miras studied here are similar to the M-Miras in their temperature fluctuations, T_{max} at $\phi = 0$, T_{min} at $\phi \sim 0.5$-0.6, and $T_{max}/T_{min} \sim 1.3$. V Cyg and T Dra have color temperatures running ~ 250 °K below V CrB and R Lep. The apparent stellar luminosity variations, derived from T_{color} and [1.04 μ] were less well behaved but seemed consistent with maximum stellar luminosity at $\phi \sim 0.1$-0.2 and ~ 1 mag variation in luminosity similar to the M stars.

To try and separate the effects of the temperature and luminosity fluctuation from those due to changes in α, a model star has been constructed. The star is assumed to be a blackbody of $T = T_*$ to which is added a blackbody excess which represents a fraction α of the total luminosity at a temperature $T_{BB} = \frac{1}{2} T_*$. T_* and α are now varied. The total luminosity is assumed to go as T_*^4, i.e. ignoring radius changes which would affect the observed colors (flux ratios) only in the second order through T_{BB}. For different $\alpha = 1 - e^{-\langle \tau_{abs} \rangle}$, the total luminosity is held constant and the star is assumed to be neutrally extinguished. The results are given in Table 3.

For R Lep, V CrB, and V Hya $\alpha \sim 0.3$ and an increase to $\alpha \sim 0.5$ ($\langle \tau_{abs} \rangle = 0.36$ to 0.69) as due to a factor of ~ 1.9 increase in the "amount of dust" results in only an -0.13 mag increase in [3.5 μ] and $\sim$ -0.21 mag increase in the [8.4 μ] - [3.5 μ] color. The color changes would be hard to distinguish from a change due to a temperature change. For V Cyg and T Dra, $\alpha \sim 0.8$ and the color changes for a given change in $\langle \tau_{abs} \rangle$ will be even smaller.

TABLE 3

Characteristics of the Hypothetical Carbon Star

T_*	α	$\langle \tau_{abs} \rangle$	[3.5 μ]	[4.9 μ] - [3.5 μ]	[8.4 μ] - [3.5 μ]	[11 μ] - [3.5 μ]
2300			- 1.97	- 0.49	- 1.07	- 1.30
2000	0.3	0.36	- 1.50	- 0.60	- 1.22	- 1.45
1700			- 0.93	- 0.69	- 1.39	- 1.75
2000	0.1	0.105	- 1.35	- 0.46	- 0.91	- 1.09
	0.5	0.69	- 1.63	- 0.72	- 1.43	- 1.65
	0.7	1.20	- 1.74	- 0.80	- 1.57	- 1.83
	0.9	2.30	- 1.84	- 0.88	- 1.65	- 1.92

Thus for the Mira carbon stars (and V Hya), changes in the "amount of dust" will be harder to detect than for M stars. This is due to:

(1) None of the infrared monitor wavelengths used here measures radiation purely from the star; the ~ 1000 °K blackbody excess can contribute significantly to the measured flux at 3.5 μ.

(2) The excess is broad and smooth in nature in contrast to the well-defined "silicate bump" in the M stars. There is a sharp feature in the excess λλ 10-12.5 μ (see Chapter V) which is monitored by the [11 μ] filter but the adjacent [8.4 μ] filter monitors a continuum which is also part of the excess. Thus an equal increase in both components of the excess may change the [11 μ] - [8.4 μ] color very little.

(3) The optical depths for the circumstellar shells deduced from the observed energy distributions ($\langle\tau_{abs}\rangle \sim 0.36$-$1.4$ for Mira variables) are no longer $\ll 1$ so the simple-minded model star presented here may be misleading.

1) Mira Variables

(a) R Lep

The light curve and polarization data for R Lep are given in Fig. 16, the format is identical to that of the M stars. As for the M and S type Miras, the 3.5 μ flux peaks somewhat after visual maximum at $\phi \sim 0.1$. The small changes in colors during the cycle are consistent with temperature changes in the excess, maximum

Fig. 16: Polarization and photometric data on R Lep.

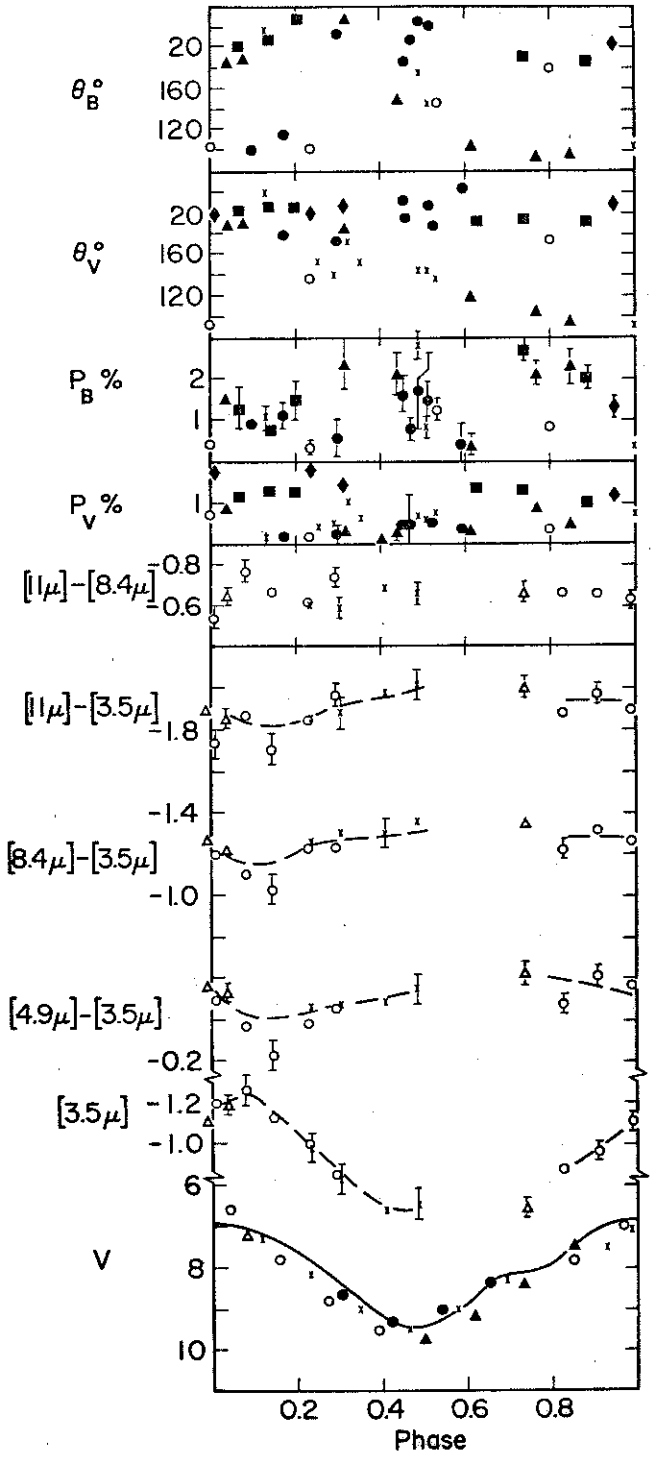

temperature coming at $\phi \sim 0.1$, i.e. bolometric maximum and minimum temperature at $\phi \sim 0.6$, bolometric minimum. The [11.2 μ] - [8.4 μ] color is approximately constant at -0.66 which is consistent with a constant amount of "silicon carbide" excess (Chapter V) relative to "blackbody" excess.

The polarization, on the other hand, shows chaotic behavior similar to that of the M and S type Miras. A suspected constant interstellar component to the polarization (P = 1% θ = 35°) has been subtracted as suggested by Serkowski (1974b), but this will not affect the existence of changes in the polarization. The degree of polarization is capable of being high (or low) during any part of the cycle. There may be some enhanced activity around $\phi \sim 0.5$ and $\phi \sim 0.8$ in the blue region, but this is not apparent in the visual region. As for many of the M and S Miras, there seems to be a "preferred angle" $\theta \sim 20°$ with occasional large excursions down to $\theta \sim 100°$. The behavior of θ_B with time is particularly intriguing. During the -3 cycle (■) $\theta_B \sim 20°$, beginning with the -2 cycle (▲) $\theta_B \sim 20°$ but around $\phi \sim 0.5$ apparently transited to $\theta_B \sim 100°$, beginning the -1 cycle (●) $\theta_B \sim 100°$ but by $\phi \sim 0.3$ $\theta_B \sim 20°$ again. Then beginning the zeroth cycle (X) $\theta_B \sim 20°$ transiting perhaps at $\theta \sim 0.5$ to reach $\theta_B \sim 100°$ by cycle's end. Continuing into the +1 cycle (○) $\theta_B \sim 100°$ transiting at perhaps $\phi \sim 0.5$ to $\theta_B \sim 0°$ by $\phi(1) \sim 0.8$. This cyclic behavior of θ_B is reminiscent of the RV Tauri star U Mon studied by Serkowski (1971), here the period of angle variation would be twice the visual period. Such quasi-periodic angle changes with double period, have been

noted by Serkowski (1970) for the Mira variables oCet and R Hya.

The polarization activity in the blue near $\phi(0) \sim 0.5$ and the aforementioned angle variations during the zeroth (X) and first (0) cycles in B and V are not accompanied by any large deviations in the infrared colors and magnitudes from the mean behavior (dotted lines in Fig. 16). In particular, there is no evidence for the production of a large amount of new dust near $\phi \sim 0.5$ to account for the position angle variations.

(b) V CrB

The infrared, visual, and polarization data for V CrB is given in Fig. 17. The increase in infrared colors toward minimum is again probably consistent with the changes expected due to luminosity and temperature changes with a constant average "amount of dust" present. The range of variation at 3.5 μ is larger for V CrB than R Lep (~ 0.9 mag vs. ~ 0.55 mag), so one might expect the larger color variations which are observed. The [11 μ] - [8.4 μ] color is approximately constant at ~ -0.65 except for one high measurement at $\phi(0) \sim 0.22$ and one low measurement at ϕ (2) ~ 0.85, again consistent with an approximately constant amount of "silicon carbide" excess relative to "blackbody" excess. One interesting and unique (among the Mira variables studied here) feature of the V CrB light curve is the apparent decrease of ~ 1.5-2 mag in the level of the visual light curve from the "mean light curve" given by Campbell (1955). The mean light curve is the average of AAVSO visual observations over the period $\sim$ 1920-1950 and so should be

Fig. 17: Polarization and photometric data on V CrB.

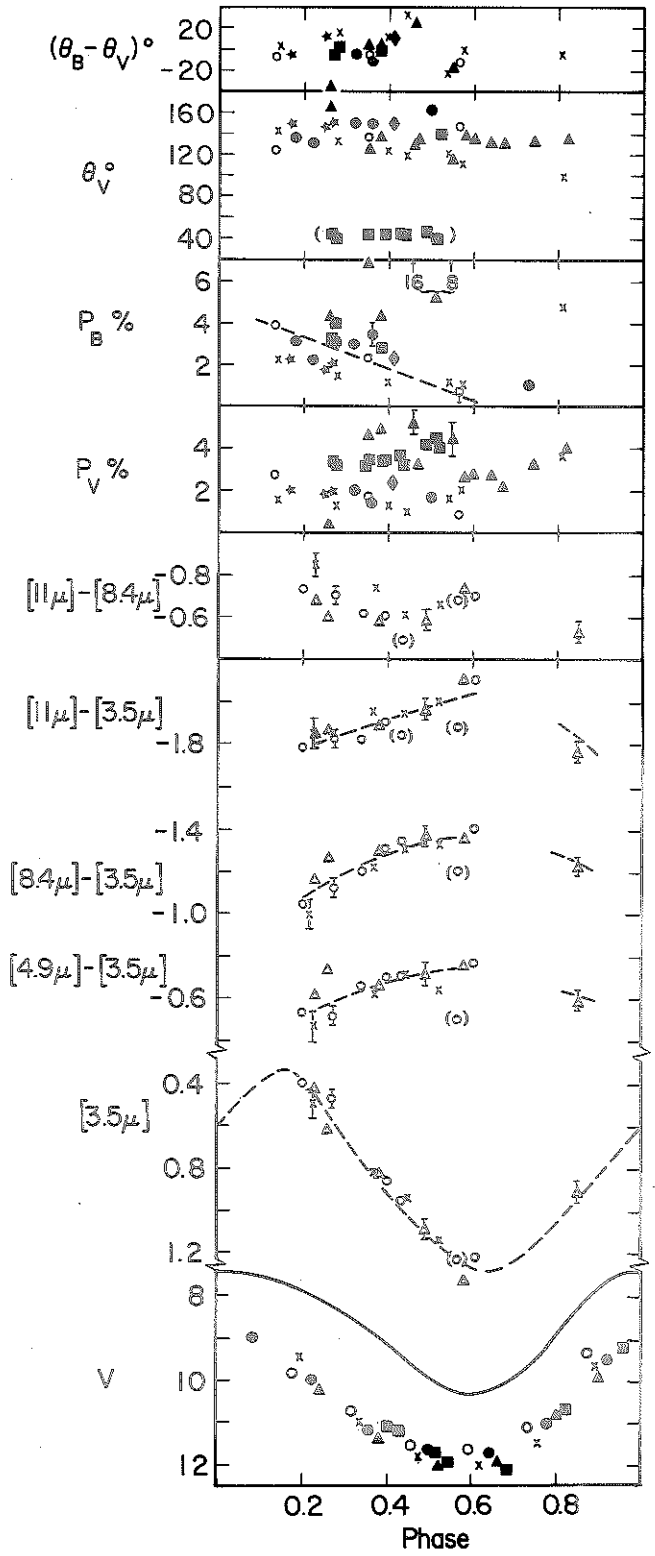

comparable to the current visual estimates; for all the other M, S and C Mira variables the current eye estimates tend to cluster around the mean light curves given by Campbell (1955). This decrease in V could be due to (1) A change in the magnitude sequence assigned to the stars around V CrB or in the AAVSO observers. However, other red stars, such as R Lep, V Cyg, don't show such an effect. In addition, photoelectric measurements by Mendoza (1967), Serkowski (1966a), Dyck (1968) and Dombrovskii et al. (1973) also indicate a decrease in the visual flux from the -7 cycle to the -3 through -1 cycles, though this result depends mostly on the early measurements by Mendoza (1967), which were close to the "mean light curve" level.

(2) A change in the actual luminosity or temperature of the star. This should be noticeable in the spectral type of the star.

(3) The appearance of or increase in the optical depth of a dust shell around V CrB. The current infrared energy distribution (Table 2a) indicates (Table 2b) a shell which radiates a fraction $\alpha \sim 0.4$ of the total energy of the system. Thus $\tau_{1.5\mu} \sim 0.5$ and if we assume the opacity of small graphite grains, $\tau_{0.55\mu} \sim 2.5$. Thus, if in the past, the shell was much thinner, $\tau_{0.55\mu} \lesssim 1$, the apparent visual flux would be increased by the required amount (~ 1.5 mag). Unfortunately, there are no earlier measurements of the infrared energy distribution to test this hypothesis. The time-scale for this $\sim$ factor of two increase in the amount of dust would be, using the photoelectric visual data, on the order of 3-4 years,

i.e. similar to the timescale for secular decrease in the amount of dust which was possibly observed in oCet.

V CrB shows a quite high degree of polarization, up to ~ 5% at V and perhaps even 10% at B. There does not seem to be a preferred phase for high polarization. The "preferred angle" for polarization appears to be $\theta_V \sim \theta_B \sim 140°$. The series of measurements during the -3 (■) cycle for which $\theta_V \sim 40°$ are all due to Dyck (1968) and may be in error because measurements by Shawl (1972) during this time gave $\theta_V \sim 140°$. Thus, V CrB may be one of the few stars in this study which does <u>not</u> show large changes in position angle of polarization. The decrease in polarization during the +1 cycle (0); P_B from ~ 4% to < 0.7%, P_V from ~ 2.7% to 0.9%; was not accompanied by any noticeable increase or decrease in the infrared magnitudes from the mean behavior. Neither was there a large difference in the visual magnitude for this cycle. Again apparent changes in the polarized flux are not accompanied by large changes in the infrared.

(c) T Dra

The infrared, visual, and polarization data for T Dra is given in Fig. 18. The AAVSO visual observations were few and scattered so the phase was not well defined. The 3.5 μ light curve is unique for this study in that it peaks <u>before</u> the adopted zero visual phase -- this probably means the phase is wrong and should be shifted ~ +0.1 to +0.2. This would probably not disagree with the available AAVSO visual estimates. The [8.4 μ] - [3.5 μ]

Fig. 18: Polarization and photometric data on T Dra.

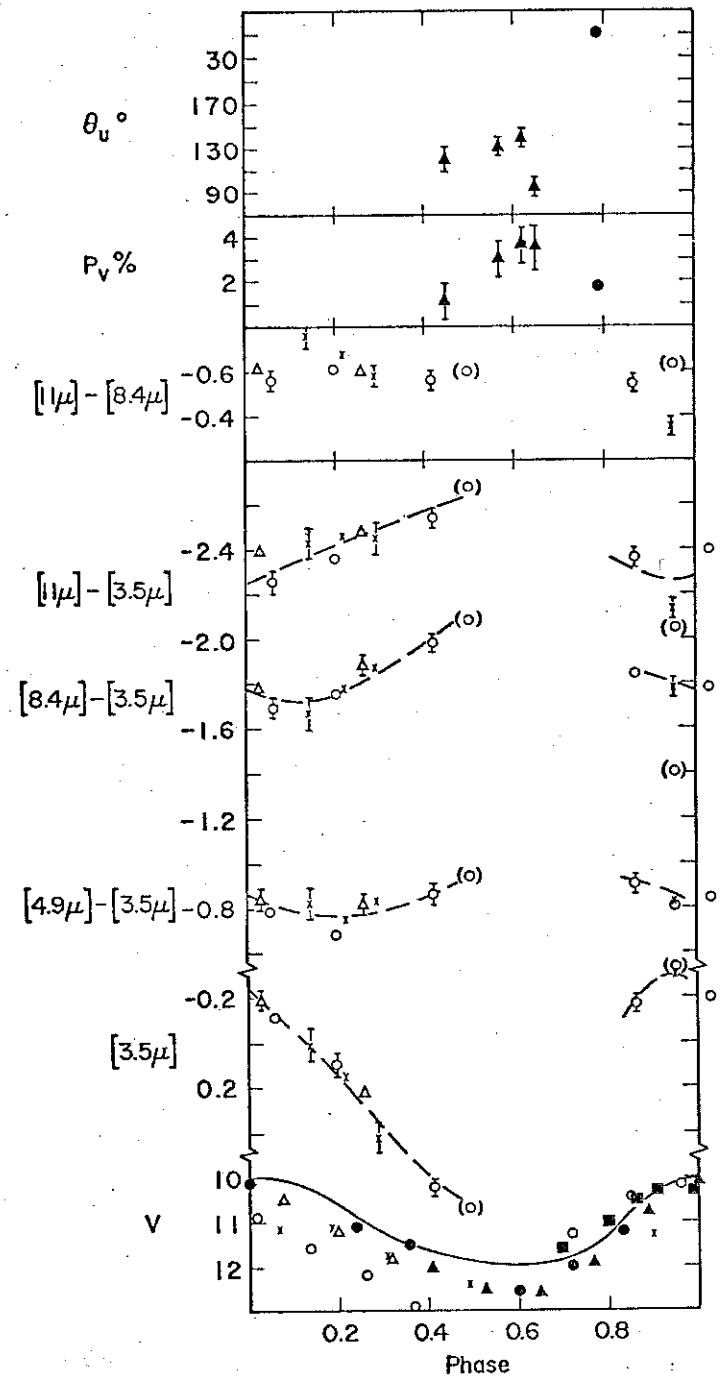

and [11 μ] - [3.5 μ] colors show small but probably real variation with phase similar to V CrB; they are probably consistent with an approximately constant "amount of dust." The [11 μ] - [8.4 μ] color is approximately constant at -0.63, indicating no large apparent change in the amount of "silicon carbide" relative to "blackbody" excess.

The polarization data is meager but does show (1) large visual polarization, up to $P_V \sim 3.5\%$, consistent with the large excess for this star (large [11 μ] - [3.5 μ] color, $\alpha \sim 0.8$). (2) Large changes in the degree of polarization, and in one case on a short (~ 50 days) timescale. (3) A large change in the position angle of polarization from $\theta_V \sim 130°$ to $\sim 90°$ in ~ 15 days during the -2(▲) cycle ending up at $\theta_V \sim 50°$ in the -1 (●) cycle, i.e. a change of at least 80° in position angle through one cycle.

(d) V Cyg

The infrared and visual data is given in Fig. 19 -- no polarization data could be located for this star. As for other Mira variables the 3.5 μ flux peaks at $\phi \sim 0.1$-0.2. The variation in flux ratios 11 μ, 8.4 μ, 4.9 μ: 3.5 μ are similar to the other carbon Miras, the minimum ratios coming approximately at 3.5 μ (~ bolometric) maximum and the maximum ratios at 3.5 μ (~ bolometric) minimum. These variations are probably consistent with a constant average amount of dust excess, the changes being due to variations in the temperature and luminosities of the star and dust, with the

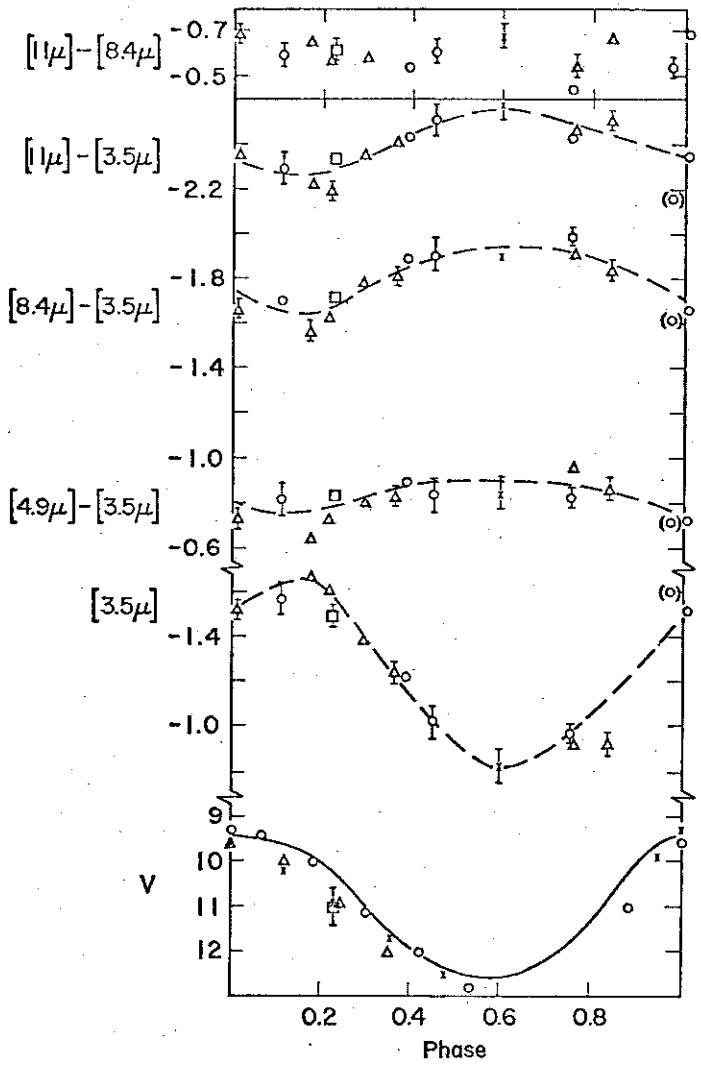

Fig. 19: Photometric data on V Cyg.

relative luminosity in dust, α, approximately constant. Again, the [11 μ] - [8.4 μ] color is approximately constant at -0.60, which is consistent with a constant ratio of "SiC" excess to "blackbody" excess.

V Cyg and T Dra have very similar energy distributions (Fig. 15) and spectra in the $\lambda\lambda$ 8-13 μ region (Chapter V). Curiously enough, these two stars have almost identical periods, differing by only 0.4 days. The energy distribution 0.55-20 μ is characterized by an $\sim$ 950 °K blackbody, a small emission feature $\lambda\lambda$ 10-12.5 μ attributed to emission from SiC grains as discussed in Chapter V, and an excess at shorter wavelengths ($\lambda \lesssim 2$ μ) which can be characterized by an $\sim$ 2000 °K blackbody. As discussed earlier, one possible explanation of the extremely cool energy distribution is re-radiation of absorbed starlight by circumstellar grains. The excess radiation at shorter wavelengths would represent transmitted starlight which is attenuated and possibly also reddened by the circumstellar shell. If this interpretation is true and the separation of star and dust as given in Fig. 15 is adopted, then the fractional amount of apparent energy radiated by the circumstellar shell is $\alpha \sim 0.8$ for these two stars, which is the largest value for α of the stars in this study. One consequence of this is that all the infrared monitor wavelengths measured here, 3.5 μ - 11 μ, refer now more or less to radiation from the dust directly; if the weakening of the stellar 2.3 μ CO bands found by Frogel and Hyland (1972) for V Cyg is due to overlying emission from the dust, then by 3.5 μ the dust will probably completely dominate because

over this range the $\sim$ 950 °K dust blackbody increases by approximately a factor of 2 while the $\sim$ 2000 °K stellar blackbody falls (ignoring possible reddening effects) by approximately a factor of 2. Assuming this to be the case, the 3.5-11 μ measurements should give information directly about the temperature and luminosity of the circumstellar shell vs. phase. The [11 μ] - [8.4 μ] color is approximately constant for these stars, indicating the strength of the "SiC" feature (discussed in Chapter V) relative to blackbody continuum is approximately constant with phase. We have used the mean [8.4 μ] - [3.5 μ] light curves to define the color temperature $T_c(3.5\mu,8.4\mu)$ of the excess vs. phase given in Fig. 20. Further, assuming the energy distribution of the excess is actually described by a blackbody of this color temperature, as indicated by Fig. 15, we have derived the apparent angular size, Ω_a, and the apparent bolometric luminosity, m_{bol}, of the excess vs. phase, also shown in Fig. 20. The apparent angular size is defined by

$$\Omega_a = \frac{F_\lambda^{obs}}{B_\lambda(T_c)} \quad ,$$

where λ = 3.5 μ or 8.4 μ. Ω_a is the angular size a blackbody of temperature T_c would have to give the observed flux. The total integrated flux is then given by

$$\mathfrak{F}^{exc} = \int F_\lambda^{exc}\, d\lambda = \Omega_a \frac{\sigma}{\pi} T_c^4 \quad ,$$

and is related to the bolometric magnitude by

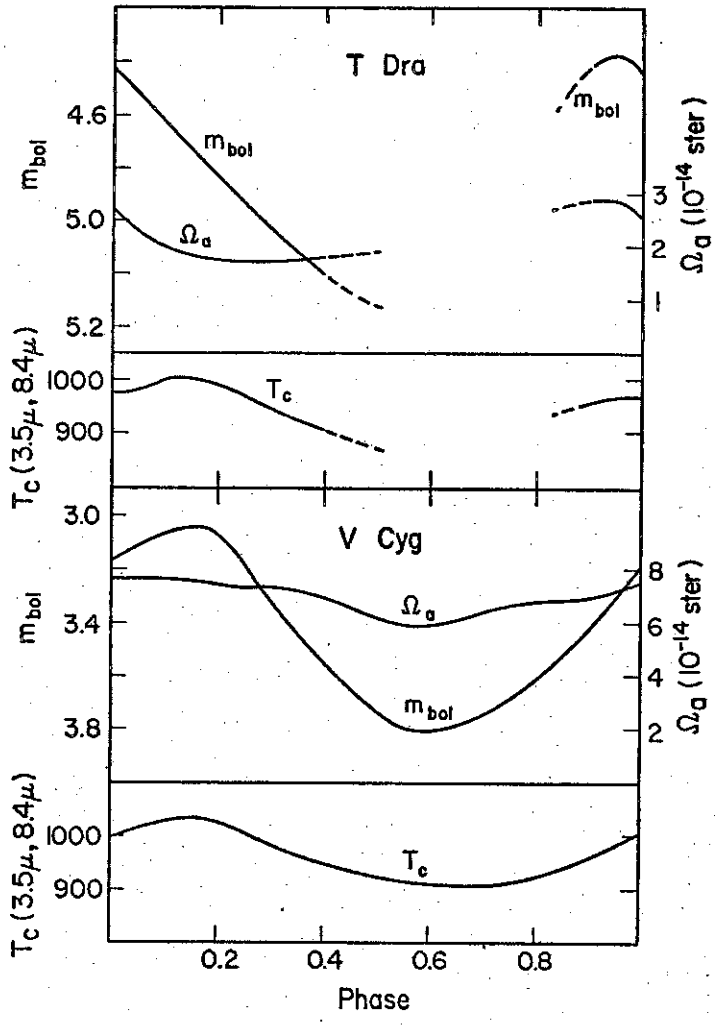

Fig. 20: Variations in the color temperature, apparent angular size, and luminosity of the excess with phase for V Cyg and T Dra as described in the text.

$$\mathcal{F}(0\text{mag})10^{-m_{bol}/2.5} = \mathcal{F}^{exc} \quad ,$$

when $\mathcal{F}(0\text{mag}) = 2.52 \times 10^{-12}$ W/cm^2 is the total apparent flux for zero bolometric magnitude (Allen 1963). In the optically thin case, where T_c referred to an actual temperature, Ω_a would be related to the total mass of dust M_d radiating (see Chapter VIII) by

$$\Omega_a = \frac{\Sigma_{grains}\sigma_{abs}}{D^2} = \frac{\kappa_\lambda M_d}{D^2} \propto M_d \quad ,$$

where κ_λ is the (constant) mass absorption coefficient of the grains and D is the (constant) star-earth distance. In an actual circumstellar shell, Ω_a will be a function of the run of density, temperature, and optical depth through the shell.

The color temperature shows only small variation with phase, $T_c(\text{max})/T_c(\text{min}) \sim 1.15$ so the bolometric magnitude essentially tracks the [3.5 μ] magnitude, with a range of ~ 0.8 magnitudes, similar to the range of bolometric magnitude found by Strecker (1973) for M and S Mira variables. The variation in Ω_a, $\Omega_a(\text{max})/\Omega_a(\text{min}) \sim 1.31$, 1.68 for V Cyg and T Dra respectively, with minimum Ω_a coming approximately at bolometric minimum could be due to a relatively smaller effective amount of dust radiating at minimum as due for instance to production of dust near the star with a larger relative absorption optical depth than the same amount of dust after it has moved further from the star.

ii) Semi-Regular Carbon Stars

(a) V Hya

The infrared, visual, and polarization data for V Hya are given in Fig. 21. V Hya has the small visual variation, $\Delta V \lesssim 1$ mag during the observing period, of the semi-regular variables and an energy distribution, Fig. 14, similar to the Mira variables R Lep and V CrB. On the circumstellar dust shell model, the excess radiation longward of $\lambda \sim 2$ μ is attributed to re-radiation of absorbed starlight and represents a fractional amount of the total flux from V Hya of $\alpha \sim 0.4$. The [3.5 μ] flux has approximately equal contributions from the star and the shell, i.e. $\beta_{3.5\mu} \sim 1.6$, and the longer wavelengths have increasingly more relative flux from the shell, i.e. $T_c^{exc}(3.5\ \mu, 8.4\ \mu) \sim 900$ °K. Thus, the colors [λ] - [3.5 μ] convey potential information about the amount of dust excess vs. time.

The variations in [3.5 μ] are probably real, i.e. Δ[3.5 μ] ~ 0.4 mag, with the 3.5 μ flux approximately in phase with the visual flux. All the colors [λ] - [3.5 μ] and [11 μ] - [8.4 μ] are statistically consistent with essentially no variation over the ~ 800 day observation period. Thus, there is no evidence for variation in the amount of dust, in either the blackbody component on the "SiC" component, over this observation period. Now the timescale for variation in flux due to a given mass of dust would be $t \sim \tau_{abs}/\dot{\tau}_{abs} \sim \frac{1}{2} R_d/\dot{R}_d$, which for the parameters given in Chapter VIII and $V_d = \dot{R}_d = 20$ km/s give $t \sim 5$ years. The lack of any variation

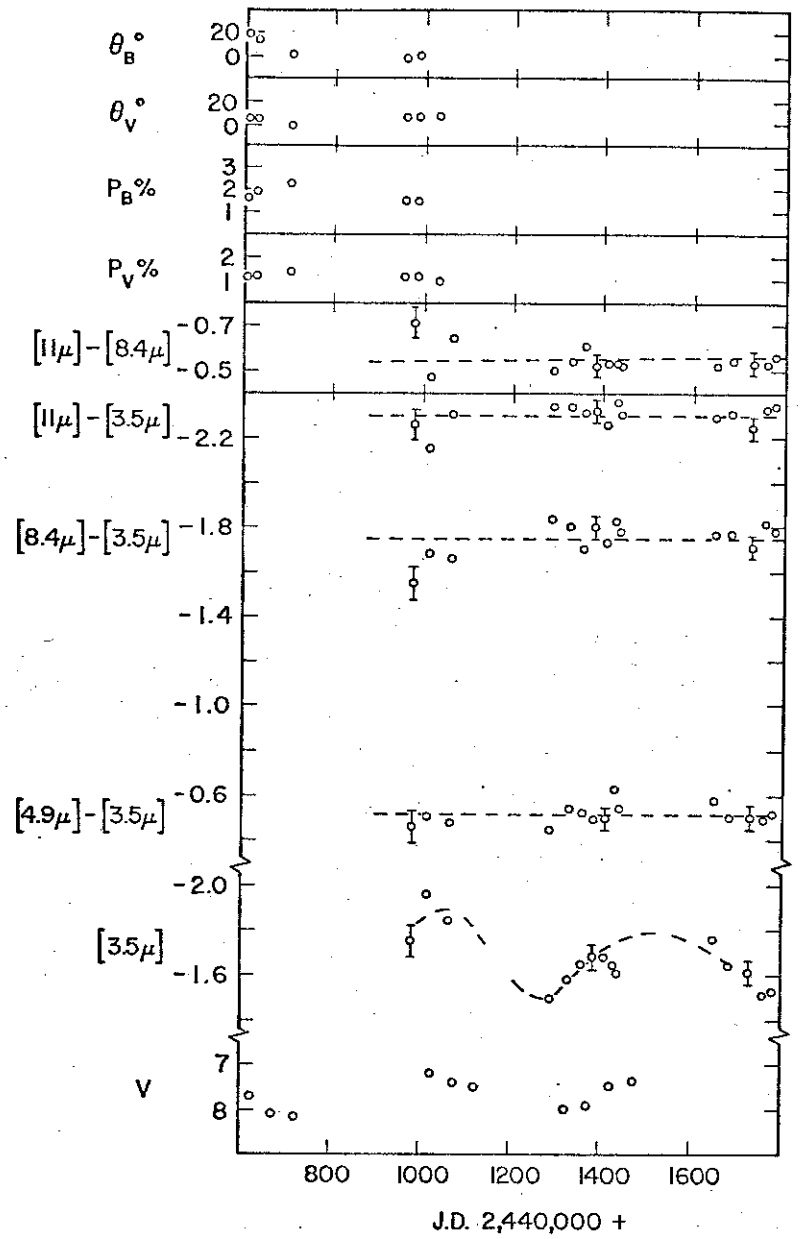

Fig. 21: Polarization and photometric data on V Hya.

over the ~ 2 1/2 year observation time and the agreement of the present measurements with earlier measurements of Gillett, Merrill and Stein (1971) indicate that over this time, dust production must have been taking place, for otherwise we would see a decrease in the infrared fluxes and an increase in the visual flux. Thus, the large oscillations in temperature, luminosity, and diameter of the Mira variable stars do not seem to be a necessary condition for the production of dust in carbon stars -- V Hya manages quite well with considerably smaller oscillations.

The polarization of V Hya does not show the large and rapid changes in degree and position angle of the Mira variables. There has been a slow decay of about a factor of 2 in amount of polarization from the earliest measurements but there are no concurrent infrared measurements to test if this is correlated with amount of dust. The position angle of polarization is remarkably stable at $\theta_V \sim \theta_B \sim 180°$; the polarization data would be consistent with an asymetric shell of approximately constant geometry or with aligned grains with approximately constant net alignment.

(b) UU Aur

The infrared, visual, and polarization data for UU Aur is given in Fig. 22. The variations in the 3.5 μ flux though small, $\Delta[3.5\ \mu] \lesssim 0.2$ mag, are probably real because they are correlated with the small variations in visual flux. The colors [λ] - [3.5 μ] and [11 μ] - [8.4 μ] are essentially constant within the ~ 5% systematic errors expected. The energy distribution of UU Aur

Fig. 22: Polarization and photometric data on UU Aur.

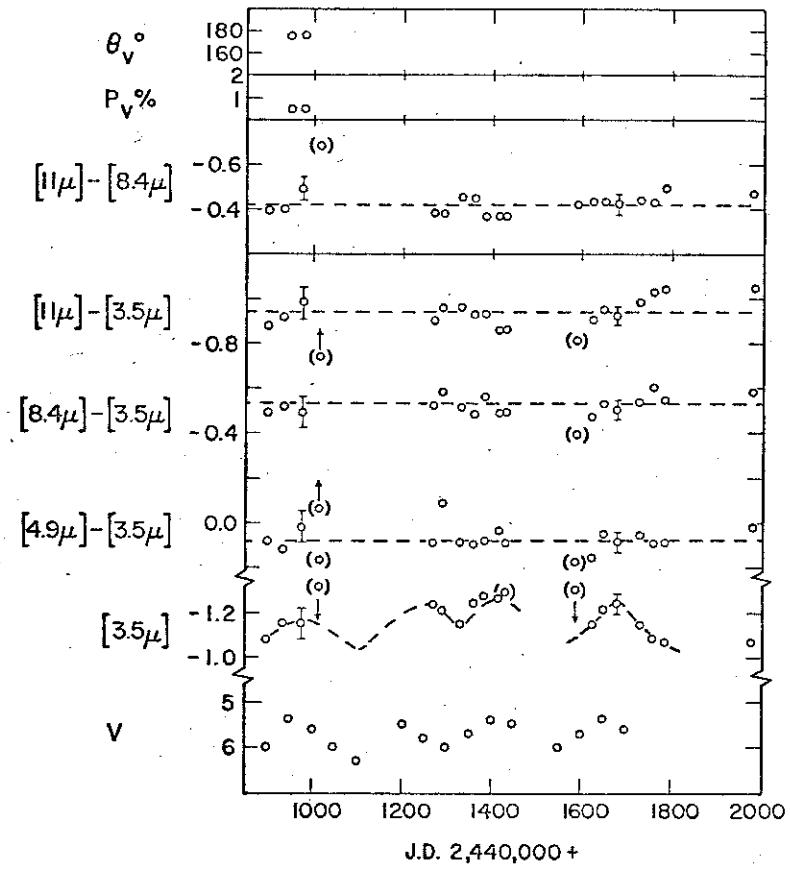

(Fig. 2) is more like the M and S stars than the carbon Miras and V Hya -- most of the energy is represented by the ~ 2400 °K stellar blackbody and only a very small fraction of the energy ($\alpha \sim 0.002$) is radiated in the 10-12.5 μ emission feature (Chapter V) which can be attributed to circumstellar SiC grains. There could be an additional smooth, blackbody excess of $\alpha \lesssim 0.05$ which could escape our notice, given the uncertainty in the true stellar continuum. Still, it seems that the ratio of flux radiated by SiC is larger relative to the blackbody excess for this star, $\alpha(\text{SiC})/\alpha(\text{blackbody}) \gtrsim 0.04$, than for, say V Cyg with $\alpha(\text{SiC})/\alpha(\text{blackbody}) \sim 0.02$, though this could be partly an optical depth effect and doesn't necessarily prove the relative abundance of SiC grains to blackbody grains is greater for UU Aur. The constancy of the [11 μ] - [8.4 μ] color (~ -0.42) and its approximate agreement with the earlier measurement of Gillett et al. (1970) again indicates continuous dust production with the (even smaller) variations of this star.

The small amount of polarization ($P_V \sim 0.5\%$) is consistent with the small amount of dust excess observed here.

(c) Y Tau

The data for Y Tau was similar to that of UU Aur and is not displayed. The variations in 3.5 μ flux for Y Tau was Δ[3.5 μ] ~ 0.3 mag. The [4.9 μ] - [3.5 μ] color was approximately constant but there may be a significant variation of ~ 0.2 mag in the [8.4 μ] - [3.5 μ] and [11 μ] - [3.5 μ] colors while the [11 μ] - [8.4 μ] color was approximately constant at -0.67. The energy distribution (Fig. 14)

is very similar to UU Aur except the emission feature at [11 μ] is relatively larger and there may be a small excess of ~ 0.5 mag at [20 μ]. Interestingly, the ratio of observed flux to continuum in the 11.2 μ broad band filter is (using the [11 μ] - [8.4 μ] color excess) $\beta_{[11\mu]} \sim 0.7$ which is the largest value for the carbon stars in this study. V CrB has about the same relative bump with $\beta_{[11\mu]} \sim 0.7$ and for the other stars it is smaller, i.e. $\beta_{[11\mu]} \sim 0.45$ for V Cyg and $\beta_{[11\mu]} \sim 0.35$ for UU Aur. A blackbody continuum, if it exists, must be small $\alpha(\text{blackbody}) \lesssim 0.05$ so the ratios $\alpha(\text{SiC})/\alpha(\text{blackbody}) \gtrsim 0.08$ which again is larger than for the Mira variables and V Hya.

The polarization for Y Tau, $P_V \sim 1\%$, is approximately twice as large as for UU Aur, consistent with the approximately twice as large 11 μ bump. It is also as large as for the present level of polarization of V Hya (Fig. 21), whose energy distribution indicates a shell with considerably larger absorption optical depth. However, since variations in the polarization of Y Tau haven't been observed over the ~ 100 days of polarization data, some of the polarization could be interstellar.

V. SPECTRA

Higher resolution spectra in the infrared are important to the interpretation of the broad energy distributions discussed in Chapter IV. If the long wavelength excesses in stars are due to thermal radiation from circumstellar dust grains, the detailed spectral shape will have information as to the identity of the radiating material. The spectrum is necessary for a comparison of the dust grains around stars studied here with (1) the expected emissivities (Appendix B) of known materials measured in the laboratory and (2) the dust grains in other celestial objects, such as H II regions, highly extinguished objects, comets, planetary nebulae, the Galactic center, and extragalactic objects. The work presented here is essentially a continuation and extension of the earlier medium resolution ($\Delta\lambda/\lambda \sim 1.5\%$) spectra by Gillett et al. (1968) and Hackwell (1971, 1972) and high resolution ($\Delta\lambda/\lambda \sim 0.2\%$) spectra by Gammon et al. (1972), Treffers and Cohen (1974), and Treffers (1973) of similar stars.

In this chapter we present medium resolution ($\Delta\lambda/\lambda \sim 0.015$) spectra in the λλ 7.5-13.5 μ region of some of the stars known to exhibit intrinsic polarization and related objects.

A. M Stars

i) Observed Excesses

The energy distributions of the M stars (Fig. 2; Table 2a) in this study are described moderately well by an ~ 2000-3000 °K

blackbody (with absorptions at some wavelengths) plus apparent excess at $\lambda \gtrsim 8$ μ. The hot blackbody is undoubtedly due to the star; as a working hypothesis we assume this is so and also that the stellar continuum F_λ^* at $\lambda > 8$ μ is represented by the continuation of the blackbody which fits the $\lambda < 6$ μ data F_λ^{cont}. Then the excess radiation due, presumably, to thermal radiation from dust grains is given by

$$F_\lambda^{exc} = F_\lambda^{obs} - F_\lambda^* \simeq F_\lambda^{obs} - F_\lambda^{cont} \quad .$$

The excesses derived in this manner for M-type Mira variables is given in Fig. 23. The parameter $\beta_\lambda \equiv (F_\lambda^{obs} - F_\lambda^{cont})/F_\lambda^{cont}$ measures the amount of excess relative to continuum. For oCet, R Cas, U Her, and U Ori the excess is seen to rise rapidly, by a factor ~ 3-4, from 8 μ to the peak at ~ 9.75 μ, fall slowly to ~ 11 μ and then fall more rapidly, by a factor ~ 2.5, to 13 μ. For RL Mi and expecially R Leo, the rise to maximum seems to be more rapid and the fall thereafter less pronounced; the ratio $F_{9.7\mu}^{exc}/F_{13\mu}^{exc} \sim 1.4$ for R Leo and ~ 3.1 for the first four stars. In addition there may be a small, ~ 15%, ~ 0.7 μ wide dip in the spectrum of R Leo centered at 11.8 μ.

The excesses of the semi-regular variable stars X Her (giant) and RW Cyg (supergiant) are compared in Fig. 24 with the total flux from the Trapezium region of the Orion nebula. The Trapezium was measured with a 22″ aperture in December 1971 -- there is essentially no contribution from the hot Trapezium stars or a free-free continuum at these wavelengths (see Fig. 2), so no subtraction has been

Fig. 23: Spectral energy distribution of excess emission from several M Mira stars as described in the text.

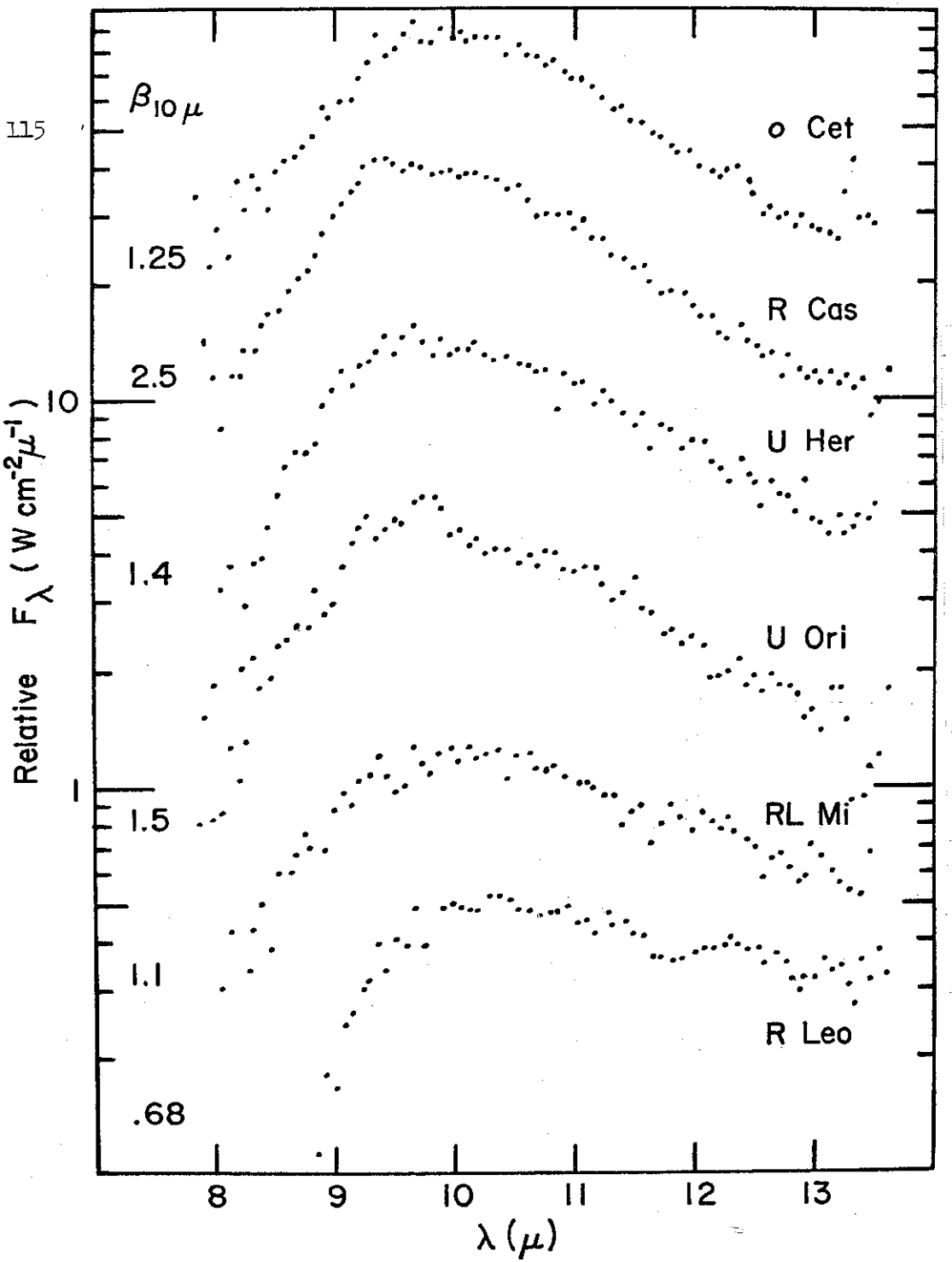

Fig. 24: Spectral energy distribution of excess emission from semi-regular M stars compared with that of the Trapezium region of the Orion Nebula.

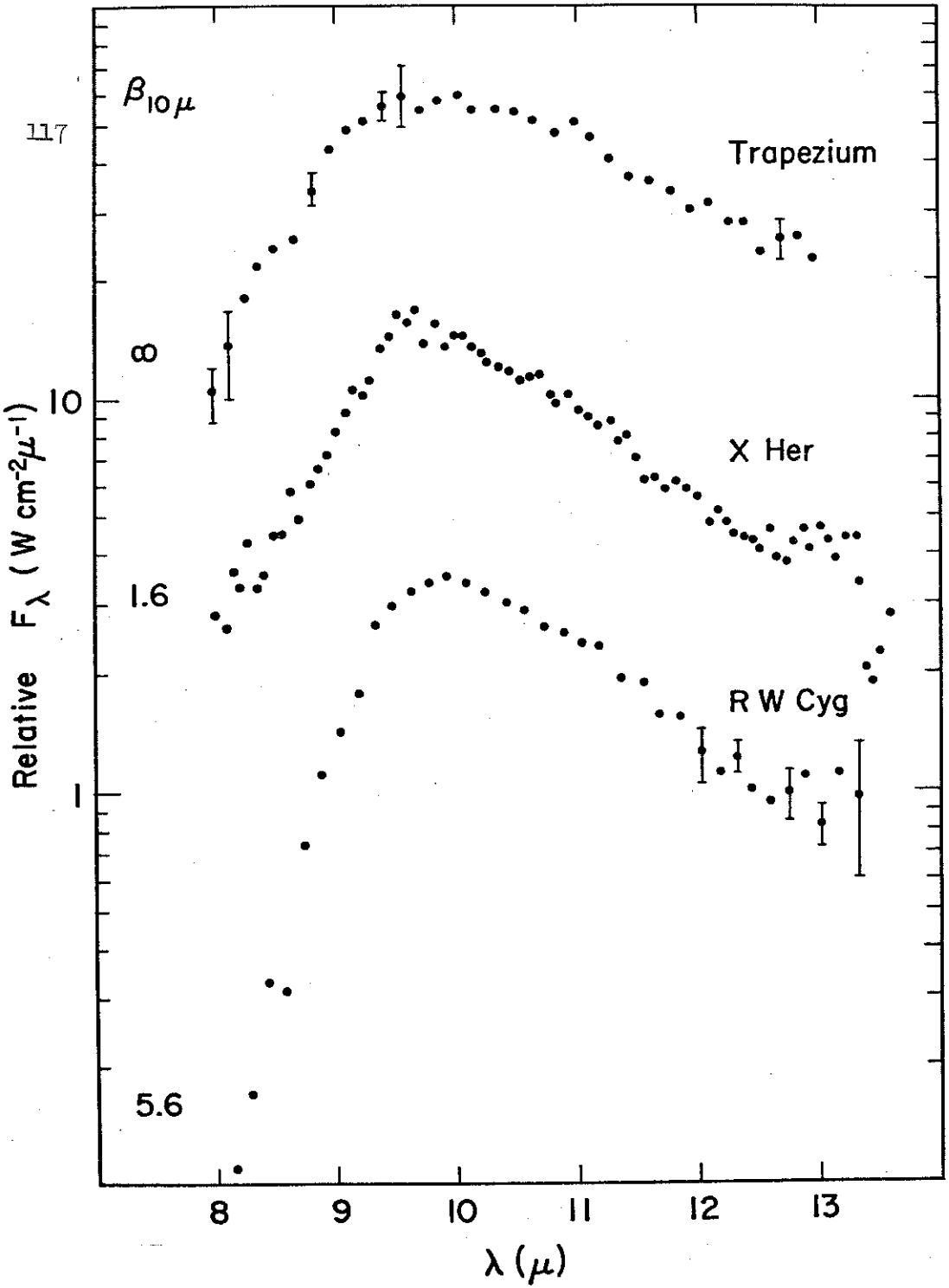

performed. The average error for all the points in this spectrum (adjacent points have been averaged) was $\sigma/S \sim \pm 5\%$ and error bars are shown if $\sigma/S \gtrsim \pm 10\%$. This spectrum essentially confirms the finding of Stein and Gillett (1969), i.e. the spectrum of the Trapezium is quite similar to the excess fluxes observed in late type M stars. The Trapezium is part of a galactic nebula where stars have recently been formed and are possibly still forming. Other hot field stars surveyed by Ney et al. (1973) don't show this characteristic excess emission so the emitting dust grains must either be part of the interstellar material which has condensed to allow the formation of stars here or possibly the dust is a by-product of star formation.

The slightly steeper rise to maximum at 9.7 μ and slower fall thereafter for the Trapezium compared to the first four Mira variables in Fig. 23 can be attributed, at least in part, to the lower temperature of the Trapezium dust -- the 11-18 μ color temperature of the Trapezium is ~ 200 °K while for the star excesses it is ~ 400-600 °K (Table 2b). Otherwise the spectra are, to within the ~ 5% measurement errors, essentially identical. The spectra of the semi-regular stars are also similar to the Trapezium, showing the peak at ~ 9.7 μ but a possibly steeper fall-off to either side. The subtraction procedure adopted should be most nearly valid for RW Cyg, it has the largest excess ($\beta_{10\mu} \sim 5.6$) of the M stars considered in this study so the true shape of the stellar continuum is much less important, especially for $\lambda > 10$ μ. The steeper spectrum

$\lambda > 10\,\mu$ may, as before, be due to hotter dust. The steeper spectrum $\lambda < 10\,\mu$ is less certain as the assumed stellar continuum is becoming more important here. It is significant, though, that before subtraction, the total flux of RW Cyg was approximately as steep as the Trapezium; if there is any stellar continuum it will be even steeper on subtraction. If real, the 8-10 μ steepness could not be due to the temperature effect (wrong sense) but could be due to (1) a slightly different material radiating (2) an additional smooth component to the radiation from the Trapezium becoming important at the shorter wavelengths. The near identity of the spectra $\lambda > 10\,\mu$ argues for the second explanation. The smooth component could be, for instance, due to "blackbody" grains such as graphite as discussed in a later section. The data here (one spectrum of RW Cyg) is insufficient to establish this rather subtle but possibly important point. What is needed is a highly accurate determination of the stellar continuum at $\lambda < 8\,\mu$, using spectra if possible, simultaneous with spectral measurements in the 8-13 μ region. Stars with large 10 μ spectral features but otherwise normal energy distributions would be the best cases, we suggest μ Cep and RW Cyg in the northern hemisphere as being the best and brightest for this. High spatial resolution measurements at $\lambda \sim 8$-13 μ to separate the star from the dust would be more direct but the necessary resolution, $\sim 0.05''$, has only been achieved to date by lunar occultation measurements of the brightest stars.

The suggestion that the excess emission in M stars found by Gillett et al. (1968) was due to small silicate mineral grains was

made by Woolf and Ney (1969). Silicates are a common terrestrial mineral composed of the anion SiO_n, $n > 2$, with metallic cation Fe, Mg, Ca, etc., in a crystal structure. There are many different types of silicates, each with its own characteristic spectrum, but they all show a resonance in the 10 μ region due to the stretching frequency of the Si-O bond and a second resonance in the 20 μ region due to the bending frequency of the O-Si-O bonds. The identification with silicates was thus strengthened by the discovery by Low and Krishna Swamy (1970) that α Ori, an M supergiant with typical "silicate" excess at 10 μ, had such a second feature at $\sim$ 20 μ. The second resonance is clearly shown for the Trapezium (Fig. 2, Ney et al. 1973), where there is no possibility of confusion with a stellar continuum. This identification with silicates is strengthened by the work of Gilman (1969) on the likely condensates in the circumstellar environment. He found that in an oxygen-rich atmosphere (i.e. $N_O > N_C$ as for M stars) the most likely mineral condensate was just this silicate material. The silicate which makes best use of the least abundant species, silicon, is $(Mg,Fe)_2SiO_4$ (olivene) for which the mass fraction for solar abundances if $f \sim 1/300$. Outside the earth, silicates are an important constituent of stony meteorites and are also found on the Moon (Perry et al. 1972). The silicate identification thus seems at least qualitatively reasonable; a positive identification would probably result if a sample of comet dust could be obtained -- some comets [Comet Bennett 1969i: Maas et al. (1970), Hackwell (1971b), Ney (1973); Comet Kohoutek 1973f: Forrest and Merrill (1974), Ney (1974), Merrill (1974)] show 10 μ and 20 μ

emission features which are quite similar to those seen around M stars and in the Trapezium.

ii) Expected Emission from Dust Grains

The flux at earth from a dust grain of radius a_i at a temperature T_i will be given by (Appendix A)

$$F_\lambda^i = \frac{\sigma_{abs}^i}{D^2} B_\lambda(T_i) = \frac{Q_{abs}^i(\lambda)\ \pi a_i^2}{D^2} B_\lambda(T_i) \quad , \qquad (V\text{-}1)$$

where D = distance, grain-earth, $B_\lambda(T_i)$ is the Planck function ($W/cm^2\ \mu$ ster) and $Q_{abs}^i(\lambda)$ is the grain absorptivity (= emissivity) at wavelength λ. In Appendix B the opacities of grains as a function of $\epsilon = m^2$ = the complex dielectric constant, grain size and shape is considered and it is shown that

$$\sigma_{abs}^i = \kappa_\lambda(\epsilon, L_j, a_i)\ M_i \quad , \qquad (V\text{-}2)$$

where κ_λ = mass absorption coefficient (cm^2/gm) M_i = mass of the grain, and the L_j are shape parameters of the grain, $L_j = 1/3$ for spheres. Further, for small grains, $2\pi a_i/\lambda \ll 1$, κ_λ is independent of grain size. Combing (V-1) and (V-2) we have

$$F_\lambda^i = \frac{\kappa_\lambda^i\ M_i\ B_\lambda(T_i)}{D^2} \quad . \qquad (V\text{-}3)$$

For an ensemble of grains in an optically thin cloud, the total flux from dust grains F_λ^d, will be the sum of the F_λ^i, i.e.

$$F_\lambda^d = \sum_i F_\lambda^i = \frac{M_d}{D^2} \langle \kappa_\lambda^i\ B_\lambda(T_i) \rangle \quad , \qquad (V\text{-}4)$$

where $M_d = \sum_i M_i$ is the total mass of dust radiating and $\langle \kappa_\lambda^i B_\lambda^i(T_i) \rangle = (\sum_i \kappa_\lambda^i\ B_\lambda(T_i) M_i)/M_d$ is the average over the cloud. We see that the physical parameters which will be important in determining the shape of the observed emission will be (1) the optical constants ϵ of the grain material(s), (2) the grain sizes and shapes, (3) the run of temperature through the cloud and (4) the optical depth of the cloud. The 11 -20 μ color temperatures of "silicate type" excesses of the stars in this study (Table 2b) are in the range 400-700 °K. Since the emissivity at 20 μ is less than at 11 μ for most silicate materials (Ney and Stein 1974, Chapter VIII), this implies grain temperatures in the range ~ 250-500 °K. It is seen from the black-body curves shown in Fig. 25 that Planck functions of these temperatures tend to be flat in the range 8-13 μ; if there is a distribution of grain temperatures, the average $\langle B_\lambda \rangle$ will be even flatter. Therefore, the temperature is of secondary importance in determining the shape of the observed emission, at most it can apply a tilt to the approximate relationship

$$F_\lambda^d \sim \langle \kappa_\lambda \rangle \quad , \qquad (V\text{-}5)$$

which will be used in the following sections.

iii) Silicates

In Fig. 25 are given the expected absorptivities (= emissitities) of lunar and meteoritic silicates and the selected blackbody functions discussed above. Curve A is the κ_λ for a lunar silicate (Moon Rock no. 14321) calculated for a = 0.2 μ sphere by Knacke and Thomson (1973) from the optical constants measured by Perry et al. (1972). Knacke and Thomson found this particular lunar sample to give the best fit to the observed emission from the Trapezium. The fit to our spectra (Fig. 23 and 24) is seen to fairly good except for (1) minor bumps and wiggles which don't show up in the observed spectra [even at the higher resolution $\Delta\lambda/\lambda \sim 0.2\%$) employed by Gammon et al. (1972), Treffers and Cohen (1974), and Treffers (1973)], and (2) a too rapid fall off longward of ~ 11 μ. These two deficiencies are actually quite general properties of most lunar and terrestrial silicates which have been measured. Hackwell (1971) studied the absorption of various ground-up silicate materials and found that some meteoritic silicates seemed to have (1) a smoother spectrum and (2) more opacity at longer wavelengths, than the terrestrial silicates he measured. Shown in Fig. 26 are his data for material from the Cold Bokkveld meteorite [(Curve B, type II carbonaceous chondrite, mostly olivene and "modified" olivene (Du Fresne and Anders 1962)] and from the Goalpara meteorite [Curve C; "ureilite," ~ 90% silicate (Urey and Craig 1953)].

The Cold Bokkveld material gives the best single material fit, with no additional assumptions, to the observed spectra. It

Fig. 25: Mass absorption coefficients of lunar and meteoritic silicate minerals and selected blackbody functions as described in the text. Curve A: Moon rock no. 14321 (Knacke and Thomson 1973; Perry et al. 1972); Curve B: Cold Bokkveld meteorite (Hackwell 1971); Curve C: Goalpara meteorite (Hackwell 1971); MIX 1: $\kappa_\lambda(\text{Mix 1}) = [\kappa_\lambda(A) + \kappa_\lambda(C)]/2$.

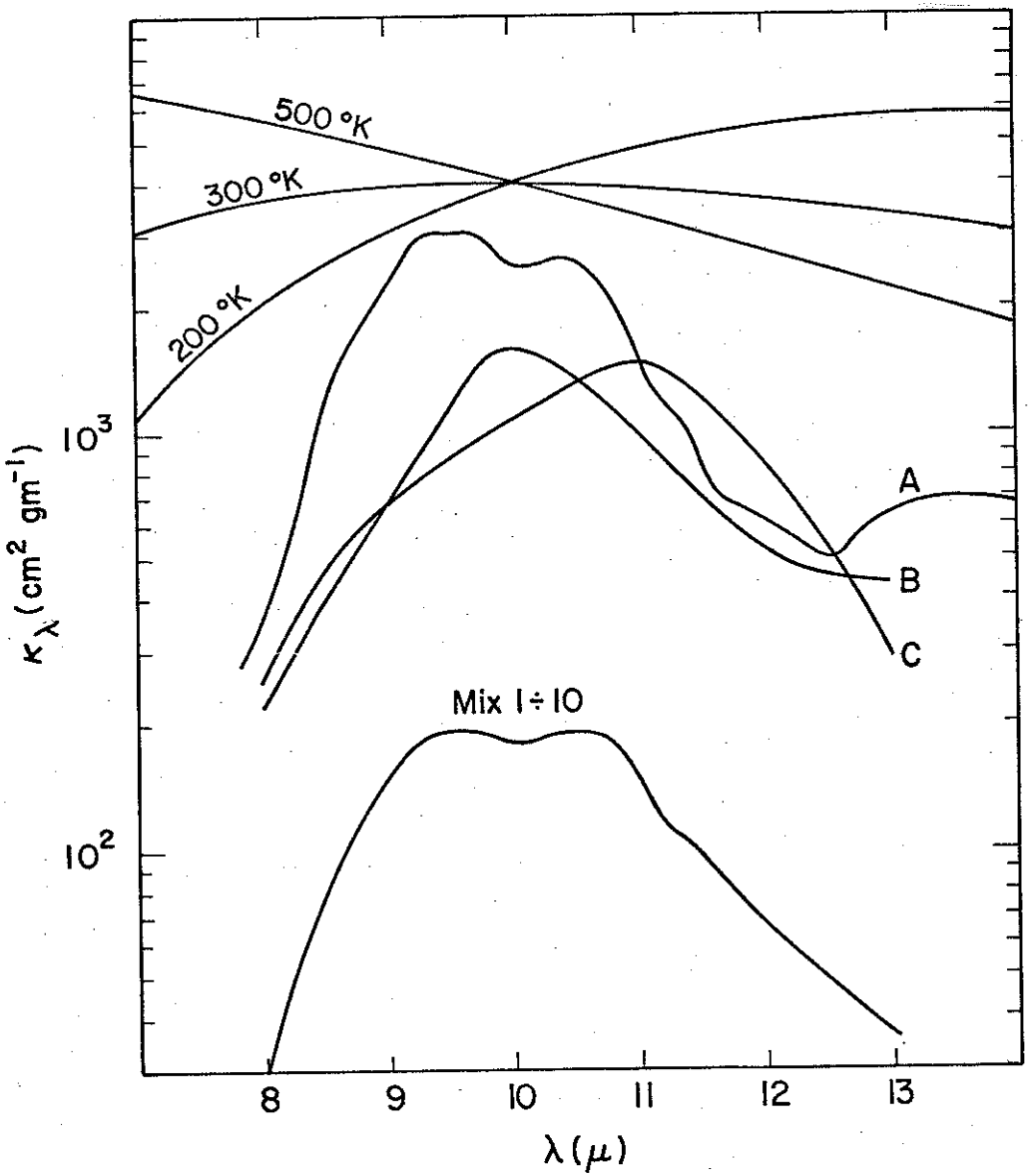

fits the spectra of X Her and RW Cyg (Fig. 24) quite well, but is somewhat too peaked to fit the Trapezium and the first four M stars in Fig. 23 -- a fit longward of 11 μ and shortward of 9.5 μ can be made but then there is too much emissivity in between. The effect of a mixture of minerals is also given in Fig. 25 -- the expected emissivity of equal parts of Moon rock no. 14321 spheres and the Goalpara mineral is shown (Mix 1). The addition of Goalpara ureilite boosts the emissivity at longer wavelengths and gives a better fit to the observed spectra.

Another effect which may be important in determining the observed spectra of silicate grains is their possibly non-spherical shapes. The observation of linear polarization of the Becklin-Neugebauer object in the Orion Nebula (Dyck et al. 1973) which was correlated with the 10 μ absorption feature attributed to cold silicate grains (Gillett and Forrest 1973) can most easily be understood in terms of absorption by aligned, non-spherical grains in our line of sight. Non-spherical silicate grains are also indicated by the work of Arrhenius and Asunmaa (1973) on the structure of the carbonaceous chondrite meteorite Allende. They found that the low density "matrix" or "ground mass" structure was actually made up of silicate flakes, ~ 0.1 μ x 0.1 μ x 0.01 μ, loosely adhering to each other. Again, samples of cometary dust might shed light on the likely shapes of circumstellar silicate condensates.

The importance of shape effects on grain opacities has been emphasized by Gilra (1972a). The effect of different shapes on the opacity is discussed in Appendix B; a general ellipsoidal particle

will have different polarizability and hence opacity depending on the orientation of the electric vector with respect to the grain axes. For small grains, the mass opacity $\kappa_\lambda(L_j)$ simplifies to eq. 8, Appendix B, where ϵ_1, ϵ_2 are the optical constants of the material and the L_j's are the (three) shape parameters of the grain, $L_j = 1/3$ for a sphere. Using the optical constant data for Moon rock no. 14321 from Perry et al. (1972) we have calculated the expected opacities as a function of the shape parameter L_j, the results for some shapes are given in Fig. 26. It is seen that since $\epsilon_1(\lambda) > 0$ for this material, there are no strong sharp resonances. The effect of a lower L_j is to (1) increase the overall emissivity and (2) push the peak emissivity to longer wavelengths. The first effect is easy to understand as small L_j corresponds to the electric vector along one of the longer axes of an asymmetric grain and hence higher polarizability and opacity. The second effect is due to the increasing importance of ϵ_2, which peaks at $\lambda = 11$ μ, in determining the shape of the resonance (eq. 8, Appendix B). The existence of some asymmetric grains, with $L_j < 1/3$ will thus (1) tend to smooth out the emissivity structure and (2) boost the emissivity at longer wavelengths. A simple mixture of one part sphere [L = (1/3, 1/3, 1/3)] plus three parts of asymmetric spheroid [L = (0.1, 0.35, 0.55)] denoted "Mix 2" is shown in Fig. 26. The resulting emissivity is almost identical in shape to "Mix 1" considered earlier, without the objectional bump at ~ 10.5 μ. It gives a closer representation, though not exact, of the observed spectra than spheres alone.

The grain size will also affect the emissivity; for large grains calculations are only tractable (Appendix B) for spheres, so

Fig. 26: Effects of particle shape and size on the absorption coefficient of a lunar silicate. L_j is the shape parameter, Mix 2 is the absorption coefficient for a mixture of shapes, and Mix 3 is the absorption coefficient for a mixture of equal masses of $a \leq 0.2$ μ and $a = 2$ μ grains as described in the text.

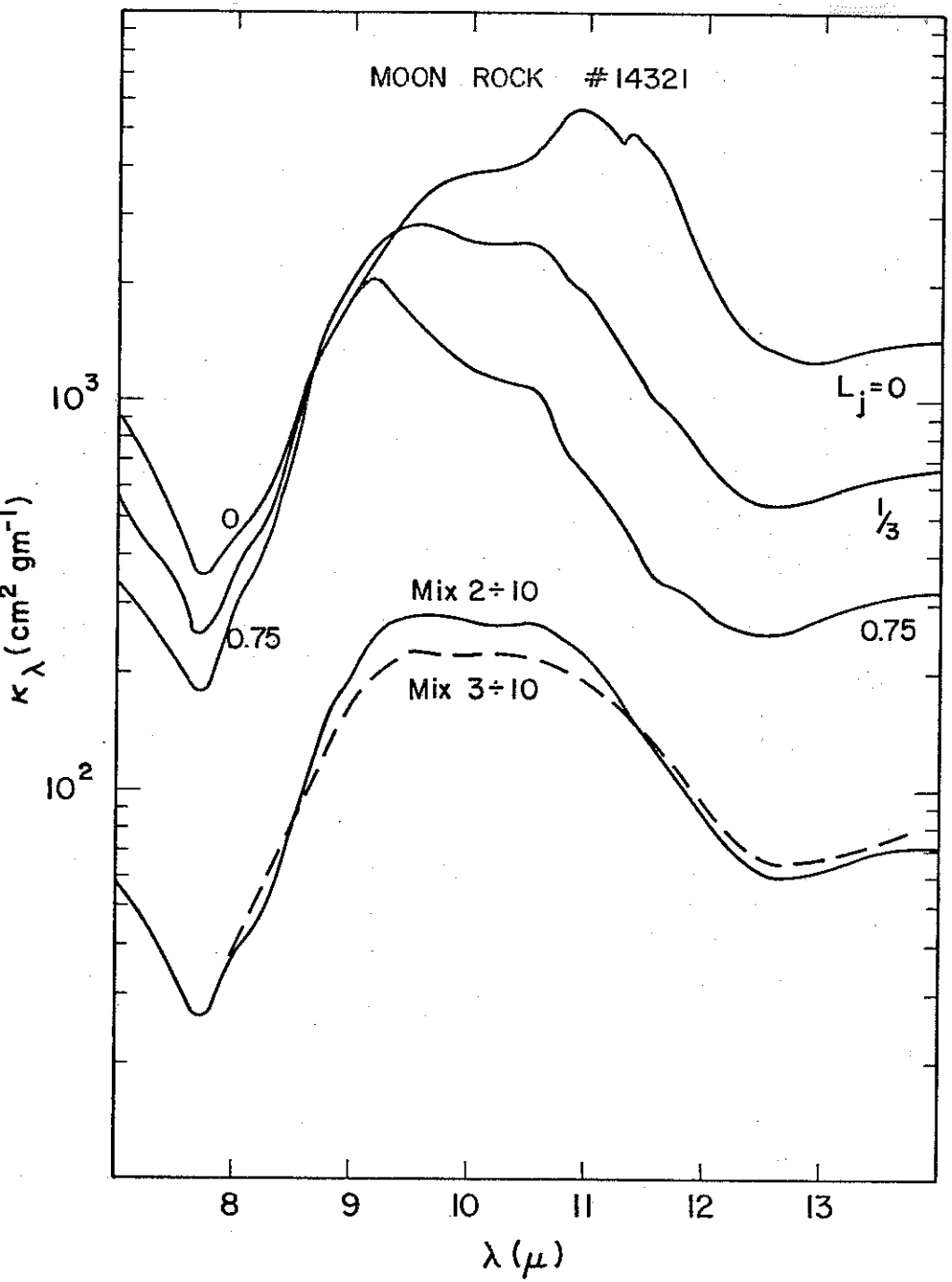

we will only consider large spheres here. The opacity for Moon rock no. 14321 in the 10 μ region is nearly that of small spheres for a, the grain radius, < 1 μ. For a ≥ 1 μ the opacity at λ ≃ 8 μ is unchanged, the peak opacity is decreased, and the opacity at longer wavelengths is increased; i.e. the 10 μ feature is flattened out. The result for a = 1 μ (i.e. $2\pi a/\lambda \simeq 0.63$) is nearly identical to the Curve "Mix 1" in Fig. 25. The result for a = 4 μ is shown in Fig. 27 in comparison to the spectrum of R Leo. The result for a mixture of equal masses of a ≤ 0.2 μ grains and a = 2 μ grains (="Mix 3") is given in Fig. 26; it provides the best fit to the observed silicate features of the mixes considered here. The question of the existence of some larger grains is uncertain; the interstellar grain models (Aanestad and Purcell 1973) and circumstellar polarization models (Shawl 1972) indicate a ≲ 0.1 μ, i.e. small grains. However, an admixture of larger grains, which would have relatively less opacity/mass and give nearly neutral extinction at visual wavelengths does not appear to be ruled out. The problem of growing such larger grains in the circumstellar environment may be more difficult.

In summary, by considering only a few reasonable physical effects, chemical composition, grain size and shape, a fairly good fit to the observed emission spectra in some M stars and the Trapezium can be obtained from the available data on lunar and/or meteoritic silicates. We consider this as supportive of the silicate hypothesis. It should be pointed out that whatever mechanism is invoked, it must be fairly ubiquitous, many stars showing nearly

identical spectra which are in turn nearly identical to the emission spectrum of the Trapezium which in turn provides a good fit to the 10 μ absorption features found in highly extinguished objects all over the galaxy (Gillett and Forrest 1973; Gillett et al. 1974; Aitken and Jones 1973; Merrill and Soifer 1974) and at the galactic center (Woolf 1972). Again, samples of comet dust could help answer some of these questions. In addition, further information about the optical constants of meteoritic silicates, such as the silicate flakes described by Arrhenius and Asunmara (1973), or on other amorphous silicate material, would aid in the interpretation of the observed spectra.

iv) R Leo

The excess emission from R Leo (Fig. 23) seems to be significantly different than some other M-Miras and the Trapezium in that there is relatively less flux $\lambda < 9$ μ and more flux $\lambda > 11$ μ than for these other objects. These peculiarities have been noted by Hackwell (1971, 1972) and Treffers and Cohen (1974); the difference can't entirely be due to the normalization of the stellar continuum which is subtracted because the spectrum of R Leo is different than, say, oCet even before subtraction. To improve the statistical significance, excesses from the three available spectra of R Leo (taken in January, March, and May of 1972) have been derived by subtraction as described above, normalized and averaged together; the result is shown in Fig. 27 with error bars plotted if $\sigma/S \geq \pm 10\%$ plus some typical error

Fig. 27: Spectral energy distribution of the average excess emission from R Leo compared to the absorption coefficient of large lunar silicate spheres and the possible effect of optical depth on the Trapezium spectrum as described in the text.

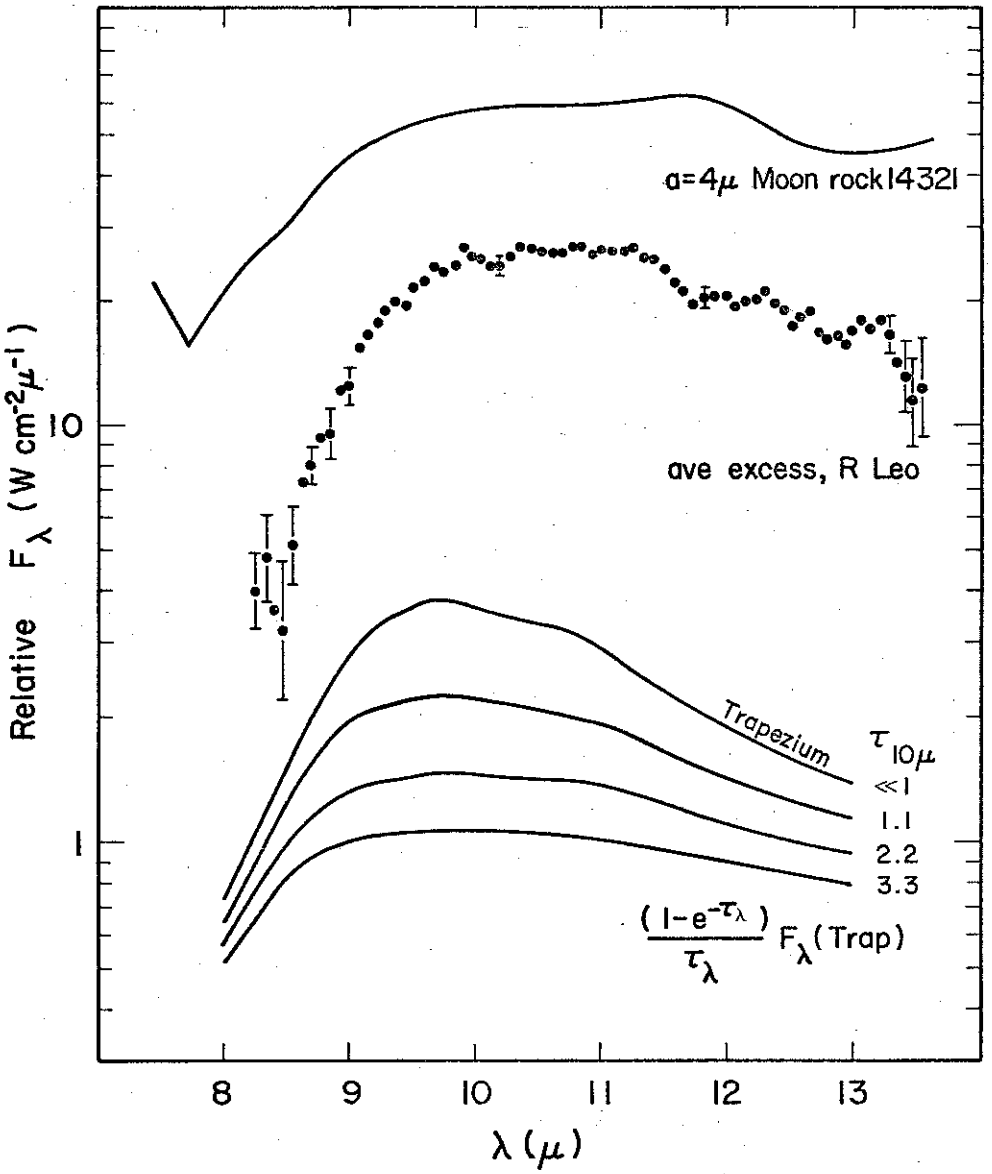

bars in the range 9-13 μ. The features noted above are evident and the ~ 15% "dip" centered at ~ 11.8 μ mentioned earlier is still present. The "dip," if real, could be due to a grain material of different chemical composition, as there is no such dip in the Trapezium or the Trapezium-like excesses, or, alternatively, an ~ 15% dip in the stellar continuum. The "dip" is not seen in the (albeit noisier) spectrum of Hackwell (1971, 1972) so it may be spurious. We will consider possible physical effects which might explain the different spectrum of R Leo.

First, assume the grain material is the same for R Leo as for, say, oCet and the Trapezium. Then the grain temperature, size and shape of the grains, and the optical depth of the shell may affect the observed spectrum.

First consider grain temperature: to give the observed deficiency for $\lambda < 9\ \mu$ and enhancement for $\lambda > 11\ \mu$, a grain temperature < 200 °K (see Fig. 25) would be required. However, the 11-20 μ color temperature of the excess in R Leo is (Table 2b) ~ 500 °K, and this implies, as discussed earlier, probable grain temperatures in the range ~ 300-400 °K. Further, this color temperature is typical of other M stars and much higher than for the Trapezium; therefore, independent of the emissivity ratio $\epsilon_{11\mu}/\epsilon_{20\mu}$, a much lower grain temperature for the dust around R Leo relative to other M stars and the Trapezium is ruled out if the grain material is the same. Thus, grain temperature alone is insufficient to explain the observed spectrum.

The 10 μ emission from the Trapezium is known to be optically thin ($\tau_{10\mu} \sim 10^{-4}$, Ney et al. 1973). If the optical depth is increased, the emission peak will tend to be flattened out. As a first approximation, neglecting the radiation transfer problem in an optically thick cloud, we consider the radiation from the Trapezium to be given by

$$F_\lambda^{Trap} = \tau_\lambda \, \Omega_{beam} \, \langle B_\lambda \rangle \quad ,$$

where $\tau_\lambda \ll 1$, Ω_{beam} is the angular size of the observing diaphragm and $\langle B_\lambda \rangle$ is the average Planck function for the beam used. Then, if $\langle B_\lambda \rangle \sim$ const λλ 8-13 μ, $\tau_\lambda \sim F_\lambda^{Trap}$ and the effect of increasing the optical depth will be, neglecting temperature structure in the nebula, given by

$$F_\lambda(\tau) = (1 - e^{-\tau_\lambda}) \, \Omega_{beam} \, \langle B_\lambda \rangle$$

$$\simeq \frac{1 - e^{-\tau_\lambda}}{\tau_\lambda} \; F_\lambda^{Trap} \; (\tau = 0) \quad .$$

The resulting spectra, with $\tau_\lambda \sim F_\lambda^{Trap}$(observed), for different values of $\tau_{10\mu}$ is shown in Fig. 27. The curve for $\tau_{10\mu} \ll 1$ corresponds to the observed Trapezium spectrum. It is seen that $\tau_{10\mu} \sim 2$-3 is required to give the necessary enhancement at longer wavelengths. In this case the simple subtraction of stellar continuum is no longer valid -- the continuum will be modified by the opacity of the envelope. The possibility of optical depth as the sole explanation of the long wave excess appears to be ruled out by (1) lack of corresponding increase at $\lambda < 9\,\mu$ in the observed

spectra and (2) the fact that R Leo has, if anything, less bolometric excess than the average Mira variable; if the shell were going optically thick at 10 μ we would expect an increased optical depth at 1.5 μ and therefore more absorption and re-emission of starlight by the shell (i.e. larger α). This is not observed (Tables 2a, b).

Grain size and shape will affect the emissivity. Using Moon rock no. 14321 as an example, we see (Fig. 26) that shape alone is insufficient to explain the emission longward of 11 μ. The calculated emissivity for a = 4 μ grains of Moon rock no. 14321 is shown in Fig. 27; the flatter spectrum with emission at longer wavelengths is just what is needed to explain the R Leo excess. However, the more rapid fall off $\lambda < 9\,\mu$ is not reproduced, but this feature is sensitive to the level of the assumed continuum of the star for R Leo. This requires very large grains, more than 10 times the size normally thought to exist in circumstellar and interstellar space. In addition, the intrinsic polarization of R Leo doesn't suggest such large grains (Shawl 1972). Large grains appear to be one possibility for explaining the observed spectrum, but questions such as other observable consequences of large grains and the problem of growing such grains around stars would have to considered also.

The chemical composition of grains will certainly affect the spectrum. However, it is not trivial to find a silicate material, which appear to be the most likely circumstellar condensates, which give as much emission $\lambda > 11\,\mu$ as seen in R Leo. In addition, if large grains and/or a different chemical composition are invoked, one has to explain how they occur in R Leo, which is believed to be a

perfectly normal M-type Mira, and not, say, oCet or R Cas. Further, the mechanism can't be too prevalent because there is little if any of this material present in the presumably interstellar dust grains of the Trapezium. A larger grain albedo 1-5 μ is a possible alternative.

The final possibility which will be considered is deviation of the stellar continuum from the assumed $\sim$ 2500 °K blackbody. Since the peculiar R Leo type spectrum only occurs in stars with small excess (i.e. $\beta_{10\mu} \lesssim 1$), this seems entirely possible. In stars with a large excess, i.e. $\beta_{10\mu} \geq 2.5$ as for R Cas, RW Cyg, μ Cep, the derived excess is seen to be quite similar to the Trapezium. There are, however, some M stars with small excess, i.e. oCet, $\beta_{10\mu} \sim 1.25$, whose derived excess isn't noticeably peculiar -- one now has to explain why only some stars have peculiar continua. On the other hand, it is significant that the "excess" as derived by subtraction is always positive, $F_\lambda^{exc} > 0$; whereas an apparently negative "excess" would be possible for a sufficiently depressed stellar continuum. This question could be resolved by high spatial resolution measurements to separate the stellar and circumstellar contributions to the observed flux.

We conclude that large grains, a different chemical composition of the grains, or a non-blackbody stellar continuum may be the cause(s) of the anomalous spectral excess of R Leo.

B. S Stars

The excesses of the "pure" S star R And (Sp:S6,6e), the S(M) star χ Cyg (Sp:S7,1e) and the M(S) star T Cas (Sp:M6e, S star characteristics noted by Spinrad and Newburn 1965) derived as for the M stars is shown in Fig. 28, along with the total observed flux from the "pure" S star W Aql (Sp:S3,9e). For W Aql the energy distribution could be described by an $\sim$ 1500 °K blackbody plus an excess described by an $\sim$ 550 °K blackbody at longer wavelengths. If the cool blackbody is ascribed to circumstellar emission from dust, the fractional amount of energy from dust is $\alpha(550\ °K) \sim 0.66$ and $\beta_{10\mu} \sim 13$, so contribution from the star is negligible here. The spectrum of W Aql is seen to be quite smooth. A "silicate" emission feature, if present, is $\lesssim 10\%$ of the continuum.

The other S stars have excesses which are similar to the M stars considered earlier. For χ Cyg and especially T Cas the peak at 10 μ is less pronounced and there is relatively more excess at longer wavelengths; the same considerations which apply to R Leo will apply here.

In summary, for some S stars the excess is quite similar to that observed for M stars; an explanation in terms of silicate grains is indicated. For W Aql, the excess is smooth and blackbody-like, similar to the spectrum of R CrB (Chapter VI). In addition, the bolometric excess, $\alpha \sim 0.66$, is much larger than the other M and S stars considered here and is more like that seen in the carbon Miras and R CrB. An explanation in terms of silicate grains in an optically thick cloud is possible but the optical depth (Fig. 27) necessary to suppress the 10 μ "silicate feature" is on the order $\tau_{10\mu} \gtrsim 3$. Alternatively, a different, "blackbody" grain material could be present as is seen in R CrB and the carbon Miras.

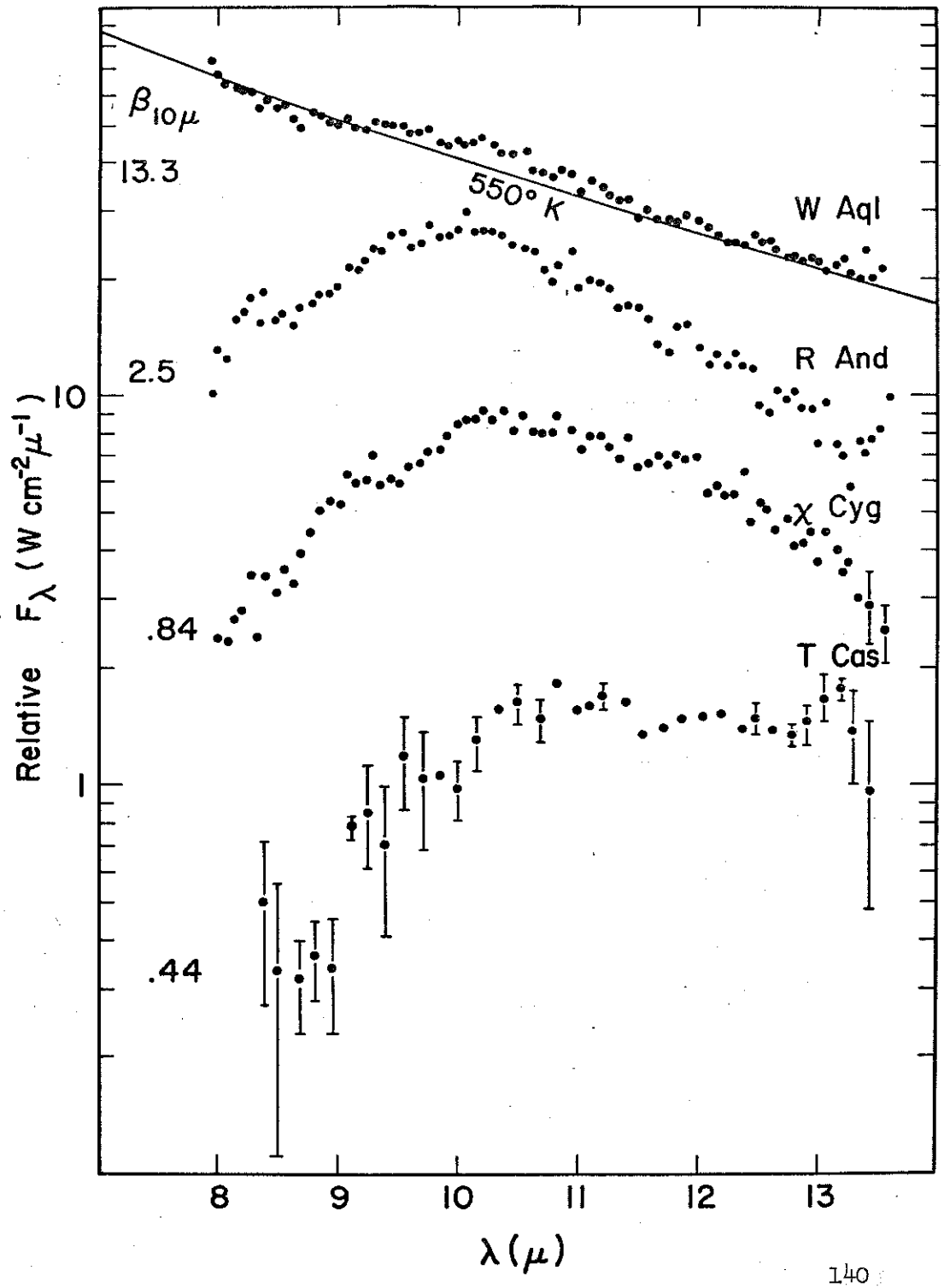

Fig. 28: Spectral energy distribution of excess emission from S and M(S) stars. The total observed flux from W Aql is plotted as discussed in the text.

C. Carbon Stars

i) Observed Emission

The spectra of the carbon stars in the 8-13 μ region consists of a smooth continuum on which is superimposed an emission feature in the range λλ 10-12.5 μ. In the case of the Mira variables and V Hya it is believed (Fig. 14, 15, Chapter IV) the continuum is in excess of that expected from the star alone and is ascribed to radiation from circumstellar grains with opacity at all wavelengths observed. Such "blackbody" grains also would explain the broad, smooth spectra seen in W Aql and R CrB. The additional emission feature λλ 10-12.5 μ has been observed by Hackwell (1971, 1972) and Treffers and Cohen (1974) and attributed by Treffers and Cohen (1974) and Gilra (1972a,b) to radiation from small silicon carbide (SiC) grains.

The total observed spectrum for V Cyg is shown at the top of Fig. 29. It is seen to consist of the aforementioned smooth continuum, with a possible downturn $\lambda < 8$ μ, plus the emission feature. The continuum $\lambda < 10$ μ and $\lambda > 12.5$ μ for the carbon stars has been fit with a single blackbody function, as shown in the figure for V Cyg. The continuum is then subtracted, the resultant excess emission features are also shown in Fig. 29. The parameter $\beta_\lambda \equiv [F_\lambda(\text{observed}) - F_\lambda(\text{continuum})]\, F_\lambda^{-1}(\text{continuum})$ measures the strength of the emission feature relative to the continuum, $\beta_{11\mu}$ reaches a maximum of ~ 0.75 for V Cyg and T Dra and a minimum of ~ 0.23 for the extreme infrared carbon star IRC +10216. In addition,

Fig. 29: Spectral energy distribution of the emission feature of carbon stars and the total flux from V Cyg. The average of the normalized excesses of V Cyg, T Dra, R Lep, and V Hya is plotted with error bars if $\sigma/S \geq \pm 6\%$.

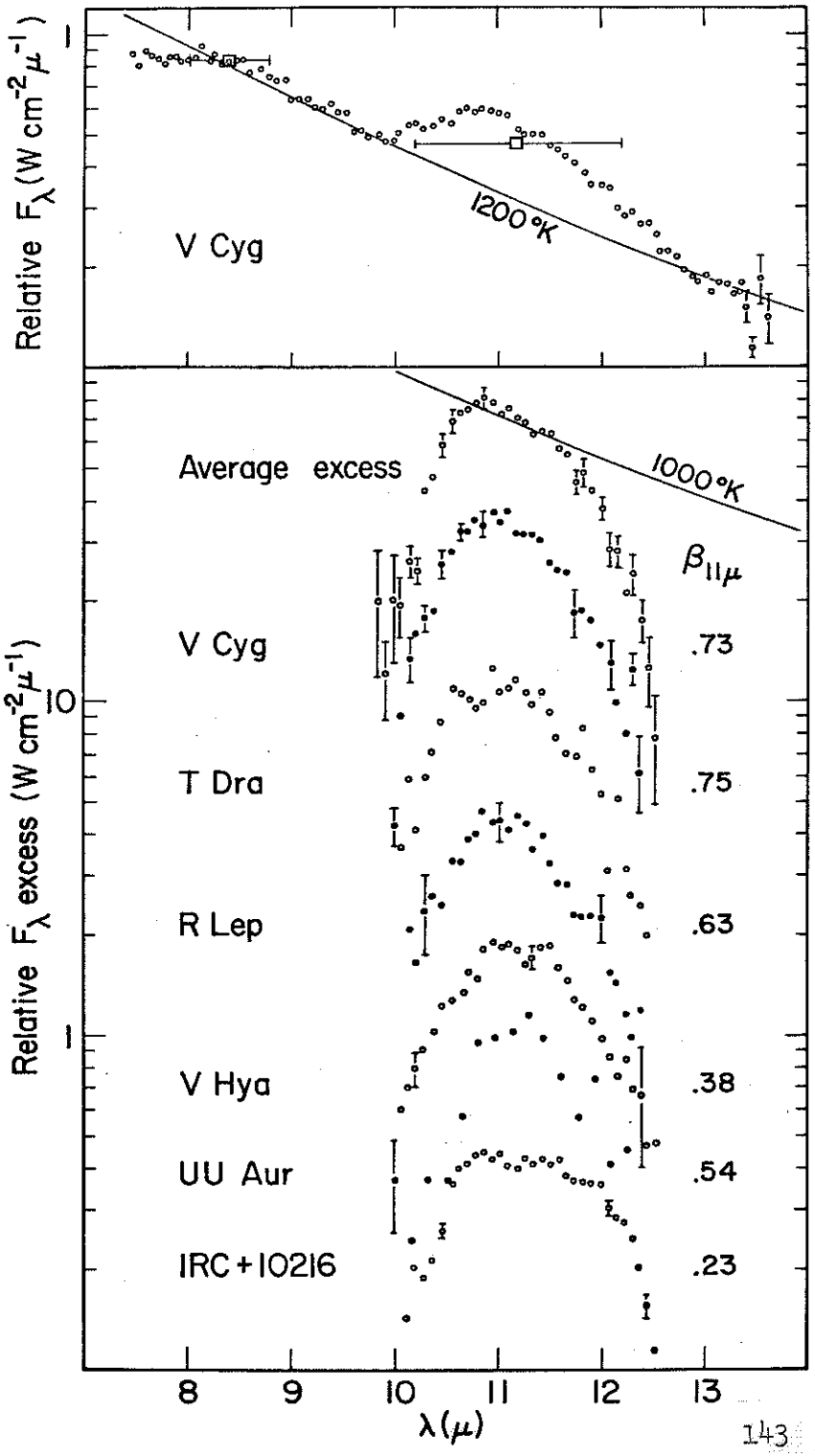

143

the normalized excesses of V Cyg, T Dra, R Lep, and V Hya have been averaged and are shown in Fig. 29 with error bars if $\sigma/S \geq \pm 6\%$.

The emission features are all contained between ~ 10 μ and ~ 12.5 μ. The composite average shows a smooth "bump" with a broad peak at λ ~ 11 μ, a possible "step" at λ ~ 10.3 μ before the steep rise to maximum, and a relatively slower rolloff longward of maximum. The higher resolution ($\Delta\lambda/\lambda \sim 0.2\%$) employed by Treffers and Cohen (1974) revealed no further structure in this feature. The identification with silicon carbide comes from (1) the well-defined extent of the emission discussed in Section ii)(a) below; (2) the prediction of Gilman (1969) that SiC would, along with graphite, be the most likely condensate for stars with $N_C > N_O$, i.e. carbon stars. In addition, Gilra (1972b) has suggested that the well-known "violet depression" in late-type carbon stars could be due to absorption by SiC grains; the absorption edge of SiC occurs at λ ~ 0.43 μ.

ii) Expected Emission

(a) SiC

Measurements of the optical constants of pure SiC by Spitzer et al. (1959a,b) show that its optical properties longward of the intrinsic absorption edge at λ ~ 0.43 μ are particularly simple. The main features are described in terms of a single, strong fundamental lattice absorption band at 12.6 μ. For small grains, the peak emissivity (Appendix B) will depend on the shape parameter L_j and will range from $\lambda_{max}(L_j = 0) = 12.6\ \mu = \lambda_{transverse}$ where ϵ_2, the

imaginary part of the dielectric constant, peaks to $\lambda_{max}(L_j = 1) = 10.3\ \mu = \lambda_{longitudinal}$ where $\epsilon_1 = 0$. Thus one main feature of the observed emission feature, its limited extent, is explained. Further, Spitzer et al. (1959a) show there are no other strong resonances for $\lambda > 12.6\ \mu$ so the lack of features at $20\ \mu$ is also understood.

The mass absorption coefficient for a sphere, $L_j = 1/3$, is shown in Fig. 30. The emissivity is in the form of a sharp resonance, of approximately Lorentzian line shape,

$$\kappa_\lambda \simeq \frac{\kappa_{max}}{1 + \left[\frac{2(\lambda - \lambda_o)}{\Delta\lambda}\right]^2} \quad ,$$

centered at $\lambda_o = 10.7\ \mu$ and with a full width half maximum given by $\Delta\lambda \sim 0.06\ \mu$. For a general ellipsoidal grain with three shape parameters, there will be 3 resonances, each with its own set of parameters λ_o, κ_{max}, $\Delta\lambda$. For $1 \geq L_j \geq 0$ the λ_o lie between $\lambda_{long} \leq \lambda_o \leq \lambda_{trans}$, the κ_{max} lie between $2 \times 10^4\ cm^2/gm \leq \kappa_{max} \leq 8.5 \times 10^5\ cm^2/gm$, and the $\Delta\lambda$ lie between $0.05\ \mu \leq \Delta\lambda \leq 0.08\ \mu$. For non-ellipsoidal grains or a mixture of shapes these strong resonances will tend to be washed out. The results for two particular shape mixtures taken from Treffers and Cohen (1974) is shown in Fig. 30. It is seen that a smooth distribution in absorptivity between $10.3\ \mu \leq \lambda \leq 12.6\ \mu$ can be explained by a smooth distribution of shapes; it seems reasonable that by consideration of shape effects alone, a fair representation of the observed spectra (Fig. 29) may be attained.

Fig. 30: Mass absorption coefficients for small silicon carbide grains and graphite spheres. λ_L, λ_T refer to the longitudinal and transverse resonance wavelengths of silicon carbide described in the text and the shape mixtures ("All shapes," "Prolate shapes") are from Treffers and Cohen (1974).

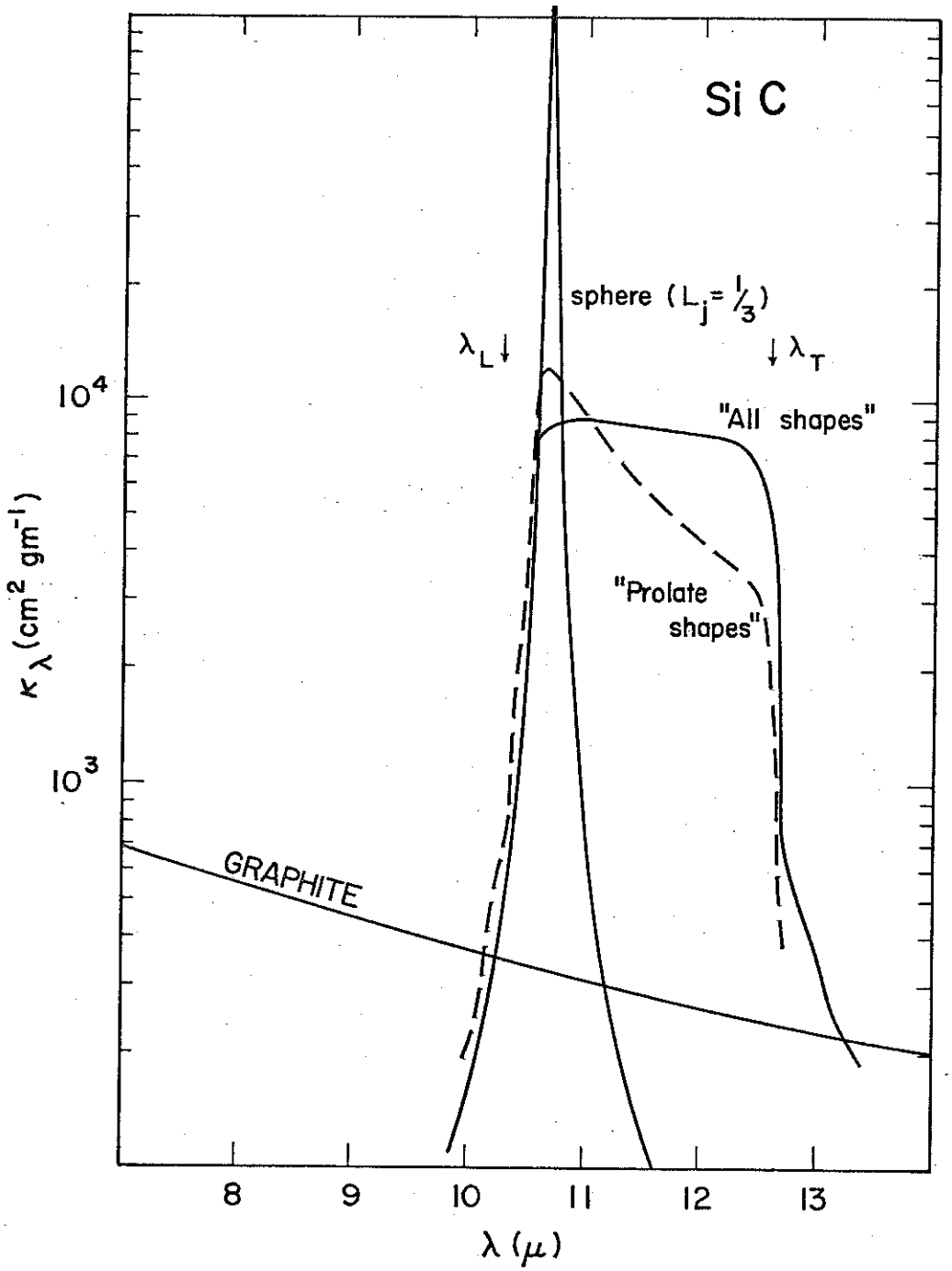

Other physical effects which may be important in determining the observed spectra are temperature, optical depth, grain size, and crystal impurities and/or imperfections. The temperature of the SiC grains is completely unknown -- there is no color temperature as for silicate grains and we only know a priori that $0 \leq T_{grain} \leq T_{vapor}$, where T_{vapor} is the vaporization temperature for SiC, 1700 °K (Gillman 1969). Because the wavelength range is small a temperature can only apply a tilt to the spectrum, such a tilt is seen between the composite average spectrum and that of IRC +10216 in Fig. 29. This is expected because the blackbody temperature needed to fit the "blackbody" excess in IRC +10216 is lower ($T \sim 600$ °K) than that needed to fit the "blackbody" excess in the other carbon Miras here ($T \sim 1000$ °K).

Optical depth will tend to flatten a peaked spectrum (see Fig. 27). It will be hard to distinguish between the effects of optical depth and the effects of different distributions of shapes, or possibly non-ellipsoidal shapes. If the optical depth is considerable, $\tau_{11\mu} \gtrsim 1$, then the method adopted here to derive the excess emission is not correct; the "continuum" will be modified in the 10-12.5 μ region by the absorption of SiC in the shell.

Since the peak strength of the absorption feature of SiC grains is very large, $\kappa_{max} \sim 10^5$ cm^2/gm, grain size effects will be important even for moderate grain sizes as the individual grain becomes optically thick. Treffers (1973) has reported the work of Gilra which shows that for a = 1 μ spheres, there will be, in addition to the primary resonance at ~ 10.7 μ, a second absorption

peak which is even larger at ~ 13.1 μ. No such excess λ > 13 μ is observed so the SiC grains around carbon stars must be smaller than 1 μ.

We conclude that small silicon carbide grains are probably responsible for the λλ 10-12.5 μ emission feature observed in late-type carbon stars. The smooth nature of the peak implies that non-spherical grains must be present; a smooth distribution of shapes between $L_j = 0$ and 1 or possibly non-ellipsoidal grains are required to explain this feature.

(b) Graphite

The smooth "blackbody" excess seen in carbon stars (Fig. 14, 15, 29) requires a grain material with opacity at all wavelengths. The most likely material, both from the standpoint of abundance [f(C) ~ 1/300] in the carbon star atmosphere and likelihood of condensation in the circumstellar environment around carbon stars (Hoyle and Wickramasinghe 1962; Gilman 1969) is solid carbon. Solid carbon comes in many forms and it is unknown which will occur; we will assume here that the carbon condenses as graphite.

Graphite grows in a hexagonal lattice with the DC conductivity parallel to the "C" axis (i.e. perpendicular to the hexagonal planes) $\sigma_{||} \sim 3 \times 10^3$ smaller than the conductivity perpendicular $\sigma_{\perp}$. This means the optical properties will be anisotropic, acting like a conductor for $E_{\perp}$ and a dielectric for $E_{||}$. The optical constants for E-field perpendicular to the "C" axis (E-vector in the "basal" =

hexagonal plane), $E_{\perp}$, has been measured by Taft and Philipp (1965). Additional work on the anisotropy and dependence on surface structure and temperature of the optical properties has been done by Autio and Scala (1966). Calculations (Appendix B) of the absorption coefficient for graphite using the data of Taft and Philipp have been made; the calculations apply to the (two) directions parallel to the hexagonal planes, the (one) direction perpendicular to the plane will probably have a much smaller absorption coefficient, at least for $2\pi a/\lambda < 1$.

For small grains, the data of Taft and Phillip imply for $\lambda \gtrsim 3\ \mu$, $L_j > 0$ (Appendix B)

$$\kappa_\lambda \sim \frac{1}{L_j^2}\ \frac{1}{\lambda^2} \quad ,$$

i.e. the absorptivity (emissivity) goes as $\sim 1/\lambda^2$. The exact result for $E_{\perp}$ in small spheres ($L_j = 1/3$) for λλ 7-14 μ is given in Fig. 30. Over a short wavelength interval, small grains at a single temperature may mimic a blackbody spectrum. Over a larger wavelength interval, however, the emission will (1) be narrower than a blackbody, (2) fall off more rapidly ($F_\lambda \sim 1/\lambda^6$) at long wavelengths than a blackbody ($B_\lambda \sim 1/\lambda^4$). The observed ~ blackbody shape, i.e. even out to 20 μ, the longest wavelength observed, the flux doesn't fall as fast as $1/\lambda^6$, could be due to (1) a distribution of temperatures in the envelope [i.e. such that $\langle \kappa_\lambda B_\lambda \rangle \sim B_\lambda(T_{BB})$ (eq. V-4)], (2) optical depth; an isothermal, optically thick shell of angular size Ω_{shell} would give a flux

$$F_\lambda^{shell} = (1 - e^{-\tau\lambda})\,\Omega_{shell}\,B_\lambda(T_{shell})$$

$$= \Omega_{shell}\,B_\lambda(T_{shell}),\quad \tau_\lambda \gg 1$$

(3) Grain size. Larger grains will have an opacity given by $\kappa_\lambda \sim$ const for $2\pi a/\lambda > 1$ and $\kappa_\lambda \sim 1/\lambda^2$ for $2\pi a/\lambda < 1$. The long wave opacity is enhanced over the small sphere value for $2\pi a/\lambda \lesssim 1$. This will have two effects: (a) grains at a single temperature will give a blackbody spectrum for $\lambda < 2\pi a$ but eventually will fall off rapidly thereafter. To explain a blackbody out to $\lambda = 10\ \mu$ requires $a \sim 1.5\ \mu$ grains. To explain a blackbody out to $\lambda = 20\ \mu$ requires $a \sim 3\ \mu$ grains. These are larger than the grains thought to exist in interstellar and circumstellar space ($a \lesssim 0.1\ \mu$) (b) The larger grains will come to a lower temperature due to their reduced ratio $(\epsilon_{vis}/\epsilon_{IR})$ as described in Appendix A. This will enhance their contribution relative to small grains at longer wavelengths but will increase the relative mass of large grains (eq. V-4) required. (4) A combination of (1)-(3).

In summary, it appears that graphite grains are good candidates for the source of the "blackbody" excesses seen in carbon stars (also R CrB and, possibly, W Aql). The abundance is large, condensation is expected, the emissivity is broad and smooth as desired, and the observed blackbody shape may result from the reasonable physical effects discussed above. The identification here is necessarily not definite because there are no characteristic features which identify graphite in this wavelength range. If the downturn $\lambda < 8\ \mu$ seen in some carbon stars is real (see Fig. 29, V Cyg), then it could give

more information about the radiating material. In addition, the narrow 3.1 μ absorption feature seen in all carbon stars observed to date (Gaustad et al. 1969; Johnson and Mendez 1970; Gillett and Forrest 1974; Merrill 1974b), including some with energy distributions which indicate large excess even at 3 μ, may indicate something about the grain material or the conditions in the circumstellar envelope where the grains reside. A positive identification with graphite would probably result if the 2200 Å absorption feature which is characteristic of the interstellar extinction curve and has been attributed to small graphite grains (Aanestad and Purcell 1973) were observed. However, these stars are cool and, in addition, have the aforementioned violet deficiency which would make this observation very difficult if not impossible. Samples of comet dust might shed some light on this; in addition to the silicate emission features at 10 μ and 20 μ there is also an ~ blackbody continuum [Comet Bennett 1969i: Maas et al. (1970), Ney (1973); Comet Kohoutek 1973f: Forrest and Merrill (1974), Ney (1974), Merrill (1974)]. In the oxygen-rich ($N_O > N_C$) solar nebula, solid carbon is not likely to condense but some of the solid material in comets could be primordial. In the case of meteorites, the "carbonaceous chondrite" type are notable for containing free carbon (Urey and Craig 1953).

D. Spectra Vs. Time

To supplement the light curves (broad band fluxes vs. time) presented in Chapter IV, spectra vs. time for oCet, R Cas and μ Cep

are presented in Fig. 31. The total observed flux, with arbitrary vertical normalization, is plotted vs. wavelength with time increasing downward. The blackbody curves are typical stellar continua, referring to the spectrum just above, which would be subtracted to derive the excesses discussed in the earlier section. The spectra of R Cas (late M Mira), covering the time November 1969 - September 1973 and phases 0.14-0.86, show no large change in the strength of the "silicate feature" centered at $\lambda \sim 9.7\,\mu$ relative to continuum with time. Likewise the earlier spectrum of μ Cep (early M supergiant) taken by Gillett et al. (1968) on 17 October 1967 UT agree well with the spectrum obtained here in June 1973. In addition, broad band observations at intermediate times indicate only small variations in actual flux for this star -- μ Cep is another semi-regular variable which has maintained a stable dust shell over the ~ 6 years of observation.

The spectra of oCet, on the other hand, indicate a decrease in the strength of the silicate feature with time between the earlier (17 October 1967 UT) observations of Gillett et al. (1968) and the present series (December 1971 - December 1973). The present series are probably consistent with a constant spectral shape, the main differences being in the 9-10 μ region where the atmospheric ozone absorption can affect the corrected spectrum as described in Chapter II. The difference between the earlier spectrum and the present series is believed to be significant; if the spectra are normalized at $\lambda \sim 8\,\mu$, there will be excess at all wavelengths $\lambda > 8\,\mu$. In addition, the early spectrum of oCet was taken on the same night with

Fig. 31: Spectral energy distribution as a function of time from oCet, R Cas and μ Cep. The dates of observation and visual phases for the various spectra are as follows:

	oCet		R Cas		μ Cep	
	Date (UT)	Phase (N)	Date (UT)	Phase (N)	Date (UT)	Phase
a	17 Oct 67	0.96(- 4)	22 Nov 69	0.86(- 1)	17 Oct 67	--
b	13 Dec 71	0.45(1)	13 Nov 70	0.71(0)	17 June 73	--
c	10 Jan 72	0.54(1)	17 Dec 71	0.64(1)		
d	4 Nov 72	0.41(2)	4 Nov 72	0.39(2)		
e	4 Dec 72	0.50(2)	21 Sep 73	0.14(3)		
f	18 Dec 73	0.64(3)				

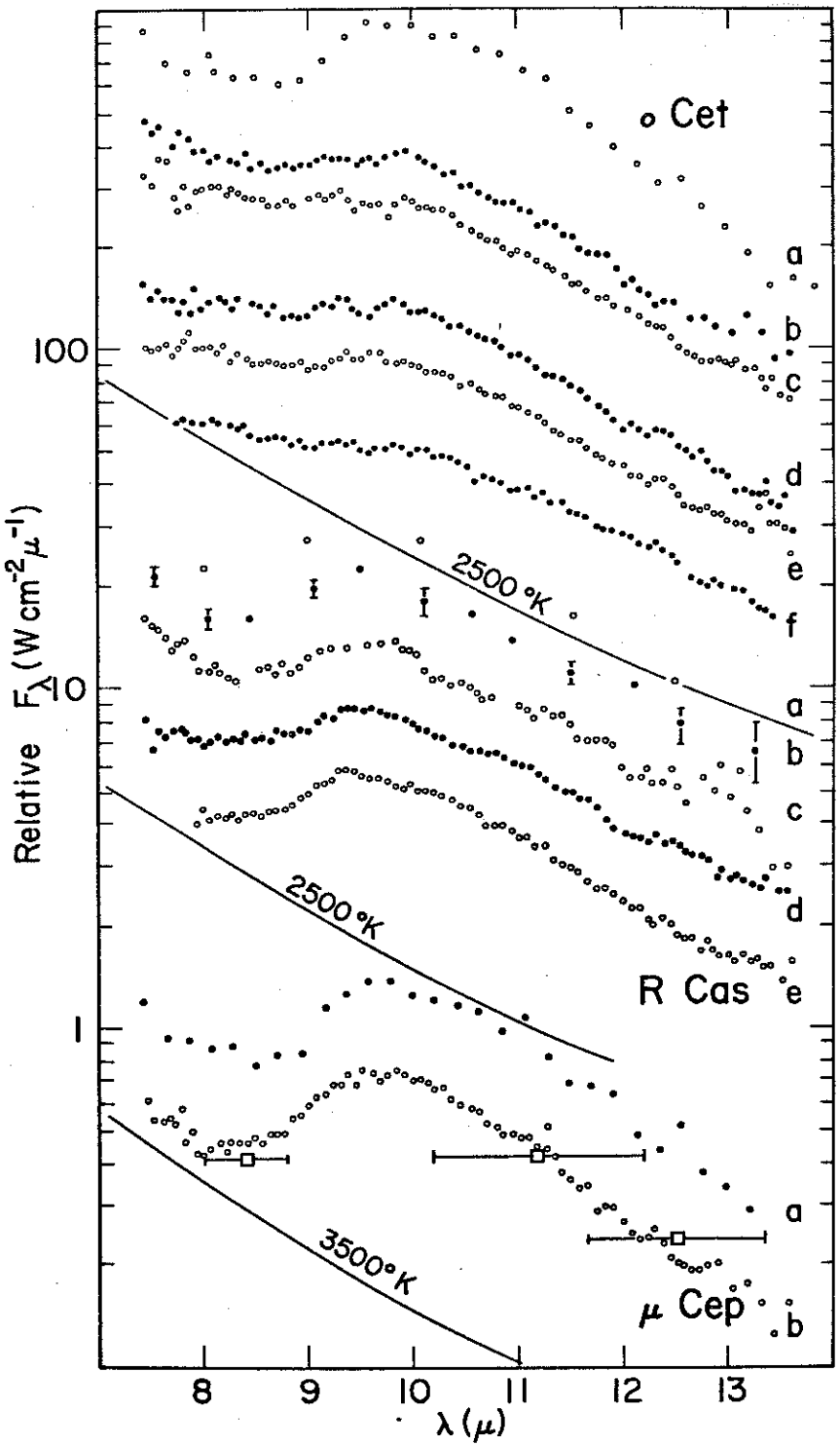

the same equipment and atmospheric correction as the early spectrum of μ Cep, which in turn agrees with the current spectrum of μ Cep using the current equipment and atmospheric correction techniques. Further, it is believed that the difference in phase (i.e. stellar temperature, luminosity) between the early observation and the present series is alone insufficient to explain the spectral difference, witness R Cas measured at different phases. Therefore, we conclude the spectra indicate a secular decrease, on a time scale of $\lesssim 4$ years, of about a factor of 2 in the amount of dust around oCet. On the other hand, the time scale for "decrease of dust" due to the departure of gas and dust indicated by mass loss (Chapter VIII) will be, in the absence of production of new dust, $t \sim \tau_{abs}/\dot{\tau}_{abs} \sim \frac{1}{2} R_d/\dot{R}_d$, where $\tau_{abs} \sim \kappa_{abs}(M_d/4\pi R_d^2)$, R_d is (average) distance of dust from the star and $\dot{R}_d$ is the recessional velocity of the dust. Taking $R_d/r_* \gtrsim 4$ as indicated by the data on mass loss and $V_d = \dot{R}_d = 20$ km/s typical for M stars (Chapter VIII), we have $t \gtrsim 1.5$ years, so a decrease over the (unobserved) four year period would seem possible, even with a moderate rate of production of new dust.

VI. R CrB

A. Characteristics of R CrB Stars -- Observations in the Visual Region

The R CrB variable stars comprise an extremely rare ($\sim$ 30 known in our Galaxy) group of carbon-rich, hydrogen-poor stars of high luminosity. The characteristic temporal behavior consists of:

(a) A fairly constant brightness at maximum which may persist for months or years but is eventually interrupted by

(b) A sudden decrease, on time scales $\lesssim$ 10 days, in the apparent visual brightness by considerable amounts ($\sim$ 1-9 mag, $\sim$ factor 2.5-4000). The faint state may last anywhere from tens of days to several years but eventually ends with

(c) A rise back to maximum. The rise to maximum tends to take longer (order of months) and be somewhat irregular following an extended minimum period but can be nearly as rapid (t $\sim$ 20 days) as the decrease following a short, sharp minimum.

The drops in brightness take place at irregular intervals; Sterne (1934) has shown statistically that for R CrB itself the times of minima were completely random over the period 1852-1933. Quoting Sterne: "Most of the known variable stars are periodic, probably with errors of period that vary from star to star; but such stars

can still be termed 'periodic.' R Coronae Borealis is not at all periodic, and the causes of such widely different types of variation must differ. So far as causes are concerned, then, variable stars of the ideally irregular type must be of a different nature from all others."

The visual light at maximum is nearly constant but superimposed on this can be small oscillations. For R CrB itself the oscillations have a range $\Delta V \sim 0.2$ mag with a period ~ 44 days, and there may also be radial velocity variations of ~ 5 km/s (Fernie et al. 1972). For RY Sgr the oscillations have been extensively studied by Alexander et al. (1972). The period is 38.6 days, $\Delta V \sim 0.5$ mag, and the radial velocity variation is ~ 30 km/s. This seems to definitely establish that at least some R CrB stars are also (small amplitude) pulsating variables. Alexander et al. (1972) also found that the regular oscillations in RY Sgr continued unabated even when the star was ~ 5 mag below maximum light. Taking $M_* = 1\ M_\odot$, $\mathcal{L}_* = 10^4\ \mathcal{L}_\odot$, $T_* = 6000$ °K (i.e. $r_* = 100\ r_\odot$), then the free fall time $\tau = (G\rho_*)^{-1/2} = 38$ days, thus it seems likely that the basic mechanism of pulsation is similar to that operating in the Mira variables. The existence of pulsation is at least qualitatively consistent with the work of Trimble (1972) on the instabilities of helium stars.

The spectra (of the ~ 15 actually observed) at maximum are distinguished by evident high luminosity (i.e. low surface gravity), high carbon abundance (including bands of C_2 and CN), and the almost complete absence of hydrogen (lines of hydrogen are only just seen at high dispersion, there is no evidence for the CH

molecule). The spectral classes range from ~ early B ($T_* \sim 15{,}000$ °K) through F (R CrB ~ F8, $T_* \sim 6000$ °K) to late C ($T_* \sim 2500$ °K). The peculiar abundances are thought to result from nuclear processing earlier in the star's life plus the possible ejection of a hydrogen-rich envelope (Warner 1967; Wallerstein 1973). The existence of helium in the stars' atmospheres has not been definitely established by direct observation but is believed to exist in order to (1) conserve the mass of the originally hydrogen-rich material (Wallerstein 1973) and (2) provide some of the continuous opacity in the stellar atmosphere (Warner 1967).

The spectra during a minimum exhibit many peculiarities of which we mention:

(1) As the star fades in light, the normal photospheric absorption spectrum appears unchanged except that as the star approaches minimum the lines become "veiled" or apparently weakened. In the case of RY Sgr the veiling has been attributed to overlying continuum emission due to the electron attachment spectrum of CN by Alexander et al. (1972). Another source of continuum emission at visual wavelengths might be the free-free radiation from a low temperature (T ~ 3000 °K) circumstellar plasma discussed by Milkey and Dyck (1973). Alternatively, the "line weakening" could be caused by scattering off an expanding circumstellar dust envelope as suggested by Woolf (1970); this possibility is discussed further in Section VIII-G.

(2) In addition to the extinguished stellar spectrum, a large number of low-excitation blue-shifted emission lines appear

near the beginning of a minimum and then gradually disappear (time scale ~ 50 days). Emission from He I may be present [λ 3888: Herbig (1949), Alexander et al. (1972); λ 10830: Wing et al. (1972)] but never has hydrogen been observed in emission. This is in distinct contrast to the Me, Se, and Ce variables which show prominent hydrogen emission during certain phases. Herbig (1949) also made the important observation that the intensity of the emission lines could not be explained merely by the weakening of the stellar continuum, i.e. their appearance and strength must be somehow linked to the mechanism which causes the reduction in visual light.

(3) There appear narrow, blue displaced (~ 30-200 km/s) absorption lines which may be due to an expanding shell. There are also broad (~ 200-300 km/s wide) emission and absorption lines which may indicate an expanding shell.

(4) After the emission lines disappear, a nearly normal stellar spectrum is recovered even when the visual light is several magnitudes below maximum. Thus, the spectroscopically determined luminosity and temperature of the star would be the same as at maximum but the observed apparent luminosity is considerably less.

B. Single Star Hypothesis -- Observations in the Infrared

These peculiar properties of the light and spectroscopic variations have led to speculation that the sudden decreases of visual light are due to occultation of the star by a cloud of

solid grains interposed between us and the star. Loretta (1934) and O'Keefe (1939) proposed that the occulting clouds originate in the star itself, with matter erupting from the surface of the star and condensing into small grains which are very efficient attenuators of visual light. O'Keefe (1939) considered the physics of graphite formation in a cloud of stellar matter as it recedes from the star and found sufficient numbers of graphite grains could condense when $R \gtrsim 8\ r_*$ on time scales of ~ 40 days (for a grain radius of 1 μ).

The discovery by Stein et al. (1969) of excess emission from R CrB over the wavelength range $\lambda\lambda$ 3.5-11.5 μ appeared to confirm the obscuration hypothesis as the amount of flux missing at visual wavelengths was approximately equal to the excess flux observed at infrared wavelengths. The infrared flux was fit well by an $\sim 900\ ^\circ K$ blackbody. A similar conclusion was reached by Lee and Feast (1969) in the case of RY Sgr, an R CrB variable quite similar spectroscopically to R CrB itself. They also found that the flux missing at visual wavelengths was approximately accounted for by the infrared excess, which again was fit by an $\sim 900\ ^\circ K$ blackbody. These observations were thus suggestive of a star of constant luminosity which is imbedded in an approximately spherically symmetric shell of dust grains which are responsible for the attenuation of visual light and thereafter re-radiate the absorbed portion in the infrared.

Further observation of R CrB in the infrared by Forrest et al. (1971, 1972) showed that this simple model for the circumstellar envelope could not be true. A light curve for R CrB, showing the visual magnitude from the AAVSO (Mayall 1973), the 2.3-11 μ

Fig. 32: Polarization and photometric data on R CrB.

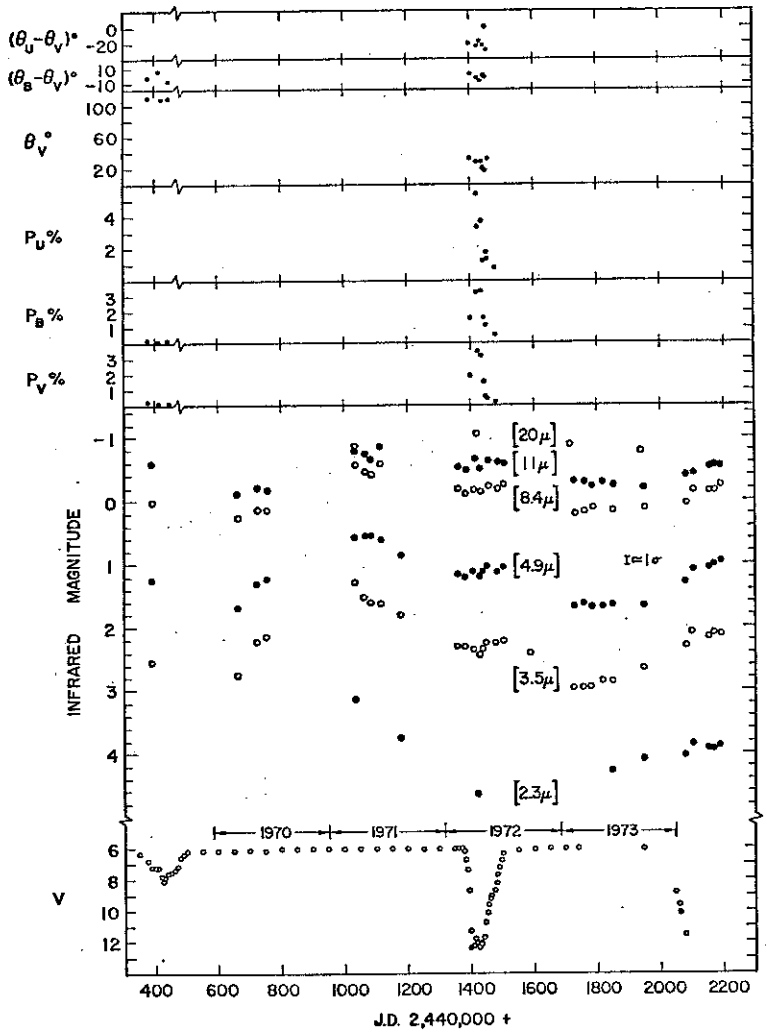

magnitudes of this study, the 20 μ magnitudes of this study, Morrison and Simon (1973) and Simon (1973), and the visual polarization measurements of Serkowski and Kruszewski (1969) and Coyne and Shawl (1973), is presented in Fig. 32. It is seen that from early 1970 to early 1971 the infrared fluxes increased dramatically while the visual flux remained approximately constant at near its normal maximum of V ~ 6.0. If we define α as the ratio of the total excess infrared flux to the total flux from the V ≃ 6.0, $T_* \simeq 6000$ °K star, assumed to be constant, i.e.:

$$\alpha \equiv \mathfrak{F}^{exc}/\mathfrak{F}_* = \mathfrak{F}^{exc}/\text{const} \quad . \qquad \text{(VI-1)}$$

Then α increased from ~ 0.2 on JD +666 (≡ JD 2,440,000+666) when the infrared flux was ~ the minimum observed to date, to ~ 0.7 on JD +1033 when the infrared flux was the maximum. A high flux level is confirmed by the infrared measurements of Hackwell (1972).

Conversely, large decreases in visual light are not necessarily accompanied by corresponding increases in the infrared. During the March-June 1972 short, sharp minimum (Fig. 32) the apparent visual luminosity decreased by at least 6 magnitudes (a factor of ~ 250) while the infrared remained nearly constant at $\alpha \sim 0.3$. The infrared and visual light are thus not anti-correlated and a spherically symmetric model for the obscuring shell appears to be ruled out. Forrest et al. (1972) concluded that the observations might be consistent with a "discrete cloud" model for the circumstellar shell of R CrB. The cloud cover would consist of

discrete, optically thick individual clouds interspersed with relatively clear areas. The apparent visual flux is determined by whether our line of sight happens to intersect a cloud or clouds or passes through the relatively clear areas between. The infrared measurements are more democratic, they sample the whole cloud complex and thus monitor the average cloud cover at any particular time. This model was supported by the fact that the average cloud cover, as monitored by the visual flux from 1852-1972, was approximately equal to the average cloud cover inferred from the infrared observations 1968-1972, $\langle\alpha\rangle \sim 0.3\text{-}0.4$ (Forrest et al. (1972).

Additional evidence for circumstellar material comes from visual polarization measurements. For RY Sgr, Serkowski and Kruszewski (1969) found the polarization increased from $\sim 0.5\%$ when the star was near maximum to at least $\sim 1.3\%$ during a minimum ($\Delta V \gtrsim 3$ mag). In addition, they found the position angle to change from $\sim 10°$ to $\sim 150°$ and noted that the polarization increased toward shorter wavelengths, similar to the red variables (Chapter VII). For R CrB the authors found (see Fig. 32) a quite small polarization, $\sim 0.2\%$, in March 1968 when $V \sim 6.6$, i.e. ~ 0.6 mag below maximum. This is approximately 180 days before Stein et al. (1969) measured R CrB in the infrared and found $\alpha \sim 0.4$, i.e. on the circumstellar shell model there was extensive cloud cover at this time. During the March-June 1972 minimum of R CrB, Coyne and Shawl (1973) found the polarization to increase to more than 3% when $V \sim 12$ mag (i.e. $\Delta V \sim 6$ mag). In addition, the position angle was $\theta \sim 25°$, an

approximately 85° change from the earlier measurements of Serkowski and Kruszewski (1969). The authors interpreted the observed wavelength dependence of polarization as due to scattering off of small ($a \sim 0.05\ \mu$ - $0.10\ \mu$) spherical graphite grains in an asymmetric optically thin ($\tau \lesssim 0.2$) envelope.

C. Double Star Hypothesis

An alternative mechanism to explain the infrared excess of R CrB has been proposed by Humphreys and Ney (1974). These authors noted that a number of high-latitude supergiant, hot stars had an apparent dual energy distribution with a fraction of the energy appearing as an $\sim 6000\text{-}7000$ °K blackbody and a fraction characterized by a much cooler $\sim 600\text{-}1200$ °K temperature. The relative amounts of energy in each region were of the same order of magnitude. They pointed out that such a dual energy distribution could be due to a cool, binary companion to the hot star and suggested the companion might be one of the well-known infrared stars which radiate the major fraction of their energy at wavelengths longer than $\sim 2\ \mu$ and can be relatively quite faint visually. In the case of R CrB the authors suggested the companion may be like the late-type carbon star CIT6. The extremely red energy distributions of some late-type carbon stars are, in turn, probably due to cool dust surrounding and obscuring a relatively hot star ($T_* \gtrsim 2000$ °K) as discussed in Chapter IV. The relative apparent luminosity of the dust compared to the star is in turn determined by the optical depth of the

circumstellar shell. Thus, in the double star model, the infrared excess is also due to thermal radiation from dust grains but, in this case, the grains are surrounding the proposed second star; changes in the infrared would then be due to changes in the luminosity of the second star and the optical depth and geometry of its circumstellar envelope. The sudden decreases in the apparent visual luminosity would presumably be due to a component of this circumstellar envelope appearing in our line of sight to the hot primary star. The authors found support for this model in the fact that the variations in the 3.5 μ flux from R CrB appears to have some of the characteristics of the variations in Mira variables. From the minimum in early 1970 (Fig. 32), the flux increased relatively rapidly to the maximum observed in early 1971, and then decayed more slowly to a second minimum in early 1973 and is now increasing again. The period, if it is periodic, would therefore be ~ 3 years. If this periodicity is confirmed by further measurements in the infrared over several cycles, it would appear to be strong evidence for the binary star hypothesis as the variations of visual light from R CrB shows no such periodicity.

D. Further Characteristics of R CrB Cloud Cover -- Optical Depth, Reddening, Time Dependence

In either model, the modulations of visual light are attributed primarily to condensed matter (i.e. dust grains) intervening in our line of sight to the hot star and thus convey potential

information about the structure, time dependence, and optical depth versus wavelength of the cloud cover on the line of sight. An immediate conclusion which can be reached, as discussed earlier, is that much of the cloud cover consists of components optically very thick ($\tau_V \gg 1$) at visual wavelengths interspersed with relatively clear areas, $\tau_V \ll 1$. The clouds appear to be optically thick at all wavelengths observed; Forrest et al. (1972) interpreted the ~ 15% dip in the 3.5 μ light curve during the March-June 1972 minimum (Fig. 32) as due to extinction of the underlying star, on this model $\tau_{3.5\mu} > 1$ during this minimum. The usually rapid onset and sometimes rapid departure of a minimum implies, as discussed in Section VI-F, either clouds with sharp edges and large velocities perpendicular to the line of sight or a rapid formation/dissipation mechanism for clouds.

With regards to the wavelength dependence of optical depth, i.e. reddening, there is evidence that there is a difference in reddening between the onset of a minimum and the rise back to maximum. The extinction during onset tends to be nearly neutral, with approximately equal extinction at all wavelengths, while during the recovery from minimum there is reddening, with relatively more extinction at shorter wavelengths. This behavior is illustrated by the March-June 1972 minimum of R CrB. One must be careful in interpreting the broad band flux measurements because of the well-known appearance of emission lines during a minimum. However, Herbig (1949) noted the emission lines only became prominent after V had dropped by more than 4 magnitudes, though this of course may

not be true for every minimum. For the 1972 minimum, the initial drop from V ~ 6 to V ~ 9.2 was accompanied by essentially no change in the B-V and U-B colors (Dürbeck 1972a) and only a slight change in the colors longward of V (Wing et al. 1972). Thus, the ratio $r \equiv (\Delta U/\Delta B/\Delta V/\Delta[0.72\ \mu]/\Delta[1.04\ \mu])$ was r ~ (0.97/1.0/1.0/1.08/0.92) for ΔV ~ 3.2 mag on JD +1396, i.e. nearly neutral. Five days later on JD +1402 ΔV ~ 5.7 and r ~ (0.91/1.02/1.0/0.90/0.67), i.e. there was apparent blueing at U, probably due to the appearance of emission lines (Pasachoff, 1972), apparently neutral extinction B to V and some reddening showing up at 0.72 μ and 1.04 μ. Reddening gradually increased at U and B as the minimum progressed (Coyne and Shawl 1973) and by JD +1455, when ΔV ~ 3.6 on the return to maximum the ratio of extinctions was r ~ (1.22/1.13/1.0/0.83/0.71). By JD +1477, ΔV ~ 2.6, there was a slight amount of further reddening at U and B (Dürbeck 1972b), i.e. r ~ (1.3/1.16/1.0/?/?). For interstellar extinction (i.e. Van de Hulst curve no. 15, Johnson 1968) or small (a = 0.06 μ) graphite spheres (Krishna Swamy 1972), these ratios would be r ~ (1.55/1.32/1.0/0.74/0.32). It would seem unreasonable to expect the appearance of emission lines to give the appearance of nearly neutral extinction, with no blueing, at the onset of minimum over the entire wavelength range λλ ~ 0.36-1.04 μ.

Herbig (1949) also noted this effect (i.e. neutral colors) on the initial decline of R CrB to the 1949 minimum before emission lines had appeared. Fernie et al. (1972) also found nearly neutral extinction at UBV on the initial decline of the short-sharp 1966 minimum. Interestingly, this sharp minimum was superimposed on the

slow return from a prolonged (1962-1968) minimum for which they found there was reddening of about r ~ (1.65/1.28/1.0), i.e. $\tau \sim (1/\lambda)^{1.2}$, which is quite similar to interstellar extinction. Also, Alexander et al. (1972) found reddening on the return of RY Sgr from its 1967-1970 minimum, after the emission lines had faded, of about r ~ (1.53/1.22/1.0), i.e. $\tau \sim (1/\lambda)^{1.0}$ which again is similar to interstellar.

A hypothesis which agrees with the observations to date on R CrB stars is that the onset of minimum can be accompanied by nearly neutral extinction while later, on the rise back to minimum, there is reddening which is not too dissimilar to interstellar reddening ($R \equiv \Delta V/(\Delta B - \Delta V)$ = 4.3 for RY Sgr, = 3.6 for R CrB, ≃ 3.1 for interstellar). If we consider the apparent extinction of R CrB during the 1972 minimum as due to a fraction μ of neutral extinction and (1 - μ) of $\tau \sim (1/\lambda)$ extinction, i.e. $\Delta[\lambda] = C[\mu + (1 - \mu)(0.55\ \mu/\lambda)]$, then μ ranged from μ ~ 1 JD ≤ +1396, μ ~ 0.7 JD+1401, μ ~ 0.4 JD+1455 and μ ~ 0.3 JD+1477. The component of extinction which is ~ "interstellar", i.e. $\tau_\lambda \sim 1/\lambda$, could be produced by a uniform cloud of small ($a \lesssim 0.1\ \mu$) graphite grains in our line of sight to the hot star. The "nearly neutral" component λλ 0.36-1 μ could be explained by either larger graphite grains ($a \gtrsim 0.25\ \mu$) in the line of sight or, alternatively, spatial inhomogeneities in the cloud structure across the face of the projected disk of the star. If the cloud structure in our line of sight to the surface of the star consisted of a fraction f of very optically thick structure $\tau_{0.55\mu} \gg 1$ with the remaining fraction

(1 - f) relatively thinner $\tau_{0.55\mu} \sim 1\text{-}5$, then the fraction f of the star's light would be completely extinguished, as in a geometric eclipse, and the remaining fraction would show reddening. The true picture will be, of course, more complicated; there must probably be a distribution of grain sizes in the first model and in the second, a distribution of optical depths across the surface of the star. In addition, a cloud (or grain) which is very optically thick at one wavelength may not be very optically thick at a longer wavelength. Further, we have not included the effects of light scattered in our direction from other cloud structures surrounding the star -- this may be important near minimum. Taking the simplest model described above and ignoring scattered light, the parameter μ represents in the first model, the relative extinction at V due to large ($a \gtrsim 0.25\ \mu$) grains as compared to small ($a \lesssim 0.1\ \mu$) grains. The decrease in μ indicates relatively more small grains were present toward the end of the minimum. On the cloud structure model, the decrease of μ indicates either (1) the cloud structure became more homogeneous as the minimum progressed and/or (2) some of the optically very thick ($\tau \gg 1$) cloud structure became just optically thick ($\tau \sim 1$) as the minimum progressed.

The questions of time-dependent reddening, large optical depths, and short time scales will be discussed in the next section in terms of their possible interpretation on the two models proposed.

E. Difficulties of Models

Each model has some problems in explaining all the characteristic visual, infrared, polarization, and spectroscopic variations of the R CrB variable stars. The single star model has the initial advantage of simplicity (i.e. Occam's razor), invoking only two components, star plus circumstellar cloud, instead of three, 2 stars plus circumstellar cloud. We will try to summarize the primary difficulties of each model -- at this time the reader must decide for himself which model seems more satisfactory, as no definitive test has as yet been made.

i) Single Star

(a) Infrared Periodicity

As mentioned above, a well-defined periodicity in the infrared, if it is established, presents grave difficulties for the single star model. If the 3.5 μ light curve is Mira-like, it would seem reasonable to attribute it to a Mira variable in the system. We discuss in the following section (VI-E-ii) characteristics of the light curve observed to date which are distinctly non-Mira-like; further infrared observations should be able to settle this point. On the single star model, variations in the infrared are attributed to variations in the cloud cover surrounding R CrB as discussed in Section VI-G; to date they do not seem to be inconsistent with this model.

(b) Lack of Visual, Infrared Correlation

The near independence of the visual and infrared light curves presents a challenge to the single star model. In particular, the aforementioned infrared maximum of R CrB indicated $\alpha \simeq 0.7$ while the star was at visual maximum. On the single star model, this is interpreted as being due to a dust-cloud complex surrounding at least 0.7 of the 4π sterradian solid angle surrounding the star, yet there was apparently no trace of this in our line of sight to the star. It can be shown, however, that if the clouds are optically thick in the infrared, an $\alpha \sim 1.0$ is possible even if only 2π sterradians around the star are covered. This is the case if the star is at the center of an optically thick hemisphere of dust with the observor in the unobscured anti-dust direction. α's much larger than this would require increasingly specialized and unlikely dust distributions to explain.

The converse behavior, represented by the March-June 1972 minimum of R CrB when the visual flux decreased by at least a factor of 250 but there was little change in the infrared, must be interpreted in terms of the geometry of the occulting cloud. Either a pre-existing cloud passed across our line of sight or a new but small cloud was formed in our line of sight to the star. Forrest et al. (1972) noted that there was a small but noticeable increase of $\sim 10\%$ in the 3.5-11 μ fluxes across this minimum (Fig. 32) which represents an increase in α by ~ 0.03. If we suppose that in the absence of the event marked by the visual minimum the flux

would have continued the decline following the maximum on JD +1033, this could indicate an actual increase of $\Delta\alpha \sim 0.1$. Thus if a new cloud was responsible for the minimum, it apparently covered at most $\Delta\alpha \sim 0.03$-0.10 of the 4π sterradians surrounding the star and we were fortunate to be in the ~ 3-10% of possible directions in space from which this event could be observed in both the infrared and the visual. On the other hand, the visual light was almost completely blocked by this cloud so that the cloud radius, r_c, must be larger than the star radius, r_*. The solid angle of this cloud, as seen from the star, will be

$$\Omega_c \simeq \frac{\pi/4\ r_c^2}{R_c^2} \simeq 4\pi\ \Delta\alpha \quad ,$$

where R_c is the star-cloud distance. Then we have

$$R_c \simeq \left(\frac{\pi/4\ r_c^2}{\Omega_c}\right)^{1/2} = \frac{r_c}{4(\Delta\alpha)^{1/2}} \simeq (0.8 - 1.4) r_c$$

for $\Delta\alpha = \Omega_c/4\pi \simeq 0.03$-$0.10$. Thus, for $R_c \gtrsim 8r_*$, which was found by O'Keefe (1939) and Galatola (1968) to be the distance at which graphite grains start to condense (i.e. for $R_c < 8r_*$, a small graphite grain would evaporate), we require $r_c \sim 6$-$10\ r_*$, so that complete occultation doesn't require perfect alignment of the cloud in our line of sight.

(c) Time Scales of Minima

On the single star hypothesis, the time scale of onset of a minimum could be due to (1) the motion of a pre-existing cloud

carrying it across our line of sight to the star or (2) the condensation of dust grains out of gaseous material already emplaced in our line of sight to the star. The AAVSO visual light curve for R CrB (Mayall 1973) has numerous examples where in the initial decline from maximum, a drop of at least one magnitude takes place on a time scale $t \lesssim 10$ days (the 1972 minimum, Fig. 32, is one example). If this is due to cloud motion, this implies a cloud must have covered at least half the projected surface of the star during this time and implies a cloud velocity perpendicular to our line of sight of

$$V_\perp \gtrsim \frac{r_*}{t} \simeq 80 \text{ km/s} \quad , \qquad \text{(VI-2)}$$

where $t = 10$ days and we have taken $r_* = 100\ r_\odot$ corresponding to $\mathcal{L}_* = 10^4\ \mathcal{L}_\odot$ and $T_* = 6000\ ^\circ\text{K} \simeq T_\odot$. On the other hand, unless the mass loss mechanism imparts a large tangential velocity to the escaping material, the tangential velocity $V_\perp$ at the star's surface, $R = r_*$, will be limited to the escape velocity.

$$V_\perp(r_*) \lesssim V_e\ (r_*) \sim 60 \text{ km/s} \quad ,$$

where we have in addition taken $M_* = 1\ M_\odot$. Now as the material moves outward the forces acting on it will be (1) gravitational attraction, (2) radiation pressure, (3) magnetic, (4) turbulence, shocks, etc. The gravitational force will be radial. The radiation field will probably be nearly radial, especially far from the star.

Thus, in the absence of large magnetic torques and other non-radial forces the net force will be $\sim$ radial and the angular momentum will be conserved so at a distance R_c from the star we will have:

$$V_\perp(R_c) \lesssim V_\perp(r_*)\ \frac{r_*}{R_c} \quad ,$$

and for $R_c \gtrsim 7\ r_*$ necessary for grain condensation we have

$$V_\perp(R_c) \lesssim 10 \text{ km/s} \quad .$$

So the time scale for changes due to motions perpendicular to our line of sight to the star would seem to be

$$t_\perp \gtrsim 80 \text{ days} \quad ,$$

which is too long.

Alternatively, the time scale could be due to the condensation process and one has to explain how (1) a suitable mass of gas of sufficient density gets to the distance from the star ($R_c \gtrsim 7\ r_*$) necessary for grain condensation and (2) how the grains can suddenly condense on these short time scales, $t \lesssim 10$ days. Since the whole question of grain formation around stars in general is not really understood in detail, this may not present too much of an obstacle in the case of R CrB. O'Keefe (1939) called to mind the action of solar prominences and suggested that analogous activity in R CrB on a much larger scale might be responsible for

the initial mass ejection. Both O'Keefe (1939) and Galatola (1968) found that once $R_c \geq 7\ r_*$ was achieved, sufficiently rapid grain condensation would be expected. On this model, there should be activity indicative of gas outflow and mass loss which precedes the onset of a minimum. In the case of R CrB there may be some evidence for such precursive activity. Espin (1890) observed the spectrum and color of R CrB visually. From March and April 1890 to September 1890 the stars' color changed from "yellowish white" to "pale orange," absorption bands appeared in the spectrum (which Berman (1935) attributed to the Swan bands of the C_2 molecule), and a possible emission line or lines appeared, all while the visual magnitude remained steady at $V \sim 6.0$. By October 1890 the absorption bands had faded and the spectrum was nearly back to that seen in March and April, the color was again "yellowish white," and the visual magnitude remained at $V \sim 6.0$. Some time in mid-1891, the visual magnitude dropped to $V \sim 12$, though a causal relationship is not proved, there is some evidence for precursive activity $\sim$ 100-200 days before the 1891 minimum. Unfortunately, since this time, there has been little discussion of possibly disturbed conditions preceding a minimum, most of the studies concentrating on the "normal" maximal spectrum or the very abnormal minimum spectra. Berman (1935) does note the abnormally low (i.e. blueshifted $\sim$ 5-10 km/s) radial velocities obtained in 1922 preceding the 1923 short-sharp minimum by $\sim$ 250 days, but this could be at least in part due to the (small) pulsations of the star noted earlier.

The recovery from minimum generally takes longer than the initial decline and this is especially true following long, protracted minima. On the single star model this could be explained by gradual dissipation and/or small tangential motions of the cloud or clouds causing the minimum. However, there are occasions following short-sharp minima where the recovery from minimum is quite rapid, the 1972 minimum of R CrB (Fig. 32) being one example. If the return to maximum results from cloud dissipation, it could be due to (1) expansion of the cloud or (2) evaporation of the dust grains. If the dust grains evaporated, we would expect a decrease in infrared flux coincident with return to maximum which is not seen for the 1972 minimum, so this can probably be rejected. If a small cloud of optical depth τ is expanding radially outward at a velocity V_r from a radius R_c, the time scale t_r for change in τ due solely to this radial expansion would be

$$t_r \sim \tau/\dot{\tau} \sim \frac{1}{2}\,\frac{R_c}{V_r} \quad .$$

So a change on an $\sim$ 20 day time scale, as for the 1972 minimum, would require a radial velocity

$$V_r \sim \frac{1}{2}\,\frac{R_c}{t_r} \gtrsim 140 \text{ km/s}$$

for $R_c \gtrsim 7\ r_*$. This is considerably larger than the apparent velocity of $\sim$ 30 km/s derived in Section G of this chapter, but is on the order of the $\sim$ 200 km/s gas velocities implied by some of the emission/absorption line observations. If the $V \sim 30$ km/s

is to be accepted as a typical dust cloud radial velocity, a rapid rise of light on time scales of $t \sim 20$ days would seem to require either rapid tangential expansion or tangential mass motions, the latter implying non-radial forces such as magnetic torque act on the cloud.

(d) Low Albedo of Dust Clouds

During the March-June 1972 minimum of R CrB the visual flux decreased by a factor of ~ 250 while the infrared was nearly constant at $\alpha \sim 0.3$. On the single star hypothesis this implies that at least 30% of the solid angle surrounding the star was covered by dust clouds, yet this dust was not seen in reflected light to at least a factor of 250. This implies that the geometric visual albedo, A_c, of the dust cloud complex must be exceedingly small. We define the geometric visual albedo of the cloud complex by

$$A_c = \frac{\mathfrak{F}^c(\text{scattered})}{\mathfrak{F}^c(\text{absorbed}) + \mathfrak{F}^c(\text{scattered})} \quad ,$$

where $\mathfrak{F}^c(\text{abs})$ is the apparent total flux absorbed and then re-emitted in the infrared by the clouds and $\mathfrak{F}^c(\text{scatt})$ is the total flux scattered by the cloud complex. Then for the March-June 1972 minimum, $\mathfrak{F}^c(\text{abs}) \sim 0.3\ \mathfrak{F}^*$ and $\mathfrak{F}^c(\text{scatt}) \lesssim 1/250\ \mathfrak{F}^*$, so

$$A_c \lesssim \frac{0.004}{0.004 + 0.3} \lesssim 1.3 \times 10^{-2} \quad ,$$

which is much smaller than the $A \sim 0.5$ thought to be appropriate for interstellar grains. As pointed out by Solomon (1973), it should be emphasized that this refers to the apparent geometric albedo of the cloud complex as a whole and not necessarily to the individual dust grains. It does seem to imply that very few of the photons incident on the front surface of the cloud manage to escape by scattering. This condition could possibly be met by invoking (1) very small, $a \lesssim 0.02\ \mu$ graphite grains which scatter very little because of the $(2\pi a/\lambda)^4$ scattering dependence (Appendix B), (2) very large $a \gtrsim 1\ \mu$ grains with roughened surfaces or (3) cloud geometries during this minimum which inhibited scattering to observors at earth. It might be pointed out that the fact that there appears to be an absolute minimum to the visual flux from R CrB, i.e. V never drops below $V \sim 14$, may be evidence that there is some scattering from the clouds which limits the depth a minimum can reach.

(e) Time Dependent Reddening

As discussed earlier the wavelength dependence extinction during a minimum appears to be time variable, with the initial decline showing nearly neutral extinction but later, on the rise to maximum, reddening not too dissimilar to interstellar extinction occurs. Nearly neutral extinction could be due to large grains but one would probably not expect large grains to appear first and small grains afterward because the growth process would lead to just

the opposite. One would have to invoke some sort of destructive or dispersive mechanism to convert initially large grains into smaller grains. On the other hand, the appearance of localized condensations within the (small) cloud causing the minimum is not too unreasonable and we might expect these knots to expand with time thus giving relatively more reddening (due to the small grains within the cloud) as the minimum progressed and the cloud became more homogeneous across our line of sight to the star. On this model, one has to include the contribution to the observed flux due to scattering from other components of the cloud cover around the star; because of the low effective albedo ($A \lesssim 10^{-2}$) this will only be important near minimum. The initial inhomogeneity could be due to (1) inhomogeneity in the gaseous material out of which the grains condense or (2) grain growth which starts at different times in this material, thus certain volume elements may condense all their condensible material, be optically thick, and give geometric (i.e. neutral) extinction while other volume elements are still in the process of condensation, are relatively optically thinner, and give reddening.

ii) Double Star

(a) Statistics

The double star model requires an apparent coincidence of an unusual hydrogen-deficient, carbon-rich (HdC) star in orbit with the also somewhat unusual infrared star. If there are, say, 10^3 such HdC stars and, say, 10^4 infrared stars, out of a total of $\sim 10^{11}$ stars in the galaxy, and every HdC star is in a binary system, the a priori probability that this association would happen even once by mere chance is

$$p \sim 10^3 \times \frac{10^4}{10^{11}} \sim 10^{-4} \quad ,$$

which seems rather unlikely. Thus, this situation, which holds for at least 30 stars in our Galaxy, would seem to require a common evolutionary history of the pair of stars. We show in the succeeding sections that the stars must be well separated ($R_{12} \gtrsim 70$ AU) in space so this common evolution must be a rather subtle effect.

(b) Dust Exclusion -- Large Star Separation

One severe constraint on the double star model is posed by the strong repulsive field for dust grains set up by the hot star due to radiation pressure. This force will tend to exclude dust from the immediate vicinity of the hot star, thus making occultation events quite unlikely if the system is viewed from directions opposite to the cool star. Such a radiation pressure mechanism has been invoked by Gehrz, Ney and Strecker (1970) and Humphreys, Strecker and Ney (1972) to explain the absence of excess emission due to dust for certain cool stars with hot companions. Whether or not the hot companion here actually prevents the formation of a circumstellar shell around the cool star, its radiation pressure field will most certainly affect the motion of the dust streaming away from the cool star. In the case of R CrB, the

luminosity of the cool component relative to the hot star has been observed to range from $\alpha \sim 0.7$ to $\alpha \sim 0.2$ with a time average of $\langle\alpha\rangle \sim 0.3$-$0.4$. In the case of small grains, the average radiation pressure efficiency of a grain, $\langle Q_{rp} \rangle$ (see Chapter VIII), will be relatively larger for the ~ 6000 °K radiation field of the hot star than the ~ 2500 °K radiation field of the cool star, which will tend to enhance the repusion of grains from the vicinity of the hot star.

An approximate treatment of the dust grain orbital problem indicates that dust exclusion from more than 2π sterradians surrounding the hot star will result unless $R_{12} > 100$ AU, where R_{12} is the separation between the two stars. Now the visual light curve indicates there has been no modulation of the characteristic R CrB light curve over the last ~ 120 years. This means our line of sight has not passed through the excluded region over this period. Therefore, the orbital period T must be longer than ~ 240 years, i.e.

$$T = \frac{R_{12}^{3/2}(AU)}{M^{1/2}(\odot)} \text{ years} > 240 \text{ years} \quad ,$$

or

$$R_{12} \gtrsim 70 \text{ AU} \quad ,$$

where $M = M_1 + M_2$ is the sum of the stars' masses, taken to be $\sim 6\ M_\odot$ here.

(c) Constant Radial Velocity -- Large Separation

A similar result would follow from the lack of radial velocity variation for R CrB found by various observers. Berman (1935) from many spectra over the period 1902-1934 found a radial velocity $V_r \sim 25 \pm 5$ km/s, which agrees with the velocities found in later years: Herbig (1949) $V_r \sim 26$ km/s; Keenan and Greenstein (1963) $V_r \sim 24$ km/s; Fernie et al. (1972) $V_r \sim 27 \pm 2$ km/s. Thus over 70 years the radial velocity has changed by less than ~ 5 km/s, which would imply $R_{12} \gtrsim 50$ AU (unless the orbital plane is nearly perpendicular to our viewing direction), for otherwise we would see radial velocity variations due to orbital motion. Any symbiotic relationship vis a vis evolutionary history would be difficult to maintain at such a large separation, though the stars could, perhaps, have been closer together in the past and moved apart as a result of mass loss from one or both stars.

(d) Large Separation -- Occultation at a Distance

This large separation and the dust exclusion effect mean that on the double-star model, minima in the visual flux must be due to occultation at a distance, i.e. the optically thick cloudlet traversing our line of sight to the hot star must be far from the hot star. There are several problems with this interpretation. Spectra of R CrB stars during minima show evidence for activity which cannot easily be explained by a remote occultation mechanism. First are the emission lines. Of the 382 emission lines observed by Alexander et al. (1972) during a minimum of RY Sgr, none could be identified with hydrogen. Thus, the emission lines must arise from the hot, hydrogen-deficient star, unless one is to suppose both stars are hydrogen deficient. The absolute strength of the emission lines is observed to decay with time after the initial drop from

maximum (Herbig 1949; Payne-Gaposchkin 1963; Alexander et al. 1972), indicating dynamic activity in the hot star during the event. Herbig (1949) has also presented evidence that some of the emission lines actually grow in absolute strength during the onset of minimum, which is further evidence for activity at the hot star. The velocities of emission lines also indicate activity at the hot star. The narrow emission lines are observed (Herbig 1949; Payne-Gaposchkin 1963) to have radial velocities which are blueshifted $\sim$ 12-15 km/s relative to the stellar spectrum, thus indicating matter is streaming toward the observor. There are also broad emission lines indicating velocities of $\sim$ 300 km/s in expansion or turbulence (Herbig 1949; Payne-Gaposchkin 1963). There are also both broad and narrow absorption lines blueshifted $\sim$ 200 km/s and possibly $\sim$ 40 km/s from the stellar velocity (Payne-Gaposchkin 1963; Alexander et al. 1972) again indicating material is streaming toward the observor.

In summary, the spectroscopic evidence points to activity around the hot star and indicates mass loss is occurring from the hot star during a minimum. Redshifted circumstellar lines, as due to material streaming toward the hot star, are not seen. Hydrogen emission lines are not seen. It is difficult to see how this activity could result from occultation at a distance as required by the double star model. On the other hand, one naturally would expect to see such stellar activity in coincidence with minima on the single star model; if we did not see evidence for activity, we would be suspicious of the single star model and might be led to consider a remote occultation mechanism.

(e) Time Scales of Minima

If the minima are to be explained by remote occultation by an optically thick cloud, the $\sim$ 10 day time scale for onset which is not uncommon requires (1) a sharp leading edge to the cloud and (2) a cloud velocity $V_\perp \gtrsim 80$ km/s (eq. VI-2) perpendicular to our line of sight to the hot star. If the leading edge is not sharp, the velocity would have to be higher. On the other hand, the observations of mass loss from late-type stars (Chapter VIII) indicate radial dust velocities of $\sim$ 15-30 km/s. In particular, the observations of CO absorption in the late-type "infrared" carbon star IRC +10216 indicate a gas outflow velocity of $\sim$ 20 km/s (Geballe et al. 1973) and from the considerations given in Chapter VIII this will imply a dust velocity $\lesssim$ 30 km/s. The projection of these velocities perpendicular to our line of sight will be even smaller so the large $V_\perp \sim 80$ km/s implied by the light curve is difficult to explain. This velocity requirement depends on the somewhat uncertain r_* and could be reduced if the luminosity were lower or the temperature were higher than we have assumed for R CrB ($\mathcal{L}_* = 10^4\ \mathcal{L}_\odot$, $T_* = 6000$ °K).

If the rapid onset of minimum can be explained by remote occultation on the double star model, then the nearly as rapid (t $\sim$ 20 days) rise back to maximum must be explained by the characteristics of the trailing edge of the cloud, i.e. in addition to the fairly sharp leading edge, the cloud must also have a trailing edge which is nearly as sharp. We are forced to consider the clouds as being very optically thick entities which also have fairly sharp

($\lesssim r_*$) edges. On the other hand, the clouds must have been produced at the cool star and travelled a distance on the order of the star-star separation, R_{12}, before occultation and this will take a time

$$t \sim \frac{R_{12}}{V} \gtrsim \frac{70 \text{ AU}}{80 \text{ km/s}} \sim 4 \text{ years} \quad .$$

It is hard to see how the cloud integrity could be maintained over the several year period between production and occultation.

(f) Time-Dependent Reddening

On the double star model, the apparent increase in reddening with time discussed earlier could be explained by postulating that the leading edge of the cloud, which initiates a minimum, is either composed of large grains or has a very patchy structure, while the trailing edge has progressively smaller grains or a more homogeneous structure. As discussed above, unless we are viewing the system from a special direction, the travel time of the cloud between production and occultation is several years. In the absence of specialized mechanisms (shock front, ?) it is difficult to see how the necessary inhomogeneity of a cloud could be maintained during this long journey.

A mechanism which may be capable of differentiating the cloud with respect to grain size, at least for an optically thin cloud, is radiation pressure on the grains. In Chapter VIII we found that the terminal velocity ΔV_t of a grain with respect to the gas for a given mass loss rate is proportional to $\langle Q_{pr} \rangle^{1/2}$,

where $\langle Q_{pr} \rangle$ is the extinction efficiency for radiation pressure of a grain averaged over the radiation field of the star. For pure graphite grains and a $T_* \sim 2500$ °K, $\langle Q_{pr} \rangle \sim 1\text{-}2$ for a grain radius $a \gtrsim 0.25$ μ and $\langle Q_{pr} \rangle \lesssim 0.5$ for $a \lesssim 0.1$ μ. Thus small grains will reach a terminal velocity a factor of two less than the large grains. If the dust velocity $V_d = V_{gas} + \Delta V_t \simeq 80$ km/s for the large grains and $V_{gas} \lesssim 20$ km/s, as is indicated for late-type stars, then for the small grains $V_d \sim (20 + 30) \sim 50$ km/s, and these grains would only arrive at the occultation region in a time $t \simeq R_{12}/V_d \sim 6.5$ years, i.e. ~ 2.5 years after the large grains. Thus, the time-dependent reddening during a short ($t \lesssim 0.5$ years) minimum, as for instance the 1972 minimum of R CrB, is difficult to explain. Perhaps by including the effects of optical depth and the strong repulsive force due to the hot star such a compact, rapidly moving, differentiated cloud could be produced.

(g) Infrared Spectra

On the double star model, the infrared excess is attributed to radiation from the cool companion and its associated dust shell. We might therefore hope to identify the companion through a comparison of the detailed spectral energy distribution in the infrared to that of other, known, objects. The broad band energy distribution in the infrared of the excess of R CrB (Fig. 33) is fit well by a blackbody function of a single temperature. This immediately rules out a star with a large, optically thin "silicate"

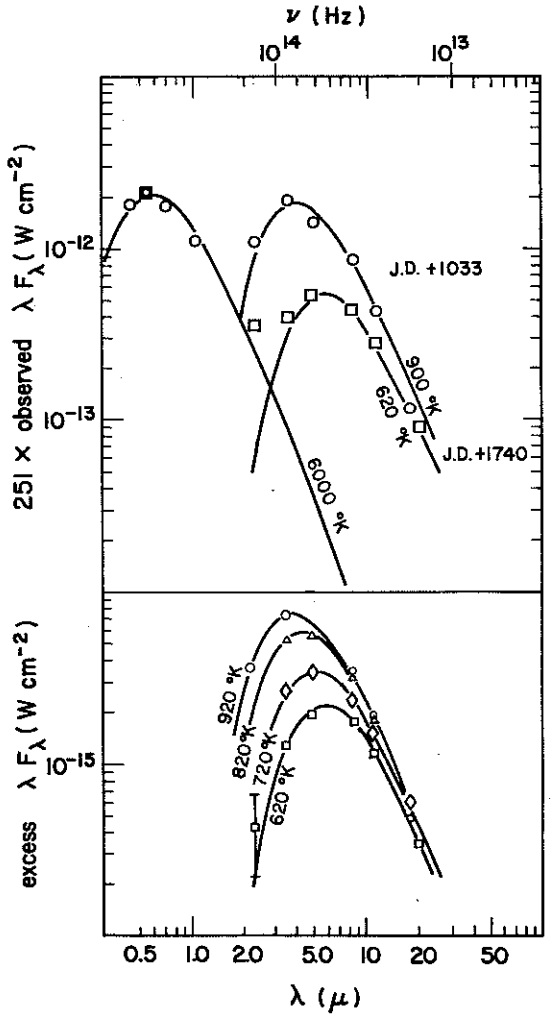

Fig. 33: Broad band energy distribution of R CrB as a function of time. The data for JD +1033 (≡ JD 2,441,033) and JD +1740 is from Table 2a. These epochs represent respectively the maximum and minimum of the infrared flux and apparent temperature of the excess observed to date. The data below represents the average infrared excess for the following observing periods:

Symbol:	○	△	◇	□
JD 2,440,000+	1033	1063-1115	1360-1500	1728-1850

emission feature at 10 μ (see Chapter V) as the companion star. High resolution spectra in the 2-2.5 μ region of R CrB and 89 Her were obtained by Gillett et al. (1970). The spectra are essentially smooth, in particular there is no indication of the absorption bands due to CO for $\lambda \geq 2.3$ μ which have been found in all late-type M stars observed to date. In particular, the extreme infrared M stars NML Cyg, IRC +10011 (CIT 3) and IRC +50137, which have broad, blackbody-like energy distributions and the less extreme M stars VY CMa, NML Tau, and VX Sgr, which show evidence of the 10 μ "silicate" feature all show these 2.3 μ CO absorptions (Hyland et al. 1972). Infrared S stars, such as W Aql described in Chapter V, have not been studied as yet in this wavelength range, so the appearance of the 2.3 μ CO bands is unknown. The carbon stars show progressive weakening of the 2.3 μ CO bands as the energy distribution becomes redder (Frogel and Hyland 1972). In Chapters IV and V this has been attributed to overlying emission from the circumstellar shell. An extreme example of this is the extreme infrared carbon star IRC +10216 in which the bands are entirely absent (Becklin et al. 1969). Thus, the binary companion, if it is to be a known star, would seem to be limited to the extreme infrared carbon stars, as red or redder than V Cyg and T Dra (Chapter IV) of this study. Typical examples would be IRC +10216, CIT 6 (= IRC +30219) and IRC +40540. On closer inspection, however, the late-type carbon stars do show features. In the 8-13.5 μ region there is an emission feature from $\sim$ 10-12.5 μ which has been attributed to emission from small, non-spherical, silicon carbide (SiC) grains

as discussed in Chapter V. In particular, the above mentioned examples all show this "SiC" feature on several spectra taken (Fig. 29, Gillett and Forrest 1974; Merrill 1974). The narrow band spectrum of R CrB appears in Fig. 34. The λλ 8-12.5 μ spectrum ($\Delta\lambda/\lambda \sim 0.015$) was taken point-by-point in March and April 1973 (normalized to March 1973) and calibrated vs. α Tau, assumed to be a 3500 °K blackbody normalized to its broad band fluxes (Table 2a). The total integration time was ~ 8000 sec and the error bars represent the 1 σ_m statistical deviation. It is seen that, within the statistical errors, the spectrum appears smooth and is fit by the ~ 600 °K blackbody which also fits the broad band energy distribution (Fig. 33) except for a possible slight upturn at $\lambda < 9$ μ. The upturn may not be real because (1) a somewhat uncertain air mass correction $\lambda \lesssim 8.5$ μ is possible and (2) the broad band 8.4 μ flux (open triangles Fig. 34) taken on the same night as the first spectrum is also higher than subsequent broad band measures (open squares) during that period. In particular, there is no "silicate" feature peaking at $\lambda \sim 9.7$ μ or "SiC" feature λλ 10-12.5 μ, either in emission or absorption, apparent in this spectrum within the statistical errors.

If, as usual, we define $\beta_\lambda = [F_\lambda(\text{excess}) - F_\lambda(\text{continuum})]\, F_\lambda^{-1}(\text{continuum})$, then we estimate the spectrum would be inconsistent with a "silicon carbide" feature as displayed for several carbon stars in Fig. 29 unless $\beta_{11\mu} \lesssim 0.1$. This is smaller than observed for all carbon stars in this program (Fig. 29) including the spectrum of IRC +10216 in that figure taken in April 1973 when the star was

Fig. 34: Spectral energy distribution of total observed flux from R CrB as described in the text.

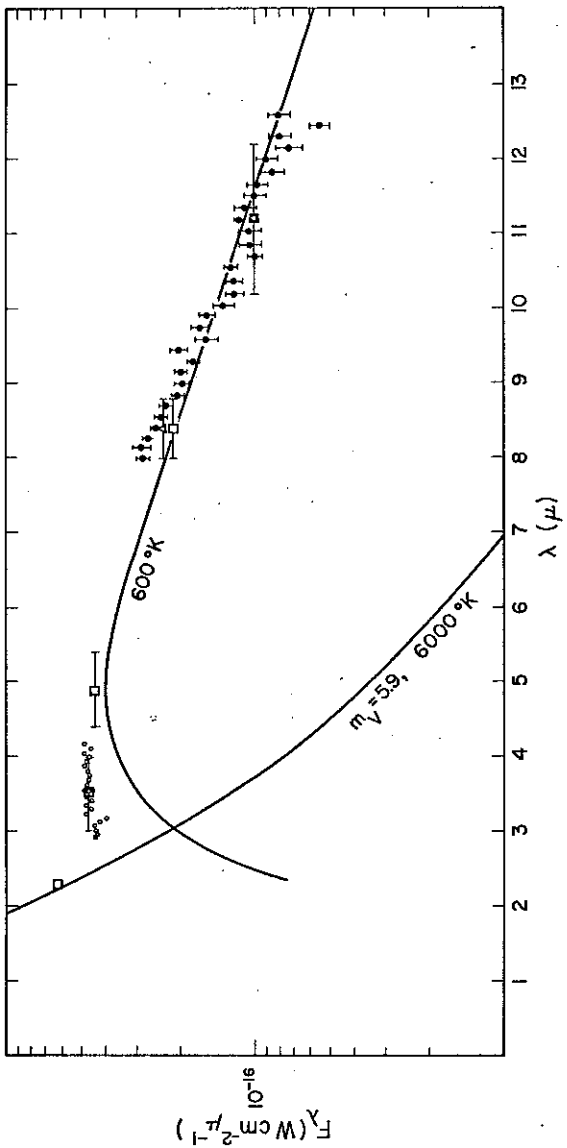

near maximum and $\beta_{11\mu} \sim 0.23$. It is also smaller than the observed feature in ~ 5 independent spectra of CIT 6 taken from 1971-1973 (Gillett and Forrest 1974; Merrill 1974) for which $\beta_{11\mu} \sim 0.3$-0.4 and that obtained by Hackwell (1971, 1972) of CIT 6 for which $\beta_{11\mu} \sim 0.4$. It is also smaller than the feature observed in IRC +40540 (Merrill 1974). The reddest carbon star considered here, IRC +10216, has the smallest "SiC" feature and there is an indication that the strength of the feature has decreased toward minimum (i.e. $\beta_{11\mu} \lesssim 0.1$ in early 1974, Merrill and Forrest 1974), so it is not inconceivable that an optically thicker version of IRC +10216 could accompany R CrB and still not be distinguishable in the 8-13 μ region.

The λλ 3-4 μ filter wheel spectrum ($\Delta\lambda/\lambda \sim 2\%$) which also appears in Fig. 34 was actually obtained a year earlier, in March 1972, and is arbitrarily normalized to the 1973 broad band fluxes. This portion of the spectrum is also smooth and featureless. In particular, the narrow absorption feature at 3.1 μ seen in all seven of the carbon stars studied by Johnson and Mendez (1970) in the carbon stars V Hya and Y CVn by Gillett and Forrest (1974) in the carbon star R Lep by Forrest and Merrill (1974) and in the extreme infrared carbon star IRC +40540 by Merrill (1974b), is not evident in this spectrum.

In summary, the λλ 2-2.5 μ, 3-4 μ, and 8-12.5 μ spectra of R CrB are, to the accuracy obtained, completely smooth and featureless. This is in distinct contrast to most late-type M, S and C stars studied to date which show some emission or absorption

features in these regions. There, of course, may be extreme infrared stars, such as the S star W Aql, Fig. 28, with smooth, featureless continua, but they are probably rarer than the well-known stars discussed above which do show features and this would seem to make the chance association with the unusual R CrB star even less likely.

(h) Infrared Light Curve

Though the observed infrared light curve of R CrB may superficially resemble that of Mira variables, as pointed out by Humphreys and Ney (1974), there are at least two characteristics which differ in detail. Firstly, the detailed shape of the 3.5 μ light curve of R CrB (Fig. 32) is unlike that of the Mira variables studied here (Chapter IV) and by Strecker (1973). In particular, consider the behavior through the March-June 1972 minimum; the flux actually increased by ~ 10% over a period of ~ 150 days while, on the double star model, the second star would be on the declining branch of its light curve. Such behavior is never seen in the M, S and C Mira variables in this study and that of Strecker; the fall of 3.5 μ fluxes to minimum is always observed to be monotonic with time. If the minimum were due to a mere chance occultation-at-a-distance, we would expect no such hesitation in the infrared light curve. On the single star model, on the other hand, this hesitation can be naturally explained as due to a small, $\Delta\alpha \sim 0.03$-0.10, additional component to the already existing cloud cover surrounding R CrB, possibly associated with the minimum.

Secondly, the variations in infrared colors (Table 1) and in the color temperature of the excess of R CrB (Figs. 33, 35) are greater than those observed for V Cyg and T Dra (Table 1, Fig. 20) which are late-type carbon stars with large infrared excesses. For V Cyg and T Dra $T_{max}/T_{min} \sim 1.1$-1.2, while for R CrB $T_{max}/T_{min} \sim 1.4$-1.5.

(i) Final Point

Finally, we wish to point out that the "infrared" stars (for instance W Aql) proposed as the binary companion to R CrB are not known also to be R CrB stars when observed in non-binary systems. That is, they don't show the characteristic sudden, unpredictable, large drops in visual light of the R CrB stars. If these stars were continuously emitting discrete, very optically thick cloudlets of matter interspersed with nearly clear areas, one might expect some R CrB-like behavior in their visual light curves. This question should be investigated for some of the extreme infrared stars which can be quite faint at visual wavelengths.

iii) Summary

In summary, the entire mass of observations present a challenge to either the single or double star model to explain in toto. For the single star model the primary difficulties would seem to arise from (1) the short time scale of minima, especially the relatively rapid rise back to maximum sometimes observed, (2) the

apparent lack of strong visual and infrared correlation in the case of R CrB and possibly (3) the low apparent albedo, $A_c \lesssim 10^{-2}$, inferred for the cloud complex. For the double star model the principle of dust exclusion from the vicinity of the hot star and the lack of periodicity in the visual light curve implies a large star-star separation and, consequently, that the minima be due to remote occultation. Then there is difficulty in explaining (1) the short time scale of minima and the apparent time-dependent reddening, (2) the visual spectroscopic observations which indicate activity at and mass loss from the hot star during minima and (3) the (weak) correlation in the infrared light curve with the March-June 1972 visual minimum of R CrB. Further, the completely smooth infrared spectrum requires additional assumptions on the double-star model but is naturally explained on the single star model as due to radiation from graphite grains, which are expected to give featureless emission in this region. Infrared periodicity, if it exists, would argue for the double star model. We believe that the observations available at present are insufficient to definitely rule out either model; however, we believe that the single star model more naturally and simply explains these observations and will adopt this point of view in what follows.

A truly definitive test of this question would be given by the short pulsation period of the hot star ($t \sim 40$ days) mentioned earlier. On the single star model, the infrared luminosity, which derives from absorbed and then re-emitted starlight, should also show this periodicity while on the double star model it should not.

What is needed are simultaneous photoelectric measurements in the visual region and the infrared. R CrB itself is not so favorable because the amplitude of visual oscillation is small, $\Delta V \sim 0.2$ mag, but this still should be attempted. RY Sgr is a better case, $\Delta V \sim 0.5$ mag, and fluctuations in the infrared of this amount would be easily detected.

F. Consequences of the Single Star Model for the Dust Surrounding R CrB

i) Evidence for Dust Ejection

The infrared and optical observations of R CrB indicate the circumstellar dust grains are distributed asymmetrically about the star. Cloudlets optically thick at visual wavelengths are interspersed with relatively clear areas. The depression at 3.5 μ during the March-June 1972 minimum (Fig. 32) when $\Delta V > 4$ mag may indicate that even $\tau_{3.5\mu} > 1$ for some cloudlets some of the time. Thus, an analysis of the observed infrared fluxes in terms of absorption and emission by independent grains as has been applied in Chapter VIII and considered in Appendix A is of questionable validity for R CrB. However, we may consider the optical properties of the cloudlets themselves -- in many respects they seem to approximate the "ideal blackbody" as defined by Van de Hulst (1957). The aforementioned low visual albedo, $A_c \lesssim 10^{-2}$ implies the cloudlets absorb almost all of the visual flux incident on them and scatter very little of it (besides the forward scattered diffraction pattern).

The broad band infrared energy distribution at various epochs, Fig. 33, seems to fit well by a blackbody of a single temperature from 3.5 μ to 20 μ. The higher resolution ($\Delta\lambda/\lambda \sim 2\%$) infrared spectrum (Fig. 34) is remarkably smooth, showing no obvious emission or absorption features λλ 3-4 μ or λλ 8-12.5 μ. The ensemble of cloudlets thus would seem, on average, to emit as blackbodies of a single temperature over the range 3 μ to 20 μ. Now as a cloudlet moves away from the star, possibly because of the action of radiation pressure on the grains (Chapter VIII), the temperature will be a decreasing function of the distance from the star, R_i. A cloudlet of radius r_i will absorb stellar radiation at a rate

$$\left(\frac{dE}{dt}\right)_{in} = \pi r_i^2 \, \epsilon_{vis}^c \, \frac{\mathfrak{L}_*}{4\pi R_i^2} \quad , \qquad \text{(VI-3)}$$

where $\mathfrak{L}_*$ is the total stellar luminosity (ergs/sec) and ϵ_{vis}^c is the absorption (and therefore emission) efficiency of the cloud averaged over the stellar radiation field. The aforementioned low albedo and large optical depth imply $\epsilon_{vis}^c \simeq 1$. The infrared emission observed from a particular cloud at a given wavelength will, in general, depend on the viewing direction. In the limit $\tau_\lambda \gg 1$, the cloudlet appears somewhat as a planet, with the apparent brightness temperature depending on the phase angle and the wavelength of observation. On the average of many cloudlets with many phase angles, the infrared observations indicate the flux can be described by a unique apparent temperature, T_a, i.e.

$$F_\lambda^{exc} = \Omega_d \, \epsilon_{IR}^c \, B_\lambda(T_a) \quad , \qquad \text{(VI-4)}$$

where $\Omega_d = \sum_i \pi r_i^2/D^2$, D is the distance star-earth, and $\epsilon_{IR}^c = \epsilon_\lambda^c \simeq$ const is the effective average emissivity vs. wavelength for the cloud complex and $F_\lambda^{exc} = F_\lambda^{obs} - F_\lambda^*$, where F_λ^* is here represented by a ~ 6000 °K blackbody run through V = 6.0 and is assumed constant, aside from occultation events. Defining, as usual $\mathfrak{F} \equiv \int_0^\infty F_\lambda \, d\lambda$, the parameter α defined by eq. (VI-1) is a relative measure of the amount of excess emission. T_a has been derived by fitting a blackbody function by eye to the derived excesses, as in Fig. 33. The quantities T_a, α, and the apparent angular size $\Omega_a \equiv \Omega_d \, \epsilon_{IR}^c = F_\lambda^{exc}/B_\lambda(T_a)$ are plotted vs. time in Fig. 35 for the time period JD 2,441,033 to JD 2,441,780 (early 1971 to early 1973). The three quantities are not all independent, i.e.

$$\alpha = \Omega_a \frac{\sigma}{\pi} T_a^4/\mathfrak{F}^* = \Omega_a \frac{\sigma}{\pi} T_a^4/\text{const} \quad .$$

From the figure it is seen that following JD +1033, when the infrared flux was the maximum which has been observed to date, α and T_a decreased monotonically with time, while Ω_a increased by small amounts. This is just what would be expected if a dust cloud or clouds formed on or about JD +1033 subsequently moved away from the star. We know that the dust distribution surrounding R CrB is highly asymmetric. In the infrared, however, we can potentially receive radiation from the dust grains in clouds in all directions around the star. If we are not in a preferred direction with respect to the infrared emission, then the total emission by the

Fig. 35: Derived source parameters of the excess as a function of time for R CrB as described in the text.

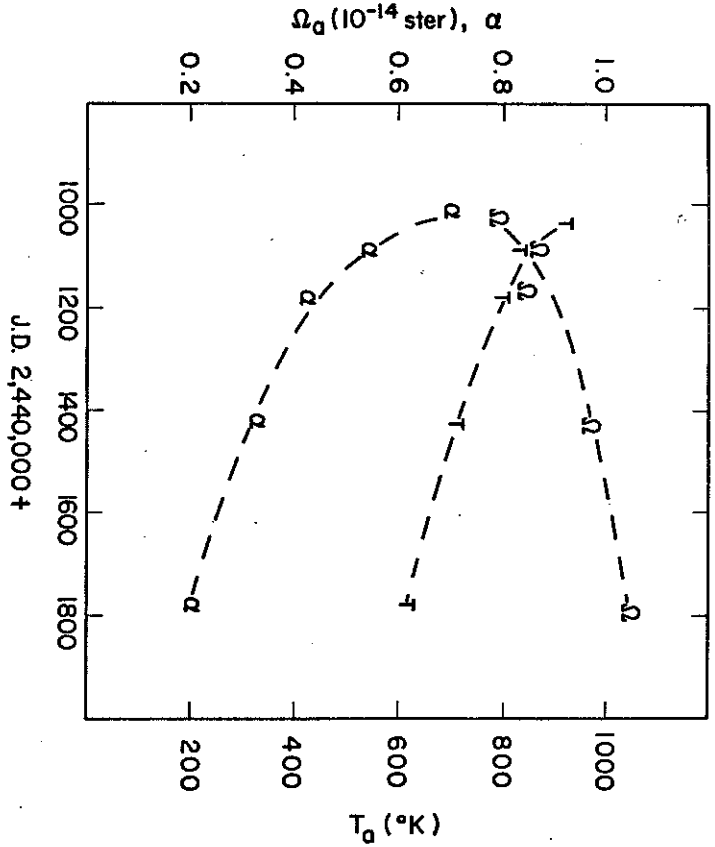

dust cloud or clouds surrounding R CrB will be

$$\mathcal{L}_d = \alpha \mathcal{L}_* \quad .$$

This must be supplied by the absorbed starlight (eq. VI-3) so we have

$$\mathcal{L}_d = \sum_i (dE/dt)_{in}$$

which reduces to

$$R_d = \frac{1}{2} r_* \left(\frac{T_*}{T_a}\right)^2 \left(\frac{\epsilon_{vis}^c}{\epsilon_{IR}^c}\right)^{1/2} \quad ,$$

where R_d is the average distance of the clouds from the star and the star's luminosity has been represented by $\mathcal{L}_* = 4\pi r_*^2 \sigma T_*^4$. This is identical to the expression given in Appendix A (Eq. A-10c) for the temperature of a single dust grain at a distance R_d from a star, only here the ϵ's refer to the apparent effective emissivities of the cloud or clouds and T_a refer to the observed apparent temperature of the infrared excess. Assuming $T_* = 6000$ °K and $\mathcal{L}_* = 10^4 \mathcal{L}_\odot$, the quantity $R_a \equiv (\epsilon_{IR}^c/\epsilon_{vis}^c)^{1/2} R_d = \frac{1}{2} r_* (T_*/T_a)^2$ has been plotted vs. time in Fig. 36. It is seen that, as advertised, the apparent distance from the star R_a, increased with time following the maximum on JD +1033. In fact, it appears that the increase is approximately linear, i.e. at apparently constant velocity. The straight line in the figure has a slope

$$V_a = \frac{\Delta R_a}{\Delta t} = 27 \text{ km/s} \quad . \qquad \text{(VI-5)}$$

Fig. 36: Apparent distance of the dust from the star as a function of time for R CrB as described in the text.

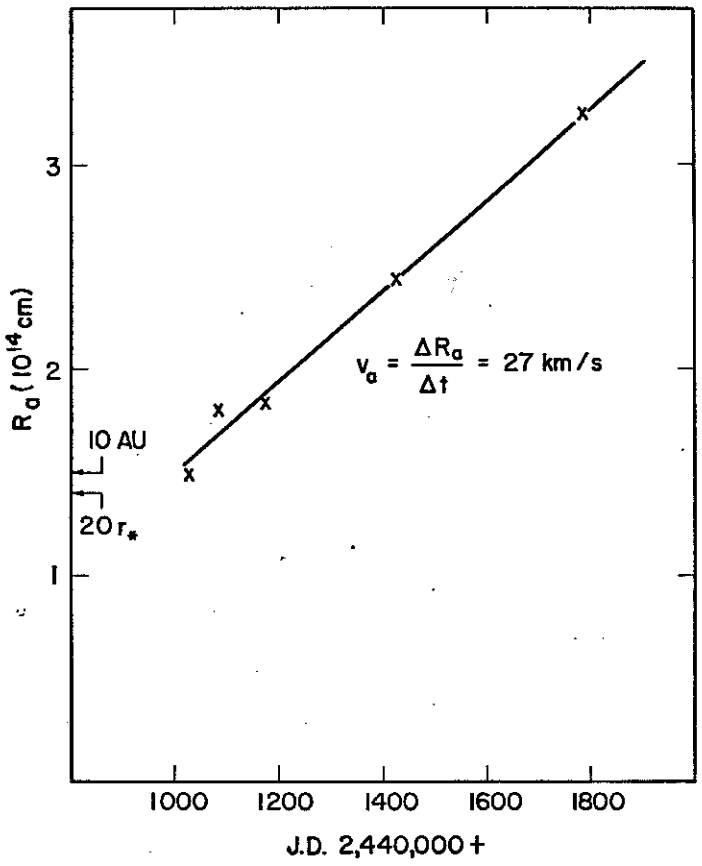

For the apparent average recessional velocity of the dust cloud or clouds. If this model for the infrared radiation from R CrB is correct, this would represent the first direct observation of dust leaving a star, without depending on Doppler velocities which refer to the gas. Interestingly enough, this velocity is also in the range one would derive from the apparent redshift of stellar absorption lines found by Payne-Gaposchkin (1963) for R CrB ($V_d \sim 5$-35 km/s) during the 1961 minimum if the shift is due to scattering off of a radially expanding dust cloud.

Whatever the true velocity of recession, intriguing support for the single star model of dust leaving the star is found if we run the recession linearly backward in time (i.e. continue the straight line in Fig. 36 to the left). We have the relationship between the true and apparent distance from the star

$$R_d \simeq (\epsilon_{IR}^{c})^{-1/2} R_a \quad ,$$

and if $d/dt\ (\epsilon_{IR}^{c})^{-1/2} \simeq 0$ following JD +1033, i.e. the cloud structure was fairly stable with time, then the true velocity is

$$V_d \simeq (\epsilon_{IR}^{c})^{-1/2} V_a \quad ,$$

and if this recession was also occurring with approximately constant velocity before JD +1033, as it appeared to after, then the material must have left the stellar surface, $R_d \simeq 0$, a time

$$\Delta t \simeq \frac{R_d(\text{JD } +1033)}{V_d} \simeq \frac{R_a(\text{JD } +1033)}{V_a} = 640 \text{ days}$$

earlier, i.e. on or about JD $\sim$ 2,440,390. Interestingly enough, there was a brief minimum in the visual light from R CrB (Fig. 32) at about this time. A causal relationship between the earlier visual event and subsequent infrared event is not proved but this agreement does seem very suggestive.

To interpret this apparent velocity in terms of an actual velocity we must treat the problem of radiation transfer in the clouds surrounding R CrB. The geometry and optical depth of the clouds not in our line of sight to the star is unknown. If we assume that we are not in a preferred direction with respect to the infrared radiation, then a lower limit to the average visual absorptivity, ϵ_{vis}^{c}, is given by

$$\alpha = \frac{\gtrsim \left(\frac{dE}{dt}\right)_{in}}{\mathfrak{L}_*} = \epsilon_{vis}^{c} \gtrsim \frac{\pi r_i^2}{4\pi R_d^2} \leq \epsilon_{vis}^{c} \quad .$$

Therefore, on JD +1033, we have

$$\epsilon_{vis}^{c} \geq 0.7 \quad .$$

This agrees with the observations of clouds which have appeared in our line of sight, i.e. $\tau_{vis} \gg 1$, and the low cloud albedo derived from the March-June 1972 minimum, i.e. $A_{vis}^{c} \lesssim 10^{-2}$. These data would imply $\epsilon_{vis}^{c} \sim 1$ for the clouds. If we assume

$\epsilon_{vis}^{c} \sim 1$ for the cloud cover between JD +1033 and JD +1780, then the remaining unknown quantity is

$$\epsilon_\lambda^{c} = \frac{1}{\Omega_d} \frac{F_\lambda^{exc}}{B_\lambda(T_a)} = \frac{1}{\Omega_d} \frac{\alpha \mathfrak{L}_*}{\frac{\sigma}{\pi} T_a^4} = \epsilon_{IR}^{c} \quad .$$

Now the apparent infrared flux from the cloud complex can be represented by $F_\lambda^{exc} = \Omega_d B_\lambda[T_B(\lambda)]$ where $T_B(\lambda)$ is the average brightness temperature of the clouds at the wavelength λ. The fact that ϵ_λ^{c} is approximately constant (i.e. the spectrum appears to be a blackbody) implies $\epsilon_\lambda^{c} = B_\lambda[T_B(\lambda)]/B_\lambda(T_a) = \text{const}$. One solution to this is $T_B(\lambda) = T_a$ and then $\epsilon_\lambda^{c} = 1$. Other solutions are possible, if $T_B(\lambda) \gtrless T_a$, then $\epsilon_\lambda^{c} \gtrless 1$, i.e. ϵ_{IR}^{c} can be greater or less than one and the actual average cloud velocity could be greater or less than the apparent velocity, 27 km/s.

An aspect of the minima which may be related to the cloud cover surrounding R CrB stars is the appearance of "veiling" or apparent weakening of the stellar absorption lines during a minimum. Payne-Gaposchkin (1963) has interpreted this as due to incipient emission in the core of the absorption line, but Herbig (1949) points out the line weakening occurs even in lines which are never seen strongly in emission. Alexander et al. (1972) have interpreted this as at least partially due to the appearance of a continuum of overlying emission during minimum which they suggest may be due to the electron attachment spectrum of CN. An interesting alternative explanation has been suggested by Woolf (1970) and Jones (1973). They point out that the photons scattered off of dust grains in an

expanding envelope surrounding a star will be redshifted. For scattering at an angle θ, the linear momentum transferred to a grain of mass M will be $\delta P \sim (1 - \cos\theta)\, h\nu/c$, and the change in energy of the photon will be $\delta E \sim h\nu(1 - \cos\theta)\, V_d/c$, where ν is the original frequency of the photon and V_d is the radial velocity of the dust grain. This predicts that a narrow line will be broadened and redshifted by a relative amount $\delta\nu/\nu \sim V_d/c$ upon scattering off the envelope. The line broadening will mean a reduction in the central depth of an absorption line and may contribute to the line weakening which occurs during a minimum. Interestingly, Payne-Gaposchkin (1963) has reported an apparent redshift of the stellar absorption lines during the 1960 minimum of R CrB. The shift amounted to $\sim$ 5-35 km/s and was only apparent when $\Delta V > 4.5$ mag. The author attributed this shift to the appearance of blueshifted emission lines distorting the spectrum, however, a shift was observed in lines which never appear in emission so an interpretation in terms of scattering off an expanding circumstellar envelope would seem to be a possible alternative. This could be further support for the $V_a \sim 27$ km/s recessional velocity found above.

ii) Mass Loss From R CrB

The previous section indicated that dust grains produced on or before JD +1033 were subsequently ejected at a velocity $\sim$ 27 km/s. This implies mass loss is occurring from the star; the aforementioned appearance of blueshifted emission and circumstellar absorption lines during a minimum also indicate mass loss is occurring. For the R CrB stars, the mass loss is apparently of an impulsive nature, rather than the more or less steady state mass loss which is observed (Chapter VIII) in late-type stars. We will apply the methods developed in Chapter VIII to measure mass loss to the impulsive event occurring on or before JD +1033.

(a) Weighing the Dust

In the case of R CrB, the visual spectra indicate the photosphere is carbon-rich, i.e. $N_C > N_O$, so we would expect, as for the carbon stars, graphite to be a primary constituent of the condensed grains. The detailed spectrum (Fig. 34) supports this suspicion -- the spectrum appears smooth, as would be expected for graphite, and in particular there doesn't appear to be any large emission or absorption features which could be attributed to the silicates or SiC which are seen in the 8-13 μ spectra M stars and carbon stars, respectively. The actual relative abundance of carbon in the photosphere is somewhat uncertain because of the near absence of hydrogen and the unobservability of helium in the photosphere. Helium is believed to be the most abundant constituent in the atmosphere in order to (1) provide the necessary continuous opacity in the photosphere (Berman 1935; Warner 1967) and (2) conserve the mass of the presumably initially normally abundant material which has presumably undergone nuclear processing to give the observed anomalous abundances (low H, high C). Wallerstein (1973)

under the second assumption gives a mass fraction of carbon in the photosphere of $f(C) \sim 1/13.3$ but also suggests that it may be a factor ~ 4–10 less, i.e. $f(C) \sim 1/50 - 1/133$.

In Chapter VIII, we derive an expression for the mass of dust radiating at a temperature T_d around a star of radius r_* and temperature T_* in the optically thin case (eq. VIII-4):

$$M_d = \beta_\lambda \frac{B_\lambda(T_*)}{B_\lambda(T_d)} \frac{\pi r_*^2}{\kappa_\lambda} \quad ,$$

where $\beta_\lambda \equiv [F_\lambda(\text{observed}) - F_\lambda(\text{star})]\, F_\lambda^{-1}(\text{star})$ and κ_λ is the mass absorption coefficient of the radiating dust grains. If the cloud is optically thick at a given wavelength, the actual mass of dust will be greater than this. If we associate the apparent blackbody temperature T_a with the dust temperature, this becomes

$$M_d(\lambda,t) = \left(\frac{F_\lambda^{exc}}{B_\lambda(T_a)}\right)\left(\frac{1}{\kappa_\lambda} \frac{B_\lambda(T_*)}{F_\lambda^*}\right) \pi r_*^2$$

$$\simeq \Omega_a(t)\, M(\lambda) \quad ,$$

i.e. the inferred mass is directly proportional (aside from the small deviations from a blackbody) to the apparent solid angle, Ω_a, which is plotted vs. time in Fig. 35. The proportionality constant $M(\lambda)$ is given in Table 4, assuming $T_* = 6000\ ^\circ K$, $\mathcal{L}_* = 10^4\ \mathcal{L}_\odot$ and κ_λ appropriate for small graphite grains (Appendix B, Chapter V).

From $\sim$ JD +1100 to $\sim$ JD +1800 the Ω_a and therefore the inferred mass of dust at any given wavelength increased only $\sim$ 20%,

TABLE 4

M_d/Ω_a for R CrB

$\lambda(\mu)$	3.5	4.9	8.4	11	18	Ave 3.5-11
$M(\lambda)$	1.37	2.37	6.0	10.0	25	4.9

$\times 10^{40}$ gm/ster

which is consistent with the model of dust made on or about JD +1033 being subsequently ejected from the vicinity of the star. The apparent increase of mass with wavelength could be due to (1) optical constants less wavelength dependent than those of small pure graphite grains, for which $\kappa_\lambda \sim 1/\lambda^2$. This could be due to (a) larger grains, though the aforementioned reddening seems to imply at least some small, $a \lesssim 0.1\ \mu$, grains. Graphite grains larger than $a \sim 1\ \mu$ would be required, (b) impure graphite or some other grain material; though the detailed spectrum (Fig. 34) indicates any proposed radiating material must have quite smooth emissivity vs. wavelength; (2) at the longer wavelengths, we are detecting cooler dust grains which are left over from earlier dust production or (3) the cloud or clouds are optically thick, thus at longer wavelengths we see deeper into the clouds and, correctly infer a greater mass of dust. Assuming (3) to be the case, the longer wavelengths would give the best estimate of the total amount of dust. To investigate the possible optical depth we consider what the optical depths of a given inferred mass would be if the mass

were distributed in a thin uniform shell at $R \sim R_a$ from the star. Taking $M(\lambda) \sim 5 \times 10^{40}$ gm/ster, $\Omega_a \sim 0.8 \times 10^{-14}$ ster and $R_a \sim 1.5 \times 10^{9}$ cm, i.e. as at the beginning of expansion on JD +1033 we get, for $\tau_\lambda = \kappa_\lambda (M_d/4\pi R_a^2)$ = the absorption optical depth through one thickness of the shell, the result shown in Table 5.

TABLE 5

Inferred Optical Depth of Shell Surrounding R CrB

$\lambda(\mu)$	0.55	3.5	8.4	11	18
τ_λ	64	3.1	0.71	0.42	0.17

On this shell model, our line of sight passes through more than one thickness of the thin shell, so this shell would be optically thick at all wavelengths except possibly 11 μ and 18 μ. Since the shell must be inhomogeneous, as on JD +1033 there was, for instance, no dust ($V \sim 6.0$) on our line of sight to the star, the actual distribution of dust will probably have an even larger optical depth. Therefore, we take as our estimate of the mass of dust associated with the JD +1033 event the mass inferred at 11 μ, i.e.

$$M_d \sim 10 \times 10^{-26} \text{ gm} \sim 50 \times 10^{-8} M_\odot \quad . \qquad \text{(VI-6)}$$

Now if events of this type occur, on the average, every three years, the dust loss rate will be

$$\dot{M}_d \sim \frac{M_d}{3 \text{ years}} \sim 17 \times 10^{-8} M_\odot/\text{yr} \quad . \qquad \text{(VI-7)}$$

And, if a mass fraction f' of the gaseous material is in the form of dust grains, the total mass loss rate will be

$$\dot{M}_g \sim \frac{1}{f'} \dot{M}_d \quad ,$$

where $f' \lesssim f(C)$, the mass fraction of carbon in the photosphere. From the previous discussion, $f(C)$ is thought to be $f \sim V_{13.3}$ but could be as low as $f \sim \frac{1}{50} - \frac{1}{133}$ so

$$\dot{M}_g \geq 2.3\text{-}23 \times 10^{-6} M_\odot/\text{yr} \quad . \qquad \text{(VI-8)}$$

(b) Conservation of Momentum

The mass of dust produced on or about JD +1033 was thereafter continuously absorbing linear momentum from the stellar radiation field (see Chapter VIII) at a rate

$$\frac{dP}{dt} \geq \alpha \frac{\mathcal{L}_*}{c} \quad .$$

Therefore, from JD +1033-1800 it received an impulse

$$\Delta P \geq \frac{\mathcal{L}_*}{c} \int_{1033}^{1800} \alpha \, dt \quad ,$$

which,is, integrating Fig. 35

$$\Delta P \geq \frac{\mathcal{L}_*}{c} \; 2.4 \times 10^{7} \text{ sec} \quad .$$

For a given total mass M_{tot}, this would result in a change of velocity

$$\Delta V = \frac{\Delta P}{M_{tot}} \quad .$$

But the observed apparent velocity, V_a, was approximately constant (Fig. 36), i.e. $\Delta V_a \lesssim 5$ km/s, so

$$M_{tot} = \frac{\Delta P}{\Delta V} \gtrsim \frac{\Delta P}{5 \text{ km/s}} \quad ,$$

taking $\mathcal{L}_* = 10^4 \mathcal{L}_\odot$ we get

$$M_{tot} \gtrsim 32 \times 10^{-6} M_\odot \quad . \qquad \text{(VI-9)}$$

This is to be compared with the total mass derived by weighing the dust, i.e.

$$M_{tot} = \frac{1}{f'} M_d \geq \frac{1}{f} M_d \gtrsim 6.7\text{-}67 \times 10^{-6} M_\odot \quad ,$$

and the two methods agree fairly well, the second method being independent of the uncertain quantity f(C). Again, if such events typically occur every ~ 3 years, the inferred mass loss rate is

$$\dot{M}_{tot} \gtrsim 11 \times 10^{-6} M_\odot/\text{yr} \quad .$$

This result is quite comparable to the $\sim 3\text{-}20 \times 10^{-6}$ $M_\odot$/year mass loss rates derived in Chapter VIII for the quasi-steady-state mass loss rates from M and C type Mira variables. The dust loss rate is, however, considerably higher (factor $\sim 3\text{-}10$) thus supporting the belief that the fraction of condensible material, f(C), is higher in the atmosphere of R CrB and also that much that is condensible does condense.

iii) Intrinsic Polarization of R CrB

The large polarization ($\sim 3\%$ at B and V) during the March-June 1972 minimum was explained (Coyne and Shawl 1973) in terms of scattering off an asymmetric envelope surrounding the star. The authors, however, assumed optically thin ($\tau_{0.55\mu} \lesssim 0.2$) clouds and it is not clear what will be the effect of the optically very thick clouds indicated by the visual light curve and the dust mass considerations above. On the other hand, a small net alignment of grains on our line of sight to the star, as discussed in Chapter VII, could give the observed polarization. The low apparent albedo of the clouds would seem to favor this mechanism over one requiring scattering. The $\sim 3\%$ polarization at V on JD +1425-+1435, when $\Delta V \sim 6$ mag requires an alignment of grains $a = (\tau_{max} - \tau_{min})/(\tau_{max} + \tau_{min})$ as discussed in Chapter VII, so

$$a \sim \frac{P_V}{\tau_V} \sim \frac{0.03}{5.5} \sim 0.0055 \quad ,$$

i.e. less than 1% net alignment. The $\sim 0.2\%$ polarization found by Serkowski and Kruszewski (1969) when $\Delta V \sim 0.6$ would require

$$a \sim \frac{2 \times 10^{-3}}{0.55} \sim 0.0036 \quad ,$$

i.e. a similar small net alignment. The $\sim 80\text{-}90°$ change in position angle of polarization between these two measurements (see Fig. 32) could be due to a change in the alignment of the grains, similar to what could explain the position angle variation in the long period variable stars. Similar values of P_λ/τ_λ and large position

angle changes have been observed in RY Sgr by Serkowski and Kruszewski (1969).

Alternatively, a model of an optically thick, asymmetric envelope with absorption, such as that discussed by Gaedin et al. (1973) may be able to account for these rather modest polarizations. Then the $\sim 90°$ position angle change would represent a re-alignment of the envelope. Also net polarization could possibly result from scattering off of discrete, optically thick cloudlets distributed asymmetrically about the star.

VII. INTRINSIC POLARIZATION

A. Introduction

Observations of intrinsic polarization from a celestial source potentially conveys information on the geometry of the radiation mechanisms which are operating in that source. Here we take the term radiation in its broadest sense, including emission, scattering, and absorption of photons. The linear polarization of the stars in this program has several characteristics which any proposed mechanism must be able to explain. The polarization is time variable, in both degree and position angle. Polarization at a particular wavelength can increase (or decrease) by a factor of 2-3 or more in a short time, $\lesssim$ 30 days. The position angle can also change by a large amount ($\Delta\theta \sim 90^{\circ}$) on these short time scales. There is a tendency for the polarization to increase toward shorter wavelengths and when the polarization is high the wavelength dependence tends to be steeper (i.e. there is less relative change in polarization at the longer wavelengths). There may be some regularity in the variation of polarization with time, i.e. peaking at visual minimum or on the rise to maximum, but superimposed on this are more or less random variations in degree and position angle of polarization. The average amount of polarization of a star is well correlated with its infrared excess, as measured by the flux ratio $F_{11\mu}/F_{3.5\mu}$ (Dyck et al. 1971, Fig. 1).

Harrington (1969) has proposed that scattering on molecules in the stellar atmosphere may produce the required amount of

polarization. High spectral resolution polarimetry by the Russians (Dombrovskii 1970; Derbiz and Dombrovskii 1973) indicates the same amount of polarization in the depths of a strong TiO absorption band as in the continuum. The fluxes in and out of the band must originate in quite different layers in the stellar atmosphere so this result would seem to rule out an atmospheric origin for the polarization. It would also seem to rule out polarization due to an additional overlying polarized emission mechanism, as for example, synchrotron radiation. For then, when the stellar continuum is depressed by a factor of two, as is the case in the TiO bands, one would expect the relative amount of polarization to increase by a factor of two, which is not observed. In addition, both these mechanisms fail to explain the correlation of polarization with the infrared excess, which is presumably due to emission from a shell of circumstellar grains. One mechanism which is consistent with the above observations and the correlation of polarization with infrared excess is the conversion of initially unpolarized starlight to the partially polarized light observed through absorption and/or scattering by dust grains in the circumstellar envelope surrounding the star. We will explore the implications of this model in the following discussion.

Discussions of the production of polarization in a circumstellar shell of dust grains have centered on two possible mechanisms: (1) scattering of light off an asymmetric, aligned envelope of freely oriented (un-aligned) grains and (2) scattering and absorption of light by aligned grains in a symmetric (or un-aligned)

envelope. In either case, if the mechanism is shown to be capable of producing the characteristics of the observed polarization, a physically reasonable mechanism for producing the necessary alignment must also be considered. In the first case, one must explain how the envelope as a whole came to be asymmetric, and how this asymmetry may vary in order to give the observed variation of a polarization with time. In the second case, one must explain (a) how the grains came to be asymmetric, (b) how asymmetric grains come to be aligned, and (c) how the changes in polarization may be related to this alignment. In order to guide this discussion we present a highly simplified, phenomenological model which displays the parameters which each of these models must hope to explain.

B. Polarization Model

The linear polarization at a particular wavelength λ is, by definition,

$$P_\lambda = \frac{I_{max}(\lambda) - I_{min}(\lambda)}{I_{max}(\lambda) + I_{min}(\lambda)} \quad , \qquad \text{(VII-1)}$$

where $I_\phi(\lambda)$ is the intensity of light linearly polarized at an angle ϕ and I_{max} is the intensity maximum obtained at $\phi_{max} = \theta$, the position angle of polarization. We have

$$I_{min} = \frac{1}{2} I_* e^{-\tau_T(\lambda,\phi_{min})} + \frac{1}{2} I_U \quad ,$$

and

$$I_{max} = \frac{1}{2} I_* e^{-\tau_T(\lambda,\phi_{max})} + \frac{1}{2} I_U + I_P \quad ,$$

where I_* = total unpolarized intensity of the star in the absence of a circumstellar shell, $\tau_T(\lambda,\phi)$ = total optical depth of the shell along our line of sight to the star to radiation with E-vector in the ϕ direction, I_U = intensity of unpolarized scattered light and I_P = intensity of polarized scattered light. If $\tau_T(\phi_{min}) = \tau_T(\phi_{max}) + \Delta\tau_T$ and $\Delta\tau_T \ll 1$, eq. (VII-1) reduces to

$$P = \frac{I_P + \frac{1}{2}\Delta\tau_T I_* e^{-\tau_T}}{I_S + I_* e^{-\tau_T}} \quad , \qquad \text{(VII-2)}$$

where $I_S = I_U + I_P$ = total intensity of scattered light and $\tau_T = [\tau_T(\phi_{max}) + \tau_T(\phi_{min})]/2 \simeq \tau_T(\phi_{max})$ for $\Delta\tau_T \ll \tau_T$. If we further define an alignment parameter a, by:

$$a \equiv \frac{\tau_T(\phi_{min}) - \tau_T(\phi_{max})}{\tau_T(\phi_{min}) + \tau_T(\phi_{max})} \simeq \frac{\Delta\tau_T}{2\tau_T} \quad , \qquad \text{(VII-3)}$$

this becomes, for $a \ll 1$,

$$P = \frac{I_P + a\,\tau_T I_* e^{-\tau_T}}{I_S + I_* e^{-\tau_T}} \quad . \qquad \text{(VII-4)}$$

The total intensity of light scattered to a given observor will depend on the shell geometry and the optical depths for scattering and absorption. If a fraction g of the light is polarized, the polarized intensity will be

$$I_P = g\, I_S \quad ,$$

and eq. (VII-4) becomes

$$P = \frac{g\, I_S + a\, \tau_T\, I_* e^{-\tau_T}}{I_S + I_* e^{-\tau_T}} \quad . \qquad \text{(VII-5)}$$

On the aligned envelope model, a is taken to be zero and the polarization properties are ascribed to g, which is a function of shell geometry and optical depth. For single 90° scattering off of small grains $g \sim 1$ is possible. For aligned envelopes of the type considered by Kruszewski et al. (1968) and Shawl (1971, 1972) there is a maximum of $g \sim 0.3$. The polarization of scattered light, g, is "diluted" by the unpolarized transmitted starlight $I_* e^{-\tau_T}$ so that $P \leq g$. On the aligned grain model, $a \neq 0$ and g may be positive or negative, i.e. the scattered light may increase or decrease the polarization due to extinction by aligned grains on our line of sight to the star.

C. Aligned Asymmetric Envelope

Models of the aligned envelope type have been presented by Kruszewski et al. (1968) and, in more detail and generality by Shawl (1971, 1972). Kruszewski et al. considered the maximum polarization attainable from a "double sector" shell geometry, which can be visualized by imagining one were viewing a peeled orange pole on with all but two opposite sections removed. They found the maximum polarization was given when the opening angle of each sector was $\lesssim 90°$. With this most favorable envelope they found a limit to the amount of polarization for non-absorptive particles (albedo A = 1, $\tau_a = 0$) when $x = 2\pi a/\lambda \lesssim 1$ and $\tau_{max} = 0.88$, for which $P_{max} \simeq 5.5\%$. For optical depths greater or less than this, the polarization was decreased. For absorptive particles with optical constants approximately those of graphite at $\lambda = 0.55\ \mu$ they found a somewhat lower maximum polarization ($P_{max} \sim 3\%$) at a somewhat higher optical depth ($\tau_{max} \sim 1.2$) for $x \simeq 1$ [there is an error in Kruszewski et al. (1968) on this point. Eq. (A17) should read $Z_{max} = e^{-\tau_{max}} = [A/(2 - A)]\ (\sqrt{2/A} - 1)$ for the optical depth giving maximum polarization. In the paper the third "A" is missing, so the results only differ for $A \neq 1$]. The authors suggested that higher polarizations may be produced if there is an additional component of the cloud which happens to be on our line of sight to the star, thus blocking the direct, unpolarized starlight.

Shawl (1972) considered other shell geometries in addition to the double sector and found, in the optically thin limit, the wavelength dependence was relatively invariant with respect to shell geometry but the degree of polarization was greatest for the double sector. He thereafter considered the wavelength dependence of polarization which would be produced by grains of a specified size with specified optical constants. In particular he considered the optical constants that would be appropriate for silicates, graphite, and iron. He then compared the observed wavelength dependence of polarization for a number of stars with the wavelength dependence derived from this (optically thin) model to derive

particle species, size, and column density. In general most of the stars could be fit, at one time or another, by one or more of the models, but often no fit could be obtained. In addition, no attempt was made to fit the degree of polarization or the position angle of polarization. The optical depth of the envelopes was limited to $\tau \lesssim 0.4$ in order that secondary scattering be negligible.

One objection to these well-ordered asymmetric envelope models is the limited amount of polarization they can produce. The maximum polarization given by the (thin) envelopes considered by Shawl (1972) was $P_{max} \lesssim 2.5\%$. Kruszewski et al. (1968) considered the dependence on optical depth and found there was a limiting polarization (the "Kruszewski limit") of $P_{max} \lesssim 5.5\%$ for dielectric (non-absorptive) grains and $P_{max} \lesssim 3\%$ for absorptive grains (~ like graphite or iron). On the other hand, many late-type stars show intrinsic polarization as large or larger than this. For example V CVn: $P_{max} \sim 9\%$ (Kruszewski et al. 1968), V CrB: $P_{max} \sim 10\%$ (Shawl 1972), R Gem: $P_{max} \sim 5\%$ (Dyck 1968). And stars with large infrared excesses can have even larger polarization: VY CMa $P_{max} \sim 20\%$ (Shawl 1972), IRC +10216 $P_{max} = 24\%$ (Dyck et al. 1971), NML Tau $P_{max} \sim 10\%$ (Kruszewski 1971a), CIT 6 $P_{max} \sim 15\%$ (Kruszewski 1973). Neither can large polarization always be due to a fortuitously placed cloud blocking the direct, unpolarized starlight for in several cases (e.g. R Leo, oCet, R Gem, χ Cyg, S CrB, R Hya in Chapter IV) large changes in the degree of polarization are not accompanied by corresponding changes in the visual light.

In summary, a well ordered, asymmetric envelope model seems able, at least semi-quantitatively, to fit the observed polarization of at least some of the stars at least some of the time. We will consider physical mechanisms which might produce such an asymmetric envelope. Consideration of the mass loss from these stars (Chapter VIII) indicates that a dust grain, once it has condensed, will be driven out from the star by the very strong stellar radiation field. If the radiation field is radial, then the subsequent motion of the particles will also be radial and the asymmetry of the envelope must be introduced at the time of particle condensation. Possible sources of this initial asymmetry are the angular momentum, the magnetic field and possible non-radial oscillations of the star. The angular momentum of the star provides a symmetry axis with respect to which the physical characteristics of the star may depend. Rotation will result in a non-spherical shape for the star. The equatorial radius will be larger than the polar radius which will result in the surface gravity g, being relatively smaller on the equator. By Von Zeiples theorem, the surface temperature on the equator will also be smaller ($T_{surface} \sim g^{1/4}$). The net effect will be to increase the scale height ($h \sim kT/mg \sim g^{-3/4}$) and reduce the surface temperature in the equatorial regions, which should enhance the grain production rate near the equatorial regions. Another physical process which may be important in the production of grains and which will be affected by the stellar rotation and magnetic field is convection. It is believed that for late-type giant and supergiant stars the energy which is generated by nuclear reactions deep in the stellar interior is

transported by convection to the stellar surface and thence radiated to the observor. This picture is supported by the observed surface abundance anomalies in these stars, which would naturally result from nuclear-processed material from the core being transported to the surface. The existence of stellar rotation and magnetic field will affect this convection and it will not necessarily be spherically symmetric. The appearance of convective cells at the stellar surface may, in turn, affect the production rate of dust grains, which will then be asymmetric. As a specific example, consider the sun -- sun spots are relatively cooler areas on the sun's surface which are believed to be due to a local condensation of magnetic field which inhibits the convection at that point. Further, sunspots are observed to be confined between $\sim \pm 45°$ of solar latitude, i.e. they appear in an asymmetric manner. If any dust grains were produced in a sunspot and repelled radially by solar radiation pressure, an asymmetric envelope would result. For such a mechanism to be effective in producing an observable envelope, the stellar analogs of sunspots would have to be much more extensive and active than those on the sun. In summary, it is not difficult to think of mechanisms which, at least qualitatively, might lead to the production of an asymmetric envelope which may be properly aligned with respect to an external observor. A quantitative treatment of the possible effects would be much more difficult, combining little known aspects of stellar structure in which geometry is important with the little known process of grain formation in a stellar atmosphere.

A major difficulty facing explanations of the observed polarization in terms of an asymmetric envelope is the optical depth of the envelope (see Chapter VIII). As usual, we define α as the ratio of the total excess flux in the infrared to the total observed flux $\alpha = \mathcal{F}^{exc}/\mathcal{F}^{tot}$; α is a measure of the amount of dust and is given approximately by (Appendix A) $\alpha \sim 1 - e^{-\langle\tau_{abs}\rangle}$, where $\langle\tau_{abs}\rangle$ is the average absorption optical depth of the shell. For the Mira carbon stars, α ranges from ~ 0.3 to 0.8. This means that the absorption optical depth averaged over the star's ~ 2300 °K radiation field and the <u>whole</u> 4π sterradians surrounding the star ranges from ~ 0.35 to ~ 1.6. If the grains are concentrated in asymmetric directions around the star, the optical depth must be even greater in those directions. Now, if the grains are assumed to be graphite and of small size, $a \lesssim 0.1\ \mu$, an absorption optical depth of 1 at $\lambda = 1.5\ \mu$ will mean an absorption optical depth of ~ 3.5-5 at $\lambda = 0.55\ \mu$. These shells should be quite optically thick to absorption at visual wavelengths. If some of the particles are large enough so that $2\pi a/\lambda \sim 1$ at these wavelengths, they will also be optically thick to scattering. For the M and S stars the evidence for large visual optical depths is less direct. The observed α's are small but the computed mass loss rates are large, ~ 3-7 $\times 10^{-6}\ M_\odot$/yr. If this mass loss is to be radiation pressure driven, this implies $\alpha_{pr} \sim \alpha_{scatt} \gtrsim 0.25$ for these stars. Thus, the scattering optical depth at ~ 1-2 μ must be quite large, $\tau_{scatt} \gtrsim 0.29$. Small grains ($a \sim 0.1$-$0.2\ \mu$) will

have an approximately 10 times larger scattering cross section at $\lambda = 0.55\ \mu$. Thus, we expect $\tau_{scatt}(0.55\ \mu) \gtrsim 3$ for these shells. As an example, consider the double sector model introduced by Kruszewski et al. (1968). The circumstellar envelope only covers 2π sterradians surrounding the star so, to explain the mass loss, $\alpha_{pr} \gtrsim 0.5$ over this portion of the envelope. Then $\tau_{scatt}(1\text{-}2\ \mu) \gtrsim 0.7$ and $\tau_{scatt}(0.55\ \mu) \gtrsim 7$. For $\tau = 7$, the model gives only $\sim 0.03\%$ polarization. Even for $\tau = 3.5$ the model gives only $\sim 1\%$ polarization. Thus, even the most idealized, maximally efficient envelope configuration will fail to give large polarizations as the optical depth is increased. It is not at all clear what the wavelength dependence of polarization will be in this case. One might suppose that as the optical depth decreases to longer wavelengths, the polarization should increase (since we are on the other side of the "Kruszewski limit" at $\tau_{max} = 0.88$) which is opposite to what is observed.

Further problems with regard to optical depth are encountered if the more extreme "infrared stars" mentioned earlier are considered. For these stars (for example, the M stars VY CMa, NML Cyg, NML Tau and the carbon stars IRC +10216 and CIT 6) more of the observed energy appears in the infrared which is presumably due to thicker shells around these stars. Eventually one would expect some sort of a "Kruszewski limit" to be reached and thereafter the polarization would decrease due to multiple scattering and the resultant loss of memory of asymmetry. Observations of these more extreme stars (for example Kruszewski 1971a; Dyck et al. 1971) do not show this.

The thicker shelled stars also show more intrinsic polarization, even at the shortest wavelengths observed. Thus, if Fig. 1 is extended to include these infrared objects the trend indicated there is merely continued, stars with a large $F_{11\mu}/F_{3.5\mu}$ flux ratio invariably show large intrinsic polarization. This effect has been independently noted by Kruszewski (1971b) who further emphasized that there is no case of a late-type star with large excess which also has small average polarization. He concluded that this was hard to understand on the asymmetric envelope model and was led to consider aligned grains as a source of polarization.

Gnedin et al. (1973) treated the problem of polarization produced in an optically thick, disk shaped envelope and found that if there was some absorption, i.e $A < 1$, then a net polarization can result even if $\tau \gg 1$. In this case, as in Harrington's (1969) model for the production of polarization in the stellar atmosphere, the preferred direction, with respect to which polarization is produced, is provided by the gradient of the radiation density which for $A < 1$ is maintained in an asymmetric envelope even as $\tau \gg 1$. Their model gave a maximum polarization of $P_{max} \simeq 5\%$ at $A_{max} \sim 0.6$ for viewing the thin disk edge on. This result was independent of τ for $\tau \gg 1$. For dielectric silicate grains, for which $A \sim 1$ is possible, a gradient might be established by the tendency of grains with $2\pi a/\lambda \gtrsim 1$ to forward scatter, as discussed by Jones (1973). Though this model appears to give polarization for large optical depths, it still fails to (1) explain the $P_{max} > 5\%$ which are

observed and (2) explain the apparent increase of P_{max} with optical depth.

A final difficulty that any of the models must face is the observed rapid variability of the degree and position angle of polarization, especially at shorter wavelengths. It is hard to imagine how an extensive asymmetric envelope could suddenly appear (or disappear) on a time scale as short as 30 days, which is a typical time scale over which the polarization can increase (or decrease) by factors of 2 or 3. It is even harder to imagine how such an envelope, once developed, can shift in angle by $\sim 90°$ as would seem to be required by the observed variations of the angle of polarization. The characteristic time scale for mechanical rearrangement of a circumstellar shell will be, in the absence of magnetic forces, $\tau \sim R/V \gtrsim r_*/V_{max}$, where r_* is the stellar radius and V_{max} is the maximum mechanical velocity in the problem. For late-type stars, $r_* \sim 4 \times 10^{13}$ cm and $V_{max} \lesssim 20$ km/s, so $\tau \gtrsim 0.6$ years which is longer than the observed ~ 0.1 year time scales.

As discussed earlier, sudden increases in polarization cannot be due solely to a decrease in the direct, unpolarized starlight [i.e. an increase in τ_T in eq. (VII-5)] as due to a cloud structure which suddenly appears in our line of sight to the star because there are many cases where an increase in polarization of more than a factor of two is not accompanied by a decrease in visual light by a factor of two (~ 1 mag). Rather, the increases in polarization would seem, on the asymmetric envelope model, to be due to actual increases in g and/or I_S is eq. (VII-5), i.e.

an actual increase in the amount of scattered light (I_S) or in the efficiency of conversion of scattered light to polarized light (i.e. g). Further, if I_S were to be increased by a substantial amount, it would imply a corresponding increase in the scattering optical depth at visual wavelengths which would imply an increase in optical depth at infrared (~ 1-2 μ) wavelengths which would imply an increase in absorption of the stellar luminosity by the circumstellar envelope which should result in a relative increase in the observed infrared flux at the wavelengths where the shell is radiating (i.e. $\lambda\lambda$ 8-13 μ). This also is not observed (Chapter IV), i.e. there doesn't appear to be any large increase in shell luminosity (i.e. α) coincident with the observed large increases in polarization. (The time scale for a small grain to heat up to its equilibrium temperature is $\lesssim 1$ sec for any reasonable grain parameters.)

Thus, it would seem that if the same grains which are responsible for the infrared excess are also responsible for the intrinsic polarization as indicated by Fig. 1, the large and rapid changes in polarization must be due, in large part, to changes in g, the efficiency of the envelope in producing polarization. Further, the time scale argument above seems to rule out changes of the whole envelope, for which $R \gtrsim 4\ r_*$, on the observed short time scales. Rather, on the asymmetric shell model, the rapid changes must be due to much smaller regions, $\Delta R < r_*$, perhaps closer to the star which represent only a small fraction of the total "amount of dust."

It appears that "well ordered" asymmetric envelopes of the double section type are hard pressed to explain the observed characteristics of intrinsic polarization, both with respect to optical depth and with respect to rapid time variability. A model which may still be able to account for the observations without resorting to aligned grains or some other mechanism is the "discrete cloud" model. Here the star is imagined to be surrounded by an extremely patchy cloud cover, with dense blobs of matter interspersed with relatively clear spaces. The average cloud cover, as monitored by α, could remain relatively constant, while the detailed distribution of cloud cover, as monitored by g and the observed polarization, could change with time. Such extremely patchy distribution of circumstellar dust grains is in fact indicated in the case of R CrB (Chapter VI), whether it be a single or a double star. However, the late-type long period variable stars do not, in general, show the characteristic sudden diminution of visual light which is one of the defining characteristics of the R CrB variables. In addition, the observations of the absorption lines due to circumstellar gas (Weymann 1963) indicate both constant velocity and constant strength with time; thus at some point the outflow of circumstellar material must become fairly uniform. In addition, the time scale problem is still important and would seem to limit the sizes of the polarizing regions, possibly suggesting small clouds quite close to the star as being responsible. The polarization which results from such an array of discrete clouds surrounding the star should be worked out in detail and compared with observation to see if this mechanism will work.

D. Aligned Asymmetric Grains

Aligned grains are familiar as they have been invoked to explain interstellar polarization. The situation in a circumstellar environment is, however, quite different, with higher gas densities, higher temperatures, probable turbulence, and supersonic streaming of grains relative to gas. It is not clear that a mechanism which may work perfectly well in interstellar space will work in a circumstellar shell. Even if alignment can be achieved, it must be shown that the desired polarization properties are produced. The existence of interstellar polarization implies the existence of asymmetric, alignable grains. It is probable that interstellar grains either are entirely produced or subsequently grow from nuclei which are produced in circumstellar space. In either case, we would expect at least some circumstellar grains to be asymmetric. In the case of carbon stars, the well known hexagonal, flaky structure of graphite leads one to expect small grains of graphite to exhibit some asymmetry. In the case of M and S stars with silicate minerals as the probable grain material, the observation of infrared polarization in the Orion Nebula (Dyck et al. 1973) which is correlated with a silicate absorption feature (Gillett and Forrest 1973) probably indicates that some silicate grains may also be asymmetric and alignable. We will therefore consider some possible alignment mechanisms and the polarization, both visual and infrared, which might be expected due to aligned grains.

Some of the grain alignment mechanisms which have been proposed and may be important in the circumstellar environment are

(1) gas streaming (Gold 1952, Zirin 1952), (2) photon streaming Harwit 1970), (3) magnetic: (a) paramagnetic relaxation (Davis and Greenstein 1951), (b) "compass needle" (Spitzer and Tukey 1951), (c) eddy currents (Davis and Greenstein 1951). We will consider the likelihood of these in turn.

1) Alignment by Streaming

Since the grains are being driven by radiation pressure through the gas in a circumstellar envelope (see Chapter VIII), it would seem natural to consider alignment mechanisms which might derive from this situation. Unfortunately for any such alignment scheme, there can be no net alignment of grains when viewed along the streaming direction because then there is no further symmetry which provides a preferred direction θ. Assuming the photons are streaming approximately radially away from the star, the grains will also be streaming radially with respect to the gas. Then there can be no net alignment of grains along our line of sight to the star, which is necessarily radial. This implies that $a = 0$ in equation (VII-5) and the primary advantage of aligned grains, that polarization be directly proportional to τ, is lost. Further, though grains along any particular radial direction may appear aligned to an external observor in another radial direction, there will be no net alignment unless the streaming motion, projected on the plane of the sky, has some net asymmetry. Thus, for net alignment there must also be an asymmetric envelope. Further, the streaming will always be present as long as the star is luminous

and the rapid variability of polarization is left unexplained. We therefore reject grain alignment purely by radial streaming as it has no apparent advantages over the asymmetric envelopes considered earlier.

ii) Magnetic Alignment

It is important to note at the outset that if the magnetic field is radial along our line of sight to the star, there again can be no net alignment (i.e. $a = \Delta\tau = 0$) perpendicular to our line of sight to the star, as for the purely streaming mechanisms, since there would be no further preferred direction for grains to be aligned with respect to. It is only if there is a component of magnetic field perpendicular to our lines of sight to the star that grains along those directions can have a net alignment and $a \neq 0$ in eq. (VII-5).

We will consider the general rotational motion of an asymmetric dust grain subjected to all the forces (torques) which can act on it in circumstellar space. First, we list the possible forces which can act on a grain:

(1) Magnetic
(2) Photon pressure
(3) Collisions with gas atoms
(4) Collisions with other dust grains
(5) Gravitation
(6) Other (shocks, turbulence, etc.)
(7) Dipole radiation reaction.

Since we will be interested in alignment and therefore in rotation, only forces which can couple to produce torques on a grain need be considered. Three rotational parameters will be important in this problem

(A) torques Γ_i

(B) rotational and alignment energies, E_i

(C) time scales τ_i for rotational equilibrium to be achieved.

The radiation reaction force (7) will limit the angular velocity ω that a grain can spin at. The disalignment forces, (2)-(6), will act in a statistical manner to try and destroy any alignment that the coherent magnetic forces, (1) may result in. This means that we must treat the effects of (2)-(6) differently than those of (1), the torques Γ_i in the first case must be handled statistically while the magnetic torque Γ_1 is coherent and can result in ordering. The most convenient way of doing this is by considering (B) and (C) above. A magnetic mechanism will be considered to be potentially effective for alignment if the (negative) magnetic alignment energy E_1 satisfies

$$|E_1| \gtrsim \sum_{i \neq 1} E_i \quad , \qquad \text{(VII-6)}$$

or if the time necessary for magnetic alignment τ_1 satisfies

$$1/\tau_1 \gtrsim \sum_{i \neq 1} 1/\tau_i \quad . \qquad \text{(VII-7)}$$

Now if a statistical process is is occurring at an event rate $\dot{N}_i$ and transferring an average angular momentum to the grain ΔL_i per event, the time τ_i for this to result in a transfer of net angular momentum L to the grain is

$$\tau_i = \left(\frac{L}{\Delta L_i}\right)^2 \frac{1}{\dot{N}_i} \quad . \qquad \text{(VII-8)}$$

To determine the appropriate L^2 which will control all of these time scales we note that, as shown in Chapter VIII, the grains are streaming through the gas with a terminal velocity ΔV_t which is greater than the thermal velocity of the gas, V_{th}. From the point of view of the grain, gas atoms are seen to be racing around it with random velocities of order V_{th} plus a net translational velocity ΔV_t in the anti-radial direction. Thus, the average rms velocity of gas atoms as seen by a dust grain is

$$V^2 = \langle(\vec{V}_i + \Delta\vec{V}_t)^2\rangle = V_{th}^2 + \Delta V_t^2 \quad .$$

Now if the grain were at rest in the gas, it would acquire, in thermal equilibrium (3 degrees of freedom), a rms angular momentum given by

$$E_{rot} = \frac{L^2}{2I} = \frac{1}{2} m V_{th}^2 = \frac{3}{2} kT \quad ,$$

where m = average mass of gas atoms. In a one-dimensional stream of velocity V, a grain would acquire a rotational energy

$$E_{rot} = \frac{L^2}{2I} = \frac{1}{2} m V^2 = \frac{3}{2} k\, "T_{stream}" \quad .$$

This is the angular momentum at which the drag due to differential rotation in the stream just balances the random walking rate of L. Then in the combined case it should reach

$$E_{rot} = \frac{L^2}{2I} = m\left(\frac{1}{2}(V_{th})^2 + \frac{1}{2}\Delta V_t^2\right) = \frac{3}{2}kT_{eff} \quad ,$$

where $T_{eff} = T_g + "T_{stream}"$. Taking $m = m_{H_2}$, $T_g = 10^3$ °K, ΔV_t = 7.5 km/s typical of circumstellar streaming, we have

$$T_{eff} = 5600 \text{ °K} \qquad \text{and}$$

$$E_{rot} \simeq 1.16 \times 10^{-12} \text{ ergs} \quad .$$

Now assume the grain is of characteristic size $a \sim 0.1\ \mu$ with characteristic mass $M \sim \frac{4}{3}\pi\, \rho_{grain}\, a^3$ with $\rho_{grain} \sim 3$ gm/cm^3, and characteristic moment of inertia $I \sim M a^2$. Then

$$I \sim 1.26 \times 10^{-24} \text{ gm cm}^2$$

and

$$L \sim 1.72 \times 10^{-18} \text{ gm cm}^2 \text{ sec}^{-1}$$

and

$$\omega = L/I \sim 1.36 \times 10^6 \text{ sec}^{-1} \quad (\nu \sim 2 \times 10^5 \text{ Hz}) \quad .$$

The time needed to establish this angular momentum is given by (VII-8) with L given above, $\Delta L_3 \simeq (a\ V\ m)\ \dot{N}_3 \simeq \pi a^2 V \rho_g m^{-1}$, $V = (\Delta V_t^2 + V_{th}^2)^{1/2} \sim 8.3$ km/s, where ρ_g is the gas density, so

$$\tau_3 = \frac{M}{\pi a^2 V \rho_g} = \frac{M}{\dot{M}} \quad ,$$

which is the time necessary for the grain to sweep out its mass of gas atoms (Purcell and Spitzer 1971). Numerically, for $a = 0.1\ \mu$, $\rho_{grain} = 3$ g/cm^3, $\dot{M}_g = 5 \times 10^{-6}\ M_\odot$/year for the stellar gas loss rate and V = 10 km/s, we get for the disalignment (equilibrium) time

for a grain a distance R from a star of radius r_*:

$$\tau_3 = 2.9 \times 10^3 \text{ sec } (a/0.1\ \mu)\ (R/r_*)^2 \quad ,$$

which is much less than the ~ 1 year time scale for a dust grain to move $\sim r_*$.

Now photon pressure, which is providing the terminal velocity, will have

$$\dot{N}_2\, \Delta L_2 \sim \dot{N}_3\, \Delta L_3 \quad ,$$

but much smaller ΔL's

$$\Delta L_{2a} \sim \frac{h\nu}{c}\, a \ll m\, Va \sim \Delta L_3$$

$$\Delta L_{2b} = \hbar \ll m\, Va \sim 3.2 \times 10^{-23}$$

i.e. $$\Delta L_2 \lesssim 10^{-4}\, \Delta L_3 \quad ,$$

so $\tau_2 \gtrsim 10^4\, \tau_3$ and is therefore negligible.

Likewise collisions with dust grains are negligible because the mass density of dust ρ_d is approximately

$$\rho_d \sim f\, \rho_g \sim \frac{1}{300}\, \rho_g \ll \rho_g \quad .$$

So the time necessary to sweep out a grain's mass in other grains will be

$$\tau_4 \sim 300\, \tau_3 \quad .$$

Gravitation can apply no torques so $\tau_5 \sim \infty$. A grain rotating with angular velocity ω with some dipole moment p will

radiate at a rate

$$\frac{dE}{dt} = \frac{2}{3} p^2 c^{-3} \omega^4 \quad .$$

Thus,

$$\tau_7 = \frac{E}{dE/dt} = \frac{\frac{1}{2} I}{\frac{2}{3} p^2 c^{-3} \omega^2} \quad .$$

Spitzer (1968) shows that in equilibrium a grain in an ionized gas acquires a negative charge such that the grain potential U is given by

$$e\,U = -2.5\ kT \quad .$$

This is the potential necessary to repel electrons so that the collision rate of the grain with the faster moving electrons equals that with the positive ions. For $T \simeq 10^3$ °K, a = 0.1 μ this means a charge

$$Z_g = 15\ e \quad ,$$

so $$p \sim a \sqrt{N_Z}\, e \sim a\ 4e$$

and $$\tau_7 \sim 4 \times 10^{22} \text{ sec} \gg \tau_3 \quad .$$

Other forces [i.e. (6)] may be present in the circumstellar environment. The appearance of strong emission lines is suggestive of shocks, turbulence, convection, etc. However, no models of these processes are available so τ_6 must remain an unknown quantity.

If the magnetic field is not zero, there are several magnetic field-grain interactions which can result in torques on a

grain. We consider:

(a) Paramagnetic Relaxation

This is the magnetic interation considered by Davis and Greenstein (1951) as a possible source of alignment of interstellar grains and currently believed (Purcell and Spitzer 1971) to be the most favorable alignment mechanism in interstellar space. From Purcell and Spitzer, the relaxation time for this mechanism is

$$\tau_{1a} = \frac{L}{\Gamma_{1a}} = \frac{I}{K\,V\,B^2} \quad , \text{ independent of L}$$

where $K_\omega = \chi''$, the imaginary part of the volume magnetic susceptibility, V = volume of grain, and B = the magnetic field. Taking $K \sim 3 \times 10^{-12}/T_d$ appropriate for a dielectric (i.e. silicate, silicon carbide) at a temperature T_d(°K) (Spitzer 1968) we get, for a = 0.1 μ, $T_d \sim 500$ °K:

$$\tau_{1a} \simeq 5 \times 10^4 \frac{1}{B^2} \quad \text{sec} \quad .$$

Therefore, for this to be effective in alignment we require (eq. VII-7)

$$\tau_{1a} \lesssim \tau_3$$

or

$$B \gtrsim 4.1 \text{ gauss } (r_*/R)\ (0.1\ \mu/a)^{1/2} \quad . \qquad \text{(VII-9)}$$

Now if the star's field is dipole, $B(R) \sim B_*(r_*/R)^3$, so

$$B_* \gtrsim 4.1\ (R/r_*)^2\ (0.1\ \mu/a)^{1/2} \qquad \text{(VII-10)}$$

is implied for the surface field. Taking $R \sim 2r_*$, we need B = 2 gauss and $B_* = 16$ gauss. These seem like entirely moderate magnetic fields. Even if $R \sim 4r_*$, $B \sim 1$ gauss and $B_* \sim 100$ gauss. In addition, Jones and Spitzer (1967) speculate that if iron atoms in a grain (as, for example, $(Mg,Fe)_2SiO_4$ silicate) are present in clumps, the necessary magnetic field may be reduced by an order of magnitude or more ("super paramagnetism").

(b) Diamagnetic Relaxation

Graphite is a fairly good conductor so it exhibits diamagnetism (induced magnetic moment opposite to B field). Wickramasinghe (1967) claims that measurements at room temperature in oscillating fields imply a χ'', if spin-lattice interactions are negligible, given by

$$K = \frac{\chi''}{\omega} \simeq 2.9 \times 10^{-10} \left(\frac{1}{T_d}\right) \quad .$$

This is $\sim 10^2$ higher than the K used above, so the magnetic field strengths required to align graphite flakes around carbon stars would be ~ 10 times lower, i.e. $B \sim 0.2\text{-}0.1$ gauss and $B_* \sim 1.6\text{-}10$ gauss. However, Greenberg (1968) reports and modifies the work of Cayrel and Schatzman (1954) which indicates

$$\frac{\chi''}{\omega} \sim 8 \times 10^{-13} \left(\frac{1}{T_d}\right)^2$$

for graphite. At $T_d = 500$ °K this is ~ 2000 less than the K used for paramagnetic relaxation so it would indicate pure graphite flakes would require magnetic fields ~ 45 times larger.

(c) "Compass Needle"

If a material has an anisotropic magnetic susceptibility or a permanent magnetic moment, there will be a tendency for it to line up in a magnetic field. In the first case, if the volume magnetic susceptibility is χ_{max} in one direction and χ_{min} in another, there will be a tendency for the χ_{max} direction to align with the magnetic field and the negative energy of alignment will be

$$E_{1c} = -\ (\chi_{max} - \chi_{min})\ V\ B^2 \quad ,$$

where V is the volume of the particle. In the second case, if the permanent magnetic moment is μ, there will be a tendency for μ to line up with the magnetic field with an energy of alignment

$$E_{1c'} = -\ \mu\ B \quad .$$

This second is the reason a compass needle points north. Pure iron grains have not been positively identified in interstellar or circumstellar space. In addition, the abundance of iron (the mass fraction of iron for cosmic abundances is $f(Fe) \sim 1/900$) lower than for silicates and graphite ($f \sim 1/300$). We thus don't

expect iron grains in great quantities in circumstellar space, though they aren't ruled out by observation. A small grain of iron might take the form of a "whisker" (i.e. as in iron filings). Then the magnetic moment would be $\mu = IV$, where V is the volume of the grain $\sim 4 \times 10^{-15}$ cm^3 for a ~ 0.1 μ and I = 2000 cgs (Greenberg 1968) and the condition for alignment is

$$|E_{1c'}| = \mu B \gtrsim E_{rot}$$

or

$$B \gtrsim 0.145 \text{ gauss} \quad ,$$

providing the grain temperature is below the Curie temperature for iron (1043 °K, Kittel 1966). This condition is independent of the distance from the star. If the star's magnetic field is dipole, grains at $\sim 2\ r_*$ require $B_* \sim 1.2$ gauss and grains at $\sim 5r_*$ require $B_* \sim 18$ gauss for alignment. These are quite small fields. If pure iron were present as a 10% impurity in a dielectric or graphite grain, the magnetic field requirements would be ~ 10 times higher, though the direction of alignment might not conform to one of the natural axes of the whole grain.

Graphite can form in flat hexagonal plates with grossly different physical properties along the short ("C") axis as compared to the long axes. In particular, as graphite is a fairly good conductor it is diamagnetic and has a volume susceptibility parallel and perpendicular to the C axis of:

$$\chi_{||} \simeq -48 \times 10^{-6} \text{cgs}$$

Wickramasinghe (1967)

$$\chi_{\perp} \simeq -1.1 \times 10^{-6} \text{ cgs} \quad .$$

Thus, there will be a tendency for the "C" axis to lie perpendicular to the magnetic field ($\chi_{min} = \chi_{||}$). The condition for alignment is

$$|E_{1c}| = (\chi_{\perp} - \chi_{||})\ V\ B^2 \gtrsim E_{rot} \quad ,$$

which for a ~ 0.1 μ particle implies

$$B \gtrsim 2500 \text{ gauss.}$$

This mechanism is therefore much less effective than the ones previously discussed and can probably be ignored. This conclusion is quite different than that arrived at by Donn et al. (1966) but I believe they made two errors. Firstly, they concluded the C-axis would align parallel to the magnetic field, which is not so serious but, I believe, wrong. Secondly, they stated the condition for alignment to be

$$|E_{mag}| \gtrsim \frac{m_{H_2}}{M_{grain}} K T_{gas} \sim \frac{m_{H_2}}{M_{grain}} E_{rot} \quad ,$$

which is thermodynamically untenable.

(d) Eddy Currents

This mechanism was considered by Davis and Greenstein (1951) and found to be negligible in the interstellar case. The basis is the fact that in a conductor placed in a time varying magnetic field eddy currents will be generated which will exert torques on the grain. The condition for alignment to be possible is (Davis and Greenstein 1951):

$$\frac{L_E}{L_R} = 0.65 \times 10^{19} \frac{a B^2 \sigma}{n_{H_2} T^{1/2}} \gtrsim 1 \quad ,$$

where σ is the conductivity. For the circumstellar case, $T = T_{eff} = 5600\ ^\circ K$, $a = 0.1\ \mu$, $\dot{M}_g = 5 \times 10^{-6}\ M_\odot/yr$, $\mathcal{L}_* = 10^4\ \mathcal{L}_\odot$, this becomes

$$B \gtrsim 7.2 \times 10^{-2} \frac{1}{\sigma^{1/2}} (r_*/R) \quad \text{gauss} \quad .$$

For pure iron at 573 °K, $\rho \simeq 25 \times 10^{-6}$ ohm cm $\Rightarrow 1/\sigma = 25 \times 10^3$ cgs, so

$$B(\text{iron}) \gtrsim 360\ (r_*/R) \quad \text{gauss} \quad .$$

For graphite, the conductivity is a factor of ~ 30 less, so

$$B(\text{graphite}) \gtrsim 2000\ (r_*/R) \quad \text{gauss} \quad .$$

The result is thus similar to 1c above, i.e. not very effective for alignment.

(e) Summary

In summary, it appears that the "paramagnetic relaxation" mechanism is potentially able to align dielectric grains (i.e. silicate, silicon carbide) in the circumstellar environment with the required field at the grain's radius $\sim$ 2-1 gauss and an implied field at the star's surface, if the field is dipole, of $\sim$ 16-100 gauss. If "super paramagnetism" is important, the field requirements may be reduced by a factor of ~ 10. Jones and Spitzer (1967) re-examined the Davis-Greenstein mechanism from a statistical mechanics point of view. Their approximate but analytic treatment of the problem essentially confirmed the results of Davis-Greenstein, i.e. that under the stated conditions there would be net alignment of a non-spherical grain. In addition, they found the condition $T_{gas} \neq T_d$ to be necessary for alignment. If $T_d < T_{gas}$ alignment is such that the axes having the largest moment of inertia tend to aligned with the magnetic field. If $T_d > T_{gas}$, the reverse is true. In the circumstellar case, $T_{gas} \sim T_{eff} \sim 5600\ ^\circ K \gg T_d$, so the first case will always hold -- polarization reversals cannot be due to alignment reversals in a fixed magnetic field. Purcell and Spitzer (1971) presented a more general, Monte-Carlo analysis of the same situation and, again found alignment to occur, in agreement with the earlier analyses. In addition, they concluded that alignment was more favorable for nearly spherical than for highly elongated grains because of the larger surface/volume ratio of the latter -- disalignment being proportional roughly to surface area and alignment proportional to volume. Thus all studies indicate that this

mechanism will give net alignment in a sufficiently strong magnetic field, if $T_{gas} \neq T_d$.

To see if rapid changes in polarization are allowed under this mechanism, we note that if alignment is to occur, the magnetic alignment time in a given magnetic field will be (eq. VII-7):

$$\tau_1 \lesssim \tau_3 \sim 3 \times 10^3 \ (a/0.1\ \mu) \ (R/r_*)^2 \quad \text{sec} \quad .$$

So for $R = 2r_*$, $\tau_1 \lesssim 1.2 \times 10^3$ sec ~ 3 hrs and for $R = 5r_*$, $\tau_1 \lesssim$ 20 hrs and alignment changes on time scales of ~ 1 day are possible. The time scale for a change of the magnetic field in the circumstellar envelope will be given by $\tau_B = r_*/V_a$, where V_a is the Alvén speed. For $\dot{M}_g = 5 \times 10^{-6}\ M_\odot$/yr, $R = 2r_*$, $V_g = 10$ km/s, we have $\rho_g \sim 4.1 \times 10^{-15}$ gm/cm^3 or $N_H \sim 2.6 \times 10^9$ cm^{-3}. And

$$\frac{V_a}{c} = \sqrt{\frac{B^2}{4\pi \rho_{plasma}}} \simeq \frac{7\ B}{\sqrt{N_e}\sqrt{\frac{m_{ion}}{m_H}}} \quad .$$

In the low temperature ($T_* \sim 2500\ ^\circ$K) radiation field of the star, the ionization will be supplied by the abundant metals with low ionization potential. Assuming all the metals (Mg, Fe, etc.) are singly ionized, $N_e \sim 10^{-4}\ N_H$ and $m_{ion}/m_H \sim 40$, so for B = 2 gauss,

$$V_a \simeq 4.4 \times 10^{-3}\ c \sim 1300 \text{ km/s} \quad .$$

So the characteristic time scale will be

$$\tau_B \sim 3 \times 10^5 \text{ sec} \sim 10^{-2} \text{ yr} \quad .$$

And changes on time scales of $\sim 10^{-1}$ yr would seem to be allowed, even for extensive regions of the whole circumstellar envelope ($R \gtrsim 4r_*$), if the magnetic field of the star changes on these times.

For graphite flakes, the same mechanism will work but the magnetic field required is uncertain because of the uncertainty in the χ''/ω appropriate for graphite. The magnetic field required may be ~ 10 times lower or ~ 45 times higher than the fields quoted above. In addition, Purcell and Spitzer (1971) point out that very thin graphite flakes will take $\gtrsim 10$ times larger field for alignment than for dielectric cylinders because of their large surface/volume. On the positive side, because of the very anisotropic optical properties of a small graphite flake, a smaller net alignment would be sufficient to produce a given amount of polarization.

Small iron needles may also be aligned by fields which are ~ 5-10 times smaller than those required for dielectric grains. If the iron is present as an $\sim 10\%$ ferromagnetic "impurity" in a 0.1 μ grain, the fields required would be about the same as for paramagnetic relaxation. The orientation given by this "compass needle" mechanism is such that the magnetic axis of a needle lines up with the magnetic field, which is orthogonal to Davis-Greenstein orientation. In addition, the field requirement is independent of distance from the star so a dielectric grain with ferromagnetic impurity might be aligned by the "compass needle" mechanism while near the star and the orthogonal Davis-Greenstein mechanism when further away.

iii) Magnetic Field Measurements

The status of direct measurements of magnetic field strengths in and around late-type stars is unsatisfactory. In the method of Babcock (1960) the longitudinal magnetic field averaged over the surface of a star is measured by observing the splitting of the opposite circularly polarized components due to the transverse Zeeman effect. The photographic technique employed limits one to stars which are bright visually, have narrow lines, large ($\sim$ 200 gauss) average fields and even then requires a large telescope. In the comprehensive catalog by Babcock (1958) there are several giant and supergiant M and S stars with large ($\sim$ 500 gauss) and sometimes variable magnetic fields. Of the stars included in the present study, R Gem was found to have an $\sim$ 400 gauss field and R Leo and R CrB were thought to have probable but not certain magnetic fields. Unfortunately, since the important and fundamental work by Babcock, there have been no further published studies of the magnetic fields of these types of star. Babcock (1960), in his review of the significance and prevalence of stellar magnetic fields, says "there is support for the view that a majority of all stars possess magnetic fields of significant intensity" and speculates that significant convection zones may be necessary for the generation of magnetic fields. He also states that "all stellar magnetic fields adequately observed are found to be variable..." Thus, there is at least a prima facie case for time variable surface magnetic fields on the order of several hundred gauss in the late-

type stars of this study and R CrB. What is needed are studies, possibly using sensitive photoelectric techniques, of the magnetic fields of these stars.

Woolf (1973) has suggested that the observed OH and H_2O maser emission lines may contain information on the circumstellar magnetic fields of these stars. The same longitudinal Zeeman effect would cause the positive and negative circularly polarized components to have slightly different energies and result in a splitting. The magnitude of splitting due to a magnetic field B will be

$$\Delta E_Z \simeq 2 \mu B$$

and

$$\Delta E_Z = h\Delta\nu \quad ,$$

so

$$\frac{\Delta\nu}{\nu} \simeq \frac{1}{h\nu} 2 \mu B \quad , \qquad \text{(VII-11)}$$

where μ is the magnetic moment of the upper (or lower) energy state. In an atom or molecule with non-zero angular momentum, μ will be of the order of μ_B, the Bohr magneton. Note that for a given magnetic field, the Zeeman splitting will be relatively greater for a transition with lower energy ($h\nu$). Thus, the splitting of the radio transitions of a molecule are relatively much larger than the splittings of the optical transitions which are used to determine the surface fields of a star. For the OH 18 cm $\sim$ 1700 MHz maser transition the splitting will be

$$\frac{\Delta\nu}{\nu B} \sim 1.66 \times 10^{-3} \text{ gauss}^{-1}$$

or

$$\frac{B}{\Delta\nu} \sim 0.45 \times \frac{10^{-3} \text{ gauss}}{\text{KHz}} \quad ,$$

or in terms of Doppler shift, $\Delta V = c(\Delta\nu/\nu)$,

$$\frac{B}{\Delta V} \sim 2 \times \frac{10^{-3} \text{ gauss}}{\text{km/s}}$$

For the $H_2O \sim 1.35$ cm transition the corresponding sensitivities will be

$$\frac{B}{\Delta\nu} \sim 0.45 \times \frac{10^{-3} \text{ gauss}}{\text{KHz}}$$

or

$$\frac{B}{\Delta V} \sim 27 \times \frac{10^{-3} \text{ gauss}}{\text{km/s}} \quad .$$

The observed OH maser emission from late-type long-period variable stars consists generally of two lines, one at approximately the stellar photospheric velocity and one blueshifted from that velocity $\sim$ 10-50 km/s. There is a good correlation (Dickinson and Chaisson 1973) between the velocity separation and the pulsation period of the variable, the longer period stars showing greater separation, but the interpretation of this in terms of shell geometry, etc. is not certain. The individual lines are narrow, $\lesssim 5$ km/s wide, and may be more or less unpolarized, though in some cases there is some linear and circular polarization. If we interpret the lack of splitting of the lines as due to a lack of magnetic field then

$$B_{OH} \lesssim 10^{-2} \text{ gauss}$$

is indicated, which is a quite small field. A model for the OH emission presented by Wilson and Barrett (1970) indicates the emitting region is characterized by a kinetic temperature $\sim$ 500-1000 °K, density $\lesssim 10^{-16}$ gm/cm^3 and an OH cloud length $\gtrsim 2 \times 10^{15}$ cm. For a mass loss of $\sim 5 \times 10^{-6}$ $M_\odot$/yr, the density requirement implies $R_{OH} \gtrsim 5 \times 10^{14}$ cm ~ 10 R_*. Thus, the OH emission regions must be well separated from the star. If R_{OH} is taken to be $\sim 2 \times 10^{15}$ cm $\sim$ 50 R_*, and the star's field is dipole, $B_{OH} \lesssim 10^{-2}$ gauss implies $B_* \lesssim 1250$ gauss. Thus, the low magnetic fields indicated by the OH observations may not be inconsistent with the possible high surface fields indicated by the work of Babcock. In addition, Scoville (1974) has pointed out that the interpretation of maser emission features in terms of Zeeman splitting due to magnetic fields, or the lack thereof, is not straightforward due to the complicated radiation-transfer problem presented by maser emission.

The H_2O 1.35 cm maser emission from long-period variable stars appears as a single line, $\lesssim$ 2 km/s wide, at a velocity between the velocity of the star and that of the blueshifted OH component (Schwartz and Barrett 1970a,b). The emission is variable in strength, but constant in velocity to $\lesssim \pm 0.5$ km/s (Schwartz *et al.* 1974). If eq. (VII-11) is now applied blindly, we would infer

$$B_{H_2O} \lesssim 0.05 \text{ gauss} \quad .$$

Models of the H_2O emitting region are in an even less satisfactory state than for OH. The lack of velocity variation implies that $R_{H_2O} > r_*$ (Schwartz et al. 1974) and Schwartz and Barrett (1970a) indicate that $N_{H_2O}dR \gtrsim 10^{16}$ cm^{-2} is necessary in order to support maser action. The model atmosphere of Tsuji (1966) indicates that in the extreme outer layers of a late-type M star, $N_{gas}/N_{H_2O} \sim 1800$. If this is taken to hold in the circumstellar envelope and a mass loss rate of $\sim 5 \times 10^{-6}$ $M_\odot$/yr at $V_{gas} \sim 10$ km/s is assumed, $N_{H_2O}dR \gtrsim 10^{16}$ cm^{-2} implies $R_{H_2O} \lesssim 3 \times 10^{17}$ cm $\sim 10^4$ R^* for masing action to be possible. Thus, we have $r_* < R_{H_2O} \lesssim 0.8 \times 10^4$ r_*. Taking $R_{H_2O} \sim 10^{15}$ cm ~ 25 R_* and assuming a dipole field, the above limit on B_{H_2O} implies

$$B_* \lesssim 800 \text{ gauss} \quad ,$$

which is not a strong constraint. Again this interpretation in terms of a lack of Zeeman splitting is uncertain because of the complicated nature of the radiation transfer problem in a masing source.

Scoville (1974) also pointed out that the thermal transitions of the CO molecule in the radio region are potentially more informative regarding magnetic fields because the radiation transfer problem is better understood. Thermal emission from the $J = 1 \rightarrow 0$ rotational transitions of CO (2.6 mm) and HCN (3.4 mm) has been detected from the late-type carbon Mira variables IRC +10216 and IRC +30219 (CIT 6) (Wilson et al. 1973). The lines are broad

($\gtrsim 20$ km/s) and flat-topped, suggesting saturation and/or expansion in the sources. Applying eq. (VII-11) we have

$$B_{CO,HCN} \lesssim 0.12 \frac{\text{gauss}}{\text{km/s}} \lesssim 2.4 \text{ gauss}.$$

Thus, the magnetic field in the region of line formation could be quite high. In the case of IRC +10216 the CO emission source was resolved on the sky and found to have an angular diameter of $\sim 138''$ which is much larger than the inferred diameter of the star ($\theta_* \sim 0.05''$) and the diameters of the optically thick ($\theta \sim 0.4''$) and optically thin ($\theta \sim 2''$) components of the dust shell surrounding the star measured by lunar occultation (Toombs et al. 1972). Thus, the magnetic field at the emitting dust shell could be as high as $\sim 10^6$ gauss and not result in a detectable Zeeman splitting in the extended CO emitting cloud. The HCN source was unresolved and therefore $\lesssim 40''$ in diameter. This limits the magnetic field to $\lesssim 1.5 \times 10^5$ gauss at the emitting dust shell which again isn't a very stringent limit.

Geballe et al. (1973) have observed absorption due to the fundamental $\Delta v = 1$ vibration-rotation bands of CO at 4.7 μ in IRC +10216. The lines were all narrower than the instrumental resolution (~ 20 km/s) and were blueshifted by ~ 20 km/s from the radial velocity of the star measured by Herbig and Zappalla (1971). From the existence of absorption from high rotational levels, $J = 23$, of the CO molecule the authors concluded that the CO giving rise to the observed absorptions was probably associated with the $\sim 2''$, 400 °K component of the shell. The magnetic moment of a $J = 23$

level of CO will be

$$\mu_{23} \sim 23\ \mu_B \quad ,$$

and eq. (VII-11) becomes

$$\frac{B}{\Delta V} \lesssim 3.3\ \frac{\text{gauss}}{\text{km/s}} \quad .$$

And since $\Delta V \lesssim 10$ km/s (i.e. half the instrumental resolution)

$$B(2^{m}_{shell}) \lesssim 33 \text{ gauss} \quad .$$

This is probably the most stringent limit on the magnetic field in a circumstellar shell, free of the complications of masing, which is available at the present time. If the field is dipole, this implies $B_* \lesssim 2 \times 10^6$ gauss, which again is not much of a limit.

In summary, the direct measurement of stellar magnetic fields (Babcock 1958, 1960) indicate surface fields on the order of several hundred gauss are possible. Measurements of the magnetic fields in circumstellar space are in a more primitive state but so far do not seem to contradict this. It would seem that the magnetic fields necessary for grain alignment ($\sim$ 2-1 gauss in circumstellar space, $\sim$ 16-100 gauss at the stellar surface) may well exist. Further, it appears that the time scales for magnetic propagation and magnetic alignment in circumstellar space are sufficiently small to allow the observed rapid changes in polarization to be due to changes in alignment.

iv) Polarization Resulting from Grain Alignment

If asymmetric grains in a circumstellar envelope are aligned by the action of a magnetic field, the resultant linear polarization as seen by an observor in a particular direction but far from the star will be a complicated function of cloud geometry (grain distribution, with respect to R, θ, and ϕ), grain opacities, magnetic field geometry, grain alignment (with respect to R, θ, ϕ), optical depth, etc. A realistic model which takes into account all the relevant parameters would be quite difficult, even if the relevant parameters were known, and is beyond the scope of this thesis. This is especially so because the inferred optical depths of these shells (Chapter VIII) are in the range $\tau_{vis} \gtrsim 1$, which is the most difficult radiation transfer problem to treat. If the particle albedos are high, which is the case for silicate and SiC grains and, to a lesser degree, large graphite grains, the contribution to the observed polarization due to (multiply) scattered light (i.e. g in eq. VII-5) must be included. The condensation of grains near a stellar surface may depend on the magnetic field strength which may be modified by or may modify the convection patterns of the star.

In order to make progress at this point, we will consider a simplified model for the star + magnetic field + circumstellar grains. Consider the star to be inert, the magnetic field to be dipolar, and the circumstellar shell to be, aside from the magnetic field, spherically symmetric with respect to the star.

Consider first an observor who views this system along the magnetic pole. He will see radial symmetry of the magnetic field-lines and therefore of the aligned grains and no net linear polarization will result. In this way, the aligned grain model is like the aligned envelope models in that the polarization goes to zero when viewed along certain symmetry directions. However, in the aligned grain case, a change in the axis of the magnetic field can introduce changes in polarization on time scales $\lesssim 3$ days without requiring the envelope as a whole to be re-aligned. The maximum radial asymmetry will obtain for an observor in a direction perpendicular to the magnetic axis of the system, so we consider observation from this direction. In the Davis-Greenstein alignment scheme, asymmetric grains end up spinning preferentially about the grain axes which have the largest momentum of inertia and these axes are also aligned along the magnetic field. A needle-like grain ends up spinning about its short axis and its time-averaged extinction efficiency will be approximately the same as a flat disk with its short axis aligned along the magnetic field line.

Consider a magnetic field $\vec{B}$ due to a magnetic dipole $\vec{m}$ at the origin aligned in the +Z direction with the observor in the +Y direction. The magnetic field at a point $\vec{R}$ from the origin will be given by

$$\vec{B}(\vec{R}) = \frac{3\hat{R}(\hat{R}\cdot\vec{m}) - \vec{m}}{R^3}\,, \quad \vec{m} = m\,\hat{Z}$$

(Jackson 1962). At a given distance R from the star there will be regions on the sphere where $\vec{B}$ points in each of the $\pm$ Z, $\pm$ X, and

$\pm$ Y directions. However, there is more surface area of the sphere corresponding to alignment in the $\pm$ Z directions, i.e. $\langle(\hat{B}\cdot\hat{Z})^2\rangle^{1/2} = 0.65$ while $\langle(\hat{B}\cdot\hat{X})^2\rangle^{1/2} = \langle(\hat{B}\cdot\hat{Y})^2\rangle^{1/2} = 0.54$. On our line of sight to the ($\vec{R} = R\,\hat{Y}$) the magnetic field is in the - Z direction and grain alignment will be in the $\pm$ Z directions (i.e. long axes in the $\pm$ X directions) which will result in a net alignment, $a \neq 0$ in eq. (VII-5), on our line of sight. The polarization will be such that the electric field lies in the $\pm$ Z direction. These grains can also emit polarized light in the infrared (E-vector in $\pm$ X direction). In addition, grains in other directions can scatter polarized light [i.e. $g \neq 0$ in eq. (VII-5)] and will also emit polarized light. We will consider these possible effects.

The grains aligned in the $\pm$ Y directions will give no net polarization in emission or by scattering. The grains aligned in $\pm$ X and $\pm$ Z directions will tend to emit and scatter light preferentially in a direction perpendicular to the alignment direction so, in the optically thin, spherically symmetric case, we might expect a net polarization from these processes. If the (emission or scattering) opacities of the grain perpendicular and parallel to $\vec{B}$ are A and B respectively, with A > B, the net polarization will be (for the emitted or scattered light)

$$P = \frac{I_X - I_Z}{I_X + I_Z} \simeq \frac{0.11(A - B)}{1.19(A + B) + 1.08\,A} \quad \pm\hat{X} \text{ direction}\,,$$

where we assume

$$I_X \simeq I_o \left\{ A[\langle(\hat{B} \cdot \hat{Z})^2\rangle^{1/2} + \langle(\hat{B} \cdot \hat{Y})^2\rangle^{1/2}] + B[\langle(\hat{B} \cdot \hat{X})^2\rangle^{1/2}] \right\}$$

and

$$I_Z \simeq I_o \left\{ A[\langle(\hat{B} \cdot \hat{X})^2\rangle^{1/2} + \langle(\hat{B} \cdot \hat{Y})^2\rangle^{1/2}] + B[\langle(\hat{B} \cdot \hat{Z})^2\rangle^{1/2}] \right\}$$

for B = 0.5A, i.e. $a = (\tau_X - \tau_Z)/(\tau_X + \tau_Z) \simeq (A - B)/(A + B) \sim 0.33$ in eq. (VII-3), which corresponds to either ~ 33% alignment of perfect polarizers or ~ 100% alignment of ~ 33% polarizers, we have

$$P \sim 0.019 \sim 1.9\%, \pm X \text{ direction.}$$

The net polarization of the scattered starlight and the thermal emission from the grains may not be too large even if there is extensive alignment. Thus, the aligned grain model may be consistent with the small ($P \lesssim 1\%$) 10 μ polarizations found by Capps and Dyck (1972) for stars with intrinsic polarization and infrared excesses. In addition, we shall find later that smaller net alignments, $a \lesssim 0.1$, are probably sufficient to explain the observed visual polarizations, so this polarization would be decreased even more. Finally, as the optical depth increases, the net polarization in the scattered (or emitted) light will decrease. Therefore, we shall consider the case that the scattered light from the star is, on average, unpolarized. This means g = 0 in eq. (VII-5) and the polarization will be

$$P \simeq \frac{a\, \tau_T\, I_*\, e^{-\tau_T}}{I_S + I_*\, e^{-\tau_T}} \quad , \pm \hat{Z} \text{ direction} \quad , \qquad \text{(VII-12)}$$

where, as usual, $\tau_T = (\tau_X + \tau_Z)/2 \sim \tau_X$ is the mean total optical depth on our line of sight to the star, the alignment parameter $a = (\tau_X - \tau_Y)/(\tau_X + \tau_Z)$ and we require $a \ll 1$ and $a\tau_T \ll 1$ for this expression for P to hold.

The effect of the scattered light, I_S, is to dilute the polarization imposed on the direct starlight by the grains aligned preferentially in the ± Z direction. If the grain albedo, A, is zero at a particular wavelength, $I_S = 0$. If $A \neq 0$, then the determination of I_S is again a difficult problem in radiation transfer which is further complicated by the assumed grain alignment. We define an effective average overall optical depth of the shell, τ_e, by

$$I_{obs}(\lambda) = I_*(\lambda)\, e^{-\tau_e} \quad ,$$

where I_* is the intrinsic monochromatic apparent flux and $I_{obs}(\lambda)$ is the observed apparent monochromatic flux at a wavelength λ short enough that grain emission can be ignored. Now we also have

$$I_{obs} = I_{scatt} + I_*\, e^{-\tau_T} \quad ,$$

i.e. the observed flux is the sum of the extinguished direct starlight plus the light which is scattered and transmitted through the shell. Then

$$I_{scatt} = I_{obs} - I_*\, e^{-\tau_T}$$

$$= I_*\, (e^{-\tau_e} - e^{-\tau_T})$$

and eq. (VII-12) becomes

$$P \simeq a\ \tau_T \frac{e^{-\tau_T}}{e^{-\tau_e}} = a\ \tau_T\, e^{-(\tau_T - \tau_e)} \quad .$$

Jones (1973) has considered the problem of optical transmission through a spherically symmetric cloud as a function of grain albedo, A, and phase function, $g = \langle \cos\theta \rangle$. This solution is only strictly valid in the limit $\tau \gg 1$, but the results may apply, at least qualitatively, in the $\tau \sim 1$ region which is appropriate for most of the stars considered here. We identify our τ_T with his τ_g, i.e. the geometric line-of-sight, optical depth of the shell. For most reasonable grain parameters, he found

$$\tau_e \gtrsim 0.5\ \tau_T \quad .$$

Thus, we immediately have

$$P \gtrsim P_{min} = a\ \tau_T [e^{-\tau_T}]^{1/2} \quad (\text{for } a,\ a\ \tau_T \ll 1) \quad .$$

For a given a, P_{min} will be $\sim$ linear with τ for $\tau \lesssim 1$ will reach a peak at $\tau \sim 2.0$, and thereafter decline. To get $\sim 5\%$ polarization with $\tau \sim 1$, we require $a \lesssim 0.08$, i.e. $\sim 8\%$ net alignment of the grains on our line of sight to the star. For small ($a \lesssim 0.05\ \mu$) graphite grains, $A \lesssim 0.2$ and $g \lesssim 0.02$ for $\lambda = 0.55\ \mu$ and for these parameters,

$$\tau_e \simeq \tau_T \quad ,$$

so

$$P \sim a\ \tau_T \quad (a,\ a\ \tau_T \ll 1) \quad .$$

And 5% polarization for $\tau_T = 1$ requires $a \gtrsim 0.05$, and a smaller net alignment would suffice.

In conclusion it appears that, within the limits of the discussion above, a moderate proportion ($a \sim 0.1$) of aligned grains on our line of sight to the star would be sufficient to give the degree of polarization which is observed in the late-type stars. The rapid changes in amount and position angle of the polarization could then be due to rapid changes in a, the alignment of the grains, without requiring an overall change in the amount of dust (i.e. τ). The increase of polarization toward shorter wavelengths and the continuing increase of polarization for more extreme infrared stars could be due to increases in τ_T. In addition, it appears that the modest amount of alignment required may be consistent with the observed small infrared polarizations, $P_{10\mu} \lesssim 1\%$, if the dust cloud is roughly spherically symmetric and the grains are aligned by a dipole-like field rather than being in a "picket fence" array. This, of course, does not prove the case for aligned grains but only indicates the plausibility of the mechanism and some of the features which might be expected under the admittedly highly simplified model considered here. More detailed calculations, using realistic grain opacities, etc. should be attempted to see if other details, such as the time-variable wavelength dependence of polarization, could be explained by such a model.

We suggest two key tests which should be able to distinguish between the aligned grain and asymmetric envelope models. Firstly, measurements of the stellar magnetic field simultaneous with the linear polarization could be made. If magnetic fields can be detected and changes in the magnetic field are correlated with changes in intrinsic polarization, it would support the magnetic alignment model. Conversely, if low limits can be set on the surface ($B_* \lesssim 10$ gauss) or circumstellar ($B_{CS} \lesssim 1$ gauss) magnetic fields, the magnetic alignment mechanism will be in trouble. Secondly, high spatial resolution, polarimetric studies of some of these stars should be able to distinguish between the models. The aligned grain model predicts that the core of the observed image, corresponding to θ_*, should be polarized while the aligned envelope models predict that polarization will only arise from regions of the shell which are away from the star, so that 90° scattering can occur.

E. Conclusion

In conclusion, it appears that scattering and absorption by circumstellar dust grains is able to account for at least some of the properties of the observed intrinsic linear polarization. Models of the aligned, asymmetric envelope type (Kruszewski et al. 1968; Gnedin et al. 1973) give a maximum polarization of $P_{max} \sim 5\%$. In addition, Shawl (1971, 1972) has shown, using the optical constants of realistic grain materials, that the wavelength

dependence of polarization can also be explained on these models, at least in the optically thin limit. The primary difficulties of these models are the apparent continuing increase of polarization with optical depth of the shell and the rapid changes in polarization which are not correlated with the infrared or visual light. If the radiation from the star is spherically symmetric, the rapid changes in polarization seem to limit the region responsible for polarization to $R \sim r_*$ so perhaps a model in terms of discrete clouds of gas and dust close to the star is more appropriate.

The aligned asymmetric grain model has been investigated and it is found that (1) alignment can be expected for moderate magnetic fields ($B_{shell} \sim 1$-2 gauss, $B_* \sim 16$-100 gauss), (2) the expected infrared polarization from the aligned grains may be small, (3) polarization proportional to optical depth is expected in the simplest model, with $P > 5\%$ possible for moderate degrees of alignment, and (4) rapid changes in polarization are possible through rapid changes in alignment without requiring an overall change in the optical depth and infrared excess of the shell. Further, this model predicts that (1) changes in polarization should be correlated with changes in the magnetic field and (2) most of the observed polarization should come from the central regions of the circumstellar shell.

If either of the above models are shown to be insufficient to explain the observed polarization, perhaps a combination of the two, or an asymmetric stellar light source, or an entirely different mechanism will have to be considered.

VIII. MASS LOSS FROM M, S, AND C STARS

A. Introduction

Mass loss from stars is potentially important for at least three reasons. For the star itself, if a mass loss at a steady rate $\dot{M}$ is occurring, the lifetime τ of this phase of a star's life is limited to $\tau \leq M_*/\dot{M}$. In addition, if some of the mass lost is converted to solid grains, the appearance of a star to an outside observor may be quite different due to the scattering and absorptive properties of the grains. For the galaxy, the existence of very luminous stars with theoretical lifetimes much less than the age of the galaxy ($\sim 10^{10}$ years) implies there is a continuous production of such stars from the interstellar medium. Unless the interstellar medium was much more dense in the past, this implies a constant replenishment of the interstellar medium, and stars could be an important source. Finally, observations in our Galaxy and others indicate the presence of dust grains in the interstellar medium. The average visual extinction in our Galaxy, ~ 1 mag/kpc, implies a fraction of mass in grains to mass in gas of $\sim 1/200$. In addition, these grains are not uniformly distributed but are concentrated along the spiral arms and in association with regions where stars are being formed. Thus the dust grains may be important to the process of star birth. Production of dust grains from gas in interstellar space is difficult because of the low densities, $N_H \sim 1$ cm^{-3}. Grain growth may occur in the denser cloud

regions, $N_H \sim 10^2 - 10^5$ cm^{-3}, but this process requires seed nuclei to be initially present. If some fraction of the mass lost from stars is in the form of dust grains, this may help explain the existence of interstellar dust.

B. Observations

The spectroscopic evidence at visual wavelengths for mass loss from stars has been summarized and discussed by Deutsch (1960) and Weymann (1963). The observational evidence is the existence of very narrow, very deep absorption lines from the ground state of atoms which are blueshifted by $\sim$ 10-20 km/s from the stellar velocity indicated by the normal stellar absorption lines. The supposition that these lines arise in cool, circumstellar gas leaving the stars is strongly supported by the discovery by Deutsch that the same lines are seen in the G-type visual companion to α Her which is at least 700 AU away from the M5 primary (Deutsch 1960). A notable feature of these circumstellar lines is that they remain quite constant in both velocity and strength, to the accuracy of measurement, with time.

The difficulty in explaining this mass loss by hydrodynamic means (analogous to the explanations of the solar wind) is evident in reading the account of Weymann (1963). Most troublesome are the low temperatures and turbulence of the circumstellar gas (narrow lines, low excitation) and the moderate and evidently constant velocity of outflow. On the other hand, Gilman (1972) has shown

that solid grains in a circumstellar envelope which are being accelerated outward by the strong ($\mathcal{L}_* \sim 10^4\ \mathcal{L}_\odot$) radiation field will be effectively momentum coupled to the gas, that is collisions with gas atoms occur frequently enough to transfer the momentum derived from the stellar radiation field to the gas. Thus, radiation pressure on the dust grains could be the agent driving mass loss. Gehrz and Woolf (1971) have used infrared observations to estimate the density and radii of circumstellar envelopes and the spectroscopically determined velocities to give the rate of outflow to derive mass loss rates for M stars. This technique will be re-examined here and two other ways of deriving mass loss rates from observations of infrared emission by circumstellar dust will be considered.

C. Two Methods for Measuring Mass Loss

1) Weighing the Dust

If a particular species of dust can be identified through its observed spectrum (e.g. silicates, SiC) or inferred on theoretical grounds (e.g. graphite, iron), then the observed fluxes can be interpreted in terms of the amounts of material, its temperature, and its distribution relative to the exciting source (star), using opacities derived from laboratory measurements of the optical constants of that material. The probable identification of silicates around M and S stars and silicon carbide around C stars has been discussed in Chapter V. Graphite is expected to

condense in the atmosphere of cool C stars characterized by $N_C > N_O$ (O'Keefe 1939; Hoyle and Wickramasinghe 1962; Gilman 1969) and is the most plausible explanation for the blackbody-like excesses seen in the carbon Miras (Chapters IV, V). The optical constants for pure graphite (Taft and Phillip 1965) and pure SiC (Spitzer et al. 1959) have been measured and the relevant opacities are discussed in Appendix B. The situation for silicates is less clear-cut but we will assume that at least the opacity in the 10 μ region is fairly well established.

(a) Observed Emission

The monochromatic flux observed from an optically thin shell of dust grains at an average temperature T_d will be

$$F_\lambda^d = \frac{\kappa_\lambda M_d}{D^2} B_\lambda(T_d) \quad , \qquad \text{(VIII-1)}$$

where κ_λ is the absorptive opacity per unit mass (cm^2/gm) for the grains (see Appendix B), $M_d = \sum_i m_i$ is the total mass of dust radiating, D is the distance, star-earth and $B_\lambda(T)$ is the Planck function ($W\ cm^{-2}\ \mu^{-1}\ ster^{-1}$). This result is discussed, from a slightly more general point of view, in Appendix A [see eqs. (A-3, -20 and -21)]. If either the shell as a whole or the individual particles go optically thick, the flux will be reduced from this value. If the particles resonate ($2\pi a/\lambda \sim 1$), the flux may be increased. The star, of radius r_* characterized by a temperature

T_*, as observed at distance D will radiate approximately:

$$F_\lambda{}^* \simeq \frac{\pi r_*^2}{D^2} B_\lambda(T_*) \quad , \qquad \text{(VIII-2)}$$

and in the case of a shell optically thin at a wavelength λ the observed flux will be the sum of (VIII-1) and (VIII-2). Now from Appendix A, eq. (A-14) the definition of β_λ gives, with the continuum being identified with the star:

$$\beta_\lambda = \frac{F_\lambda^d}{F_\lambda^*} = \frac{\kappa_\lambda M_d B_\lambda(T_d)}{\pi r_*^2 B_\lambda(T_*)} \qquad \text{(VIII-3)}$$

or

$$M_d = \beta_\lambda \frac{B_\lambda(T_*)}{B_\lambda(T_d)} \frac{\pi r_*^2}{\kappa_\lambda} \quad , \qquad \text{(VIII-4)}$$

and the initial result, namely "weighing the dust," has been achieved. Here we are using the star itself as a "standard candle" to estimate the quantity D^2 in eq. (VIII-1). We will assume the total luminosity of these stars is known (roughly) and can be used to estimate D from $\mathcal{F}^{obs} = \mathcal{L}_*/4\pi D^2$. This observed luminosity is represented here by the best blackbody fit to the energy distribution, though it is not crucial to this discussion that the temperatures assigned by this method, T_*, represent an actual stellar surface temperature. The blackbody fit can be thought of as a fiducial mark for scaling $F_\lambda{}^d$.

For M and S Mira variables, $\mathcal{L}_* \sim 10^4\ \mathcal{L}_\odot$, $T_* \sim 2500$ °K $\Rightarrow$ $r_* \sim 600\ r_\odot \sim 4.2 \times 10^{13}$ cm. The broad band [11 μ] opacity of small silicate grains is $\kappa_{11\mu} \sim 2 \times 10^3$ cm^2/gm and it is probable that $\kappa_{20\mu} < \kappa_{11\mu}$ so that the true temperature, T_d, will be somewhat less than the observed color temperature of the excess $T_c(11\ \mu, 20\ \mu)$. From Table 2b $T_c \sim 350$-900 °K so we will take $T_c \sim 500$ °K as typical. Also $\beta_{11\mu} \sim 1$-2 for these stars. Eq. (VIII-4) now gives

$$M_d \sim \beta_{11\mu} \frac{\mathcal{L}_*}{10^4\ \mathcal{L}_\odot} \ 5 \times 10^{25} \ \text{gm}$$

$$\sim 2.5\text{-}5 \times 10^{-8}\ M_\odot \quad .$$

If $T_d < T_c(11\ \mu, 20\ \mu)$, the masses would be correspondingly higher. For Moon rock no. 14321 (Perry et al. 1972, Table 6), $\kappa_{11\mu} \sim 2\ \kappa_{20\mu}$ so $T_c = 500$ °K indicates $T_d = 300$ °K, and these masses should be multiplied by ~ 6.

For the M supergiants W Per and RW Cyg, which have "silicate" features (Table 2a, Chapter V), $\mathcal{L}_* \sim 10^5\ \mathcal{L}_\odot$ and $\beta_{11\mu} \sim 6$ so the above mass is multiplied by ~ 30. It should be emphasized that this mass refers to the observed radiating material fairly close to the star. For a constant mass loss rate (eq. VIII-5) $\rho_d \sim 1/R^2$ so a true total mass of dust $\sim \int_{R_1}^{R_2} \rho_d\ 4\pi R^2\ dR$ will diverge as $R_2 \to \infty$. The mass calculated here refers to the dust at a characteristic temperature T_d which by eq. (A-10c) of Appendix A means dust at a characteristic radius R_d.

For the Mira carbon stars the circumstellar shells may be going optically thick at shorter wavelengths. In addition, the observed β_λ's must be corrected due to the extinction of the star by the shell. To first order (neutral extinction) this will be

$$\beta_\lambda' \simeq (1 - \alpha)\, \beta_\lambda^{obs} \quad ,$$

where $\alpha = \mathfrak{F}^{dust}/\mathfrak{F}^{tot}$ is the relative bolometric excess as defined in Appendix A. The color temperatures for the "blackbody" excesses of carbon stars is (Table 2b, Chapter IV) $T_c(3.5\ \mu, 8.4\ \mu) \sim$ 900-1000 °K. As discussed later $T_d \sim 0.65\ T_{BB}$ for small graphite grains, so taking $T_d = 620$ °K for a = 0.1 μ grains but $T_d \sim 950$ °K for a = 1 μ grains which are more nearly grey-bodies, the opacity appropriate for graphite grains (Appendix B), and R Lep as an example, assuming $\mathfrak{L}_* = 10^4\ \mathfrak{L}_\odot$, we use eq. (VIII-4) to calculate the graphite dust mass M_d. The result is shown in Table 6.

TABLE 6

M_d for R Lep (Graphite Component)

	3.5 μ	4.9 μ	8.4 μ	20 μ	
β_λ^{obs}:	1.1	1.8	3.5	5.0	
					T_d
a = 0.1 μ	12.6	10.5	16.5	53	620 °K
a = 1.0 μ	2.4	2.1	2.8	7.8	950 °K
	M_d, $10^{-8}\ M_\odot$				

The masses determined at 3.5 μ and 4.9 μ around the peak of the energy distribution of the excess are comparable to those derived for M stars. At longer wavelengths, especially 20 μ, the derived masses are much larger for small grains ($a \lesssim 0.1\ \mu$) because of the steep wavelength dependence of the opacity of graphite ($\kappa_\lambda \sim 1/\lambda^2$, Appendix B). One has to invoke quite large grains $a \gtrsim 1\ \mu$, to increase the relative opacity at longer wavelengths (this is due to resonance effects) and bring the estimates more nearly into agreement. Perhaps at longer wavelengths we are seeing the effects of a much more extended, cool shell which does not contribute at 3-5 μ because of its lower temperature. Perhaps there really are some grains which are large ($a \gtrsim 1\ \mu$) in at least one dimension and thus able to radiate effectively at 20 μ. Perhaps the radiating material is not graphite. The masses of dust observed for V CrB and V Hya would be about the same as for R Lep while those for V Cyg and T Dra would be ~ 2-3 times higher.

The total mass loss rate from material of space density ρ, at a distance R from the star leaving at a velocity V is

$$\dot{M} = 4\pi R^2\, \rho\, V \quad . \qquad \text{(VIII-5)}$$

Observations of the gas indicate V_{gas} = constant so, in the steady state, $\rho_{gas} \sim 1/R^2$. A dust grain of radius a will have at least three forces acting on it. (1) The outward force due to radiation pressure is given by:

$$F_{pr} = \frac{\mathcal{L}_*}{4 \pi R^2} \frac{\langle Q_{pr} \rangle \pi a^2}{c} \quad , \qquad \text{(VIII-6)}$$

where $\langle Q_{pr} \rangle$ is the efficiency factor for radiation pressure averaged over the star's radiation field. Q_{pr} may be expressed (Van de Hulst 1957, p. 128) in terms of the absorption efficiency, scattering efficiency and the phase function $g = \langle \cos \theta \rangle$

$$Q_{pr} = Q_{abs} + (1 - g) Q_{sca} \qquad \text{(VIII-7)}$$

(see Appendix B).

(2) The inward force due to gravity:

$$F_{grav} = \frac{G M_* m_{grain}}{R^2} = \frac{G M_* \frac{4}{3} \pi a^3 \rho_{grain}}{R^2} \, . \qquad \text{(VIII-8)}$$

And (3) the force due to gas drag. For $\mathcal{L}_* \sim 10^4 \, \mathcal{L}_\odot$, $a \sim 0.1 \, \mu$ and $M_* \sim 1\text{-}5 \, M_\odot$, $F_{pr} \gg F_{grav}$ and the grain will be rapidly accelerated outward to supersonic velocities, $V > V_{th} = \sqrt{3kT/m_{H_2}} \sim$ 3.5 km/s, so the gas drag will be given by the supersonic drag

$$F_{drag} = \frac{\Delta P}{\Delta t} = \pi a^2 (\Delta V)^2 \rho_{gas} \quad , \qquad \text{(VIII-9)}$$

where $\Delta V = V_{dust} - V_{gas}$. The dust grain will be accelerated until it reaches a terminal velocity ΔV_t, where $F_{pr} = F_{drag}$, i.e.

$$\Delta V_t = \left(\frac{\mathcal{L}_*}{4 \pi R^2 \rho_{gas}} \frac{\langle Q_{pr} \rangle}{c} \right)^{1/2} \qquad \text{(VIII-10a)}$$

or, using Eq. (VIII-5)

$$\Delta V_t = \left(\frac{\mathcal{L}_* \langle Q_{pr} \rangle V_{gas}}{c \dot{M}_{gas}} \right)^{1/2} \, . \qquad \text{(VIII-10b)}$$

The terminal velocity is independent of R and depends on the Mie-theoretical $\langle Q_{pr} \rangle$, the observed V_{gas} and $\mathcal{L}_*$, and $\dot{M}_{gas}$ which is one of the quantities we wish to calculate.

An important point to note here is that if a <u>small</u> mass loss rate $\dot{M}_{gas}$ is claimed, this will imply a <u>large</u> ΔV_t which, for a given observed infrared excess will, by eq. (VIII-5), imply a <u>large</u> dust loss rate, $\dot{M}_{dust}$. Putting in numbers eq. (VIII-10b) becomes

$$\Delta V_t = 45 \langle Q_{pr} \rangle^{1/2} \left(\frac{V_{gas}}{10 \text{ km/s}} \right)^{1/2} \left(\frac{10^{-6} \, M_\odot/\text{yr}}{\dot{M}_{gas}} \right)^{1/2} \left(\frac{\mathcal{L}_*}{10^4 \, \mathcal{L}_\odot} \right)^{1/2} \text{km/s} \, . \qquad \text{(VIII-10c)}$$

$\dot{M}_{gas}$ has been estimated by Deutsch (1960) and Weymann (1963) for M stars. If Deutsch's results on earlier spectral types (M1-M5 III) are extrapolated to $\sim$ M7 appropriate for the Mira variables studied here, $\dot{M} \sim 10^{-6} - 10^{-7} \, M_\odot$/yr. Weymann arrives at mass loss rates approximately an order of magnitude higher than Deutsch. Thus, we expect

$$\Delta V_t \sim 0 \; (45 \langle Q_{pr} \rangle^{1/2} \text{ km/s}) \, .$$

If $\dot{M}_{gas}$ is <u>much</u> less than this, so that gas drag is negligible, a grain of radius a, density 3 gm/cm^3 initially formed at

a R_o from the star will be accelerated by radiation pressure (eq. VIII-6) to a velocity

$$V_{pr}(R_o,R) = \left(\frac{\mathcal{L}_*}{10^4\ \mathcal{L}_\odot}\right)^{1/2}\left(\frac{T_*}{2500\ ^\circ K}\right)\left(\frac{0.1\ \mu}{a}\right)^{1/2}\langle Q_{pr}\rangle^{1/2}$$

$$\left(\frac{r_*}{R_o}\right)^{1/2}(1 - R_o/R)^{1/2}\ 6700\ \text{km/s} \quad , \qquad \text{(VIII-10d)}$$

which for any reasonable values of $\langle Q_{pr}\rangle$ and R_o will be much greater than the observed V_{gas} and much greater than the escape velocity for that radius which by eq. (VIII-8) is

$$V_e(R) = \left(\frac{M_*}{M_\odot}\right)^{1/2}\left(\frac{10^4\ \mathcal{L}_\odot}{\mathcal{L}_*}\right)^{1/2}\left(\frac{T_*}{2500\ ^\circ K}\right)\left(\frac{r_*}{R_o}\right)^{1/2} 25\ \text{km/s} \quad . \qquad \text{(VIII-10e)}$$

Gilman (1972) showed that for M stars this terminal velocity is reached in a time short compared to the time for mass motions of the shell $\tau \sim R/V$, and that thereafter the momentum given to the dust via radiation pressure was dumped into the gas. The outward velocity of the dust grains V_d will be given by

$$V_d = V_{gas} + \Delta V_t > V_{gas} \quad . \qquad \text{(VIII-11)}$$

Now consider the two observed species in a circumstellar envelope, gas and dust. The steady state mass loss rates (eq. VIII-5) for the gas and dust, respectively, will be

$$\dot{M}_{gas} = 4\pi R^2\ \rho_{gas}\ V_{gas} \qquad \text{(VIII-12a)}$$

$$\dot{M}_{dust} = 4\pi R^2\ \rho_d\ V_{dust} \quad . \qquad \text{(VIII-12b)}$$

Using eq. (VIII-11) we have immediately

$$\dot{M}_{dust} = 4\pi R^2\ \rho_d\ V_d \gtrsim 4\pi R^2\ \rho_d\ V_{gas} \quad . \qquad \text{(VIII-13)}$$

V_{gas} is given by the optical observations and $R^2\ \rho_d$ can be estimated from the infrared observations. Further, only a mass fraction f of the gas in the stellar photosphere is available for condensation into a particular species of dust grain. For $(Fe,Mg)_2SiO_4$ silicates in an M star $f \sim 1/300$. For graphite in a C star $f \sim 1/300$. For SiC in a C star $f \sim 1/1000$ (abundances from Allen 1963; Wallerstein 1973). If the outer layers of a star are not to be depleted of the condensed elements, we must have

$$\dot{M}_{gas} \geq \frac{1}{f}\dot{M}_{dust} \quad . \qquad \text{(VIII-14)}$$

In the case there is convective mixing from deeper layers in the star, the factor 1/f may be determined by the detailed balancing of dust loss, $\dot{M}_{dust}$, with the re-supply of condensing elements due to mixing. In the steady state the f's should not differ too much from the values quoted above for otherwise the observed relative surface abundances of stars losing mass would depend on the mass loss rate.

If the run of density of dust in the envelope is ρ_d and

the run of temperature is T(R), the total emission observed will be:

$$F_\lambda^d = \frac{\int_0^\infty 4\pi R^2 \kappa_\lambda \rho_d B_\lambda(T)\, dR}{D^2} \qquad \text{(VIII-15a)}$$

or, using eq. (VIII-12b)

$$F_\lambda^d = \frac{\int_0^\infty (\dot{M}_d/V_d) \kappa_\lambda B_\lambda(T)\, dR}{D^2} \quad . \qquad \text{(VIII-15b)}$$

This is an integral equation involving the unknown quantity $\dot{M}_d$, which may be a function of R if condensation continues as the dust and gas move outward. Our knowledge about the amount of dust and its distribution with respect to the star essentially amounts to two facts: (1) The relative flux level β_λ (or α) and (2) a color temperature T_c. Assuming the optical constants κ_λ are known, these may be interpreted as an average dust temperature T_d which, in turn, implies an average distance from the star R_d by eqs. (A-10) Appendix A, and a "mass of dust" radiating M_d as discussed earlier. Thus, solution of the integral equation will not be attempted at this time and instead we adopt a simplified order of magnitude model, which hopefully will display the important physical parameters, to derive a mass loss rate.

The "observed mass" of dust M_d will be assumed to be uniformly distributed in a region at a characteristic distance R_d from the star of a characteristic volume $\frac{4}{3}\pi R_d^3$ (i.e. as if

spread between $0.85\ R_d \lesssim R \lesssim 1.2\ R_d$). Then

$$\rho_d \simeq \frac{M_d}{\frac{4}{3}\pi R_d^3}$$

and, using eq. (VIII-12b)

$$\dot{M}_d \simeq \frac{3 M_d V_d}{R_d} \quad . \qquad \text{(VIII-16)}$$

From eq. (A-10c), Appendix A, we have

$$R_d = \frac{1}{2} r_* \left(\frac{T_*}{T_d}\right)^2 \left(\frac{\epsilon_{vis}}{\epsilon_{IR}}\right)^{1/2} \quad . \qquad \text{(VIII-17)}$$

Combining eqs. (VIII-17), (VIII-16), and (VIII-4) we get

$$\dot{M}_d = 6 \beta_\lambda \frac{\pi r_*}{\kappa_\lambda} \left(\frac{\epsilon_{IR}}{\epsilon_{vis}}\right)^{1/2} V_d \left(\frac{B_\lambda(T_*)}{B_\lambda(T_d)}\right) \left(\frac{T_d}{T_*}\right)^2 . \qquad \text{(VIII-18)}$$

(1) M and S Stars -- Silicate Excess

For M and S Miras β_λ is observed at 11 μ and T_d is estimated from the 11-20 μ color of the excess. Defining $S_\lambda(T_d,T_*) \equiv [B_\lambda(T_*)/B_\lambda(T_d)](T_d/T_*)^2$, we get the results shown in Table 7. $S_{11\mu}$ is only weakly dependent on temperatures and $S_{11\mu} \sim 1$ for typical observed temperatures. Taking $S_{11\mu} \simeq 1$, eq. (VIII-18) reduces to:

TABLE 7

$S_{11\mu}(T_d, T_*)$

T_*/T_d	300	500	800
2000	1.78	0.84	0.70
2500	1.52	0.72	0.61
3000	1.33	0.63	0.53

$$\dot{M}_d \simeq 6\ \beta_{11\mu}\ \frac{\pi\ r_*}{\kappa_{11\mu}}\ \left(\frac{\epsilon_{IR}}{\epsilon_{vis}}\right)^{1/2}\ V_d \qquad \text{(VIII-19a)}$$

$$\dot{M}_d \simeq \beta_{11\mu}\left(\frac{2\times 10^3\ \mathrm{cm^2/gm}}{\kappa_{11\mu}}\right)\left(\frac{\mathcal{L}_*}{10^4\ \mathcal{L}_\odot}\right)^{1/2}\left(\frac{\epsilon_{IR}}{\epsilon_{vis}}\right)^{1/2}\left(\frac{V_d}{10\ \mathrm{km/s}}\right)\ \times$$

$$6.1\times 10^{-9}\ \frac{M_\odot}{\mathrm{yr}}\ . \qquad \text{(VIII-19b)}$$

The chief uncertainties in these equations are now in V_d and $(\epsilon_{IR}/\epsilon_{vis})$, both of which depend on the grain opacities in the crucial $\lambda\lambda$ 1-3 μ region where the stellar energy distribution is peaking. Unfortunately, no optical constant measurements of any silicate material in the range $\lambda\lambda$ 1-5 μ have been published.

Fortunately, a stringent lower limit on $\dot{M}_{gas}$ can be set for any star in which silicate emission is observed, even in the absence of knowledge of ϵ_{vis}. We have

$$V_d = V_g + \Delta V_t \geq \Delta V_t\ ,$$

where ΔV_t is given by eq. (VIII-10c). Now (eq. VIII-7)

$$\langle Q_{pr}\rangle = \langle Q_{abs} + (1-g)\ Q_{scatt}\rangle\ .$$

$$\geq \langle Q_{abs}\rangle \equiv \epsilon_{vis}$$

by definition of ϵ_{vis} (Appendix A). So eq. (VIII-19b) becomes

$$\dot{M}_d \geq \beta_{11\mu} \left(\frac{2 \times 10^3}{\kappa_{11\mu}}\right) (\epsilon_{IR})^{1/2} \left(\frac{\mathcal{L}_*}{10^4\ \mathcal{L}_\odot}\right) \left(\frac{V_{gas}}{10\ km/s}\right)^{1/2} \left(\frac{10^{-6}\ M_\odot/yr}{\dot{M}_{gas}}\right)^{1/2}$$

$$\times\ 2.8 \times 10^{-8}\ M_\odot/yr \quad . \qquad \text{(VIII-20)}$$

The dependence on ϵ_{vis} has been cancelled and a small $\dot{M}_{gas}$ now implies a large $\dot{M}_d$. Invoking eq. (VIII-14) with $1/f \sim 300$ for silicates and solving for $\dot{M}_{gas}$ we have

$$\dot{M}_g \geq \beta_{11\mu}^{2/3} \left(\frac{2 \times 10^3}{\kappa_{11\mu}}\right)^{2/3} \epsilon_{IR}^{1/3} \left(\frac{\mathcal{L}_*}{10^4\ \mathcal{L}_\odot}\right)^{2/3} \left(\frac{V_{gas}}{10\ km/s}\right)^{1/3} \left(\frac{1}{300\ f}\right)$$

$$\times\ 4.1 \times 10^{-6}\ M_\odot/yr \quad . \qquad \text{(VIII-21)}$$

This represents the minimum amount of gas which is needed to keep the observed dust grains from rapidly escaping. By definition:

$$\epsilon_{IR} \equiv \frac{\int \epsilon_\lambda\ B_\lambda(T_d)\ d\lambda}{\int B_\lambda(T_d)\ d\lambda} = \langle \epsilon_\lambda \rangle_{T_d}$$

and, assuming $2\pi a/\lambda \ll 1$

$$\epsilon_\lambda \equiv Q_{abs}(\lambda) = \frac{4}{3}\ \rho_{grain}\ a\ \kappa_\lambda \quad ,$$

so

$$\epsilon_{IR} = \langle \kappa_\lambda \rangle_{T_d}\ \frac{1}{3}\ \rho_{grain}\ a \quad ,$$

where κ_λ is the mass opacity for small grains, a is the grain radius and $\rho_{grain} = 3\ gm/cm^3$ for silicates. Taking as an example the κ_λ for "Mix 2" of Moon rock no. 14321 (Perry et al. 1972) discussed in Chapter V, we calculate the broad band opacities $\langle \kappa_\lambda \rangle_{\lambda_o}$ (averaged over the filter bandpasses) and the $\kappa_{IR} \equiv \langle \kappa_\lambda \rangle_{T_d}$ (averaged over the blackbody function); the results are shown in Table 8.

TABLE 8

Average Opacities, "Mix 2" of Moon Rock No. 14321

λ_o:	8.4 μ	11 μ	18 μ	20 μ
$\langle \kappa_\lambda \rangle_{\lambda_o}$ (10^3 cm^2/gm):	0.76	1.85	1.15	0.92
T_d (°K):	200	300	500	800
$\langle \kappa_\lambda \rangle$ (10^3 cm^2/gm):	0.76	1.0	0.97-1.10	0.62-1.05

The opacities λλ 1-5 μ are not known, the smaller numbers for $\langle \kappa_\lambda \rangle_{T_d}$ in Table 8 hold if the opacities are zero there.

Thus, for the likely temperature range $T_d \sim 300$-500 °K, $\langle \kappa_\lambda \rangle_{T_d} \sim 1.0$-$1.1 \times 10^3$ cm^2/gm and eq. (VIII-21) becomes

$$\dot{M}_g \geq \beta_{11\mu}^{2/3} \left(\frac{1.85 \times 10^3}{\kappa_{11\mu}}\right)^{2/3} \left(\frac{\kappa_{IR}}{1.05 \times 10^3}\right)^{1/3} \left(\frac{a}{0.1\ \mu}\right)^{1/3} \left(\frac{\mathcal{L}_*}{10^4\ \mathcal{L}_\odot}\right)^{2/3}$$

$$\left(\frac{V_{gas}}{10\ km/s}\right)^{1/3} \left(\frac{1}{300\ f}\right) \times 1.5 \times 10^{-6}\ M_\odot/yr \quad .$$

This represents the minimum amount of mass loss in gas consistent with the observed infrared emission. For $\beta_{11\mu} \sim 1$, the IR opacities given above, $a \sim 0.1\ \mu$, $\mathcal{L}_* \sim 10^4\ \mathcal{L}_\odot$, $V_{gas} \sim 10\text{-}20$ km/s, $f \sim 1/300$, we get

$$\dot{M}_g \gtrsim 1.5 \times 10^{-6}\ M_\odot/yr \quad .$$

This result is independent of the uncertain quantity ϵ_{vis} and doesn't even require that the radiation pressure on dust grains is responsible for the mass loss. For example, if $\dot{M}_g$ were claimed to be much less than this, V_d would be given by V_{pr} (eq. VIII-10d) and for $R_d > R_o > r_*$, but of the same order of magnitude, we have

$$V_d \to V_{pr}(R_d) \simeq 0\ [(0.1\ \mu/a)^{1/2}\ \langle Q_{pr}\rangle^{1/2}\ 1000\ km/s]$$

so eq. (VIII-19b) becomes

$$\dot{M}_d \simeq \beta_{11\mu} \left(\frac{2 \times 10^3\ cm^2/gm}{\kappa_{11\mu}}\right) \left(\frac{\epsilon_{IR}}{\epsilon_{vis}}\right)^{1/2} \left(\frac{0.1\ \mu}{a}\right)^{1/2} \langle Q_{pr}\rangle^{1/2}$$

$$\times\ 6.1 \times 10^{-7}\ M_\odot/yr \quad .$$

And again $\langle Q_{pr}\rangle \geq \epsilon_{vis}$ so, using the broad band opacities of Table 8

$$\dot{M}_d \geq \beta_{11\mu}\ \ 1.2 \times 10^{-7}\ M_\odot/yr$$

independent of grain radius a. This now implies, by eq. (VIII-14) that

$$\dot{M}_g \geq \beta_{11\mu}\ 4 \times 10^{-5}\ M_\odot/yr$$

which is much larger than the lower limit above. Basically, the gas is needed to keep the dust grains from being rapidly ejected by the very strong stellar radiation field. For the M supergiants RW Cyg and W Per, $\mathcal{L}_* \sim 10^5\ \mathcal{L}_\odot$, $\beta_{11\mu} \sim 6$, and the minimum gas loss rate is increased to $\sim 23 \times 10^{-6}\ M_\odot/yr$.

For a lower limit on the dust loss rate we need an upper limit on $\dot{M}_{gas}$ in eq. (VIII-20). If the mass loss is driven by radiation pressure as discussed in Section C-ii) of this chapter, there is an upper limit to the mass loss vis:

$$\dot{M}_{total} \leq \left(\frac{\mathcal{L}_*}{10^4\ \mathcal{L}_\odot}\right) \left(\frac{10\ km/s}{V_{gas}}\right)\ 20 \times 10^{-6}\ M_\odot/yr \quad .$$

Inserting this into eq. (VIII-20) with the opacities discussed above gives

$$\dot{M}_d \geq \beta_{11\mu} \left(\frac{\mathcal{L}_*}{10^4\ \mathcal{L}_\odot}\right)^{1/2} \left(\frac{V_{gas}}{10\ km/s}\right)^{3/2} \left(\frac{a}{0.1\ \mu}\right)^{1/2}$$

$$\times\ 1.2 \times 10^{-9}\ M_\odot/yr \quad . \qquad \text{(VIII-23)}$$

These rather roundabout methods of determining the $\dot{M}$'s have been forced upon us by lack of knowledge of ϵ_{vis} for silicates.

However, the foregoing discussion has given a minimum for $\dot{M}_g$ and if we assume the mass loss is radiation pressure drive the discussion in Section C-ii) allows us to set limits on ϵ_{vis}. As discussed there

$$\alpha_{pr} \frac{\mathcal{L}_*}{V_g c} \gtrsim \dot{M}_g$$

and using the lower limit on $\dot{M}_g$ of eq. (VIII-22) with $a \sim 0.1\ \mu$, $f \sim 1/300$, we get

$$\alpha_{pr} \gtrsim \beta_{11\mu}^{2/3} \left(\frac{V_g}{10\ km/s}\right)^{2/3} \left(\frac{10^4\ \mathcal{L}_\odot}{\mathcal{L}_*}\right)^{1/3} 0.075 \quad .$$

But α_{pr} is related to the observed quantity α by eq. (VIII-36). Taking $\beta_{11\mu} \sim 1.4$, $V_g \sim 10$ km/s, $\mathcal{L}_* \sim 10^4\ \mathcal{L}_\odot$ and $\alpha \sim 0.014$ (i.e. as for oCet), we get

$$\alpha_{pr} = \frac{\langle Q_{pr} \rangle}{\epsilon_{vis}} \alpha \gtrsim 0.095$$

so

$$\frac{\langle Q_{pr} \rangle}{\epsilon_{vis}} \gtrsim 6.7$$

using eq. (VIII-7)

$$\epsilon_{vis} \leq \frac{\langle (1 - g)\ Q_{scatt} \rangle}{5.7} \quad .$$

Now, for any size grain, $g \gtrsim 0$ and $Q_{scatt} \lesssim 2$, so

$$\epsilon_{vis} \leq 0.35 \quad .$$

For small grains ($a \lesssim 0.1\ \mu$) we have (from Section C-ii) $\langle (1 - g)\ Q_{scatt} \rangle \lesssim 0.3$ so, using the silicate opacities above,

$$\frac{\epsilon_{iR}}{\epsilon_{vis}} \gtrsim 0.75\ (a/0.1\ \mu)$$

must hold for the silicate material around the Mira variables if the mass loss is to be radiation pressure driven.

We can now safely take $(\epsilon_{IR}/\epsilon_{vis})^{1/2} \gtrsim 1$ in eq. (VIII-19b) which, with $\kappa_{11\mu} \sim 2 \times 10^3$ cm^2/gm gives $\dot{M}_d \sim 5$ times higher than the lower limit given by eq. (VIII-23). Now $\dot{M}_g \gtrsim 1/f\ \dot{M}_d$ so

$$\dot{M}_g \gtrsim \beta_{11\mu} \left(\frac{\mathcal{L}_*}{10^4\ \mathcal{L}_\odot}\right)\left(\frac{V_g}{10\ km/s}\right)\left[1 + \frac{\Delta V_t}{V_g}\right] 1.8 \times 10^{-6}\ M_\odot/yr \quad , \qquad \text{(VIII-24)}$$

where $\Delta V_t \sim \langle Q_{pr} \rangle^{1/2} (\dot{M}_g)^{-1/2} V_g^{1/2}$ is given by eq. (VIII-10c). This is therefore a cubic equation in $\dot{M}_g^{1/2}$ which has one real solution. Taking $\langle Q_{pr} \rangle \sim 0.1$, as indicated in Section C-ii), the real solution is given in Table 9 for various stellar parameters.

For the Mira variables $\beta_{11\mu} \sim 1$-2 (Table 2b, Chapter V) and $\mathcal{L}_* \sim 10^4\ \mathcal{L}_\odot$, so

$$\dot{M}_g \sim 3\text{-}7 \times 10^{-6}\ M_\odot/yr$$
$$\dot{M}_d \sim 1\text{-}2 \times 10^{-8}\ M_\odot/yr$$
$$\Delta V_t \sim 5\text{-}8\ km/s \quad .$$

TABLE 9

Mass Loss Rates and Terminal Velocities for Stars with Silicate Emission Features

$\mathcal{L}_*$	V_g	$\beta_{11\mu}$	ΔV_t	$\dot{M}_g$	$\dot{M}_d$
			$\lesssim$	$\gtrsim$	$\lesssim$
	10	1	7.8	3.2	1.1
	10	3	4.9	8.1	2.7
$10^4\ \mathcal{L}_\odot$	10	5	4.0	12.5	4.2
	20	1	8.8	5.2	1.7
	10	1	12.5	12.7	4.2
	10	3	8	31	10
$10^5\ \mathcal{L}_\odot$	10	5	6.5	47	15.6
	20	1	14.2	19.5	6.5
	km/s		km/s	$\times 10^{-6}\ M_\odot$/yr	$\times 10^{-8}\ M_\odot$/yr

For the M supergiants W Per and RW Cyg, $\beta_{11\mu} \sim 5\text{-}6$ (Table 2b, Chapter V) and $\mathcal{L}_* \sim 10^5\ \mathcal{L}_\odot$ so

$$\dot{M}_g \sim 50 \times 10^{-6}\ M_\odot/\text{yr}$$
$$\dot{M}_d \sim 16 \times 10^{-8}\ M_\odot/\text{yr}$$
$$\Delta V_t \sim 6\ \text{km/s} \quad ,$$

i.e. ~ 10 times the rates for the Mira variables. The mass losses for the other M and S stars with silicate emission features in this program will be somewhere between these values. These mass losses are larger but comparable to the $\dot{M}_g \sim 2 \times 10^{-6}\ M_\odot$/yr estimated by Gehrz and Woolf (1971) for Mira variables. The more general analysis presented here, which applies to any star with a silicate feature and $T_d \sim 300\text{-}800\ ^\circ K$, actually increases the (already large) mass loss rates given by those authors. We find that if there is <u>any</u> observable silicate features ($\beta_{11\mu} \gtrsim 0.2$), then there is a minimum mass loss rate (eq. VIII-22) of $\dot{M}_g > 0.5 \times 10^{-6}\ M_\odot$/yr.

One important additional result which follows from the analysis presented here is that the terminal velocity of the dust grains relative to the gas is limited to $\Delta V_t \lesssim 5\text{-}10$ km/s for these stars because of the requirement $\dot{M}_g \gtrsim 1/f\ \dot{M}_d$ on the gas loss rate for a given dust loss rate. If a large terminal velocity is supposed, this implies a large $\dot{M}_d$ which implies a large $\dot{M}_g$ which, in turn, limits the terminal velocity through eq. (VIII-10c).

The mass loss rates are also comparable but smaller than the limiting value for radiation pressure driven mass loss derived

in Section C-ii), i.e. $\alpha_{pr} \leq 1 \Rightarrow \dot{M}_g \leq 20 \times 10^{-6}\ M_\odot/yr$ for the Mira variables. We can now turn this argument around and derive a limit on $(\epsilon_{IR}/\epsilon_{vis})^{1/2}$ which will imply a limit on R_d/r_*. Using the above limit on $\dot{M}_g$, eqs. (VIII-19b) and (VIII-14), and $\beta_{11\mu} \sim 1\text{-}2.5$ we have

$$\left(\frac{\epsilon_{IR}}{\epsilon_{vis}}\right)^{1/2} \leq 5\text{-}3$$

which, from eq. (VIII-17) and assuming $T_d \lesssim T_c(11\ \mu,\ 20\ \mu) \sim 400\text{-}500$ °K (Table 2b) implies

$$R_d/r_* \gtrsim 3.5$$

for the Mira variables oCet, R Leo, R Cas, and S CrB. Thus the shells would appear to be well separated from the stellar surface.

Another result of this analysis is, since

$$\alpha_{pr} \gtrsim 0.25 \quad .$$

In order to drive the mass loss, the scattering optical depth of these shells at visual wavelengths must be quite large. We have

$$\tau_{0.55\mu} \sim \alpha_{pr}\ \frac{Q_{scatt}(0.55\ \mu)}{\langle Q_{pr}\rangle} \quad .$$

And for small grains ($a \lesssim 0.1\ \mu$) $\langle Q_{pr}\rangle \lesssim 0.1$ but $Q_{scatt}(0.55\ \mu) \gtrsim 1$ so

$$\tau^{scatt}_{0.55\mu} \gtrsim 0.25 \times 10 \sim 2.5 \quad .$$

These shells appear to be optically thick ($\tau > 1$) to scattering at visual and shorter wavelengths. Any analysis of the observed polarization at these wavelengths must take this into account. This also predicts that angular size measurements at visual wavelengths will be larger than the actual stellar size, i.e.

$$\theta_d \gtrsim \theta_{obs} \gtrsim \theta_* \quad .$$

The large scattering envelope may be hard to detect in comparison to a central condensation from the forward-scattered image of the star because of its low surface brightness, i.e. $R_d/r_* \gtrsim 4 \Rightarrow$ the shell will have only $\sim 1/16$ the stellar surface brightness. Attempts should be made to detect this low surface brightness halo around these stars.

(2) Carbon Stars

The emission feature λλ 10-12.5 μ seen in the spectra of carbon stars is probably due to SiC grains (Chapter V) and in this way could play a role analogous to silicates in M stars regarding "weighing the dust" and estimating mass loss. Unfortunately, there is no way of estimating the characteristic temperature, T_d, of the SiC grains so the techniques developed in the preceding section for observed silicate features no longer apply. There will still be

a limit of the type given by eq. (VIII-22) on mass loss, i.e. $\dot{M}_g \geq$ order of $(10^{-6}\ M_\odot/yr)$ in order that we observe any SiC feature, for otherwise the grains would be too rapidly ejected by radiation pressure.

If the "blackbody" excess discussed in Chapters IV and V is ascribed to thermal emission from circumstellar grains, the most likely candidate is graphite (Hoyle and Wickramasinghe 1962; Gilman 1969). Since $\epsilon_\lambda \sim 1/\lambda^2$ for small ($a \lesssim 0.25\ \mu$) graphite grains (Appendix B), the observed blackbody spectrum $\lambda\lambda$ 3.5-20 μ implies either: (1) There is a range of temperatures in the shell, the cooler grains contributing relatively more at 20 μ, (2) the grains are large ($a \gtrsim 2\ \mu$) in at least one dimension and so can radiate effectively at $\lambda \sim 20\ \mu$, (3) a combination of (1) and (2), or (4) the emission is due to some other type of grain with a more nearly "grey body" emissivity. We will tentatively assume (1) is the case in the following discussions.

The expression for dust loss given by eq. (VIII-18) could be applied to the observed β_λ's for carbon stars (assuming the κ_λ, ϵ_λ appropriate for graphite) as for the M and S stars. However, as the discussion on the mass of dust indicated, this procedure is not well defined for graphite, as we would infer larger masses at longer wavelengths. Therefore, we adopt an integrated form of this equation for the carbon stars. The total observed flux from a cloud of small dust grains optically thin at infrared wavelengths is given approximately by

$$\mathcal{F}^d = \frac{M_d\ \kappa_{IR}\ \frac{\sigma}{\pi}\ T_d^4}{D^2} \quad ,$$

where M_d is the total mass of dust radiating at a characteristic temperature T_d and κ_{IR} is the mass absorption coefficient averaged over $B_\lambda(T_d)$. The total flux from the star in the absence of a dust shell can be written

$$\mathcal{F}^{tot} = \frac{\mathcal{L}_*}{4\ \pi\ D^2} \quad .$$

From the definition of α we have

$$\alpha = \frac{\mathcal{F}^d}{\mathcal{F}^{tot}}$$

so

$$M_d = \alpha\ \frac{\mathcal{L}_*}{4\ \kappa_{IR}\ \sigma\ T_d^4} \qquad \text{(VIII-25)}$$

$$= \alpha \left(\frac{\mathcal{L}_*}{10^4\ \mathcal{L}_\odot}\right)\left(\frac{10^3\ cm^2/gm}{\kappa_{IR}}\right)\left(\frac{10^3\ {}^\circ K}{T_d}\right)^4 \times 8.8 \times 10^{-8}\ M_\odot \quad .$$

For the range of temperatures appropriate for these stars $\sim$ 500-1200 °K, κ_{IR} for small ($a \lesssim 0.1\ \mu$) spherical graphite grains can be represented by (Appendix B)

$$\kappa_{IR}(T_d) \simeq 2.45 \times 10^3\ (T_d/10^3\ {}^\circ K)^2\ cm^2/gm \quad ,$$

so we have

$$M_d = \alpha \left(\frac{\mathcal{L}_*}{10^4\ \mathcal{L}_\odot}\right)\left(\frac{10^3\ ^\circ K}{T_d}\right)^6 \times 3.6 \times 10^{-8}\ M_\odot \quad .$$

It is seen that the calculated M_d's will critically depend on the characteristic T_d which is assigned to the observed excess. For the "characteristic temperature" T_d we will choose the temperature such that $\epsilon_\lambda B_\lambda(T_d)$ peaks at the same wavelengths as the energy distribution of the excess. The energy distribution of the excess (see Chapter IV) is fit quite well by $B_\lambda(T_{BB})$ and since (Appendix B) $\epsilon_\lambda \sim 1/\lambda^2$ the relationship between T_d and T_{BB} is

$$T_d \sim 0.65\ T_{BB} \quad ,$$

so

$$M_d = \alpha \left(\frac{\mathcal{L}_*}{10^4\ \mathcal{L}_\odot}\right)\left(\frac{10^3\ ^\circ K}{T_{BB}}\right)^6 \times 50 \times 10^{-8}\ M_\odot \quad .$$

T_{BB} is in the range $\sim$ 900-1000 °K so $T_d \sim 600$ °K. α ranges from $\sim$ 0.3-0.4 for R Lep, V CrB, and V Hya to $\sim$ 0.8 for V Cyg and T Dra (Table 2b) so $M_d \sim 18\text{-}54 \times 10^{-8}\ M_\odot$ for the Mira carbon stars here. This is higher than the $\sim 2.5\text{-}5 \times 10^{-8}\ M_\odot$ estimated earlier for M and S Miras using $T_d \sim T_c(11\ \mu, 20\ \mu)$ but is comparable to the masses inferred if $\kappa_{11\mu} \sim 2\ \kappa_{20\mu}$ which gives approximately 6 times higher masses.

Proceeding to mass loss using eq. (VIII-16) we have (using eq. A-10b) for $R_d(\alpha = 0)$

$$\dot{M}_d = \alpha \left(\frac{\mathcal{L}_*}{10^4\ \mathcal{L}_\odot}\right)^{1/2}\left(\frac{V_d}{10\ km/s}\right)\left(\frac{10^3\ ^\circ K}{T_d}\right)^4\left(\frac{\epsilon_{IR}}{\epsilon_{vis}}\right)^{1/2} g^{-1}(\alpha)$$

$$\times\ 2.9 \times 10^{-8}\ M_\odot/yr \quad .$$

The factor $g(\alpha)$ is necessary to correct eq. (A-10b), Appendix A, for the R_d^o appropriate for an optically thin shell, i.e.

$$R_d = g(\alpha)\ R_d^o \quad .$$

To calculate $g(\alpha)$ requires, even if the scattering is small, solution of the radiation transfer equations through the envelope.

There are (at least) two competing effects here. The first is, as R_1 increases, a dust grain sees more and more of the 1000 °K radiation field. Thus, the effective ϵ_{vis} for the outer grains is more like $\langle\epsilon_\lambda\rangle_{1000^\circ K}$ which, for small graphite grains, is less than the $\langle\epsilon_\lambda\rangle_{2300^\circ K}$ appropriate for the stellar radiation field. This would make $R_d < R_d^o$, i.e. $g < 1$. The second is, if a considerable fraction of starlight is converted into dust emission in the shell, the radiation field no longer goes down as fast as $1/R^2$ (i.e. there is back-heating of the inner shell regions by the outer shell regions). This implies the temperature of a grain no longer goes down as fast as $1/\sqrt{R}$ which means $R_d > R_d^o$, i.e. $g > 1$. $g(\alpha)$ thus could be greater or less than 1. This unknown factor will become increasingly important as $\alpha \to 1$.

Again using the opacities appropriate for small ($a < 0.1\ \mu$) graphite spheres (Appendix B) for which $\kappa_{vis} \simeq \langle \kappa_\lambda \rangle_{2250°K} \sim 8 \times 10^3$ cm^2/gm, and converting from T_d to $T_{BB} \sim 10^3$ °K, the apparent blackbody temperature, we have

$$\dot{M}_d = \alpha \left(\frac{\mathcal{L}_*}{10^4\ \mathcal{L}_\odot}\right)^{1/2} \left(\frac{V_d}{10\ \text{km/s}}\right) \left(\frac{10^3\ °K}{T_{BB}}\right)^3 g^{-1}(\alpha) \times 5.7 \times 10^{-8}\ M_\odot/\text{yr} \quad . \tag{VIII-26}$$

So for $V_d \gtrsim 10$ km/s and $g \sim 1$ we get for the carbon Miras and V Hya,

$$\dot{M}_d \gtrsim 1.7\text{-}4.6 \times 10^{-8}\ M_\odot/\text{yr} \quad .$$

This compares quite favorably with the dust production rate $\dot{M}_d \sim 2.5 \times 10^{-8}\ M_\odot$/yr in small graphite grains predicted by Hoyle and Wickramasinghe (1962) for late-type carbon stars. Now, using $f(c) = 1/300$ and $V_d = V_g + \Delta V_t$ as before we have for $\dot{M}_g \gtrsim 1/f\ \dot{M}_d$:

$$\dot{M}_g \gtrsim \alpha \left(\frac{\mathcal{L}_*}{10^4\ \mathcal{L}_\odot}\right)^{1/2} \left(\frac{V_g}{10\ \text{km/s}}\right) \left(\frac{10^3\ °K}{T_{BB}}\right)^3 g^{-1}(\alpha) \left[1 + \frac{\Delta V_t}{V_g}\right] \times 17.1 \times 10^{-6}\ M_\odot/\text{yr} \quad , \tag{VIII-27}$$

where ΔV_t is given by eq. (VIII-10c). Gilra (1974) reports measurements of circumstellar absorption lines for some semi-regular variable carbon stars indicating $V_g \sim 15$ km/s, which is similar to the M stars discussed earlier. As in Section (1)

previous, eq. (VIII-27) is solved for the mass loss rates and the terminal velocity, the results are shown in Table 10.

It is seen that, as for the M and S stars, the terminal velocity is limited by the necessary minimum gas loss rate, $\dot{M}_g \gtrsim \frac{1}{f} \dot{M}_d$, to the range $\Delta V_t \sim 5\text{-}10$ km/s. The gas and dust loss rates for the Mira carbon stars are approximately a factor of 2 higher than those derived for the M and S Mira stars (they, of course, depend on the $\mathcal{L}_*$ and V_g assumed). The unknown factor $g(\alpha)$ which accounts for optical depth effects will become increasingly important as $\alpha \to 1$.

(b) Absorption of Starlight

The absorption optical depth of a circumstellar shell of dust grains is given by eq. (A-17) Appendix A which, for $\langle 1/R_i^2 \rangle = 1/R_d^2$, $\epsilon_{vis} \pi a_i^2 = \kappa_{vis} m_i$ becomes, solving for $M_d = \Sigma m_i$

$$M_d(\tau) = \frac{4\pi R_d^2 \langle \tau_{abs} \rangle_{vis}}{\kappa_{vis}} \quad . \tag{VIII-28}$$

This equation will hold if the shell is optically thin to scattering near the peak of the stellar energy distribution, $\sim 1\text{-}3\ \mu$ for late-type stars. As discussed in the previous section $R_d = g(\alpha) R_d^o$, where R_d^o is given by eq. (A-10b) Appendix A, and using eq. (VIII-25) for $M_d(\alpha)$, the mass inferred from the observed emission, we have

$$M_d(\tau) = g^2(\alpha)\ M_d(\alpha)\ \frac{\langle \tau_{abs} \rangle_{vis}}{\alpha} \quad .$$

TABLE 10

Mass Loss Rates and Terminal Velocities

for Stars with Graphite Emission

$\mathcal{L}_*$	V_g	α	ΔV_t $\lesssim$	$g(\alpha)\,\dot{M}_g$ $\gtrsim$	$g(\alpha)\,\dot{M}_d$ $\lesssim$
$10^4\,\mathcal{L}_\odot$	10	0.1	11.6	3.7	1.2
	10	0.3	7.3	8.9	3.0
	10	0.5	6.0	13.7	4.6
	10	0.8	4.9	20	6.8
	20	0.3	8.3	14.4	4.8
	20	0.8	5.4	34.7	11.6
$10^5\,\mathcal{L}_\odot$	10	0.1	17.9	15.2	5.1
	10	0.3	11.8	35.5	11.8
	10	0.5	9.6	53	17.8
	10	0.8	8	78	26
	20	0.3	13	54	18
	20	0.8	8.8	125	42
	km/s		km/s	$10^{-6}\,M_\odot$/yr	$10^{-8}\,M_\odot$/yr

NOTE: These results apply to small grains ($a < 0.1\ \mu$), if $a = 0.1\ \mu$, κ_{IR} is increased by ~ 1.37 and κ_{vis} is increased by ~ 1.9 due to resonance effects. This means M_d would be reduced by ~ 1.37 and R_d would be increased by ~ 1.18 which would reduce these mass loss rates by a factor of ~ 1.6.

So in the optically thin limit $\langle\tau_{abs}\rangle_{vis} \to \alpha \ll 1$, $g(\alpha) \to 1$ and the two expressions for M_d agree as expected since they were derived from the same phenomenological model. The choice of which expression, eq. (VIII-25) or (VIII-28), to use in this case reduces to which pair, (T_d, κ_{IR}) or (R_d, κ_{vis}) is better known. For the stars in this study there is little or no high spatial resolution information so R_d is not a directly observed quantity and eq. (VIII-25) must be used.

The bolometrically derived mass of dust given by eq. (VIII-25) may be compared with the masses derived monochromatically (i.e. β_λ) in the earlier discussion of M and S stars with a "silicate" excess. Taking $\mathcal{L}_* = 10^4\,\mathcal{L}_\odot$, $\kappa_{IR} \sim 10^3$ cm^2/gm, $T_d = 500$ °K, and $\alpha \sim 0.01$-0.02 appropriate for the Mira variables gives

$$M_d \sim 1.4\text{-}2.8 \times 10^{-8}\ M_\odot \quad .$$

For $T_d = 300$ °K these masses would be approximately 7.7 times larger. The agreement with the earlier estimates is quite good, which means we have at least been self-consistent in the calculations.

As the optical depth increases, the two expressions for M_d may diverge, depending on the (unknown) correction factor $g(\alpha)$. For the purposes of estimating mass loss eq. (VIII-25) is to be preferred in this case because it more directly refers to the dust grains whose distance from the star, R_d, we can estimate from the observed color temperatures of the excess.

In conclusion, the identity of the dust mass estimates given by eqs. (VIII-25) and (VIII-28) in the optically thin limit means that the mass loss rates will also be the same. Thus, we have shown that "absorption of starlight" is on the other side of the coin from "thermal emission by dust" as could be expected.

ii) Conservation of Momentum -- the Inverse Rocket Problem

If the mechanism driving the mass loss in a star is radiation pressure on some component of the circumstellar envelope, we can measure the rate by applying Newton's second law:

$$\frac{dP}{dt} = F = F_{pr} - F_{grav} \qquad \text{(VIII-29)}$$

to the radial motion of the envelope as a whole. F_{pr} is the total (outward) force of radiation pressure on the envelope and F_{grav} is the total (inward) force of gravity. We define α_{pr} as the fraction of the star's radiation field which goes into driving mass loss, i.e.

$$F_{pr} = \alpha_{pr} \frac{\mathcal{L}_*}{c} \quad . \qquad \text{(VIII-30)}$$

Now consider the circumstellar shell to be composed of many discrete radial elements with masses m_i moving at an average velocity V radially outward from the star. Then the total radial momentum is given by

$$P = \Sigma m_i V = M V \quad , \qquad \text{(VIII-31)}$$

where M represents the total mass of the envelope which is being accelerated by radiation pressure. Therefore,

$$\frac{dP}{dt} = \dot{M} V + M \dot{V} \quad , \qquad \text{(VIII-32)}$$

where $\dot{V}$ is the change of radial velocity with time and $\dot{M}$ is the rate of change of mass moving in the radial direction with velocity V. Solving for $\dot{M}$:

$$\dot{M} = \left(\frac{dP}{dt} - M\dot{V}\right)/V = \left(\alpha_{pr} \frac{\mathcal{L}_*}{c} - F_{grav} - M\dot{V}\right)/V \quad . \qquad \text{(VIII-33)}$$

This is essentially an "inverse rocket problem" with $\dot{M}$ representing the accretion rate of the circumstellar envelope and, therefore, the mass loss rate of the star. In the case $V \sim$ const appropriate for the gas loss in late-type stars, $\dot{V} \sim 0$ and we have

$$\dot{M} = \frac{1}{V}\left(\alpha_{pr} \frac{\mathcal{L}_*}{c} - F_{grav}\right) \lesssim \frac{\alpha_{pr} \mathcal{L}_*}{V c} \quad . \qquad \text{(VIII-34)}$$

In order for radiation pressure to be effective in driving mass loss, we must have $F_{pr} > F_{grav}$. If we assume photons cannot scatter back and forth across the envelope and impart more than $h\nu/c$ of momentum to the envelope, then an upper limit to radiation pressure driven mass loss is given by $\alpha_{pr} \leq 1$, which, for $\mathcal{L}_* = 10^4\ \mathcal{L}_\odot$ and V = 10 km/s, implies

$$\dot{M} \leq 20 \times 10^{-6}\ M_\odot/\mathrm{yr} \quad .$$

Further consider a circumstellar shell where the radiation pressure is exerted on the dust grains and then transferred to the gas via collisions as discussed by Gilman (1972). In the optically thin case the net force F_{pr} is the sum of the forces on the individual grains, eq. (VIII-6), so

$$\alpha_{pr} = \sum_i \frac{\langle Q_{pr}\rangle_{vis}\ \pi\ a_i^2}{4\ \pi\ R_i^2} \quad , \qquad \text{(VIII-35)}$$

which can be related to the relative bolometric excess α defined in Appendix A (i.e. eq. A-17) by

$$\alpha_{pr} = \frac{\langle Q_{pr}\rangle_{vis}}{\langle Q_a\rangle_{vis}}\ \alpha \geq \alpha \quad , \qquad \text{(VIII-36)}$$

where the subscript "vis" means averaged over the stellar radiation field. This shows that the same grains which are responsible for the excess emission (i.e. α, β_λ) observed in the infrared must also be responsible for the mass loss if this mechanism is to be effective.

The condition for positive mass loss to occur can be written

$$\frac{F_{pr}}{F_{grav}} = \frac{\rho_d\ g_{pr}}{\rho_g\ g_{grav}} > 1 \quad , \qquad \text{(VIII-37)}$$

where

$$g_{pr} = \left(\frac{\mathcal{L}_*}{c\ 4\ \pi\ R^2}\right)\left(\frac{\langle Q_{pr}\rangle\ \pi\ a^2}{\frac{4}{3}\ \pi\ a^3\ \rho_{grain}}\right) \qquad \text{(VIII-38)}$$

is the outward radiative acceleration per unit mass of dust and

$$g_{grav} = \frac{G\ M_*}{R^2} \qquad \text{(VIII-39)}$$

is the inward gravitational acceleration per unit mass. The gas and dust densities are given by eqs. (VIII-12a,b) and $V_g/V_d \gtrsim 0.7$ from the previous section so, applying eq. (VIII-14), we have

$$\frac{F_{pr}}{F_{grav}} \gtrsim (f'\ 300)\left(\frac{\mathcal{L}_*}{10^4\ \mathcal{L}_\odot}\right)\left(\frac{M_\odot}{M_*}\right)\left(\frac{0.1\ \mu}{a}\right)\left(\frac{3\ gm/cm^3}{\rho_{grain}}\right)\langle Q_{pr}\rangle$$

$$\times\ 46 > 1 \quad , \qquad \text{(VIII-40)}$$

as a necessary condition. Here $f' \lesssim f$ is the mass fraction which actually condenses to form dust, i.e. $\dot{M}_g = \frac{1}{f'}\dot{M}_d$.

(a) Carbon Stars

For small graphite grains, $a \lesssim 0.1\ \mu$, $\langle Q_{pr}\rangle \sim \langle Q_{abs}\rangle \simeq 0.25(a/0.1\ \mu)$ for $T_* = 2250$ °K and this becomes ($\rho_{graphite} = 2.2$ gm/cm^3

$$\frac{F_{pr}}{F_{grav}} \simeq (f'\ 300)\ \frac{\mathcal{L}_*}{10^4\ \mathcal{L}_\odot}\ \frac{M_\odot}{M_*}\ 15.7 \quad . \qquad \text{(VIII-41a)}$$

Gordon (1968) found that the luminosities of the late-type carbon stars is in the range $\mathcal{L}_* \sim 10^4$-$10^5\ \mathcal{L}_\odot$. Eggen (1972) argues that the masses of late-type carbon stars lie in the range $1.5\ M_\odot \lesssim$

$M_* \lesssim 5\ M_\odot$. Taking $\mathcal{L}_* = 5 \times 10^4\ \mathcal{L}_\odot$ and $M_* = 5M_\odot$ we have

$$\frac{F_{pr}}{F_{grav}} \simeq (f' 300)\ 15.7 \quad .$$

so if more than $\sim 1/5$ of the available carbon condenses to graphite $F_{pr} \gg F_{grav}$ is satisfied and it appears that radiation pressure driven mass loss must be considered. Further, since small graphite grains have a small albedo, $\langle A \rangle_{vis} \lesssim 0.1$, $Q_s \ll Q_a$ and by eqs. (VIII-7), (VIII-36) $\alpha_{pr} \simeq \alpha$, so eq. (VIII-34) becomes

$$\dot{M}_{tot} \simeq \alpha \left(\frac{\mathcal{L}_*}{10^4\ \mathcal{L}_\odot}\right)\left(\frac{10\ km/s}{V}\right)\ 20 \times 10^{-6}\ M_\odot/yr$$

independent of f. The resultant mass loss rates are given in Table 11 for various parameters.

TABLE 11

Carbon Star Mass Loss Rates Using Conservation of Momentum

$\mathcal{L}_*$	V	α	$\dot{M}_{tot}$ $\simeq$
	10	0.3	7.1
$10^4\ \mathcal{L}_\odot$	10	0.8	16
	20	0.3	3.5
	10	0.3	71
$10^5\ \mathcal{L}_\odot$	10	0.8	160
	20	0.3	35
	km/s		$\times 10^{-6}\ M_\odot/yr$

These results are to be compared with the lower limits (because of uncertainty in f') on $\dot{M}_g$ derived by the method of "weighing the dust" and given in Table 10. For $\mathcal{L}_* = 10^4\ \mathcal{L}_\odot$, $V_g = 10$ km/s the results are comparable but slightly less ($\sim 20\%$ less) than the results given there. The rather good agreement between these two widely different methods for estimating mass loss lends support to the radiation pressure driven mass loss model and to the simplified shell geometry adopted in the previous section. If both models are taken to be correct, it implies $f' \sim f$, i.e. most of the available carbon atoms are actually condensing into graphite, and the late-type carbon stars would appear to be truly efficient dust factories. Further, if $V_g = 20$ km/s the gas loss rates given here are reduced by a factor of two while the minimum gas loss rates in Table 10 are increased by ~ 1.5. If V_g is increased any more than this, there will be disagreement even if $\mathcal{L}_* = 10^5\ \mathcal{L}_\odot$ and the particles are large ($a \gtrsim 0.1\ \mu$). Thus, we would predict that measurements of V_g for carbon Miras similar to the ones studied here should give $V_g \lesssim 20$ km/s.

(b) M and S Stars

For silicate grains the opacities in the 1-3 μ region are unknown but there is a lower limit of

$$\langle Q_{pr} \rangle = \langle Q_{abs} \rangle + \langle (1 - g)\ Q_{scatt} \rangle \geq \langle (1 - g)\ Q_{scatt} \rangle$$

For small grains, $g \simeq 0$. Taking $n = 1.65$, $k = 0$ (i.e. "clean silicate", no absorption) the results shown in Table 12 are obtained.

TABLE 12

$\langle Q_{scatt} \rangle_{T_*}$

T_* (°K)	2000	2500	3000
a			
0.1 μ	0.016	0.039	0.074
0.2 μ	0.18	0.30	0.42

For small grains $\langle Q_{pr} \rangle$ will be very small because of the $\sim (2\pi a/\lambda)^4$ dependence of Q_{scatt} for $2\pi a/\lambda < 1$ (Appendix B) so that any large grains ($a > 0.1$ μ) will dominate the radiation pressure. Taking $a = 0.15$ μ, $\langle Q_{pr} \rangle \simeq 0.1$ and $\rho_{grain} = 3$ gm/cm^3 in eq. (VIII-40) gives

$$\frac{F_{pr}}{F_{grav}} \gtrsim (f'\ 300) \left(\frac{\mathcal{L}_*}{10^4\ \mathcal{L}_\odot}\right)\left(\frac{M_\odot}{M_*}\right) 3.1 \quad . \qquad \text{(VIII-41b)}$$

The situation for the M and S stars appears to be less favorable than for the carbon stars regarding radiation pressure on the grains driving the mass loss. It would seem to require that either (1) all of the available atoms must condense to silicates (i.e. $f' \sim f = 1/300$) or (2) there be some absorption λλ 1-3 μ by the grains, if

this mechanism is to work. Smak (1966) reviews the available data on M-type Miras and concludes $\mathcal{L}_* \sim 10^4\ \mathcal{L}_\odot$ and, with less certainty, $M_* \sim 1\ M_\odot$ for stars comparable to those in this study. Taking $F_{pr}/F_{grav} \sim 3.1$ eq. (VIII-34) becomes

$$\dot{M} \lesssim 0.68\ \frac{\alpha_{pr}\ \mathcal{L}_*}{V\ c} \quad .$$

So $\alpha_{pr} \gtrsim 0.25$ is required to explain the mass loss rates derived earlier (Table 9). In terms of α [eqs. (VIII-36), (VIII-7)] we have

$$\dot{M} \lesssim \frac{\alpha}{1 - \langle A \rangle}\left(\frac{\mathcal{L}_*}{10^4\ \mathcal{L}_\odot}\right)\left(\frac{10\ \text{km/s}}{V}\right)\ 13.6 \times 10^{-6}\ M_\odot/\text{yr} \quad ,$$

where $g = 0$ for small grains and $\langle A \rangle = \langle Q_s/(Q_s + Q_a) \rangle$ is the grain albedo averaged over the stellar radiation field. For the M and S stars, α is quite small (~ 0.01-0.02) so if this method is to agree with the results derived by "weighing the dust" (Table 9) we must have, even if $f' = f = 1/300$ (i.e. complete condensation),

$$\frac{1}{1 - \langle A \rangle} \gtrsim 24$$

or

$$\langle A \rangle_{vis} \gtrsim 0.96 \quad .$$

This result has been used in the previous section to derive a limit on ϵ_{vis} for silicate particles. We conclude that the silicates around the M and S stars must have very little absorption in the

wavelength range λλ 1-3 μ if they are to be effective in driving mass loss (large α_{pr}) and still show so little bolometric excess (small α). The case for this mechanism driving the mass loss in M and S stars would be strengthened if ε_{vis} could be determined by independent means, such as high spatial resolution studies giving R_d directly or measurements of the optical constants of realistic silicate materials (for instance lunar, meteoritic, and cometary silicates) in the range λλ 1-3 μ.

IX. CONCLUSIONS

This study has been concerned with the dust around stars and some of its consequences. The time behavior and detailed spectral distribution of the infrared excess due to dust have been observed and are interpreted, using other observations, laboratory measurements and the laws of physics, in terms of the type of dust, the amount of dust, the possible polarization due to dust, and the distribution and dynamics of dust in the circumstellar envelope leading to information about mass loss.

1. As a result of the study of the variability of cool stars at infrared wavelengths, it must be concluded that:

(a) There is no evidence that changes in the intrinsic polarization of starlight can be attributed to a significant change in the total amount of circumstellar dust. Infrared emission is interpreted in terms of the large scale emission of grains around the star -- condensing and being blown out through the gas by radiation pressure (Gilman 1972; Gehrz and Woolf 1971). The changes in intrinsic polarization should be interpreted in terms of scattering and absorption by much more localized and transient regions of gas and dust or perhaps by aligned grains.

(b) There is some evidence from the dependence of the observed [11 μ] - [8.4 μ] color of M-type Mira variables with phase compared with that expected due to a constant amount of dust heated by a variable stellar luminosity and temperature that perhaps on average there is more circumstellar dust at minimum phase than at

maximum phase. This evidence is indirect in that no [11 μ] - [8.4 μ] color change has been observed whereas a decrease in this color is expected at minimum phase due to a decrease in the stellar luminosity and temperature.

(c) There is evidence for a secular decrease, of about a factor of two, in the amount of dust surrounding oCet over the period 1967 to 1971. There is weaker evidence for possible secular changes in the dust surrounding R Gem and V CrB. The 21 other cool stars showed no evidence for secular variation, over the three year monitoring period and in comparison with the earlier measurements by Gillett et al. (1971), in the total amount of dust.

(d) There is no evidence for any large sudden change, on time scales much less than the visual period, of the overall amount of dust surrounding any of the cool stars.

2. The data that has been obtained on the spectral energy distribution of excess radiation from the stars indicate that:

(a) The characteristic "silicate" type emission profile similar to that observed from the Orion Trapezium region is found in many M and S stars. Some variations in detailed shape, e.g. R Leo, are found. Effects of optical depth and grain temperature do not sufficiently explain these variations. Large grain size, a different chemical composition of dust, or a non-blackbody stellar continuum are possibly indicated.

(b) The excess emission from cool carbon stars can probably be attributed to radiation characteristic of the emissivity with

wavelength of silicon carbide superimposed on a blackbody continuum. The amount of blackbody excess is much stronger from carbon Mira variables than from semi-regular variables.

(c) The spectral excess of the S star W Aql is unique among the M, S and C stars of this study in that it appears smooth, with no large emission or absorption features. It may be compared with R CrB, whose spectrum is also smooth.

(d) No spectra have been observed in this investigation that require interpretation in terms of grains of exceedingly different chemical composition than those discussed -- blackbody grains, silicate grains, and silicon carbide grains.

3. The data presently available is insufficient to definitely decide between a double or single star model for R CrB. It is argued that the double star model requires additional assumptions to explain some of the important characteristics of this unusual object which are a more natural consequence of the single star model and is therefore less likely. On the single star model it is found that the behavior of the infrared excess flux with time can be interpreted as the departure from the star of dust formed on or about JD 2,441,033 with an apparent recessional velocity of 27 km/s. There is no visual event near this date but if the recession is extrapolated linearly back in time the material would have had to leave the star on JD ~ 2,440,400 about which time there was a visual event. The total mass loss rate for R CrB is analyzed in terms of impulsive events and is found to be similar to that derived for the Mira variables. A larger fraction of the

mass loss appears as dust grains for R CrB. The variable intrinsic polarization of R CrB may be due to scattering off of discrete, optically thick clouds or alternatively, aligned dust grains in the line of sight.

4. It has been argued that the rapid variability of intrinsic polarization, its lack of correlation with either infrared or visual flux, and the large shell optical depths inferred from the infrared observations are difficult to reconcile with a well ordered asymmetric envelope model. On the other hand, since the optical depths are large, any polarization mechanism which is proposed must consider the effects of scattering and absorption in this shell. A model involving small clouds, perhaps close to the star, may be able to polarize the starlight and also change rapidly but this light must then transit the extended envelope which is well away from the star. A possible alternative may be asymmetric grains in the extended envelope aligned by the Davis-Greenstein paramagnetic relaxation mechanism. The alignment time scales are small, 1-3 days, and the field required is modest $\sim$ 1-2 gauss. If the field is dipolar, a stellar surface field of $\sim$ 16-100 gauss is implied and, while the grains on our line of sight to the star may be in a "picket fence" array, the net alignment over the whole envelope and the resulting infrared polarization need not be large.

5. Mass loss from late-type stars has been re-investigated. Dust grains in the circumstellar envelope will be expelled by radiation pressure, as suggested by Gilman (1972) and Gehrz and

Woolf (1971), so that the secular stability of infrared excess observed for most stars here implies a continuous condensation of new grains for both the large and small amplitude variables. In order that the surface layers of the star not be depleted of condensed elements, the observed persistence of dust grains in the circumstellar envelope in the presence of the strong radiation pressure repulsion implies a minimum gas density necessary to slow the outflow of grains leading to a minimum mass loss rate $\gtrsim 10^{-6}$ $M_\odot$/yr. The large mass loss rates found by Gehrz and Woolf (1971) are supported without necessitating large 10 μ optical depths. In addition, it is found that a self-consistent solution of the coupled equations governing mass loss leads to a limit of 5-10 km/s for the terminal velocity of grains relative to gas. Finally, it is found that for the carbon Miras, the calculated mass loss rate, assuming graphite dust, agrees with the mass loss arrived at by requiring conservation of energy and momentum in the circumstellar envelope, thus supporting the idea of Gilman (1972) and Gehrz and Woolf (1971) that radiation pressure on the grains may be the agent driving mass loss in the cool, luminous stars.

The gas and graphite loss rates for the carbon Miras are found to be approximately twice the gas and silicate loss rates of the M Miras. Thus, since $\sim$10% of Miras are carbon-rich, the Miras will contribute a ratio silicate/graphite $\sim$ 5 to the interstellar medium. If, as proposed by Gehrz and Woolf (1971) and supported by the findings here, the Mira variables contribute a

major fraction of the interstellar dust, we would expect the ratio silicate/graphite ~ 5 in interstellar space. The ratio silicon carbide/graphite in the carbon Miras is uncertain because of the uncertain temperature and optical depth of the silicon carbide emission feature.

APPENDIX A

INTERPRETATION OF OBSERVED FLUXES

The monochromatic flux (W cm^{-2} μ^{-1}) at wavelength λ observed from a star, F_λ^{obs}, can, in the absence of interstellar reddening, be characterized by approximately

$$F_\lambda^{obs} \simeq F_\lambda^{*} e^{-\tau_e(\lambda)} + F_\lambda^{shell} \quad , \qquad \text{(A-1)}$$

where F_λ^* is the flux from the star which would be observed in the absence of a shell, $\tau_e(\lambda)$ is the effective extinction optical depth of the shell for our line of sight to the star and F_λ^{shell} is the flux which would be observed from the shell in the absence of the star. In the late-type stars and R CrB the component of the shell which is important for extinction of visible light [$\tau_e(\lambda)$] and radiation (F_λ^{shell}) at infrared wavelengths is most probably dust. Jones (1973) has considered the problem of radiation transfer in a spherically-symmetric circumstellar cloud of dust grains and finds expressions for the effective optical depth τ_e in terms of the geometrical optical depth (τ_g) and the grain albedo and phase function (see Appendix B).

i) The Star

The flux observed from the star can be characterized by

$$F_\lambda^* = \Omega_* B_\lambda [T_B(\lambda)] \quad , \qquad (A\text{-}2)$$

where $\Omega_* = \pi r_*^2/D^2$ is the apparent solid angle of the star, r_* = radius of the star, D = distance, star-earth, $B_\lambda(T)$ = Planck blackbody function (W cm^{-2} μ^{-1} $ster^{-1}$), and $T_B(\lambda)$ = brightness temperature of the star at wavelength λ ≃ temperature of the radiating level where $\tau_\lambda = 1$ in the stellar atmosphere. In actual fact this brightness temperature is a very complicated function of λ depending on the temperature structure, molecular abundances, pressure, "turbulent" velocities, etc., and all these parameters are inter-related -- in short this is a difficult and still current problem of model atmosphere calculation. As the primary concern of this thesis is the properties of the circumstellar dust grains, this problem will not be discussed further here. However, we are aware that the deviations of F_λ^* from a blackbody can affect our interpretation of observed excess fluxes as due to circumstellar emission and to a certain extent make this uncertain. It is pointed out in the text when it is believed this uncertainty may be significant.

ii) The Shell

In the shell the continuous opacity at infrared wavelengths is dominated by the solid particles (dust grains) of the circumstellar envelope. The dust grains scatter and absorb stellar photons, heat up, and radiate in the infrared according to their

temperature and emissivity. For a single grain i, the observed flux F_λ^i will be

$$F_\lambda^i = \epsilon_\lambda^i \Omega_i B_\lambda(T_i) \quad , \qquad (A\text{-}3a)$$

where $\epsilon_\lambda^i = Q_{abs}^i(\lambda)$ is the emissivity of the grain, which is a function of grain composition (i.e. optical constants), size, and shape as discussed in Appendix B.

$\Omega_i = \pi a_i^2/D^2$ is the apparent solid angle of the grain of radius a, and T_i = the temperature of the grain.

For a shell going optically thick, the observed flux will be a complicated function of the run of density, temperature, and the individual particle opacities through the shell. In addition, the observed flux may depend on the viewing direction ("patchy clouds"). For an optically thin cloud, each individual dust grain is observed independently and the observed flux is given by

$$F_\lambda^{shell} = F_\lambda^{dust} = \sum_i F_\lambda^i \quad . \qquad (A\text{-}3b)$$

The temperature of each particle is, in turn, determined by an energy balance

$$\dot{E}_{in} = \dot{E}_{out} \quad . \qquad (A\text{-}4)$$

In the presence of the very intense stellar radiation field ($\mathcal{L}_* \sim 10^4 \mathcal{L}_\odot$) the $\dot{E}_{in}$ term is dominated by absorbed stellar

radiation which, for the optically thin case, is given by

$$\dot{E}_{in} = \int_{\lambda=0}^{\infty} \frac{D^2}{R_d^2} F_\lambda^* \left\{ \epsilon_\lambda \pi a^2 \right\} d\lambda \quad , \tag{A-5}$$

where R_d is the distance of the dust grain from the star. If we further define an average grain emissivity "ϵ_{vis}", averaged over the stellar radiation field as

$$\epsilon_{vis} = \langle Q_{abs} \rangle_{T_*} = \frac{\int_0^\infty F_\lambda^* \epsilon_\lambda \, d\lambda}{\mathfrak{F}^*} \quad . \tag{A-6}$$

where $\mathfrak{F}^* = \int_0^\infty F_\lambda^* \, d\lambda$ is the total flux (W cm^{-2}) received at earth from the star, eq. (A-5) reduces to, variously,

$$\dot{E}_{in} = \begin{cases} = \dfrac{\pi^2 a^2}{\Omega_{shell}} \mathfrak{F}^* \epsilon_{vis} & \text{(A-7a)} \\ = \pi a^2 \dfrac{\mathfrak{L}_*}{4 \pi R_d^2} \epsilon_{vis} & \text{(A-7b)} \\ = \pi a^2 \dfrac{4 \pi r_*^2 \sigma T_*^4}{4 \pi R_d^2} \epsilon_{vis} \quad , & \text{(A-7c)} \end{cases}$$

where $\Omega_{shell} = \pi R_d^2 / D^2$ is the solid angle subtended at earth by a spherical shell at R_d and

$$\mathfrak{L}_* = 4 \pi D^2 \mathfrak{F}^* = 4 \pi r_*^2 \sigma T_*^4$$

is the total luminosity of the star (W = 10^7 erg s^{-1}) where T_* is, by definition, the "effective temperature" of the star.

At the temperatures characteristic of the circumstellar shells in this study ($T_d \sim 300$-900 °K) the primary energy loss mechanism is thermal re-radiation. A small grain will come to thermal equilibrium at a temperature T_d and radiate over its whole surface so we have:

$$\dot{E}_{out} = 4 \pi a^2 \int_0^\infty \epsilon_\lambda \left[\pi B_\lambda(T_d) \right] d\lambda \tag{A-8}$$

$$= \epsilon_{IR} \, 4 \pi a^2 \sigma T_d^4 \quad , \tag{A-9}$$

where

$$\epsilon_{IR} \equiv \langle Q_{abs} \rangle_{T_d} \equiv \frac{\int_0^\infty \epsilon_\lambda B_\lambda(T_d) \, d\lambda}{\int_0^\infty B_\lambda(T_d) \, d\lambda}$$

is the effective average grain emissivity for the infrared radiation (radiation at $T = T_d$). Equation (A-4) now implies, using eqs. (A-7) and (A-9) that

$$T_d = \begin{cases} = \left(\dfrac{\pi \mathfrak{F}^*}{4 \sigma \Omega_{shell}} \right)^{1/4} \left(\dfrac{\epsilon_{vis}}{\epsilon_{IR}} \right)^{1/4} & \text{(A-10a)} \\ = \left(\dfrac{\mathfrak{L}_*}{16 \pi \sigma R_d^2} \right)^{1/4} \left(\dfrac{\epsilon_{vis}}{\epsilon_{IR}} \right)^{1/4} & \text{(A-10b)} \\ = T_* \left(\dfrac{1}{4} \right)^{1/4} \left(\dfrac{r_*}{R_d} \right)^{1/2} \left(\dfrac{\epsilon_{vis}}{\epsilon_{IR}} \right)^{1/4} \quad . & \text{(A-10c)} \end{cases}$$

A small grey body, defined by $\epsilon_\lambda = \epsilon$, const or a blackbody, $\epsilon_\lambda = 1$, will come to a temperature

$$T_{BB} = T_* \left(\frac{1}{4}\right)^{1/4} \left(\frac{r_*}{R_d}\right)^{1/2} \quad , \qquad \text{(A-11)}$$

and a general grain reaches

$$T_d = T_{BB} \left(\frac{\epsilon_{vis}}{\epsilon_{IR}}\right)^{1/4} \quad . \qquad \text{(A-12)}$$

The observed flux from the (optically thin) shell [i.e. eq. (A-3b)] will now be determined by (a) the run of temperature (T_d) and density of grains through the shell and (b) the detailed grain emissivities ϵ_λ. The grain opacities are discussed in Appendix B.

iii) The α and β of the Excess

As a measure of the relative importance of the grain component we define α, the relative bolometric excess, as

$$\alpha = \frac{\mathfrak{F}^{dust}}{\mathfrak{F}^{obs}} \simeq \frac{\mathfrak{F}^{d}}{\mathfrak{F}^{*} + \mathfrak{F}^{d}} \quad , \qquad \text{(A-13)}$$

where, as usual $\mathfrak{F} \equiv \int_0^\infty F_\lambda \, d\lambda$. Under the assumption that the fluxes are spherically symmetric, α represents the fractional amount of the total luminosity which is radiated by the dust grains.

Further we define a monochromatic measure of the relative excess

$$\beta_\lambda = \frac{F_\lambda^{exc}}{F_\lambda^{cont}} = \frac{F_\lambda^{obs} - F_\lambda^{cont}}{F_\lambda^{cont}} \quad , \qquad \text{(A-14)}$$

where the separation of observed flux into "excess" and "continuum" is made in the text. α, β can be related to the amount of dust in two ways:

(a) Absorption of Starlight

α represents the fraction of starlight which is absorbed by the shell so from eq. (A-1)

$$\alpha = \langle 1 - e^{-\tau_e} \rangle_{vis} \quad , \qquad \text{(A-15)}$$

where $\langle 1 - e^{-\tau_e} \rangle_{vis}$ is the effective absorption of the cloud averaged over wavelength and over the 4π sterradians surrounding the star. In the optically thin case ($\tau, \alpha \ll 1$) we have

$$1 - e^{-\tau_e} \simeq \tau_e \quad ,$$

and

$$\tau_e(\lambda) = \tau_{abs}(\lambda) = \sum_i \tau_{abs}^i(\lambda)$$

$$= \sum_i \frac{\pi a_i^2 \epsilon_\lambda}{4 \pi R_i^2} \quad , \qquad \text{(A-16)}$$

where R_i is the distance of the i^{th} grain from the star. Averaged over the stellar radiation field this becomes

$$\langle \tau_e \rangle_{vis} = \langle \tau_{abs} \rangle_{vis} = \sum_i \frac{\pi a_i^2 \epsilon_{vis}}{4 \pi R_i^2} \quad , \tag{A-17}$$

i.e. $\langle \tau_e \rangle_{vis}$ is directly proportional to the total solid angle the grains subtend at the star and is thus one measure of the "amount of dust."

The case of an optically thick ($\tau \gg 1$), spherically symmetric circumstellar dust shell has been treated by Jones (1973). He finds expressions for τ_e in terms of the geometric optical depth $\tau_g = \tau_{abs} + \tau_{scatt}$ for various combinations of the grain albedo, A, and phase function $g = \langle \cos \theta \rangle$ (see Appendix B). For most reasonable grain parameters and modest optical depths he found

$$\tau_e \cong \tau_{abs}$$

and usually

$$\tau_e \gtrsim \tau_{abs} \quad .$$

So again $\langle \tau_e \rangle_{vis}$ will be approximately linearly proportional to the "amount of dust" and $\alpha = \langle 1 - e^{-\tau_e} \rangle_{vis}$ will be an increasing function of the "amount of dust."

(b) Thermal Re-Emission of Light by Dust

By definition, in the spherically symmetric case,

$$\alpha = \mathcal{L}_d / \mathcal{L}_{obs} = \mathcal{L}_d / \mathcal{L}_* \quad , \tag{A-18}$$

where $\mathcal{L}_*$ is the stellar luminosity. Using the definition of ϵ_{IR} (eq. A-9), in the optically thin case,

$$\mathcal{L}_d = \sum_i 4 \pi a_i^2 \epsilon_{IR} \sigma T_i^4 \quad . \tag{A-19}$$

Again α is a measure of the amount of dust.

A monochromatic measure of the amount of dust is given by β_λ. In the case of the "continuum" by the flux from a star and the "excess" is due to thermal re-radiation by dust grains eq. (A-14) becomes [using eqs. (A-2) and (A-3b)] in the optically thin limit:

$$\beta_\lambda = \frac{\sum \pi a_i^2 \epsilon_\lambda [B_\lambda(T_i)]}{\pi r_*^2 B_\lambda(T_*)} \quad . \tag{A-20}$$

Further, in the case (Appendix B) $x = 2\pi a/\lambda \ll 1$, we have (eq. B-7)

$$\epsilon_\lambda \pi a^2 = Q_{abs} \pi a^2 = m_{grain} \kappa_\lambda \quad ,$$

where m_{grain} is the mass of the grain and κ_λ, the mass absorption coefficient, is independent of grain radius a. Thus eq. (A-20) becomes

$$\beta_\lambda = \frac{\kappa_\lambda M_d \langle B_\lambda(T_d) \rangle}{\pi r_*^2 B_\lambda(T_*)} \sim M_d \quad , \tag{A-21}$$

where $M_d = \sum_i m_{grain}^i$ is the total mass of dust radiating and

$$\langle B_\lambda(T_d) \rangle = \frac{\sum_i \pi a_i^2 \epsilon_\lambda B_\lambda(T_i)}{\sum_i \pi a_i^2 \epsilon_\lambda}$$

is the average "source function" for the grains. Thus, β_λ is directly proportional to the total mass of dust radiating.

APPENDIX B

GRAIN OPACITIES

i) General Formulas

A small, spherical grain of radius a of material of bulk optical constants $m = n - ik = \sqrt{\epsilon}$, where m is the complex index of refraction and $\epsilon = \epsilon_1 - i\epsilon_2$ is the complex dielectric constant, will both scatter and absorb radiation incident on it. The absorption cross-section is given by

$$\sigma_{abs}(\lambda) = Q_a(\lambda) \pi a^2 \quad . \tag{B-1}$$

The scattering diagram is in general also a complicated function of scattering angle polarization of incident light, we will only consider here the total average cross-section

$$\sigma_{scatt}(\lambda) = Q_s(\lambda) \pi a^2 \tag{B-2}$$

and the phase function

$$g = \langle \cos \theta \rangle = \int \frac{d\sigma_s}{d\Omega} \cos \theta \, d\Omega \quad . \tag{B-3}$$

Two important quantities are the albedo of the grain, $A(\lambda)$, defined as

$$A(\lambda) = \frac{\sigma_s}{\sigma_s + \sigma_a} = \frac{Q_s}{Q_s + Q_a} = \frac{Q_s}{Q_T} \quad , \qquad \text{(B-4)}$$

i.e. the ratio of scattering to total cross-section, and the efficiency for radiation pressure

$$Q_{pr} = Q_{abs} + (1 - g)\, Q_{scatt} \quad , \qquad \text{(B-5)}$$

which determines the force on a grain due to radiation pressure.

In the case $2\pi a/\lambda \gtrsim O(1)$, the opacity parameters are arrived at by applying Maxwell's electromagnetic equations with appropriate boundary conditions (= Mie theory) to the situation of (grain + incident plane wave) as described by Van de Hulst (1957). The solution involves sums of Bessell functions and requires a computer -- this will not be discussed further here but some consequences of the large grain case have been considered in the text -- in this case the computer program written by T. Jones (1974) for use on a Wang 720C computer and tested against published solutions has been used.

In the case $2\pi a/\lambda \ll 1$, the solutions greatly simplify to (Van de Hulst 1957)

$$Q_{sca} = \frac{8}{3}\left(\frac{2\pi a}{\lambda}\right)^4 \left|\frac{m^2 - 1}{m^2 + 2}\right|^2 \simeq 0$$

$$Q_{abs} = -4\left(\frac{2\pi a}{\lambda}\right) \mathrm{Im}\left(\frac{m^2 - 1}{m^2 + 2}\right) \qquad \text{(B-6)}$$

$$g \simeq 0 \quad ,$$

i.e. if $\epsilon_2 = 2nk \neq 0$, then $Q_{abs} \gg Q_{scatt}$ and $A \simeq 0$ and the absorption cross-section can be written as

$$\sigma_{abs} = Q_{abs}\, \pi a^2 = \kappa_\lambda\, m_{grain} \quad , \qquad \text{(B-7)}$$

where $m_{grain} = \frac{4}{3}\pi a^3 \rho$ and ρ = grain density, gm/cm^3 and

$$\kappa_\lambda = \frac{3}{4}\frac{Q_{abs}}{\rho a} = \frac{6\pi}{\rho}\frac{1}{\lambda}\,\mathrm{Im}\left(\frac{1 - m^2}{2 + m^2}\right)$$

$$= \frac{18\pi}{\rho}\frac{1}{\lambda}\,\frac{\epsilon_2}{(2 + \epsilon_1)^2 + \epsilon_2^2} \qquad \text{(B-8)}$$

is the mass absorption coefficient, cm^2/gm. In the case of a non-spherical grain, the absorption cross-section depends on the orientation of the electric field vector with respect to the grain axes (Van de Hulst 1957; Gilra 1972a). In the case of an ellipsoid with axes a_j, $j = 1, 2, 3$, the mass absorption coefficient for electric vector parallel to the j^{th} axis becomes

$$\kappa_\lambda(L_j) = \frac{2\pi}{\rho}\frac{1}{\lambda}\,\frac{\epsilon_2}{[L_j(\epsilon_1 - 1) + 1]^2 + L_j^2\,\epsilon_2^2} \quad , \qquad \text{(B-9)}$$

where L_j is a shape parameter with the property

$$\sum_{j=1}^{3} L_j = 1$$

and the approximate relationship

$$L_j \simeq \text{const } 1/a_j$$

(the exact formulas are given in Van de Hulst 1957). Thus, for a sphere, L = (1/3, 1/3, 1/3) and eq. (B-9) reduces to eq. (B-8). For an oblate spheroid of $a_1 = a_2 \gg a_3$ L → (0, 0, 1) and for a prolate spheroid $a_1 = a_2 \ll a_3$ L → (0.5, 0.5, 0). For freely oriented ellipsoids, the average absorption coefficient will be given by

$$\langle \kappa_\lambda \rangle = \frac{\sum_j \kappa_\lambda(L_j)}{3} \quad .$$

If $\epsilon_1 > 1$, then the absorption cross-section has a maximum for $L_j = 0$, i.e. for radiation with the electric field along the long axis of an asymmetric grain. If $\epsilon_1 < 0$, then there are strong resonances when $L_j = 1/(1 - \epsilon_1)$ or $\epsilon_1 = 1 - (1/L_j)$.

ii) Specific Materials

The optical constants which have been used in calculating grain opacities in the text are from the literature as follows:

(a) Silicates

(i) Perry et al. (1972): optical constants from ~ 5-500 μ for ~ 9 lunar silicate samples at ~ 150 °K and ~ 300 °K.

(ii) Huffman and Stapp (1971) optical constants for one terrestrial silicate (brown enstatite, $(MgFe)SiO_3$) from ~ 0.1-1.0 μ at room temperature.

(b) Silicon Carbide (SiC)

Spitzer et al. (1959a, b): optical constants from 1-25 μ for hexagonal and cubic SiC at room temperature.

(c) Graphite

Taft and Phillip (1965) optical constants from 0.04 μ to ~ 24 μ for electric vector in the basal plane (⊥ to "C" axis = optic axis, i.e. in the direction of high conductivity in plane of hexagonal plates) at room temperature. For $3\ \mu \lesssim \lambda \sim 20\ \mu$, $\epsilon_2 \simeq 5.9\ \lambda(\mu) + 10 \gg |\epsilon_1|$ and eq. (B-9) reduces to

$$\kappa_\lambda \simeq \frac{2\pi}{\rho} \frac{1}{\lambda} \frac{\epsilon_2}{1 + L_j^2\, \epsilon_2^2} \quad , \qquad \text{(B-10)}$$

which for $L_j \neq 0$ becomes

$$\kappa_\lambda \simeq \frac{2\pi}{\rho} \frac{1}{\lambda} \frac{1}{L_j^2} \frac{1}{\epsilon_2}$$

$$\simeq \frac{2\pi}{\rho} \frac{1}{L_j^2} \frac{1}{\lambda} \frac{1}{[5.9\ \lambda(\mu) + 10]}$$

$$\sim \frac{1}{L_j^2} \frac{1}{\lambda^2} \quad , \qquad \text{(B-11)}$$

i.e. the absorption cross-section goes approximately as $1/\lambda^2$.

REFERENCES

Aannestad, P. A., and Purcell, E. M. 1973, Ann. Rev. Astron. & Astrophys. Vol. 10, 309.

Aitken, D. K., and Jones, B. 1973, Ap. J. 184, 127.

Alexander, J. B., Andrews, P. J., Catchpole, R. M., Feast, M. W., Evans, T. L., Menzies, J. W., Wisse, P. N. J., and Wisse, M. 1972, Mon. Not. Roy. Astron. Soc. 158, 305.

Allen, C. W. 1963, Astrophysical Quantities (London: Athlone Press).

Arrhenius, G., and Asunmaa, S. K. 1973, The Moon 8, 368.

Auman, J. R., Jr. 1966, Colloquium on Late Type Stars, Trieste, ed. M. Hack, p. 313.

Auman, J. R., Jr. 1967, Ap. J. (Suppl.) 14, 171.

Autio, G. W., and Scala, E. 1966, Carbon 4, 13.

Babcock, H. W. 1958, Ap. J. (Suppl.) 3, No. 30.

Babcock, H. W. 1960, in Stars and Stellar Systems, Vol. VI, ed. J. L. Greenstein (Chicago: University of Chicago Press), p. 282.

Baumert, J. H. 1972, Ph.D. Thesis, Ohio State University.

Becklin, E. E., Frogel, J. A., Hyland, A. R., Kristian, J., and Neugebauer, G. 1969, Ap. J. (Letters) 158, L133.

Berman, L. 1935, Ap. J. 81, 369.

Campbell, L. 1955, Studies of Long Period Variable Stars (Mass: AAVSO).

Capps, R. W., and Dyck, H. M. 1972, Ap. J. 175, 693.

Cayrel, R., and Schatzman, E. 1954, Ann. d'Ap. 17, 555.

Coyne, George V. S. J., and Shawl, S. J. 1973, Ap. J. 186, 961.

Davis, L., Jr., and Greenstein, J. L. 1951, Ap. J. 114, 206.

Derbiz, T. E., and Dombrovskii, V. A. 1973, Trudy Leningrad 29, 65.

Deutsch, A. J. 1960, Stars and Stellar Systems, Vol. 6, ed. J. L. Greenstein (Chicago: University of Chicago Press), p. 543.

Dickinson, D. F., and Chaisson, E. J. 1973, Ap. J. (Letters) 181, L135.

Dombrovskii, V. A. 1970, Astrofizika 6, 207.

Dombrovskii, V. A., Polyakovo, T. A., Yakovleva, V. A. 1973 Trudy Leningrad 29, 45.

Du Fresne, E. R., and Anders, E. 1962, Geochimica et Cosmochimica Acta 26, 1085.

Dürbeck, H. 1972a, I.A.U. Circular No. 2395.

Dürbeck, H. 1972b, I.A.U. Circular No. 2415.

Dyck, H. M. 1968, Astron. J. 73, 688.

Dyck, H. M. 1972, unpublished observations.

Dyck, H. M., Capps, R. W., Forrest, W. J., and Gillett, F. C. 1973, Ap. J. (Letters) 183, L99.

Dyck, H. M., Forbes, F. F., and Shawl, S. J. 1971, Astron. J. 76, 901.

Dyck, H. M., Forrest, W. J., Gillett, F. C., Gehrz, R. D., Stein, W. A., Woolf, N. J., and Shawl, S. J. 1971, Ap. J. 165, 57.

Dyck, H. M., and Sanford, M. T. 1971, Astron. J. 76, 43.

Eggen, O. J. 1972, Ap. J. 174, 45.

Espin, Rev. T. E. 1890, Mon. Not. Roy. Astron. Soc. 51, 11.

Fáy, T., Honeycutt, R. K., and Warren, W. H., Jr. 1973, Proc. Conf. on Red Giant Stars, p. 130.

Fernie, J. D., Sherwood, V., and DuPuy, D. L. 1972, Ap. J. 172, 383.

Fillit, R., Gheudin, M., Nguyen-Quang-Rieu, Paschenko, M., Slysh, V. 1972, Astron. & Astrophys. 21, 317.

Forrest, W. J., Gillett, F. C., and Stein, W. A. 1971, Ap. J. (Letters) 170, L29.

Forrest, W. J., Gillett, F. C., and Stein, W. A. 1972, Ap. J. (Letters) 178, L129.

Forrest, W. J., and Merrill, K. M. 1974, unpublished data.

Frogel, J. A. 1971, Ph.D. Thesis, California Institute of Technology.

Frogel, J. A., and Hyland, A. R. 1972, Mem. Soc. Roy. Sciences Liege III, 111.

Fujita, Y. 1966, Vistas in Astronomy, Vol. 7, ed. A. Beir (New York: Pergamon Press), p. 71.

Galatola, A. 1968, Ph.D. Thesis, University of Pennsylvania.

Gammon, R. H., Gaustad, J. E., and Treffers, R. R. 1972, Ap. J. 175, 687.

Gaustad, J. E., Gillett, F. C., Knacke, R. F., and Stein, W. A. 1969, Ap. J. 158, 613.

Geballe, T. R., Wollman, E. R., and Rank, D. M. 1973, Ap. J. 183, 499.

Gehrz, R. D., Ney, E. P., and Strecker, D. W. 1970, Ap. J. (Letters) 161, L219.

Gehrz, R. D., and Woolf, N. J. 1971, Ap. J. 165, 285.

Gillett, F. C., and Forrest, W. J. 1973, Ap. J. 179, 483.

Gillett, F. C., and Forrest, W. J. 1974, unpublished data.

Gillett, F. C., Forrest, W. J., Merrill, K. M., and Capps, R. W. 1974, in preparation.

Gillett, F. C., Hyland, A. R., and Stein, W. A. 1970, Ap. J. (Letters) 162, L21.

Gillett, F. C., Low, F. J., Stein, W. A. 1968, Ap. J. 154, 677.

Gillett, F. C., Merrill, K. M., and Stein, W. A. 1971, Ap. J. 164, 83.

Gilman, R. C. 1969, Ap. J. (Letters) 155, L185.

Gilman, Robert C. 1972, Ap. J. 178, 423.

Gilra, D. P. 1972a, The Sci. Results from the OAO, NASA SP-310, p. 295.

Gilra, D. P. 1972b, Interstellar Dust and Related Topics, I.A.U. Symp. No. 52, to be published.

Gilra, D. P. 1974, in preparation.

Gnedin, Yu. N., Dolginov, A. Z., Potashnik, E. L., and Silant'ev, N. A. 1973, Soviet Astronomy A.J. 16, 809.

Gold, T. 1952, Mon. Not. Roy. Astron. Soc. 112, 215.

Gordon, C. P. 1968, Publ. Astron. Soc. Pacific 80, 597.

Greenberg, J. M. 1968, in Stars and Stellar Systems, Vol. 7, ed. B. M. Middlehurst and L. H. Aller (Chicago: University of Chicago Press), p. 221.

Hackwell, J. A. 1971a, Ph.D. Thesis, London University College.

Hackwell, J. A. 1971b, Observatory 91, 33.

Hackwell, J. A. 1972, Astron. & Astrophys. 21, 239.

Harrington, J. P. 1969, Astrophys. Letters 3, 165.

Harwit, M. 1970, Nature, 226, 61.

Herbig, G. H. 1949, Ap. J. 110, 143.

Herbig, G. H., and Zappala, R. R. 1970, Ap. J. (Letters) 162, L15.

Hoyle, F., and Wickramasinghe, N. C. 1962, Mon. Not. Roy. Astron. Soc. 124, 417.

Humphreys, R. M., and Ney, E. P. 1974, Ap. J., in press.

Humphreys, R. M., Strecker, D. W., and Ney, E. P. 1972, Ap. J. 172, 75.

Huffman, D. R., and Stapp, J. L. 1971, Nature Phys. Sci. 229, 45.

Hyland, A. R., Becklin, E. E., Frogel, J. A., and Neugebauer, G. 1972, Astron. & Astrophys. 16, 204.

Jackson, J. D. 1962, Classical Electrodynamics (New York: John Wiley & Sons, Inc.).

Johnson, H. L. 1966, Ann. Rev. Astron. & Astrophys., Vol. 4, p. 193.

Johnson, H. L. 1968, Stars and Stellar Systems, Vol. 7, ed. B. M. Middlehurst and L. H. Aller (Chicago: University of Chicago Press), p. 167.

Johnson, H. L., and Mendez, M. E. 1970, Astron. J. 75, 785.

Jones, R. V., and Spitzer, L., Jr. 1967, Ap. J. 147, 943.

Jones, T. W. 1973, Publ. Astron. Soc. Pacific 85, 811.

Jones, T. W. 1974, private communication.

Keenan, P. C., and Greenstein, J. L. 1963, Perkins Contrib. Series II, No. 13.

Kittel, C. 1966, Introduction to Solid State Physics (New York: John Wiley & Sons, Inc.).

Knacke, R. F., and Thomson, R. K. 1973, Publ. Astron. Soc. Pacific 85, 341.

Krishna Swamy, K. S. 1972, Publ. Astron. Soc. Pacific 84, 64.

Kruszewski, A. 1971a, Astron. J. 76, 576.

Kruszewski, A. 1971b, New Directions and New Frontiers in Variable Star Research, Bamberg Colloq. 32.

Kruszewski, A. 1973, I.A.U. Bulletin on Variable Stars, No. 781.

Kruszewski, A., Gehrels, T., and Serkowski, K. 1968, Astron. J. 73, 677.

Kukarkin, B. V. 1955, I.A.U. Symp. No. 3: Non-Stable Stars, p. 111.

Kukarkin, B. V., Kholopov, P. N., Efremov, Yu. N., Kukarkina, N. P., Kurochkin, N. E., Medvedeva, G. I., Perova, N. B, Fedorovich, V. P., Frolov, M. S. 1969, General Catalog of Variable Stars, Moscow.

Lee, T. A., and Feast, M. W. 1969, Ap. J. (Letters) 157, L173.

Lockwood, G. W. 1972, Ap. J. (Suppl.) 24, 375.

Lockwood, G. W., and Wing, Robert F. 1971, Ap. J. 169, 63.

Loreta, E. 1934, Astr. Nach. 254, 151.

Low, F. J., and Krishna Swamy, K. S. 1970, Nature 227, 1333.

Maas, R. W., Ney, E. P., and Woolf, N. J. 1970, Ap. J. (Letters) 160, L101.

Mayall, M. W. 1973, AAVSO Observations, private communication.

Mendoza, V. E. E. 1967, Bol. Obs. Tonatzintla Tacubaya 4, 114.

Merrill, K. M. 1974a, to be published.

Merrill, K. M. 1974b, unpublished observations.

Merrill, K. M., and Forrest, W. J. 1974, unpublished observations.

Merrill, K. M., and Soifer, B. T. 1974, Ap. J. (Letters) 189, L27.

Merrill, P. W. 1960, Stars and Stellar Systems, Vol. 6, ed. J. L. Greenstein (Chicago: University of Chicago Press), p. 509.

Milkey, R. W., and Dyck, H. M. 1973, Ap. J. 181, 833.

Miller, Joseph S. 1970, Ap. J. (Letters) 161, L95.

Morrison, D., and Simon, T. 1973, Ap. J. 186, 193.

Neugebauer, G., and Leighton, R. B. 1969, Two Micron Sky Survey (NASA, Washington, D. C., 1969).

Ney, E. P. 1973, unpublished data.

Ney, E. P. 1974, Ap. J. (Letters) 189, L141.

Ney, E. P., and Stein, W. A. 1974, P. A. S. P., in press.

Ney, E. P., Strecker, D. W., and Gehrz, R. D. 1973, Ap. J. 180, 809.

Nguyen-Quang-Rieu, Fillit, R., and Gheudin, M. 1971, Astron. & Astrophys. 14, 154.

Nussbaumer, H., and Swings, J. P. 1972, Ap. J. 172, 121.

O'Keefe, J. A. 1939, Ap. J. 90, 294.

Pasachoff, J. M. 1972, I.A.U. Circular No. 2403.

Payne-Gaposchkin, C. 1963, Ap. J. 138, 320.

Perry, C. H., Agrawal, D. K., Anastassakis, E., Lowndes, R. P., Rastogi, A., and Tornberg, N. E. 1972, The Moon 4, 315.

Pettit, E., and Nicholson, S. B. 1933, Ap. J. 78, 320.

Purcell, E. M., and Spitzer, L., Jr. 1971, Ap. J. 167, 31.

Schwartz, P. R., and Barrett, A. H. 1970a, Proceedings of the Conference on Late-Type Stars, ed. G. W. Lockwood and H. M. Dyck, p. 95.

Schwartz, P. R., and Barrett, A. H. 1970b, Ap. J. (Letters) 159, L123.

Schwartz, P. R., Harvey, P. M., and Barrett, A. H. 1974, Ap. J. 187, 491.

Scoville, N. Z. 1974, private communication.

Serkowski, K. 1966a, Ap. J. 144, 857.

Serkowski, K. 1966b, I.A.U. Information Bull. on Variable Stars, No. 141.

Serkowski, K. 1970, Proc. of the Conf. on Late-Type Stars, ed. G. W. Lockwood and H. M. Dyck, p. 107.

Serkowski, K. 1971, New Directions and New Frontiers in Variable Star Research, I.A.U. Colloquium No. 15, p. 11.

Serkowski, K. 1974a, in preparation.

Serkowski, K. 1974b, private communication.

Serkowski, K., and Kruszewski, A. 1969, Ap. J. (Letters) 155, L115.

Shakhovskoi, N. M. 1964, Soviet Ast. A.J. 7, 806.

Shawl, S. J. 1971, Bull. Amer. Astron. Soc. 3, 442.

Shawl, S. J. 1972, Ph.D. Thesis, University of Texas.

Simon, T. 1973, private communication.

Smak, J. I. 1964, Ap. J. (Suppl.) 9, 141.

Smak, J. I. 1966, Ann. Rev. Astron. & Astrophys., Vol. 4, p. 19.

Solomon, P. 1973, private communication.

Solomon, P., and Stein, W. A. 1966, Ap. J. 144, 825.

Spinrad, H., and Newburn, R. L. 1965, Ap. J. 141, 965.

Spinrad, H., Pyper, D. M., Newburn, R. L., Jr., and Younkin, R. L. 1966, Ap. J. 143, 291.

Spitzer, L., Jr. 1968, Diffuse Matter in Space (New York: Interscience Publ.).

Spitzer, L., Jr., and Tukey, J. W. 1951, Ap. J. 114, 187.

Spitzer, W. G., Kleinman, D., and Walsh, D. 1959a, Phys. Rev. 113, 127.

Spitzer, W. G., Kleinman, D. A., and Frosch, C. J. 1959b, Phys. Rev. 113, 133.

Stein, W. A., Gaustad, J. E., Gillett, F. C., and Knacke, R. F. 1969, Ap. J. (Letters) 155, L3.

Stein, W. A., and Gillett, F. C. 1969, Ap. J. (Letters) 155, L197.

Sterne, T. 1934, H. B. 896, 17.

Strecker, D. W. 1973, Ph.D. Thesis, University of Minnesota.

Taft, E. A., and Philipp, H. R. 1965, Phys. Rev. 138, A197.

Toombs, R. I., Becklin, E. E., Frogel, J. A., Law, S. K., Porter, F. C., and Westphal, J. A. 1972, Ap. J. (Letters) 173, L71.

Treffers, R. R. 1973, Ph.D. Thesis, University of California, Berkeley.

Treffers, R. R., and Cohen, M. 1974, Ap. J. (in press).

Trimble, V. 1972, Mon. Not. Roy. Astron. Soc. 156, 411.

Tsuji, T. 1966, in Colloquium on Late-Type Stars, ed. M. Hack (Observatorio Astronomico di Trieste), p. 260.

Urey, H. C., and Craig, H. 1953, Geochimica et Cosmochimica Acta 4, 36.

Van de Hulst, H. C. 1957, Light Scattering by Small Particles (New York: John Wiley & Sons, Inc.).

Vardanian, R. A. 1968, Non-Periodic Phenomena in Variable Stars, p. 339.

Wallerstein, G. 1973, Ann. Rev. Astron. & Astrophys., Vol. 10, p. 115.

Warner, B. 1967, Mon. Not. Roy. Astron. Soc. 137, 119.

Weymann, R. 1963, Ann. Rev. Astron. & Astrophys., Vol. 1, p. 97.

Wickramasinghe, N. C. 1967, Interstellar Grains (London: Chapman and Hall).

Wilson, W. J., and Barrett, A. H. 1970, Proc. of the Conf. on Late-Type Stars, ed. G. W. Lockwood and H. M. Dyck, p. 77.

Wilson, W. J., Schwartz, P. R., and Epstein, E. E. 1973, Ap. J. 183, 871.

Wing, R. F., Baumert, J. H., Strom, S. E., and Strom, K. M. 1972, paper presented at the A.S.P. Meeting, 1972 June.

Woolf, N. J. 1970, Proc. of the Conf. on Late-Type Stars, ed. G. W. Lockwood and H. M. Dyck, p. 187.

Woolf, N. J. 1972, Interstellar Dust and Related Topics, I.A.U. Symp. No. 52, to be published.

Woolf, N. J. 1973, private communication.

Woolf, N. J., and Ney, E. P. 1969, Ap. J. (Letters) 155, L181.

Woolf, N. J., Schwarzschild, M., and Rose, W. K. 1964, Ap. J. 140, 833.

Zappala, R. R. 1967, Ap. J. (Letters) 148, L81.

Zirin, H. 1952, Harvard Obs. Bull. 921, 26.